वार्षिक प्रतिवेदन
Annual Report
2011-2012

भौतिक अनुसंधान प्रयोगशाला, अहमदाबाद
Physical Research Laboratory, Ahmedabad

पी.आर.एल. में सुविधाएं
Facilities at PRL

वार्षिक प्रतिवेदन

Annual Report

2011 - 2012

भौतिक अनुसंधान प्रयोगशाला, अहमदाबाद

Physical Research Laboratory, Ahmedabad

Front Cover: Center Left Panel: Celebration of Republic Day at Thaltej Campus of Physical Research Laboratory, Ahmedabad.

Center Right Panel Synoptic view of Mt. Abu Observatory

Center Bottom Panel: Synoptic View of Udaipur Solar Observatory located in Fateh Sagar Lake, Udaipur.

Inside front cover: Facilities at PRL

Inside back cover: Events at PRL

Back cover: The sequence of photographs of Venus Transit captured by Solar Flare Telescope at Thaltej campus of Physical Research Laboratory, Ahmedabad.

Compiled by:
Office of the Dean, PRL.

Published by:
Physical Research Laboratary, Ahmedabad.

Layout & Printed by:
Creative Printers Pvt. Ltd., Ahmedabad.

Council of Management

Chairman Professor U. R. Rao ISRO Headquarters, Government of India, Bangalore	Nominee, Government of India
Members Dr. K. Radhakrishnan Secretary, DOS and Chairman, ISRO, Government of India Department of Space, Bangalore	Nominee, Government of India
Shri A Vijay Ananad Joint Secretary, Department of Space, Government of India, Bangalore	Nominee, Government of India
Shri Sanjay S. Lalbhai Ahmedabad Education Society Ahmedabad	Nominee, Ahmedabad Education Society
Shri Kartikeya V. Sarabhai Chidambaram, Usmanpura, Ahmedabad	Nominee, Karmakshetra Educational Foundation
The Principal Secretary, Department of Education (Higher & Technical Education) Government of Gujarat, Gandhinagar	Nominee, Government of Gujarat
Professor J. N. Goswami Director, Physical Research Laboratory, Ahmedabad	(Ex-Officio)
Member- Secretary Shri Y.M. Trivedi Registrar Physical Research Laboratory, Ahmedabad	(Ex-Officio)

Contents

Director's Foreword

A major landmark of the current year was the formulation of the Science Goals for PRL during the 12th five year plan period. These were derived through extensive discussions and brainstorming sessions amongst faculty members and a comprehensive and well-defined plan is now ready. The plan document contains the trajectory of science at PRL in the coming years with new initiatives and definition of pathways towards strengthening of existing research programs. The new initiatives include the plans for establishing a 2.5 meter telescope at Mt. Abu for astronomical observations, making forays into laboratory studies of molecular genesis in simulated cold astrophysical environment, an accelerator mass spectrometer for inferring precise time scales of planetary and geological processes, experiments to understand the role of volatile hydrocarbon in tropical troposphere and the development of optical parametric oscillator based sources for studies of photon entanglement.

Specific need-based augmentation of experimental facilities for research in different areas and upgrading of computational capabilities will also form a major component of the activities during the next five years. With the anticipated completion of the Space Instrumentation Facility in the PRL-Thaltej campus, PRL's commitment to actively participate in ISRO's future space-science missions in the fields of Astronomy & Astrophysics, Solar Physics and Planetary & Atmospheric Sciences will now on be a more ambitious route. PRL has played a major role in ISRO's planetary science missions to Moon and Mars and has an active role in the Solar Mission, "*Aditya*" for probing the solar corona, the outermost layer of the Sun. I anticipate an enhanced and a proactive role of PRL scientists in such missions in the years to come.

The year witnessed several landmarks, some of which were achieved using the facilities established during the 11th plan period. These include the installation of Multi Application Solar Telescope (MAST) at the Udaipur lake site that is nearing completion. With this facility, we anticipate an exciting new era of solar observations and a refined understanding of various solar phenomena and processes. First science results from the indigenously developed Echelle Spectrograph, obtained in early 2012, confirmed its capability for detection of exo-planets and routine observations will follow. Direct detection of water in microscopic mineral phases in lunar samples was made using a Secondary Ion Mass Spectrometer (Nano-SIMS) that was acquired during the last plan. In the area of space exploration, fabrication of the two payloads for the *Chandrayaan-2* mission is progressing well and development of a payload proposed for the Mars mission has been initiated. In basic geosciences, the studies at PRL delineated the role of the Ganga-Brahmaputra river system in controlling the trace element inventory of the world oceans. Theoretical analysis showed that the claim for an elementary particle (neutrino) moving at a speed faster than light, made by a European experimental group, that would require modification of Einstein theory of special relativity, is not tenable, as it conflicts with well-established results on decay of elementary particles.

The core academic faculty strength at PRL remained close to seventy and the combined number of research scholars and post-doctoral fellows is nearly hundred. A large number

of project associates are also working in different areas. Preparations for the 8th UN course on Space Sciences for the Asia-Pacific region, conducted by PRL, have been completed and fifteen students will join the course starting from July, 2012. Keeping in view the broad canvas of research areas at PRL, an MOU was signed with Indian Institute of Technology, Gandhinagar (IIT-Gn), Gujarat, to facilitate academic exchange and registration of PRL research scholars at IITGn for their PhD degree. Growing involvement of PRL in Planetary and Space Explorations also led to signing of an MOU with the Space Application Centre, Ahmedabad, for support and collaboration in realizing space qualified payloads at PRL for future ISRO space missions.

The steady and positive growth in research in different scientific areas at PRL was also reflected both via an increase in the total number of publication, and in the number of publications in high impact journals. PRL faculty members were also invited to edit special issues of journals, and to write review articles in international journals and monographs. Fifteen research scholars completed their PhD studies during the year.

The research at PRL was formally recognized by various international and national forum through fellowship, awards and honors bestowed on PRL faculty. These included the J. C. Bose fellowship, D.Sc. (Honoris Causa), Vice-Chairman, Committee on Space Sciences of International Astronautical Academy, Goyal Prize, K. R. Ramanathan Gold Medal (Indian Geophysical Union), D. M. Khaitan Gold Medal (Asiatic Society), National Geoscience Award and Young Associate, Indian Academy of Sciences. Several research scholars of PRL also received awards at various national conferences and symposia for high quality of their presentations. Senior faculty members from PRL were invited to serve in Council/Board of academic and research institutions in India and as member of international scientific working groups. Further, several faculty members continued to serve as editorial board members of international and national journals and others as guest editors of special issues of journals.

PRL was honored to be invited to host the 77th Annual Meeting of the Indian Academy of Sciences and the meeting was organized jointly with the Institute for Plasma Research, Gandhinagar, and the Space Applications Centre, Ahmedabad. About half a dozen national and international symposia were held at PRL during the year. These included the 7th Chandrayaan-1 Science Meet, with participation of scientists from US and Japanese moon missions, an International workshop on Asian greenhouse gases budget and a workshop on neutrinos beyond standard model.

PRL honored Prof. M. M. Sharma and Prof. Yash Pal with the Hari-Om-Ashram award for Senior Scientists on November 11, 2011, the Foundation Day of PRL. The weekly colloquium series had nearly twenty invited scientists from India and abroad, as well as PRL faculty member and post-doctoral fellows, presenting new science results and reviewing contemporary developments in different fields in research. The regular seminar activities of all the six major divisions, where senior research scholars are encouraged to present their work, continued with usual vigour.

As a part of its HRD activities, PRL is working hard to encourage young college and university students, by inviting them to spend some quality time and partner the academic activities at PRL and interact with its scientists. PRL had a strong summer program, driven by its own program and via its participation in the Indian Academies program and over seventy students participated in these programmes. The technical faculty members of PRL additionally guided a large number of B.Tech and M.Tech engineering students in their project work and dissertation.

PRL continued to conduct the PLANEX and RESPOND programmes of ISRO. These programs aim at enhancing participation of scientists from universities and academic institutions in the areas of space and planetary research. Nearly fifty groups across the country are currently pursing research under these two programmes.

The celebration of science day at PRL has now matured into a major Science outreach activity that covers higher secondary schools from across the state of Gujarat. PRL held events and lectures at eleven centers across the state and selected over a hundred students from over hundred schools who were invited to PRL along with their teachers on Science Day to participate in various activities. Some of the meritorious students from amongst these were awarded scholarships and other incentives.

PRL made a steady improvement in the use of Hindi in its day to day administration. The PRL website is now in a bilingual format. This year was the second consecutive year when the Town's Official Language Committee, Ahmedabad, selected PRL for the First Prize for excellence in contribution towards implementation of official language.

The multi dimension forward movement of PRL in science, articulation of the long-term science goals of the laboratory as a part of the 12th Five Year Plan along with the implementation of DOS policy for PRL Technical Staff up to SC level became possible due to the untiring effort of the scientific, technical, administrative and auxiliary staff members of the laboratory. I will like to place on record my deepest appreciations to the entire *Team-PRL* for their unstinted support. Given the generous support from DOS, the onus is now on us to ensure that the proposed long-term plans and programs are executed in time and that these lead to front-ranking science. I urge all my colleagues to strive hard to achieve these objectives and I am confident of their rising up to the challenges ahead.

I would like to express my deep sense of gratitude to Chairman, PRL Council, Chairman ISRO and the members of the Council of PRL for their guidance, constructive advice and suggestions that were critical in the smooth functioning of the laboratory and chartering its future course.

J. N. Goswami

Director

Science Highlights

Astronomy and Astrophysics

- The first successful "science" observing run with the PARAS spectrograph for observing exo-planets was carried out in early 2012, under stabilized condition of temperature and pressure. Temperature was controlled at 0.02°C to 0.03°C rms at 25°C and the net change in pressure inside the spectrograph vessel during observations, spread over a week, was of the order of ~0.15 mbar. These conditions yielded typical intrinsic Radial-velocity stability of about 1.5 to 1.7m/s.

- Infrared light curves and spectra, obtained soon after the 2011 outburst of the well-known recurrent nova T Pyx, were analyzed to study its temporal evolution. The spectral line profiles indicate enhanced mass loss near the optical maximum.

- Evidence for enhanced angular sizes of Asymptotic Giant Branch stars due to mass loss and presence of circumstellar shells was obtained based on measured uniform disk angular diameters of 45 oxygen-rich Mira variables by lunar occultation technique.

- Time resolved infrared photometry of the Intermediate Polar WX Pyx showed a strong modulation at 1559 seconds coinciding with the spin period of the magnetic white dwarf in this close binary system. There is also an indication of a second period of 5.3 hours attributed to the orbital period of the binary system.

- An upper limit on the size of the emission region of 10^{15} cm and a billion solar mass for the central source for the blazar CGRaBS J0211+1051 were estimated on the basis of the shortest variability time scale of 1.24 hrs observed in optical polarization and optical flux.

- A study of anisotropy in the sky brightness from discrete radio sources revealed a large peculiar motion of the solar system, relative to the frame of distant radio sources.

- Interplanetary scintillation (IPS) observations at 327 MHz obtained between 1983 and 2009 revealed that microturbulence levels in the entire inner heliosphere have shown a steady decline since ~1995. This result, coupled with the fact that there was also a steady decline in solar magnetic fields above 45° latitude since ~1995, suggest that the deepest solar minimum in the past 100 years, experienced at the end of solar cycle 23 was initiated in the mid 1990's.

- Centaurus X-3 is one of the few high mass X-ray binary (HMXB) sources which exhibit phase dependent dips. X-ray spectra of this pulsar show

three Iron emission lines at 6.4, 6.7 and 6.9 keV. Phase dependence of their intensities implies that the origin of the 6.4 keV line lies closer to the neutron star whereas the other two lines originate in the highly photoionized wind of the companion star or in the accretion disk corona.

- A Be/X-ray binary pulsar A0535 + 262/HDE 245770, monitored in the JHK bands at various phases of its ~111 day orbital period, showed that the spectra are dominated by hydrogen Bracket and Paschen series lines. This along with the absence of any significant change in the continuum of the Be companion during X-ray quiescent and X-ray outburst phases suggest that the near-IR line emitting regions of the disc are not significantly affected during the outburst.

Solar Physics

- Multi-wavelength signatures along with RHESSI X-ray spectra and available magnetic field measurements provided evidence that discrete, confined events of energy release during the precursor phase of a flare (which might correspond to the localized events of magnetic reconnection) act as a common trigger for the main flare and associated large-scale eruption.

- Estimation of various physical parameters as a function of time in an evolving solar active region (NOAA AR 11158) confirmed that rotational motions played a predominant role in increasing non-potentiality of magnetic structures by injecting helicity.

- Analysis of flare-induced seismicity in the active region NOAA 10930 and related enhancement of global waves in the Sun, at sites that are away from the flare location, and the hard X-ray foot points suggests that the sudden enhancement in velocity seems to be caused by the Lorentz force driven by the "magnetic jerk" in the localized penumbral region and possibility of a connection between the flare induced localized seismic signals and the excitation of global high-frequency oscillations.

- A significant weakening in field strength in the light bridge associated with its brightening was seen in high quality data from Hinode which is suggestive of strong convection in the sunspot triggering the expulsion and fragmentation of a small sunspot.

- Interplanetary Coronal Mass Ejections (ICMEs) resulting from solar eruptions appeared to contain a mixture of cold and hot plasma with presence of He^{+} ions. The rarity of finding cold, low charge state ions at 1 AU as filament plasma suggests partial ionization of elements during transit through corona.

- A novel technique for solving linear force-free field extrapolation in spherical geometry was evolved which yields finite magnetic energy for the infinite half-space outside the solar surface.

- Calibration of the tandem Fabry-Perot etalon, prior to its integration into the narrow band imager, one of the first back-end instruments for the Multi-Application-Solar Telescope, has been successfully completed.

Planetary Sciences and PLANEX Programe

- The potential of noble gas isotopes to identify and quantify the nature of the impactor responsible for formation of crater, and in particular for the Lonar crater has been demonstrated. Xe, Ne and Ar isotopic compositions of Lonar crater glasses are found to be significantly different from terrestrial ratios, and clearly suggest that these differences are related to trapping of impactor components in them. Excess ^{129}Xe, present in lonar glasses suggest up to 2 wt % contribution of the impactor.

- A laser heating system capable of analysing sub-milligram amounts of samples for nitrogen and noble gas composition has been developed, and used for studying individual ilmenite grains from lunar meteorite Y983885 to decouple their nitrogen components. A non-solar nitrogen component contributed by Interplanetary Dust Particles could be identified in nitrogen and argon isotope systematics.

- Spectral reflectance data obtained by the Chandrayaan-1, LRO and Kaguya missions for the multi-ringed Oriental basin of the Moon have been analysed. The elongated vent at the centre of the ring is found to be noritic in composition and shows pyroclastics on its surface. A large melt sheet with mafic edges has also been identified within the ring.

- Studies of the non mare domes of Moon's Gruithuisen region using M^3 and DIVINER data brought out the felsic nature of the domes as well existence of compositional variation amongst the domes.

- Analysis of high-resolution images obtained by Terrain Mapping Camera on board Chandrayaan-1 and the Lunar Reconnaissance Orbiter Camera revealed landslides and gully formation on the interior steep upper wall of a 7 km crater having a slope of ~35

degree. The gullies show a typical alcove-channel-fan morphology but with less conspicuous channels. Spectral reflectance studies suggest the gullies and landslides to be of relatively recent origin. These gullies appear similar to the gullies on Mars, occur at steeper slopes than on Mars and have poorly developed channels. The lunar gullies and landslides are products of dry granular flows generated by seismic effects due to single or multiple impacts on moon near the crater site.

- Energetic particle environment in the earth-moon space, including earth's radiation belts, during the Chandrayaan-1 mission duration, have been inferred from data obtained by the RADOM payload. The maximum flux of electron and proton components in the radiation belt reached ~15000 and ~9600 particles cm^{-2} s^{-1}, respectively. The particle flux, en route to the moon, was rather low (~3 particles cm-2 s^{-1}) that decreased to ~2.5 particles cm^{-2} s^{-1} at the final lunar orbit of 100km, reflecting shielding effect of the moon. A gradual increase in particle flux in lunar space as a function of time, over the mission duration, reflects effect of solar modulation in cosmic ray intensity.

- A mineralogical study of phyllosilicate-rich ultramafic rocks near Udaipur, Rajasthan, reflects similarities with Martian surface features and shows serpentinisation suggesting metamorphism and hydrothermal alteration of mafic minerals. Comparisons of mineralogical data at this site with reflectance data for Nilli Fossae on Mars suggest that the ancient Mg-rich Martian crust experienced sub-surface water-rock interaction resulting in formation of Mg-rich phyllosilicates and carbonates.

Space and Atmospheric Sciences

- Studies of black carbon aerosol mass concentrations over the past several years reveal that the concentrations have increased over Bay of Bengal during the last decade and are the highest in winter reflecting influence of emissions from biomass/biofuel burning that is prevalent during winter.

- Modeling studies along with the measured ozone profiles obtained from a series of balloon launches over Ahmedabad reveal that ozone in the lower troposphere is affected by regional transport (North India, Indian Ocean, and Arabian Sea) and in the middle and upper troposphere by continental transport (North Africa, Europe, North and South America).

- Analysis of intra-seasonal oscillations in the 1–100 km region in the zonal winds over India over a 3-year period suggests a coupling between the convection activity at lower atmosphere and wave dynamics in the mesosphere.

- Daytime optical investigations of the less explored region of 110 km using balloon-borne measurements of ultraviolet oxygen emission intensities at 297.2 nm reveal wave features in the scale sizes of 50 – 70 km and periodicities of 25 ± 5 minutes.

- An extreme event of prompt response of the interplanetary electric field, recorded in the equatorial- and low-latitudes ground-based magnetic and space-borne radio measurements, indicate the variability of the low-latitude ionosphere to space weather events.

- Numerical simulations of the effect of solar energetic particle event on the Martian ionosphere reveal that the enhancement in electron density can be significantly high to cause strong attenuation of radio waves.

Geosciences

- Records of Os isotope composition of the Arabian seawater since last 40 ka archived in two sediment core taken from Arabian ocean suggest variation in phase with those of the global ocean since last 40 ka, except during time period around last glacial maxima (LGM). During LGM, $^{187}Os/^{188}Os$ deviates from the trend set by the global ocean and shows an excursion towards higher $^{187}Os/^{188}Os$. Deviation of Os isotope composition and bottom anoxia present during LGM, thus, indicate reduced supply of North Atlantic Deep water (NADW) to the Arabian Sea during LGM. This resulted in partial isolation of the Arabian Sea from rest of the oceans during this era.

- The concentrations and isotope composition of dissolved Nd, measured in the water column along 87°E transect in the Bay of Bengal, show that the dissolved Nd concentration in the Bay of Bengal is significantly higher compared to that of the global ocean, suggesting presence of unradiogenic Nd. This suggests that release of Nd from particulate sinking matter and from shelf sediments derived from the Ganga-Brahmaputra river system contribute significantly to the dissolved Nd budget of the Bay of Bengal and highlight the significance of boundary exchange process in contributing to the global oceanic budget of dissolved Nd. This result underscores the

significant role of dissolved/particulate Nd from the Ganga-Brhamputra river system in contributing to the dissolved Nd budget of the global ocean.

- Simultaneous measurements of drop size distribution (DSD) and stable oxygen and hydrogen isotopic compositions ($\delta^{18}O$ and δD) of rain at Gadanki (13.5°N, 79.2°E), southern India, were made to understand cloud microphysical processes leading to rain formation. The MST radar at NARL, Gadanki, was operated continuously during rain events, while rain samples were collected at very short time intervals (<1 h), to capture small changes (~0.2‰) in their $\delta^{18}O$ and δD. The slope of the local meteoric water line (δD vs.$\delta^{18}O$) was 8.07 ± 0.47, similar to that of global meteoric water line, confirming that the precipitation occurred under isotopic equilibrium, and the evaporation of rain drops at the cloud base was insignificant. Whenever the isotopic variations were larger (>2‰) during a rain event, there was a significant negative correlation between the $\delta^{18}O$ and DSD. This suggest that the larger drops are mostly associated with convective rather than stratiform rain, and ^{18}O (and D) depletion in convective rain is relatively high.

Theoretical Physics

- Very economical description incorporating correct value for the recently measured reactor mixing angle in neutrino physics was proposed using the concept of the generalized CP symmetry that predicts the entire neutrino mass matrix in terms of only three unknowns. Maximal CP violation emerges as an important prediction of the scheme.

- A novel mechanism to incorporate the tri-bimaximal mixing at the leading order in grand unified SO(10) theory is proposed. Perturbation to this are systematically studied and those which can or which cannot account for the measured reactor mixing angle are distinguished.

- Models of dark matter which can explain and predict new features in direct detection experiments as well as high energy cosmic ray observations in terms of supersymmetry are proposed.

- Collider studies of particle physics models is made in the light of recent possible detection of Higgs particle and the limits set on supersymmetric particle masses at the large hadron collider, CERN. Specific studies include simulation of collider observables, studies of top-quark and Higgs properties at colliders.

- Strong constraints arising from the pion decay kinematics on superluminal neutrinos are placed in the light of the reported evidence for such neutrinos by the OPERA collaboration of the Grand Sasso laboratory, Italy. These findings severely constrain possible forms of modification of the special theory of relativity.

- The coupled system in which the average effect of the environment is modelled by an over-damped oscillator kept alive with feedback from the subunits was shown to lead to an interesting phenomenon in which the collective dynamics of coupled systems is quenched due to interaction with an environment. Such suppression of dynamics provides a control mechanism for stabilizing systems to steady states.

- A new limit on the permanent electron electric dipole moment (EDM) due to parity (P) and time reversal (T) symmetry violations was obtained by employing novel relativistic many-body methods and a new method to measure EDM in an atomic Indium was proposed.

- Creation of coreless vortex dipoles when a Gaussian obstacle beam traverses across vortex above a critical speed is demonstrated. As the obstacle passes through the inner component, it carries along a droplet of the outer component. Further it is shown using Thomas-Fermi approximation, that phase-separated binary condensates can either support vortices with empty or filled cores.

Awards and Honours

Faculty Members

U. R. Rao

1. Sivananda Eminent Citizen Award, 2011.

2. D.Sc. (Honoris Causa) from National Institute of Technology, Agarthala, 2012.

J. N. Goswami

3. Vice-chairman, Committee on Space Sciences, International Astronautical Academy.

4. J. C. Bose National Fellowship of the Department of Science and Technology, 2011.

5. Member, Governing Board, Inter University Centre for Astronomy & Astrophysics, Pune.

A. K. Singhvi

6. J.C. Bose National Fellowship of the Department of Science and Technology, 2011.

7. D.P. Khaitan Memorial Gold Medal by the Asiatic Society, 2011.

8. Leader, Indian Delegation to four yearly INQUA congress in Berne, 2011.

9. Member, Science Program Committee of the IGBP – PAGES, Open Science Meeting: 2013.

10. Chair, Geosciences Group for Ministry of Earth Sciences, XII Plan proposals.

V. K. B. Kota

11. Appointed as an Expert member in the Board of Studies in Physics and Meteorology and a member, Faculty Board, Faculty of Science, M. S. University of Baroda, September, 2011-2014.

P. Venkatakrishnan

12. Co-Convener of Session ST09, "Solar Physics with Hinder in the ascending phase of the solar cycle", at AOGS 2011, held in Taipei, 08-12 August, 2011.

S. Lal

13. Member, Governing Body of Wadia Institute of Himalayan Geology, Dehradun.

R. Ramesh

14. K. R. Ramanathan Memorial Gold Medal of the Indian Geophysical Union, 2011.

15. Member, Indian team for the International Earth Science Olympiad, Italy.

16. Chairman, IMD Committee for Scientific Instrumentation onboard aircraft for cyclone studies.

17. Chairman, IITM Committee for scientific instruments onboard research Aircraft for studying Aerosol-Climate Interaction.

18. Member, Intergovernmental Panel on Climate Change, WMO.

19. Member, Governing Council, Birbal Sahni Institute of Paleobotany.

20. Member, Editorial Advisory, Board, Gondwana Geological Society.

M. M. Sarin

21. Vice-Chairman, UN/GESAMP (United Nations Group of Experts on Scientific Aspects of Marine Environmental Protection).

22. Member, Scientific Advisory Committee, Space Physics Laboratory (Trivandrum).

23. Member, Research Advisory Committee, Indian Institute of Tropical Meteorology (Pune).

24. Member, National Steering Committee, RAWEX – GVAX Project (ISRO).

25. Adjunct Professor, University of Delaware (USA).

26. Member, WMO/GESAMP Working Group on "Impact of atmospheric anthropogenic nitrogen deposition on marine biogeochemistry".

Utpal Sarkar

27. Goyal Prize for Physics, Kurukshetra University, 2008.

S. A. Haider

28. Elected President of Planetary Sciences by Asia Oceania Geosciences Society (AOGS) for 2012-2014.

29. Convener, Science and Exploration of Mars and Venus, 8th annual Asia-Oceania Geosciences Society (AOGS) meeting, Taipei, Taiwan, 8-12 August, 2011.

D. Pallamraju

30. Member Secretary, Board of Studies, Centre for Space Science and Technology Education in Asia and the Pacific (CSSTEAP) (Affiliated to the United Nations).

31. Main Convener, Atmospheric Coupling Processes in the Sun-Earth System, 8th annual Asia Oceania Geosciences Society (AOGS) Meeting, Taipei, Taiwan, 8-12 August, 2011.

32. Appointed Science Discipline Representative (SDR) to Scientific Committee on Solar Terrestrial Physics (SCOSTEP).

33. Co-Convener, Session S6: Ionospheric storms and Space weather effects at low and mid latitudes in the "13th International Symposium on Equatorial Aeronomy", Paracas, Peru, 12-17 March, 2012.

34. Chairman, Session S6: Ionospheric storms and Space weather effects at low and mid latitudes in the "13th International Symposium on Equatorial Aeronomy", Paracas, Peru, 12-17 March, 2012.

Nandita Srivastava

35. Guest Investigator, on ESA's Proba2 solar mission, October 2011.

Navin Juyal

36. National Geosciences Award, 2010.

37. Member Indo-Swiss joint working group on scientific cooperation in glaciology and related areas, October 2011.

Bijaya Sahoo

38. "S N Ghosal Award" given by the Indian Physical Society as the best Young Physicist at the Colloquium for Young Physicists (YPC), 18-19 August, 2011.

Smitha V. Thampi

39. Associate of the Indian Academy of Sciences, 2011-2014.

Raghavan Rangarajan

40. Appointed member of the Academic Advisory Council of IIT Gandhinagar, September 2011.

41. Appointed member of the Board of Editors, Physics Education (a journal of the Indian Association of Physics Teachers - IAPT).

42. Appointed member of the Council of the Indian Association for General Relativity and Gravitation (IAGRG) for 2012-2016.

Young Scientists

Mala Bagiya

43. Best paper award for the paper, "A novel method based on GPS TEC to forecast L band scintillations over the equatorial region through a case study", by Sridharan, R., Mala Bagiya, and S. Sunda in the National Space Science Symposium, Sri Venkateswara University, Tirupati during 14-17 February, 2012.

A.H. Laskar

44. Awarded the first prize in the Research Scholar presentation at the ISMAS Symposium, Munnar, Kerala, 07-11 November, 2011.

Ashok Kumar

45. Poster award (1st position) for the paper "Making an optical vortex and its copies using a single spatial light modulator", by A. Kumar, P. Vaity, J. Banerji and R. P. Singh, in the Physical Sciences section, 99th Indian Science Congress, Bhubaneshwar, 03-07 January, 2012.

Rishitosh K. Sinha

46. Poster award (2nd position) for the paper "Seasonal accumulation and evacuation: Modelling forced flows of debris from cavity on an inclined plane on Mars", by R.K. Sinha. and S.V.S. Murty at NSSS-2012, Sri Venkateswara University, Tirupati, 14-17 February, 2012.

Administration

47. PRL has received First Prize conferred by Town Official Language Committee (TOLIC), Ahmedabad for excellent contribution towards implementation of Official Language Policy during 2010-2011. A certificate of appreciation has also been given to Shri R.S. Gupta, Hindi Officer-II & OSD.

Theses Submitted

Manan Vyas

1 "Some Studies on Two-body Random Matrix Ensembles", M. S. University, Baroda, May 2011.

Ashok Kumar

2 "First and second order coherence studies of optical vortices", Mohanlal Sukhadia University, Udaipur, July 2011.

J. P. Pabari

3. "Investigation of Wireless Sensor Network for In-Situ Exploration of Water Ice on the Moon", Indian Institute of Technology Bombay, Mumbai, July 2011.

Sandeep Gautam

4. "Dynamics of ultracold quantum gases in variable potentials", Mohanlal Sukhadia University, Udaipur, July 2011.

Anil Dutt Shukla

5. "Geochemical and isotopic studies of some sedimentary sequences of the Vindhyan Supergroup", India, M. S. University, Baroda, August 2011.

Nishtha Anilkumar

6. "Research Undertaken in Physical Research Laboratory (PRL): A Bibliometric study", M. S. University, Baroda, August 2011.

Pankaj Sharma

7. "Collider Signals of New Physics Beyond the Standard Model", Mohanlal Sukhadia University, Udaipur, September 2011.

Rohit Srivastava

8. "Spectral aerosol optical depths and radiative forcing: Seasonal and spatial variations", Mohanlal Sukhadia University, Udaipur, September 2011.

Anand D. Joshi

9. "Morphology and Dynamics of Solar Prominences", Mohanlal Sukhadia University, Udaipur, November 2011.

Ketan M. Patel

10. "Beyond the standard model of Physics: Grand Unification and otherwise", Mohanlal Sukhadia University, Udaipur, November 2011.

Alok Kumar

11. "Geochemical and isotopic studies of rocks from the Barren Island Volcano and Andaman subduction zone", India, M. S. University, Baroda, December 2011.

Bhaswar Chatterjee

12. "A field theoretic study of matter under extreme conditions", Mohanlal Sukhadia University, Udaipur, December 2011.

V. Sreekanth

13. "Properties of strongly interacting matter under extreme conditions", Mohanlal Sukhadia University, Udaipur, December 2011.

Vineet Goswami

14. "Spatial and temporal variations of Os, Nd, Sr isotopes and redox sensitive elements in waters and sediments of the Arabian Sea and their implications", Mohanlal Sukhadia University, Udaipur, January 2012.

Soumya Rao

15. "Constraints on particle properties from astrophysical sources", Mohanlal Sukhadia University, Udaipur, February, 2012.

Human Resource Development

Staff Structure

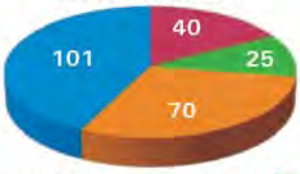

Administrative
Auxilliary
Scientific
Technical

Doctoral, Post Doctoral and Other Programmes

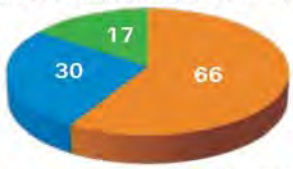

Research Fellows
Project Associates
Post - Doctoral Fellows

Technical Programmes

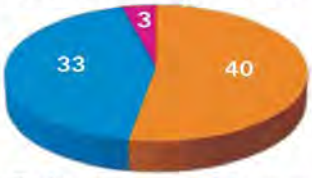

Engineering Trainees
Summer Students
Summer Teachers

Scientific Publications

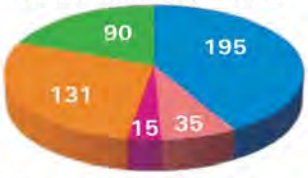

Journals
Theses
Proceedings of Coference /Workshop/Symposia
Invited Talks at Conference/ Symposia/ Workshop
Lectures at Universities/Institutions

Administrative/Technical / Allied Service Staff

Tradesman Trainees
Library Trainees
Project Engineers
Office + Computer Operator Trainees
Data/Document/Record Assistant & Office Assistant

Colloquia/Public Lectures by Visitors

Prof. Apoorva Patel

Indian Institute of Science, Bangalore

Efficient energy transport in photosynthesis: Roles of coherence and entanglement

Prof. Girish S. Agarwal

Oklahoma State University, USA

Quantum interference between independent photons

Prof. Amita Das

Institute of Plasma Research, Gandhinagar

Propagation of low frequency electromagnetic disturbances in plasma

Dr. Devendra Ojha

Tata Institute of Fundamental Research, Mumbai

Do Massive Stars Trigger New Waves of Star Formation?

Dr. J.G. Canadell

Commonwealth Scientific and Industrial Research Organization (CSIRO), Marine and Atmospheric Research, Canberra, Australia

Recent Trends in Anthropogenic Carbon Fluxes

Dr. Madan Rao

Raman Research Institute & National Centre for Biological Sciences, Bangalore

Active Cellular Mechanics and Information Processing in the Cell

Prof. Prakash D. Vyavahare

S.G.S. Institute of Technology& Science, Indore

Near Shannon Limit Channel Codes

Prof. Ajoy K. Kar

Heriot-Watt University, Edinburgh, EH14 4AS, Scotland

Femtosecond-laser-written optical waveguides for optical communications and biophotonic applications

Prof. Arjun Berera

University of Edinburgh, Scotland, U.K.

Inflationary Cosmology in the Planck Era

Prof. Supriya Chakrabarti

Centre for Space Physics, Boston University, USA

Studies Using Direct Imaging at Boston University: Current Work and Future Plans

Prof. Terrence M. Quinn

Jackson School of Geosciences, University of Texas, Austin

A Proxy Perspective on Southwest Pacific Climate Variability in the Common Era

Prof. Steven Tomcyzyk

High Altitude Observatory, Boulder, Colarado, USA

Observation of Alfven Waves in the Solar Corona

Prof. Pijushpani Bhattacharjee

Saha Institute of Nuclear Physics, Kolkata

Chasing The WIMPs of Milky Way

Dr. Bhalamurugan Sivaraman

Tata Institute of Fundamental Research, Mumbai

Elkectron, Proton and Ion Induced Molecular Synthesis and VUV Spectroscopy of Interstellar Molecules in the Ice Phase

Prof. Greg J. Evans

Southern Ontario Centre for Atmospheric Aerosol Research, University of Toronto, Canada

Every Breath You Take: The Impacts of Aerosol on Air Quality and Health

Prof. Nicholas Lancaster

Desert Research Institute, Reno, Nevada, USA

From R.A. Bagnold to A.K. Singhvi and beyond – How Physics has transformed Desert Geomorphology and why we need more of it

Prof. Narendra Kumar

Raman Research Institute, Bangalore

Re-visiting Classical Orbital Magnetism: A Surprise

Conferences / Symposia / Workshops held

1. "77th Annual Meeting of Indian Academy of Sciences", Bangalore, organized by Physical Research Laboratory, 18-22 November, 2011.

2. "RESPOND", Review meeting, Physical Research Laboratory, Ahmedabad, 28-29 February, 2012.

Planetary Sciences & PLANEX Program

3. "7th Chandrayaan-1 Science meeting", Physical Research Laboratory, Ahmedabad, 16-18 December, 2011.

4. 12th PLANEX Workshop on "Exploration of Asteroids and Comets", Physical Research Laboratory, Mt. Abu, 02-06 January, 2012.

5. PLANEX Projects PIs Review meeting, Physical Research Laboratory, Ahmedabad, 16-17 March, 2012.

Space and Atmospheric Sciences

6. "CAWSES Workshop on Space Weather and Space Climate", Physical Research Laboratory, 27-28 April, 2011.

7. "International workshop on Asian greenhouse gases budgets", Physical Research Laboratory, 27-29 September, 2011.

Geosciences

8. DST-SERC sponsored Training Workshop on "Isotope Hydrology" organized jointly with National Institute of Hydrology, Roorkee, 19-24 December, 2012.

Theoretical Physics

9. "iCaPP (interface of Cosmology and Particle Physics)" meeting on Dark Matter, Physical Research Laboratory, 06-08 April, 2011.

10. "iCaPP meeting on neutrinos beyond standard model", Physical Research Laboratory, 21-23 September, 2011.

11. "Garuda Boot Camp", jointly organized by Physical Research Laboratory, Ahmedabad and Centre for Development of Advanced Computing (CDAC), Bangalore, 16-17 February, 2012.

Computer Centre

12. "Interdisciplinary Workshop on High Performance Computing", Physical Research Laboratory, Ahmedabad, 30 January-01 February, 2012.

Invited Talks at Conference / Symposia / Workshops

Astronomy and Astrophysics

A. K. Singal

1. "Our large peculiar motion in the universe determined from the sky brightness anisotropy", at the national conference on Applied Mathematics and Computational Physics, Moradabad, 25-26 February, 2012.

2. "Large peculiar motion of the solar system from the anisotropy in sky brightness due to the distant radio sources", International Conference on Astrophysics and Cosmology, Kathmandu, Nepal, 19-21 March, 2012.

B. G. Anandarao

3. "Atomic, molecular and PAH emission in Star Forming Regions", Invited Review talk in the International Conference on Interstellar Dust, Molecules and Chemistry, IUCAA, Pune, 22-25 November, 2011.

Baliyan K.S.

4. "Some recent interesting results on Blazar variability from Mt Abu IR Observatory", delivered at the 2nd Theme meeting on VHE Gamma-ray Astronomy at GOALS, Mt. Abu, 29-31 March, 2012.

Ganesh S.

5. "Interstellar Extinction and Galactic Structure", at International Conference on Interstellar Dust, Molecules and Chemistry (IDMC-2011), at IUCAA, Pune, India, 22-25 November, 2011.

6. "Composition of Comets", 12th PLANEX Workshop on the Exploration of Asteroids and Comets at Mt. Abu, 02-06 January, 2012.

H. O. Vats

7. "Estimation of solar rotation", at Solar Radio Workshop, NCRA, Pune, 23-25 November, 2011.

8. "Solar Terrestrial Relationship", at National Seminar on Recent Trends in Physics (NSRTP-12), Punjabi University, Patiala, Punjab, 29 March, 2012.

Rajmal Jain

9. "Relationship between high energy processes in solar flares /CMEs and geomagnetic storms", at CAWSES workshop on Space Weather and Space Climate held at Physical Research Laboratory, Ahmedabad, India, 27-28 April, 2011.

10. "Solar signatures on the Earth's climate", at National Conference on Applied Mathematics & Computational Physics held at Hindu College, Moradabad, UP, 25-26 February, 2012.

Sachindra Naik

11. "Broad-band spectroscopy of HMXB pulsar Cen X-3", Advanced workshop on X-ray Timing, IUCAA, Pune, 23-28 January, 2012.

12. "Broad-band spectroscopy of X-ray Pulsars", Symposium on Accretion on to Compact Objects, Harish-Chandra Research Institute, Allahabad, 6-18 February, 2012.

S. V. Vadawale

13. "Measuring X-ray polarization with Compton scattering: Pushing to lower energies", NOW meeting held at TIFR, 12 January, 2012.

14. "Multi-pixel CZT detectors: Astrosat CZT", at Advance Workshop in X-ray Timing, IUCAA, 24-28 January, 2012.

15. "X-ray Spectral simulations for observation proposals With XSPEC", at X-ray View of Cosmos conference, PRL, 23-25 April, 2012.

T. Chandrasekhar

16. Two invited talks, "The Occultation Phenomena" and "Occultation of Kuiper belt objects and lunar transient events", at the IUCAA Workshop on Teaching and Research using small telescopes, JES College, Jalna, Maharashtra, 17-19 October, 2011.

17. "Trans-Neptunian objects" at the 12th PLANEX Workshop on Exploration of Asteroids and Comets, Mt. Abu, 02-06 January, 2012.

Solar Physics

Ashok Ambastha

18. "Solar physics in Optical Wavelengths: Measuring Solar Magnetic and Velocity Fields", Solar Radio Workshop, NCRA, Pune, 22-25 November, 2011.

19. "Spectral Line Profile Changes Associated with Energetic Solar Transients", International Workshop on Stellar Spectra Libraries (IWSSL 2011), Delhi University, 05-09 December, 2011.

20. "Photospheric Transients Driven by the X2.2 White-Light Flare of 2011 February 15 in NOAA 11158", National Space Sciences Symposium, Sri Venkateswara University, Tirupati, 14-17 February, 2012.

Bhuwan Joshi

21. "Multi-wavelength signatures of magnetic reconnection in solar flares: The RHESSI perspective", International Astrophysics Forum Alpbach IAFA 2011 - Frontiers in Space Environment Research, Alpbach, Austria, 20-24 June, 2011.

22. "Observational aspects of magnetic reconnection and energy release in solar eruptive phenomena", Workshop on Physics of the Solar Transition Region and Corona, IUCAA, Pune, India, 05-07 September, 2011.

23. "Solar flares: A multi-wavelength perspective", Solar Radio Workshop, National Centre for Radio Astronomy (NCRA-TIFR), Pune, India, 23-25 November, 2011.

Brajesh Kumar

24. "Mysteries of our daytime star: The Sun", in the Astronomical Workshop "Nakshatra-2011", The Indian School, Kingdom of Bahrain, 17-18 October, 2011.

Nandita Srivastava

25. "Solar Phenomena and their geo-effectiveness", CAWSES Workshop on Space Weather and Space Climate, PRL, Ahmedabad, 27-28 April, 2011.

26. "3D Reconstruction of CMEs: Implications on Prediction of the Arrival Time", AOGS 8th Annual meeting, Taipei, Taiwan, 08-12 August, 2011.

27. "Kinematics of two eruptive prominences observed from EUVI onboard STEREO", Workshop on the physics of the solar transition region and corona, IUCAA, Pune, 05-07 September, 2011.

28. "Challenges on predicting the space weather", International workshop on Nano Physics and Astrophysics, Pt. Ravishankar Shukla University, Raipur, 19-21 February, 2012.

P. Venkatakrishnan

29. "Electric Currents in Sunspots", Workshop on Physics of the Solar Transition Region and Corona, IUCAA, Pune, 05-07 September, 2011.

30. "Solar Astronomy" in "Galaxy Forum 2011" at Nehru Planetarium, Bangalore, 09 September, 2011.

31. "MAST Overview" in Science with upcoming Solar facilities in the Country, IIA, Bangalore, 02 November, 2011.

Ramit Bhattacharyya

32. "Variational calculus: a not so conventional but possible tool to explore the coronal field", Workshop on Physics of the Transition Region and the Corona, IUCAA, Pune, 05-07 September, 2011.

33. "An overview of the numerical magneto hydrodynamic model EULAG and its applications in solar physics", Interdisciplinary workshop on high performance computing, PRL, Ahmedabad, 30 January - 01 February, 2012.

Planetary Sciences & PLANEX Program

A. Sarbadhikari Basu

34. Two talks on "Meteorites - Primitive and Processed", and "Comets and water on Earth", at the 12th PLANEX workshop on Exploration of Asteroids and Comets, Physical Research Laboratory, Mt. Abu, Rajasthan, 02-06 January, 2012.

J. N. Goswami

35. "Exploring the unknown", Indian Institute of Remote Sensing, Dehradun, 01 June, 2011.

36. "Planetary Science and Astronomy", Karnataka Science Academy, Bangalore, 08 September, 2011.

37. "Significant Results from Chandrayaan-1 Mission", Second International Solar System Symposium, Moscow, 10-14 October, 2011.

38. "Chandrayaan-Mission: Orbiter and Rover Payloads", Second International Solar System Symposium, Moscow, 10-14 October, 2011.

39. "Exploring asteroids and comets", Planex workshop, Mt. Abu, 02 January, 2012.

40. "Space and Planetary Sciences: An Indian Perspective", Science Expo, Regional Science City, Lucknow, 01 February, 2012.

41. "Research in Space Sciences in India: Problem and Prospects", Keynote Address, 17th National Space Science Symposium, Tirupati, 14 February, 2012.

K. Durga Prasad

42. Two talks on "DAWN – Mission Objectives", "ROSETTA – Chasing a Comet", at the 12th PLANEX workshop on Exploration of Asteroids and Comets, Physical Research Laboratory, Mt. Abu, Rajasthan, 02-06 January, 2012.

K. K. Marhas

43. "Results from Stardust Mission", 12th PLANEX Workshop on Exploration of Asteroids and Comets, Mt. Abu, Rajasthan, 02-06 January, 2012.

N. Srivastava

44. "Space Weathering", 12th PLANEX Workshop on Exploration of Asteroids and Comets, Mt. Abu, Rajasthan, 02-06 January, 2012.

S.V.S. Murty

45. Chandrayaan-1: Important Results", at 7th International Conference on Microwaves, Antenna, Propagation and Remote Sensing at ICRS, Jodhpur, 07-10 December, 2011.

46. "Asteroid meteorite connection", 12th PLANEX Workshop on Exploration of Asteroids and Comets, Physical Research Laboratory, Mt. Abu, 02-06 January, 2012.

47. "Hayabusa and results from Itakowa", 12th PLANEX Workshop on Exploration of Asteroids and Comets, Physical Research Laboratory, Mt. Abu, 02-06 January, 2012.

48. "Meteorites as probes to understand evolution of solar system objects", in Introductory seminar on Astronomy, Astrophysics and our Earth, Sardar Vallabhbhai Patel University, 29 January, 2012.

49. "Impactor signatures in Lonar impact glasses", 17th National Space Science Symposium, S. V. University, Tirupati, 14-17 February, 2012.

50. "Geo-Cosmo chemistry of noble gases", at ISAGBHU-2012, Banaras Hindu University, Varanasi, 22-24 February, 2012.

Vinai K. Rai

51. "MC-ICPMS: A powerful Mass Spectrometer for precise isotope measurements", ISMAS International Discussion Meet on Elemental Mass Spectrometry in Health and Environmental Sciences at Inter University Accelerator Centre (IUAC), New Delhi, 14-15 February, 2011.

Space and Atmospheric Sciences

D. Chakrabarty

52. "Effects of space weather over low latitudes: recent results using optical and other techniques", 13th International Symposium on Equatorial Aeronomy (ISEA13), Paracas, Peru, 12-17 March, 2012.

D. Pallamraju

53. "Overview of science results from the CAWSES-India Program", Indo-US Workshop on Advancing VLF Science Through the Global AWESOME Network, Goa, 28 November-01 December, 2011.

54. "Optical investigations of the Mesosphere and Lower-Thermosphere", Growth of Geomagnetism: Challenges and Opportunities in the Next Two Decades, IIG, New Panvel, 12-13 December, 2011.

H. Chandra

55. "Ionospheric radio: Developments in 20th century, National Conference on Advances in Physics (NCAP), IIT Roorkee, 26 February, 2012.

56. "Equatorial spread-F", Workshop on recent trends in space physics, atmospheric physics, and astrophysics, BHU, Varanasi, 12-17 March, 2012.

L. Sahu

57. "Seasonal and diurnal variations of carbonaceous aerosols in Bangkok", Workshop on Aerosol Impact in the Environment: from Air Pollution to Climate Change, The Abdus Salam International Centre for Theoretical Physics (ICTP), Trieste, Italy, 08-12 August, 2011.

58. "Importance of non-methane hydrocarbons in ozone formation at a semi-arid urban site of India", IGBP, 3rd Integrated Land Ecosystem-Atmosphere Processes Study (iLEAPS) Science Conference, Garmisch-Partenkirchen, Germany, 16-23 September, 2011.

59. "Study of Arctic haze: Long range transport of aerosols and trace gases over Arctic", National Space Science Symposium (NSSS), Tirupati, 14-17 February, 2012.

R. Sridharan

60. "Future trends in Space Sciences, Solar Terrestrial Physics and Aeronomy - Indian Perspective", Growth of Geomagnetism: Challenges and Opportunities in the Next Two Decades, IIG, New Panvel, 12-13 December, 2011.

61. "CAWSES-INDIA: Objectives and Accomplishments", National Space Science Symposium (NSSS), Tirupati, 14-17 February, 2012.

S. Lal

62. "Ozone and trace gas measurements and future directions", Third National Workshop on Climate Change, NCAOR, Goa, 22 September, 2011.

63. "Trace gases measurements and modeling – an ISRO GBP initiative", International workshop on Asian greenhouse gases budgets, PRL, Ahmedabad, 27-29 September, 2011.

64. "Atmospheric Chemistry and Air Quality, Indo-German workshop", TERI University, New Delhi, 28 November, 2011.

65. "Processes in the tropical troposphere and stratosphere affecting distributions of trace gases, I-SPARC meeting", ISRO HQ Bangalore, 30 November, 2011.

66. "Environmental Pollution, Seminar on Environmental Pollution and Bioremediation", JNU, New Delhi, 28 December, 2011.

67. "Atmospheric Chemistry and Climate: Perspectives for the Indian region", Plenary Session on Frontiers in Atmospheric Sciences, Indian Science Congress, KIIT University, Bhubaneswar, 04 January, 2012.

68. Advances in Atmospheric Chemistry in India, Workshop cum Seminar on Challenges and Opportunities in Air Pollution and Climate Change Indo-German Collaboration, IITM, Pune, 17 January, 2012.

69. "Trace gases in the tropical Indian region: Some recent results and future directions," Workshop on Atmospheric Chemistry in South Asia: Progress and emerging issues IISER, Mohali, 05-06 March, 2012.

S. Ramachandran

70. "Ozone", International Ozone Day, Gujarat Science City, Ahmedabad, 16 September, 2011.

V. Sheel

71. "Numerical Modeling of Stratosphere Troposphere Exchange and its Effect on Atmospheric Chemistry", Meeting of I-SPARC (Indian Scientific Program of SPARC), ISRO HQ, Bangalore, 30 November, 2011.

72. "Dust Aerosols and Ions in the lower Atmosphere of Mars", 2nd International Workshop on Spectroscopic Signatures of Molecular Complexes/ Ions in our Atmosphere and Beyond, Varanasi, 07-10 February, 2012.

Geosciences

A. K. Singhvi

73. "The Role of Geosciences in informing about Planets Future (How does Physics help)", National Seminar on new trends in Physics and Applications, 04 March, 2011.

M. G. Yadava

74. "Long Term Solar Influence on the Indian Monsoon Rainfall", 8th Annual AOGS meetings, Taipei, 11 August, 2011.

M. M. Sarin

75. "Impact of anthropogenic sources on aerosol-Fe solubility: Comparative in Planetary study from tropical Bay of Bengal and Arabian Sea", GEOTRACES Colloquium, Liege (Belgium), 05 May, 2011.

76. "Tropospheric soot particles: Role in atmospheric chemistry" AEACI Meeting, BARC-Mumbai, 06 June 2011.

77. "Characteristics of carbonaceous aerosols from Indo-Gangetic Plain and Central Himalaya", IUGG-2011, Melbourne (Australia), 06 July, 2011.

78. "Impact of continental outflow on atmospheric dry-deposition of N, P and Fe to Bay of Bengal", ICAMG-2011, NIO, Goa, 12 October, 2011.

79. "Carbonaceous and mineral aerosols: A regional perspective", I-SPARC Meeting, ISRO-Hq (Bangaluru), 30 November, 2011.

80. "Radionuclide and nutrient fluxes: Implications to sediment transport", I2SM-2012, BARC (Mumbai), 21 March, 2012.

Navin Juyal

81. "Reconstructing the Late Quaternary climate in Himalaya", at Karnataka state council of science and technology, Bangalore, 02 December, 2011.

R. Bhushan

82. "Application of radiocarbon in oceanography", Inter-University Accelerator Centre, New Delhi, India during the workshop on Accelerator Mass Spectrometry, 15 September, 2011.

R. D. Deshpande

83. "New Hydrological Insights", the 14th ISMAS Symposium cum Workshop on Mass Spectrometry IWIN, Munnar, Kerala, 07-11 November, 2011.

R. Ramesh

84. "New Production in the Indian Ocean", SIBER International Scientific Steering Committee Meeting, Chennai, 27, July, 2011.

85. "Dendroclimatology of Tropical trees", Symposium on 'Climate Change and Geo Hydrology, BSIP, Lucknow, 28- 29 August, 2011.

86. "Monsoon onset signal in the stable oxygen and hydrogen isotopes in Rainfall", XIV ISMAS Symposium cum Workshop on Mass Spectrometry, Munnar, Kerala, 07-11 November, 2011.

87. "Holocence Paleomonsoon inferred from Indian Ocean Sediments", National Seminar on modern and Palaeo sediments: implication to climate, water resources and environmental changes & xxviii convention of Indian Association of Sedimentologists, Jawaharlal Nehru University, New Delhi, 24-26 November, 2011.

88. "Paleoclimate and Hydrology of India", two lectures at the ICTP Workshop on Paleoclimate and human dispersal during Marine isotope Stage 3, Ahhan University, Chennai, 12-17 December, 2011.

89. "Reconstruction of Paleomonsoons using oxygen isotopes in tree rings and speleothems", K. R. Ramanathan Memorial, IGU, Vishakapatnam, 20 December, 2011.

90. "Can high resolution reconstruction of Indian monsoon during Holocene tell us what may happen to Indian monsoon in 'Anthropocene'?", INSA Climate Change Symposium, Tezpur University, 28-30 December, 2011.

91. "Past as a mirror for future: Monsoon Tipping point", Golden Jubilee International Conference, IITM, Pune, 21-15 February, 2012.

92. "Wavelet applications in Paleoclimatology", National workshop on Wavelets, Multiresolution and Multifractal Analyses in Earth, Ocean and Atmospheric Sciences: Current Trends (WMMFA2012), IIT, Powai. Mumbai, 29 February-02 March, 2012.

93. "Stable isotope evidence for Antarctic melting", International Conference on the Science and Geopolitics of the Arctic and the Antarctic, New Delhi, 09-12 March, 2012.

R. Rengarajan

94. "Particle-reactive Radionuclides as Tracers of Carbon Export", Biogeochemistry in the framework of Earth System Science, National Institute of Oceanography, Goa, 03 February, 2012.

S. K. Singh

95. "Indian GEOTRACES Programme" SIBER Scientific Steering Committee Meeting, 26-28 July, 2011, Chennai, India.

96. "Re-Os systematics in organic rich sediments", Invited lecture at ISMAS workshop, Munnar, India, 10 November, 2011.

97. "Contemporary and paleo-oceanographic processes in the Northern Indian Ocean: clues from Os, Sr and Nd isotope composition of sediments and waters". Invited lecture at National Seminar in Geochemistry and Geophysics: the Indian scenario (ISAG BHU-2012), BHU, Varanasi, India, 22-24 February, 2012.

S. Krishnaswami

98. "Erosion Processes in the Himalaya: Clues from Studies of Rivers and Northern Indian Ocean Sediments", Key Note Lecture at 7th International Conference on Asian Marine Geology, National Institute of Oceanography (CSIR), Goa, India, 11-14 October, 2011.

Theoretical Physics

A. C. Das

99. "Reconnection Processes in Solar and Magnetosphere environment: A comparative View", in Recent Trends on Space Physics, Atmospheric Physics and Astrophysics, Banaras University, Varanasi, 12-17 March, 2012.

100. "Magnetosphere of Outer Planets: Many Surprises" in Recent Trends on Space Physics, Atmospheric Physics and Astrophysics, Banaras University, Varanasi, 12-17 March, 2012.

Bijaya Sahoo

101. "Singly charged atomic ions as prospective candidates for atomic clocks", ISAMP topical conference on Laser interactions with atoms, molecules and cluster (TC2012), Hyderabad Central University, Hyderabad, India, 09-12 January, 2012.

102. "Possibility of temporal variation of fine structure constant and roles of many-body methods for its investigation", National conference on "Advances in Physics", IIT Roorkee, India, 25-26 February, 2012.

103. "Variation of fine structure constant, atomic clocks and the relativistic many-body methods", Indo-UK Scientific Seminar (IUSS), NISER, Bhubaneswar, India, 07-09 March, 2012.

D. Angom

104. "Vortex dipoles in Bose-Einstein condensates", International Conference on Theoretical and applied physics, IIT Kharagpur, 01-03 December, 2011.

105. "Relativistic coupled-cluster theory of open-shell systems with additional perturbation", Recent advances in many-electron theories, Holiday Resort, Puri, 01-04 December, 2011.

Hiranmaya Mishra

106. "Kinetics of chiral transition - a toy model", Working group talk at Workshop on High Energy Physics Phenomenology, (WHEPP-12), Mahabaleswar, India, 02-08 January, 2012.

107. "Strong magnetic field and chiral transition in hot and dense matter", STAR collaboration meeting on Phase diagram of QCD VECC, Kolkata, 10-12 January, 2012.

J. Banerji

108. "Nonlinear energy spectrum and fractional revival of wave packets", Workshop on Nonlinear Dynamics (ND2011), Tezpur University, Tezpur, 26-28 April, 2011.

109. "Generating Schrödinger cats with sub-Planck spots", Workshop on Nonlinear Dynamics (ND2011), Tezpur University, Tezpur, 26-28 April, 2011.

110. "Ultra-sensitive dual-mode waveguide interferometers", 99th Indian Science Congress, KIIT University, Bhubaneswar, 03-07 January, 2012.

Partha Konar

111. "LHC as a probe on properties of Dark Matter", iCaPP Meeting on "Dark Matter", PRL, 06-08 April, 2011.

112. Discussion session on "Inverse Problem/Mass Reconstruction/MCMC at WHEPP XII," Mahabaleswar, 02-15 January, 2012.

R. Amritkar

113. "Synchronization of networks and Time delay systems", Two invited talks in National workshop on Nonlinear dynamical systems, NIT, Durgapur, 04-08 July, 2011.

114. "Introduction to nonlinear dynamics'', 8 lectures in SERC school on Nonlinear Dynamics VIII, IISER, Pune, 04-24 December, 2011.

115. "Synchronization with variable delay'', 2nd International Symposium On Complex Dynamical Systems and Applications, Presidency University, Kolkata, 09-11 January, 2012.

116. "Amplitude death in coupled dynamical systems'', invited talk in Conference on Statistical Physics and Nonlinear Dynamics, S. N. Bose National Center for Basic Sciences, Kolkata,12-16 March, 2012.

R. P. Singh

117. "A study of vortex dipoles in Bose-Einstein Condensate", ISAMP Topical Conference on Interaction of Lasers with Atoms, Molecules & Clusters (TC-2012), University of Hyderabad, India, 09-12 January, 2012.

Raghavan Rangarajan

118. "Non-Gaussian fluctuations of the inflaton and constancy of correlations of zeta outside the horizon", Indo-UK Scientific Seminar: Confronting Particle-Cosmology with Planck and LHC, IUCAA, Pune, 10-12 August, 2011.

119. "Non-Gaussian fluctuations of the inflaton and constancy of correlations of zeta outside the horizon", 7th International Conference on Gravitation and Cosmology (ICGC), Goa, 14-19 December, 2011.

Saurabh D. Rindani

120. "Going beyond the standard model of elementary particle physics", at the Symposium on Recent Trends in High Energy Physics at the Annual Meeting of the Indian Academy of Sciences, PRL, Ahmedabad,19 November, 2011.

Srubabati Goswami

121. "The bimagic baseline and optimization of a Low Energy Neutrino Factory, Invited talk in the conference Theoretical Issues in Neutrinos Physics", KIAS. Seoul, South Korea, 13-16 November, 2011.

122. "Bimagic Baseline and Low Energy neutrino Factories" Recent developments on Particle Physics Phenomenology, University of Kolkata, 05 March, 2012.

Subhendra Mohanty

123. "Dark matter signatures and models", 17th International Symposium on Particles Strings and Cosmology (PASCOS), Cambridge University, DAMTP, 03-08 July, 2011.

124. "Higgs Inflation", Indo-UK Scientific Seminar: Confronting Particle-Cosmology with Planck and LHC, IUCAA, Pune, 10-12 August, 2011.

125. "Inflation and CMB", Symposium on Recent Trends in High Energy Physics, Annual Meeting of the Indian Academy of Sciences, PRL, Ahmedabad, 19 November, 2011.

126. "Vacuum stability of the Higgs Potential", Advances in Astroparticle Physics and Cosmology (AAPCOS2012) SINP, Darjeeling, 07-12 March, 2012.

V. K. B. Kota

127. "Embedded Random Matrix Ensembles to Spectral Distributions:", Need for HPC, Interdisciplinary Workshop on High Performance Computing, Physical Research Laboratory, Ahmedabad, 30th January-01 February, 2012.

128. "Modern Shell Model with Large Configuration Spaces (3 Lectures and 2 Tutorials)", DST SERC School on "Modern Trends in Nuclear Structure and Dynamics", IIT Roorkee, Roorkee, 06-24 February, 2012.

129. "Symmetries and Random Matrices in Physics: Advances from Nuclear Physics", Gujarat Science Academy, Prof. Ajay Divatia Memorial Lecture, XXVI Gujarat Science Congress, M. S. University, Baroda, 26 February, 2012.

Computer Centre

Jigar Raval

130. "Mitigate SSH Attacks with Multi-Layer Security and Multi-Factor Authentication Approach", International Conference on IT Security organized by CSI, Ahmedabad Chapter, Ahmedabad. 01-03 December, 2011.

131. "Server Security Using Open Source Tool – A PRL perspective", Technical Paper Presentation as a part of CSI Annual National Convention organized by CSI, Ahmedabad Chapter, Ahmedabad. 01-03 December, 2011.

Lectures at Universities / Institutions

Astronomy and Astrophysics

A.K. Singal

1. "Absolute Motion of the Earth - A Journey Through Space!", Bharuch, 28 January, 2012.

2. "The universe in space and time", Narmada Vidhyalaya, Bharuch in under National Science Day, 29 January, 2012.

B.G. Anandarao

3. "Chandrasekhar Limit", Tezpur Central University, Tezpur, Assam, 19 October, 2011.

4. "Stellar Evolution and Physics of Compact Objects", Course (of 8 lectures) given to post-graduate students, Tezpur Central University, Tezpur, Assam, 08 October-09 November, 2011.

Baliyan K. S.

5. "Photopolarimetry of blazar CGRaBS J0211 + 1051: An LBL?", National Space Science Symposium 2012, Tirupati, 13-17 February, 2012.

6. "Birth and death of stars", Adarsh Vidyalaya, National Science Day program, Patan, 28 February, 2012.

H. O. Vats

7. "Sun and the solar system", DST INSPIRE Program, S. P. University, Vallabh Vidyanagar, 23 April, 2011.

8. "Learning through experiments", DST INSPIRE Program, S. P. University, Vallabh Vidyanagar, 24 April, 2011.

9. "Our Sun and the solar system", Workshop on Astronomy, Nehru Planetarium, New Delhi, 03 May, 2011.

10. "Physics concepts from nature," Science Club, NAS I/C Meerut, 09 May, 2011.

11. "Overview of Sun and the solar system", Physics Department, Saurashtra University, Rajkot, 05 August, 2011.

12. "North-South asymmetry of solar coronal rotation", Solar Group Science Meeting of Stanford University Palo Alto, USA, 23 September, 2011.

13. "Twinkling of stars and other similar phenomena in Nature", (Hindi), Hindi Technical Seminar on the "Indigenization of Space technology", at SHAR, SRIHARIKOTA, 04 November, 2011.

14. "Mysterious Universe", (Key note address), All Gujarat Amateur Astronomers Meet – 2011, Ravalsar, Jamnagar, 17-18 December, 2011.

15. "BRAHMAND AUR HAMARA SURYA", (Hindi), 100rd year of Satya, Surat, 24 December 2012.

16. "Sun as an astrophysics laboratory", National Seminar on "New Perspectives of Natural Sciences", Vidyanagar, 07 January, 2012.

17. Space Science Education with Graphic Novels, on "Science Communication for Scientific Temperament", National Institute of Science Communication Complex, New Delhi, 10-12 January, 2012.

18. "Do we know the Sunspots?", Introductory Seminar on Astronomy Astrophysics & Our Earth, S. P. University, Vidyanagar, 29 January, 2012.

19. "An overview of solar phenomena", at National conference on applied mathematics and computational physics, Hindu College, Moradabad, UP, 25-26 February, 2012.

20. "Space Science Education with Graphic Novels", National conference on applied mathematics and computational physics, Hindu College, Moradabad, UP, 25-26 February, 2012.

21. "Science education", a seminar for teachers and students of Forte Institute of Technology, Meerut, 30 March, 2012.

P. Janardhan

22. "The Unusual Solar Cycle 23: The Vanishing Solar Wind, its Cause and Impact", XXX General Assembly and Scientific Symposium of International Union of Radio Science, Istanbul, Turkey, 13-20 August, 2011.

23. "A Close look at the Deepest Solar Minimum in the Past 100 Years", at the workshop on "Physics of the Solar Transition Region and Corona", IUCAA, Pune, 04-07 September, 2011.

24. "A Overview of Solar Magnetic Fields and the Unusual Solar Cycle 23", Solar Radio Workshop, Pune, 23-25 November, 2011.

Rajmal Jain

25. "2012 – End of the World: What is Truth?", ITM University, Gwalior, 17 May, 2011.

26. "Solar and Terrestrial Relationship", Department of Physics, Jivaji University, Gwalior, 18 May, 2011.

27. "Does the Sun Change Earth's Climate?" at DST Sponsored workshop on INSPIRE Programme held at Hemchandracharya, North Gujarat University, Patan, 23-27 May, 2011.

28. "Energy-dependent timings of thermal emission in solar flares", ARIES, 23 June, 2011.

29. "Solar activity and human environment", IUAC, New Delhi, 05 December, 2011.

Sachindra Naik

30. "Properties of Accretion Powered X-ray binary pulsars", Department of Physics, Mohanlal Sukhadia University, Udaipur, 22 September, 2011.

31. "Workshop on X-ray data analysis", IUCAA Resource Center, Department of Physics, Mohanlal Sukhadia University, Udaipur, 22-24 September, 2011.

Susanta K. Bisoi

32. "Composite synthesis imaging of the quiet sun using simultaneous observations from the GMRT and the NRH", Solar Radio Workshop, Pune, 23-25 November, 2011.

S. V. Vadawale

33. "Space born research in Astronomy and Planetary Science: Indian Context", DST INSPIRE program, Chirst College, Rajkot, 07 May, 2012.

Solar Physics

Ashok Ambastha

34. "Sounding the Sun's Interior: Sub-Surface Weather of Solar Active Regions", IUCAA, Pune, 18 November, 2011.

35. "Understanding our Daytime Star from its deep Interiors to the Outer Corona", DST-INSPIRE Camp

Nathdwara Institute of Engineering & Technology, Nathdwara, 26 March, 2012.

Bhuwan Joshi

36. "Current research activities and future programs at Udaipur Solar Observatory", IGAM, University of Graz, Austria, 15 June, 2011.

37. "Observational signatures of magnetic reconnection in solar flares: The RHESSI perspective", Korea Astronomy and Space Science Institute (KASI), Daejeon, South Korea, 18 August, 2011.

Nandita Srivastava

38. "Automated Detection of Filaments Using Full-Disc H_α Images from solar observatories", SIDC, Royal Observatory of Belgium, 06 October, 2011.

Vemareddy P.

39. "Solar magnetic and Velocity fields & Energetic Activity on the Sun", in HPC workshop meeting, PRL, 31 January-02 February, 2012.

Planetary Sciences & PLANEX Program

J. Pabari

40. "Planetary Wireless Sensor Network: Communication Perspective", Venus International College of Technology, Kalol, 13 February, 2012.

Space and Atmospheric Sciences

D. Pallamraju

41. "Space weather and its effects on the earth's upper atmosphere", Pune University, Pune, 18 July 2011.

H. Chandra

42. "Lectures on Ionosphere", Gujarat University, September-October, 2011 (9 lectures).

43. "Lectures on Ionosphere", SERC School, Raja Balwant Singh College, Agra, 23-24 February, 2012 (4 lectures).

S. Lal

44. "Major role of minor constituents in atmospheric science", S. P. University, Vallabh Vidyanagar, 29 January, 2012.

S. P. Gupta

45. "Techniques used to study Electrical structures of middle atmosphere and ionosphere", SERC School, Raja Balwant Singh College, Agra, 23-24 February, 2012.

46. "Variability of stratospheric conductivity-balloon borne results", SERC School, Raja Balwant Singh College, Agra, 23-24 February, 2012.

47. "Plasma instability in equatorial-E region. Rocket and ground based results", SERC School, Raja Balwant Singh College, Agra, 23-24 February, 2012.

48. "Meteor shower induced effect in ionosphere-radar and rocket results", SERC School, Raja Balwant Singh College, Agra, 23-24 February, 2012

S. Ramachandran

49. Two lectures on "Atmospheric aerosol: Sources and sinks, effects on the atmosphere, and Radiation", Gujarat University, Ahmedabad, September, 2011.

50. "Volcanic aerosols: Physical, Optical and Radiative Effects", Dibrugarh University, 01 August, 2011.

51. "Black carbon aerosols: Characteristics and Radiative Impact", Dibrugarh University, 02 August, 2011.

S. Sharma

52. "Middle Atmospheric Temperature Climatology and Long-term Temperature Tendencies over Indian Tropical & Sub-tropical Locations", Indian Institute of Tropical Meteorology (IITM), Pune, India, 17 June, 2011.

53. "Tropical and Sub-tropical Middle Atmospheres: Possible Interconnections", Sri Venkateswara University, Tirupati, India, 26 July, 2011.

54. "Lidar and Radar Probing of Earth's Atmosphere", Saurashtra University, Rajkot, India, 05 August, 2011.

55. "Middle Atmospheric Climate Change in the Indian Region", SRM University, Chennai, India, 20 December, 2011.

56. "Middle Atmospheric Temperature Changes in Indian Tropical and a Sub-Tropical Regions", Aryabhatta Research Institute of Observational Sciences (ARIES), Nainital, India, 30 March, 2012.

Geosciences

A.K. Singhvi

57. "Luminescence of minerals: A case of synergistic mutualism between Physics and Geology", S. P. University, 02 March, 2011.

M. M. Sarin

58. "Atmospheric chemistry and environmental change", DST-INSPIRE Camp, M. S. University, Vadodara, 24 August, 2011.

Navin Juyal

59. "Himalaya: our concern", in National seminar on environmental education, concerns, sensitization and action at Department of extension and communication, M.S. University, Baroda, 24-25 January, 2012.

60. "Past and recent climate changes: evidence from the central Himalaya", given to the university teachers at the Department of Geology, Pune University, 18 February, 2012.

R. Ramesh

61. "Basics of Meteorology and Oceanography", Training Workshop on the eve of International Science Olympiad, Geological Society of India, Bengaluru, 03 September, 2011.

62. "Application of stable isotopes in Oceanography", National Seminar on Modern streams of bio-chemistry Department of Chemistry, St.Albert's College, Ernakulam, 20-22 September, 2011.

63. Three lectures on "Research Methodology", University of Hyderabad, Centre for Earth and Space Sciences, March, 2012.

64. Eight "INSPIRE", lectures, M.S. University of Baroda, S. R. Rengasami College, Tiruchngode, and Jammu University, July 2011, October 2011 and January 2012.

Theoretical Physics

A. C. Das

65. "Solar Terrestrial Relation and Space Weather" (8 Lectures), part of a course on Advanced P G Diploma in Geo-informatics and Satellite Communication, Gujarat University, December, 2011.

66. Four talks on "Solar Terrestrial Relationship and Space Weather", at DST-SERC School on Seismo Electromagnetic, Department of Physics, R. B. S. College, Bichpuri, Agra, 06-26 February, 2012.

Bijaya Sahoo

67. "Singly charged atomic ions as precise atomic clocks", Frequency standard group at WIPM, Wuhan, China, 07 December, 2011 - 05 January, 2012.

68. "Role of many-body methods in the search for variation of fine structure constants", atomic physics group at WIPM, Wuhan, China, 07 December, 2011 - 05 Januray, 2012.

69. "Relativistic coupled-cluster method to probe fundamental physics", Chemistry Department at Peiking University, Beijing, China, 31 December, 2011.

70. "Atomic clocks using singly charged ions", Institute of Physics (IoP), 31 December, 2011.

71. "Many-body methods for precision studies", Institute of Physics (IoP), 31 December, 2011.

Dilip Angom

72. "Importance of Numerical Techniques", QIP short term course on Computational Techniques in Physics, IIT-Guwahati, 01-06 August, 2011.

73. "Overview of Numerical Techniques", QIP short term course on Computational Techniques in Physics, IIT-Guwahati, 01-06 August, 2011.

74. "Vortex dipoles in Bose-Einstein condensates", Colloquium, IPR, Gandhinagar, 28 September, 2011.

75. "Modern Shell Model with Large Configuration Spaces" (3 Lectures and 2 Tutorials), DST (India), SERC School on "Modern Trends in Nuclear Structure and Dynamics", IIT Roorkee, Roorkee, 06-24 February, 2012.

D. P. Dewangan

76. "Some important discoveries", Ravishankar Shukla University, Raipur, 05-11 June, 2011.

77. "INSPIRE Internship Summer Camp", Ravishankar Shukla University, Raipur, 06-10 June, 2011.

78. Three talks on "Some important discoveries", Pt. Ravishankar Shukla University, Raipur, INSPIRE Internship Summer Camp, 06-10 June, 2011.

Hiranmay Mishra

79. "Chiral symmetry breaking in hot and dense matter in strong field", Institute of Physics Bhubaneswar, 26 December, 2011.

Partha Konar

80. "LHC as a probe on properties of Dark Matter", HRI, Allahabad, 27 April, 2011.

Raghavan Rangarajan

81. "Cosmology and General Relativity", Homi Bhabha Centre for Science Education, Mumbai, June 22, 2011.

82. "Cosmology and Particle Physics", Training and Capacity Building Workshop of the Knowledge Consortium of Gujarat, AMA, Ahmedabad, 05 November, 2011.

Srubabati Goswami

83. "Earth Matter effect in propagation of neutrinos and Bimagic Baseline", Indian Association for Cultivation of Sciences, Kolkata, 07 June, 2011.

Saurabh Rindani

84. "Introduction to Helicity Amplitudes", a series of four lectures delivered at the Centre of High Energy Physics, Indian Institute of Science, Bangalore, 14-16 March, 2012.

V. K. B. Kota

85. "Spectral Distribution Theory for Nuclear Structure: Past To Future", Michigan State University, East Lansing, Michigan, USA, 05 July, 2011.

86. "Update on Results from Shell Model Based SDM and DSM for Double Beta Decay", Laurentian University, Sudbury, Canada, 28 July, 2011.

87. "Results from Shell Model Based SDM and DSM for Double Beta Decay", IIT Roorkee, Roorkee, 19 October, 2011.

88. "Random Interaction Matrix Ensembles for Finite Quantum Systems", Andhra University, Visakapatnam, 13 March, 2012.

Computer Centre

Jigar Raval

89. "Open Source-Linux" and " Internet Security" at Refreshers' course for faculties at Rollwala Computer Center, Gujarat University, 14-22 November, 2011.

90. Delivered expert talks and conducted hands-on session during Short Term Training Program (STTP) on "Open Source Technology-Linux", R. K. University, 28-29 December 2011.

SCIENCE

Astronomy and Astrophysics

The Astronomy and Astrophysics Division is engaged in research covering a wide spectrum of topics such as explosive events like novae, massive star formation regions, variability of distant active galactic nuclei, galactic X-ray binary systems, study of solar magnetic fields and solar X-rays emission from explosive solar phenomena. The division is also actively involved in developing new instruments both for the optical/infrared observations from Mt. Abu Observatory as well as satellite based experiments for X-ray astronomy. Inner heliospheric signatures from interplanetary scintillation observations were used to study the deep solar minimum between Solar Cycles 23 – 24 and show that the build-up to the deepest solar minimum experienced in the past 100 years actually began over a decade ago. A clear evidence of enhanced angular sizes of some Mira variables due to mass loss and shell effects was obtained using high angular resolution observations.

First Science Observations with PARAS

The first successful "science" observing run with the PARAS spectrograph under stabilized condition of temperature and pressure control were carried out.The temperature was controlled at 0.02^{0}C to 0.03^{0}C rms at 25^{0}C and the net change in pressure inside the spectrograph vessel during the nights of observations was of the order of 0.15mbar. These conditions give us typical intrinsic Radial-velocity stability of about 1.5m/s to 1.7m/s. On sky on bright RV standard stars (or main sequence G, K stars > 6.5mag) we are able to reach sub-2m/s precision at least over a period of 30 days. On fainter G, K type sources between 7^{th} and 9^{th} magnitude, PARAS can attain about 7 to 10m/s precision. We have taken up studies of some of the Kepler objects apart from radial velocity monitoring of bright targets at sub-2m/s precision

We focused on a Kepler Candidate KOI 1924.01.Kepler predicted to have a transit of 2.5 days period planet of unknown mass. However, when we observed this source using PARAS from Mt. Abu we found a high mass secondary object going around the Kepler Object with a long period of the order of more than 100 days net detected by Kepler. We also got a few observations from HET (Hobby Eberly Telescope – 9m class) in August and in early September.

The PARAS observations and the HET observations together show evidence for a possible secondary object of approximately 80Jupiter Mass right at the Brown Dwarf/L Dwarf boundary with a period of 105 days and semi-major axis of about 0.6AU in high eccentric orbit of $e \sim 0.43$. The Kepler source brightness is around 8th mag and is close to the limit of PARAS on the 1.2m (limit being 9th mag). We got RV errors of around 7m/s to 10m/s. The HET HRS data has poorer error of 50m/s even though they were using a 9m telescope because their spectrograph is not designed for simultaneous precision RV measurements and also is not in stabilized environment. Further, follow up confirmation observations will take place in October – November 2012 with PARAS.

(Abhijit Chakraborty)

Studies of a possible new Herbig Ae/Be star in the open cluster NGC 7380

We present a study of a member of the young cluster NGC 7380 to identify its true nature as it has been variously proposed to be a Be star, a symbiotic object and a Herbig Ae/Be star by different groups. The spectroscopic observations were done using the HFOSC (Himalayan Faint Object Spectrograph Camera) available with the 2.0m Himalayan Chandra Telescope (HCT), operated by the Indian Institute of Astrophysics, India. The HFOSC was also used in imaging mode to obtain a broad band (6300-6740 Å) H_α image of the source and its environment. JHK photometric observations of the object were made from Mt. Abu Infrared Observatory on 21 October, 2010 using the near-infrared imager-spectrograph.

The H_α image of the star is shown in Figure 1. A nebulosity is clearly seen around the object whose principal features consist of a diffuse patch (feature 2) and a bow-shock shaped structure (feature 1) very close to the star. The bow shaped structure looks like a cometary globule (cometary nebula) with the apex, as expected in these objects, oriented towards the photoionizing source which in this particular case is DH Cep.

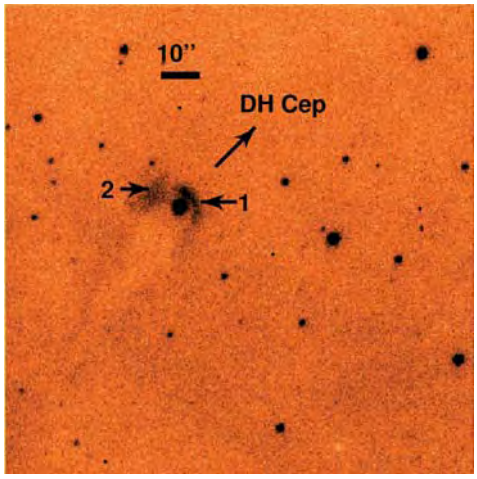

Figure 1: 2 X 2 square arcmin field around NGC 7380(4) obtained with an H_α broad band filter. Nebulosity is seen around NGC 7380(4). North is to the top and east to the left.

The optical spectra of NGC 7380(4) showed lines of hydrogen (Balmer and Paschen series), Ca II, Na I, K I, Fe II and forbidden lines of O I, S II in emission, as shown in Figure 2. An interesting aspect of the spectra is the evidence of a fast outflow (176 to 215 km s^{-1}) as inferred from the behavior of the forbidden lines of [S II] and [O I]. The presence of these forbidden lines in the spectra of HAeBe stars has long been used to infer the presence of jets/ outflows since such lines arise only in low density conditions and hence are tracers of low density material. High ionization lines (Fe VII , He II, Ca V), Raman scattered O VI lines and molecular bands of late-type giant like TiO, H_2O, CO, CN, or VO which are characteristics of symbitoic stars are not present in the spectra of NGC 7380(4) and hence the object is not a symbiotic star.

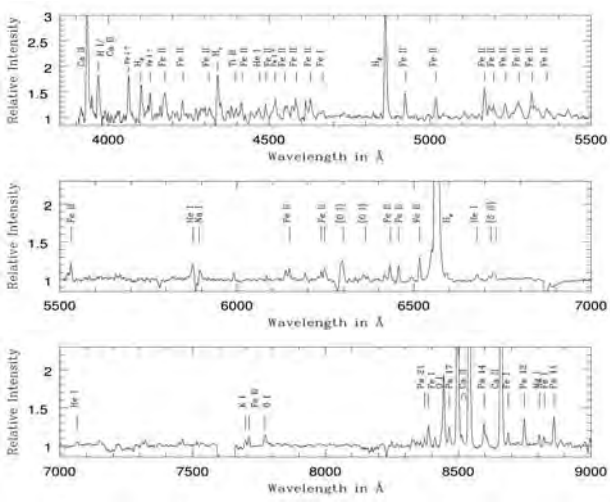

Figure 2: Optical spectrum of NGC 7380(4). The prominent emission lines are identified.

The presence of emission lines (both permitted and forbidden), infrared excess (estimated from the spectral energy distribution), association with 2 Million year open cluster NGC 7380 and the presence of nebulosity confirms the Herbig Ae/Be nature of NGC 7380(4).

This work was done in collaboration with A.Subramanian and B.Bhavya of Indian Institute of Astrophysics, Bangalore

(Blesson Mathew, D.P.K.Banerjee, N.M.Ashok and Vishal Joshi)

The 2011 outburst of recurrent nova T Pyxidis

Recurrent novae (RNe) are cataclysmic variables that undergo multiple nova outbursts in human life time. The outburst mechanism, a thermonuclear runaway on the surface of a white dwarf in a close binary system, has a short recurrence time due to high accretion rate and high mass white dwarf. The recurrent novae have a special place in the studies of cosmologically important topic of Type Ia supernova as they are considered to be their progenitor candidates.

T Pyx is historically the first recurrent nova to be discovered and has gone into outburst on six occasions between 1890 and 1966 and its next outburst was eagerly awaited for last few decades. T Pyx was discovered in outburst on April 2011 14.29 UT. We have obtained a very well sampled IR light curve starting as early as 0.4 days after the outburst and also a set of extensive IR spectra starting

from 2 days after the outburst. We also participated in the joint international observations to obtain interferometric observations. The interferometric observations suggest a two component model for the outburst ejecta with an unresolved central source and a slowly expanding extended source with a low inclination angle.

This work was done in collaboration with O. Chesneau of Observatory de la Cote Azur, France.

(D. P. K. Banerjee and N. M. Ashok)

A study of near-infrared modulations at spin and orbital period of intermediate polar WX Pyx.

Intermediate Polar(IP) is a subclass of Cataclysmic Variable stars which is a close binary system with a moderately magnetic (1MG < B < 10MG) white dwarf accreting material from the late type main sequence star.

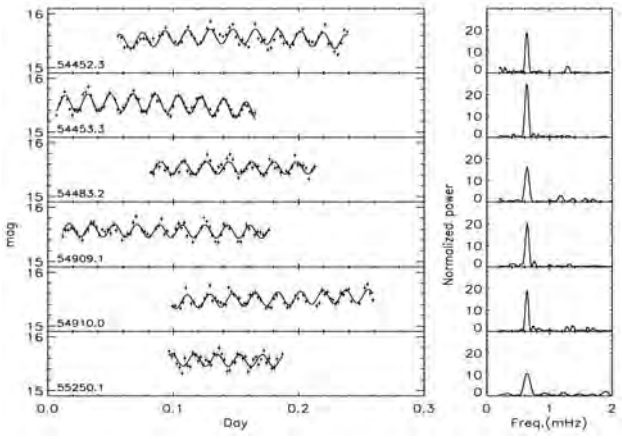

Figure 3: Light curves of WX Pyx are shown in the panels on the left. The abscissa is HJD - HJD0 where HJD0 is arbitrary and given in the lower left for each day. Solid line shows the best fit sinusoid plus a polynomial fit representing the long term variation. The Lomb-Scargle periodograms of individual runs are shown in the right hand panels.

WX Pyxidis is a poorly studied intermediate polar. We obtained first ever near-infrared J band photometry of this object. This time resolved photometry was using 256×256 HgCdTe PRLNIC array installed on the 1.2μ Mount Abu Near-Infrared Telescope. We observed WX Pyx for six nights between December 2007 and February 2010. All images were reduced to obtain J band magnitudes of WX Pyx. Lomb Scargal periodogram was produced in order to search for periodic modulations present in the resulting light curve and these are shown in the right hand panel of Figure 3.

Our period analysis of J band light curves suggests a strong modulation at 1559.2 ± 0.2 seconds. This period value coincides with the spin period of magnetic white dwarf of WX Pyx. This is the first ever indication of white dwarf spin in near-infrared light. Once the periodogram was cleaned for this period, another peak at longer period appears in the cleaned periodogram. The period corresponds to this second peak is 5.3 hours. This longer period is interpreted as the orbital period of the binary system. This first ever estimate of orbital period value allows us to infer spectral type of the secondary star to be M2 ± 2. and the distance of the system to be 1.53 kpc. This value is in agreement with the previously calculated distance using completely independent method. The absence of peak at first harmonic of orbital period in periodogram is indicative of low inclination angle of the binary system and we obtain the upper limit of inclination angle as 30°. We also obtain the mass transfer rate from secondary star to lie in the range 0.6 to 1.0×10^{17} gs^{-1} or 0.95 to 1.6×10^{-9} solar mass per year, a value fairly typical for IPs.

(Vishal Joshi, N. M. Ashok and D. P. K.Banerjee)

AGB Stars at high angular resolution – Evidence of enhanced angular sizes of some Mira variables due to mass loss and shell effects

As a part of the high angular resolution (HAR) study of Asymptotic Giant Branch (AGB) stars, especially Miras, we have investigated the possibility of high mass-loss rates and presence of a circumstellar shell enhancing the measured uniform disk (UD) angular diameters. We have used a sample of 45 oxygen-rich Miras with spectral types later than M5. We plot the ratio of observed and calculated angular diameters against (K-[12]) colour excess derived from 2MASS and IRAS catalogues and spectral type. The observed UD angular diameters include two of our Mira measurements and data taken from Charm2 catalogue of HAR measurements. The calculated angular diameter is obtained from an estimation of bolometric flux using K band fluxes and (V-K) colours and effective temperature corresponding to the spectral type. It is seen from the plot (Figure 4) that the ratio for Miras remains close to unity upto a colour excess of ~ 2.5 and then increases sharply. Our observed UD value for one of the Miras (AW Aur) at the (K-[12]) colour excess of 1.1 is in good agreement with the calculated value giving a ratio of ~ 1. However the other Mira in our observed sample BS Aur has a large (K-[12] colour excess of ~ 2.5 and its observed angular diameter is 1.4 times to its calculated value. The enhanced UD diameter suggests that BS Aur could have a high mass-loss rate and may have a circumstellar shell. The presence of a shell is also indicated by the IRAS LRS classification of this star. After correction of the enhancement both BS Aur and AW Aur are found to have similar radii within error limits.

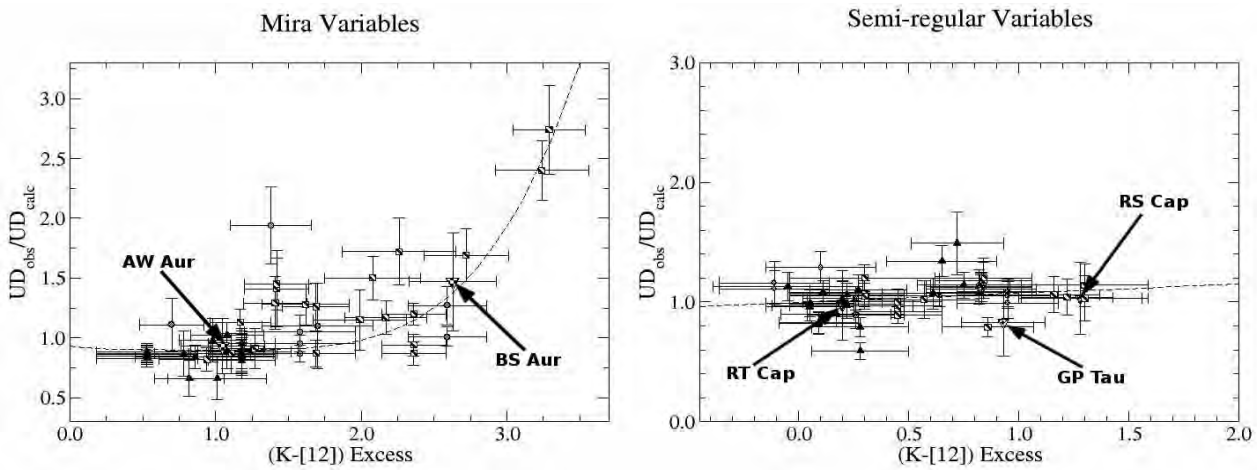

Figure 4: The (K-[12]) colour excess versus the ratio of observed and calculated angular diameters for both Mira Variables and Semi-Regular Variables. The dotted line shows a polynomial through the points to indicate the rising trend in Miras. Our observed sources are also plotted and labeled.

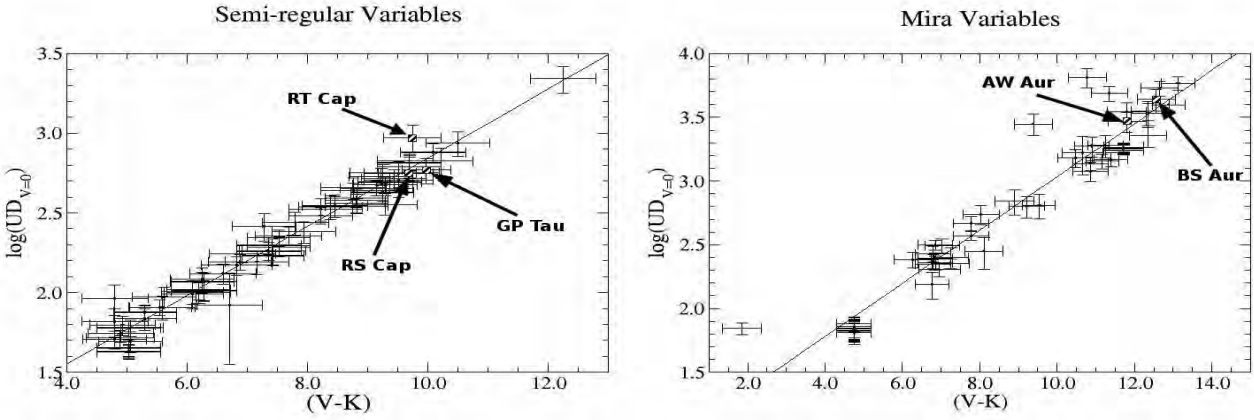

Figure 5: The (V-K) colour versus zero magnitude angular diameter calibration curve for oxygen-rich Mira Variables and Semi-Regular Variables. The solid line represents the least square fit to these points (correlation coefficients are 0.94 (Miras) and 0.98 (SRVs)). Position of sources in our measured sample also indicated.

We have also carried out a similar exercise for a sample of 52 Semi-Regular Variables (SRV) with spectral types later than M5 including our own measurements of three SRVs – RS Cap, RT Cap and GP Tau. All SRVs in our sample have a lower (K-[12]) colour excess value(<1.5). Compared to Miras and the ratio of their observed to calculated angular diameters is also close to unity. It appears unlikely that SRVs could have large mass-loss rates and shell effects. It is also consistent with the conjecture of the less active SRVs as progenitors of Miras.

As a corollary to this work we had also derived separate calibrations for Miras and SRVs with previously measured K band angular diameters and (V-K) colours. A tight correlation is seen in both cases (Figure 5). Our measured angular diameters are in good agreement with the calibrations.

(Tapas Baug and T. Chandrasekhar)

Evidence of Excess blue shifts in Coronal Green line profiles from the interferograms of the Zambian Total Solar Eclipse

The coronal green line (Fe XIV, 5303 Å) Interferometric observations during the successful PRL eclipse expedition to Zambia in 2001 continue to provide a wealth of good quality data suitable for detailed study. In the present work about 300 green line profiles in the radial range 1.0 to 1.5 $R_\odot$ and positional angle coverage of 240° were taken up for analysis. The instrumental width was 0.2 Å. The line profile were fitted with single Gaussians and their intensity, Doppler velocity and line widths were determined. Centroids of line profiles which measure asymmetry in the line were also obtained. The histogram of Doppler velocity shows excess blue shifts while the centroid data also reveals a predominant blue wing in the line profiles. The centroids and Doppler velocity are highly correlated and indicate presence of multiple components with excess of blue shifts which also depend upon solar activity. The magnitude of

the Doppler velocity of secondary component is in the range of 20-40 km/s with an increase towards poles is indicated. Possible explanation of multi components could be type II Spicules which are recently being considered important for coronal heating or nascent solar wind flow. However the presence of blue components in coronal lines above the limb is still a mystery.

The work was done in collaboration with K.P. Raju of IIA, Bangalore.

(T. Chandrasekhar and N.M. Ashok)

Monitoring of Blazars from MIRO: Fresh activity in PKS0716

A sample of blazars were monitored for variability in optical and near-IR flux using an optical CCD (1296x1152 pixels) and the NICMOS-3 mounted at the 1.2m telescope of MIRO (Mt. Abu Infra Red Observatory). A recently procured 50 cm telescope mounted with an EMCCD (1000x1000 pixels) and dedicated to variability study, was also part of the monitoring system. Since blazars vary at various time scales- ranging from years to minutes, apart from long term monitoring, fast sampling is required to detect microvariations with time scales of few tens of minutes. During the period 2011-12, we monitored 3C66A, 3C454.3, PKS0716, PKS 1510, OJ 287, Mrk501 etc for variability in flux and polarization. Last year blazar PKS0716 showed rapid variations resulting in 0.15 mag change in R-band during 2.88 Hrs, constraining the emission size and mass of the black hole. We noticed fresh activity in this source during 2011 as well. It brightened by 0.18 mag in R-band in 2.4 Hrs (Figure 6). It indicates that the source is mostly active irrespective of its status, i.e. whether it is in bright phase or quiescent phase. Such emission in the jet is produced by the relativistic shock

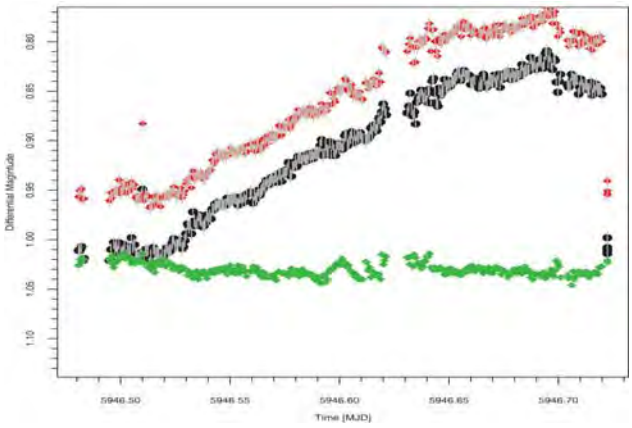

Figure 6: Intra-night variability in the R-band light-curves of the blazar PKS0716+71 during 20 January, 2012. The source varies within 2.3 Hrs with variability amplitude on 0.22 mag.

moving down the jet and its interaction with stationary sub-mm core or other relatively slowly moving plasma blob. However, during the quiescent phase, significant contribution from the disk is expected. The physical mechanisms at work are being explored.

(K S Baliyan, S Chandra, S Ganesh, U C Joshi)

Correlated multiwavelength variations in CGRaBS J0211+1051

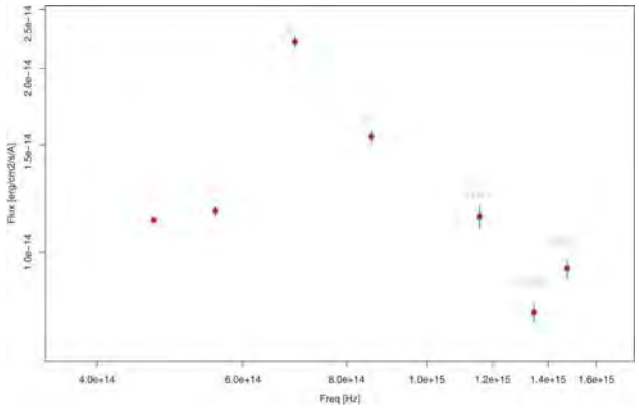

Figure 7: Spectral energy distribution for CGRaBS J0211+1051 on Jan 31, 2011. Optical data (MIRO and Swift), radio (MOJAVE program), UV, X-ray (Swift) and Gamma-ray (Fermi). Synchrotron peak is seen at $3x10^{14}$ Hz.

Active galactic nuclei emit profusely at all frequencies ranging from radio to very high energy gamma-rays. Since these objects are very compact and hence un-resolvable by any existing facility, variability in flux and polarization is used as a tool to understand structure and energy processes of their central engine. Blazars are best candidate for this purpose as they probe the deepest regions of the central region and show strong variation at all energy regimes. In a study on CGRaBS J0211+1051 blazar, we analyzed the gamma-ray data from Fermi, X-ray and UV data from SWIFT space missions and radio-mm data from MOJAVE program. Results from the quasi-simultaneously observed radio, mm, UV, X-ray and gamma-ray data were combined with our own values in optical and light curves were generated. It is interesting to note a significant correlation among different energy emissions. There is an indication of the enhanced variation amplitude at higher energies. The multiwavelength data available in the radio, UV, X-ray and gamma-rays from MOJAVE, Metsahovi observatory (radio), SWIFT (optical, UV and X-ray) and Fermi (gamma-rays) quasi-simultaneous with our observations was used to construct spectral energy distribution revealing that the synchrotron peak lies in optical region (Figure 7).

(S Chandra, K S Baliyan, S Ganesh, UC Joshi)

Polarization: a tool for blazar classification

Blazar continuum spectral energy distribution (SED) shows two broad peaks at low and high frequencies. The low frequency peak is mostly due to synchrotron radiation from the relativistic electrons while high energy peak is proposed to be due to upscattering of soft photons. Depending upon synchrotron peaking frequency, blazars are classified into a sequence: blazar sequence. FSRQs and RBLs (LBLs) peak at low (IR to optical) frequencies while XBL (HBL) synchrotron peak lies in UV or X-ray/Gamma-ray region. These subclasses have several distinct properties in the sense that luminosity and Compton dominance decrease from FSRQ to XBL. Variability duty cycle also decreases towards HBL.

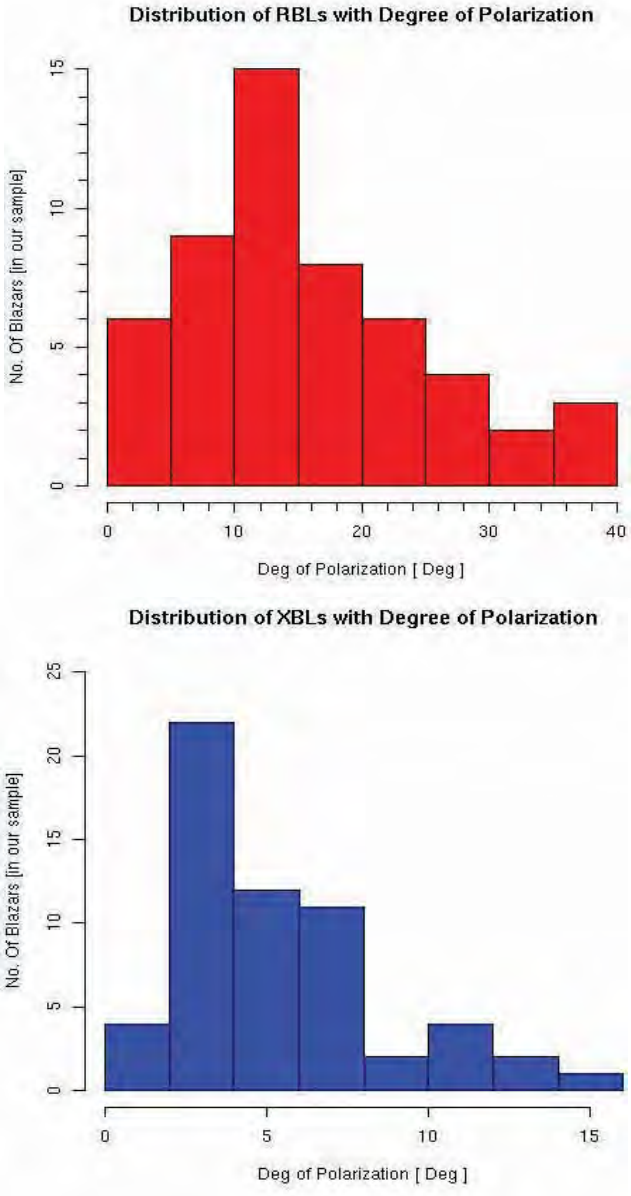

Figure 8: Distribution of blazars as a function of optical polarization: (a) RBL (b) XBL

While a source is confirmed to be a RBL or XBL by constructing its SED, it is difficult to have simultaneous observed data at all the frequencies. Since blazars show significant polarization, we performed a statistical study on a sample of blazars including RBLs and XBLs with detected polarization. We noticed that RBLs distinctly show higher degree of polarization (DP) as compared to XBLs. While majority of XBLs show DP between 2-7%, RBLs population peaks between 20-35%. Though polarization values are not available for many blazars, we intend to improve the sample. Based on our study, we propose DP as a tool for blazar classification. We have used it to suggest CGRaBS J0211+1051 to be an RBL, which was confirmed later by constructing its SED. Figure 8 shows the number distribution of RBLs and XBLs as a function of polarization.

(K S Baliyan, Sunil Chandra)

Constraining the sites of blazar emissions

Apart from the problems in understanding the site and processes responsible for the origin of jet, other major uncertainty is to pinpoint the location of the origin of various emissions in the jet. We broadly know that radio emission comes from extended jet and IR/opt/UV comes from synchrotron emission from the jet. During flares, optical to gamma-rays emission is generated either very close to the central engine, near BLR or at several pc away from it. The emission at high energy requires seed photons which are upscattered to produce it. We intend to use nature of variability to settle the issue of location of such emission. For this we used Fermi data obtained during flaring. We used high and low energy GeV data to generate light curves and photon indices. If high energy emission is produced near BLR region (0.1pc from central engine) where UV photons are upscattered in the Klein Nishina (KN) regime and electron cooling is practically energy independent. The photon index will be almost constant and variations achromatic. The time scale of variation is expected to be few hours. On the other hand, if GeV emission is produced far (~10pc) from central engine, IR photons from torus will be upscattered in Thomson regime with cooling time decreasing with energy and flare amplitude increasing with energy. We analyzed data on PKS1510 at three epochs. At one epoch, we notice significant change in photon index while at other, there is almost no change. Perhaps high energy emissions are produced at different locations. However, we would like to study more flaring events in several blazars before arriving at any definitive conclusion.

(S Chandra, K S Baliyan)

Convection zone study of white dwarf EC14012-1446 using optical light curves

Understanding the stellar interiors and their atmospheres is an area of great interest. Stellar mass, effective temperature, carbon/oxygen ratio etc of white dwarfs can be estimated using their linear pulsations and seismological models. These pulsations manifest themselves in the variation of their light curves. In addition to linear pulsations, some cooler white dwarfs with large amplitude fluctuations also show non-linearity in their pulsations, supposed to be caused by the interaction with the outer convection zone layer. This helps improving the knowledge of convection zone-a significant contributor to the errors in stellar models. However, for such study, continuous long duration light curves are must. That was made possible with a large number of ground based observatories participating in the Whole Earth telescope (WET) campaign. During 14-18 April, 2008, we took part in the campaign on pulsating DA white dwarf, EC14012-1446 using a 1kx1k ccd. During this period, the source was observed for 2.5 hrs to 4 hrs every night. Fractional amplitudes were obtained and plotted as a function of time to get light curves. The Fourier transform of the light curves was used to obtain periods of pulsation. By combining light curves from all participating observatories, more than 30 observed frequencies, which are normal modes of oscillations described by spherical harmonics are obtained. By combining asteroseismology of the source with nonlinear analysis of its light curves an empirical description of the convection zone is obtained. From the analysis of more than 300 hrs WET data, 19 independent frequencies are identified along with a dozen of l = 1 modes.

This work was done in collaboration with WET team.

(KS Baliyan, H O Vats)

The Deep Solar minimum between Solar Cycles 23 – 24: Inner Heliospheric Signatures from Interplanetary Scintillation Observations.

We have reported earlier from extensive measurements of solar photospheric fields that solar polar fields have been declining since ~1995. These solar polar fields measurements, in the latitude range 45°-78°, were obtained using synoptic Carrington maps from the database of the National Solar Observatory, Kitt-Peak, and coves the period 1975 to 2010. Figure 9 shows a plot of measured polar fields in cycles 22 and 23 that show a steady drop starting from ~1995 and continuing through solar cycle 23. The vertical grey band indicates the extended period of solar minimum that was experienced at the end of cycle 23.

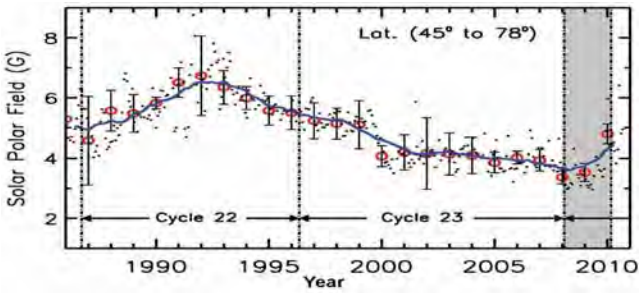

Figure 9: Solar polar field variations as a function of time in years in latitude range 45°-78° covering solar cycles 22 and 23. The black solid dots are actual polar field measurements while red open circles are annual means of polar field measurements. The overlaid blue solid line is a smoother curve. A steady decline in polar fields since ~1995 can be clearly seen. The dotted lines demarcate the solar minimum of cycles 21, 22 and 23 and the grey shaded region shows the extended period of solar minimum at the end of cycle 23.

Since the Interplanetary Magnetic Field (IMF) is basically the result of the photospheric magnetic field coupled with solar rotation being continuously swept into the inner heliosphere, one would expect to see these changes reflected globally in the solar wind and the interplanetary medium as a reduced level of microturbulence. We have used extensive interplanetary scintillation (IPS) observations at 327 MHz in the distance range 0.3 to 0.8 AU, obtained between 1983 and 2009 from the Solar Terrestrial Environmental Laboratory, Toyokawa, Japan to show that microturbulence levels in the entire inner heliosphere, as inferred through IPS observations, have also shown a steady decline since ~1995. Figure 10 shows plots of m as a function of time in years for a sample of 9 out of 27 observed radio sources. The grey crosses and red dots are observations at helio latitudes ≤ 45° and > 45° respectively and the blue open circles are annual means.

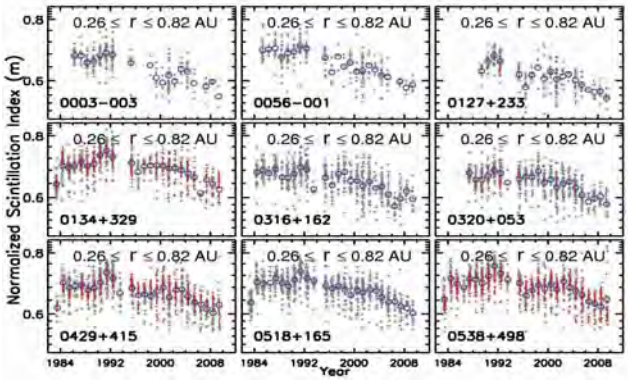

Figure 10: Plots of m as a function of time in years for a sample of 9 out of 27 observed sources. The values of m have been normalized by the value of m for the point source 1148-001 to make it independent of distance from the Sun. The grey crosses are observations at source heliolatitudes ≤ 45° while the fine red dots are observations when the source heliolatitudes are > 45°. The open circles are yearly averages by excluding the high latitude observations. The IAU name of each source is indicated at the bottom left in each panel.

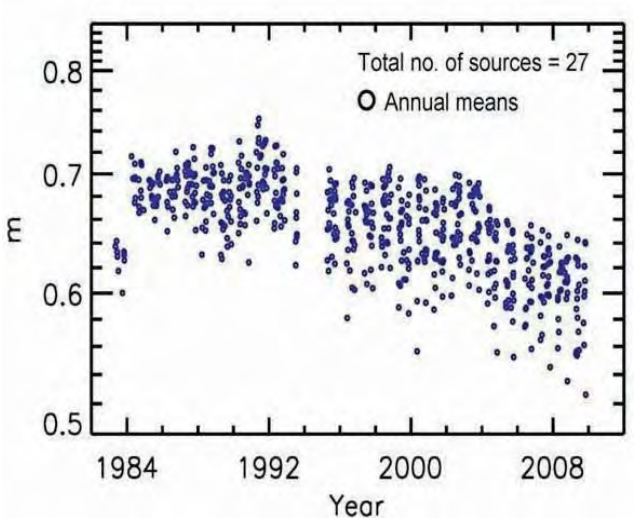

Figure 11: Plots of annual means of m, blue open circles,(as depicted in Fig 10) as a function of time in years for 27 sources.

Figure 11 shows only the annual means for all 27 observed sources. The decrease in m after ~1995 for all sources is clearly visible. We believe that this large-scale IPS signature, in the inner heliosphere, coupled with the fact that solar polar fields have also been declining since ~1995, provide a consistent result showing the build up to the deepest solar minimum in 100 years actually began more than a decade earlier.

(P. Janardhan and Susanta K. Bisoi)

Near-infrared Observations of Be/X-ray Binary Pulsar A0535+262

Be/X-ray binaries, consisting of a compact object in orbit around the Be star, form the largest subclass (about 2/3) of High Mass X-ray Binaries (HMXBs). The orbit of the compact object around the Be star is wide and highly eccentric, limiting interactions with the circumstellar disk to when the objects are closest (periastron passage). Be/X-ray binaries are generally quiescent. The transient X-ray outbursts seen in these objects are thought to be due to interactions between the compact object and the circumstellar disk surrounding the Be star. Among the ~96 HMXB pulsars, 67% of the identified systems are Be/X-ray systems and 33% of the systems have no known optical/IR counter parts. These Be/X-ray binary systems attract interests in several branches of astrophysics: stellar astrophysics, accretion theory, close binary evolution, etc. Progress towards the understanding of the physics of these systems depends on multi-wavelength program of observations (in Optical, IR, and X-ray wavebands). Using IR and Optical observations of these objects, the physical conditions under which the neutron star accretes matter can be determined. In combination with the X-ray timing and flux observations, we can get a complete picture of the accretion process.

We present results obtained from an extensive near-infrared spectroscopic and photometric observations of the Be/X-ray binary A0535+262/HDE 245770 at different phases of its ~111 day orbital period (Figure 12). This observation campaign is a part of the monitoring programme of selective Be/X-ray binary systems aimed at understanding the X-ray and near-IR properties at different orbital phases, especially during the periastron passage of the neutron star. The near-IR observations presented here were carried out using the 1.2 m telescope at Mt. Abu IR observatory. Though the source was relatively faint for spectroscopic observations with the 1.2 m telescope, we monitored the source closely during the February-March, 2011 giant X-ray outburst to primarily investigate whether any drastic changes in the near-IR JHK spectra take place at the periastron passage. Changes of such a striking nature were expected to be detectable in our spectra. Photometric observations of the Be star show a gradual and systematic fading in the JHK light curves since the onset of the X-ray outburst, Figure 13. This gradual and systematic changes in the JHK magnitudes could suggest a mild evacuation/truncation of the circumstellar disc of the Be companion. Near-IR spectroscopy of the object shows that the JHK spectra are dominated by the emission lines of hydrogen Brackett and Paschen series and HeI lines at 1.0830 micron, 1.7002 micron, and 2.0585 micron. The presence of all hydrogen emission lines in the JHK spectra, along with the absence of any significant change in the continuum of the Be companion during X-ray quiescent and X-ray outburst phases suggest that the near-IR line emitting regions of the disc are not significantly affected during the X-ray outburst.

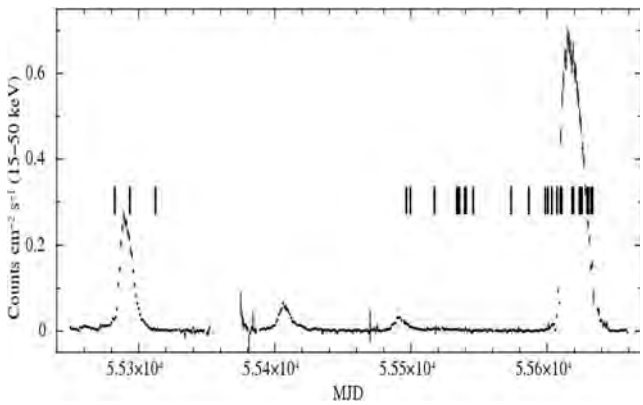

Figure 12: The X-ray light curve (obtained from Swift/BAT observations) of A0535+262 in 15-50 keV energy band, is shown from 23 February 2010 (MJD 55250) to 08 April 2011 (MJD 55659). The regular and periodic X-ray outbursts in the transient Be/X-ray binary pulsar are seen in the light curve. The epochs of our near-infrared observations are marked by vertical lines in the figure.

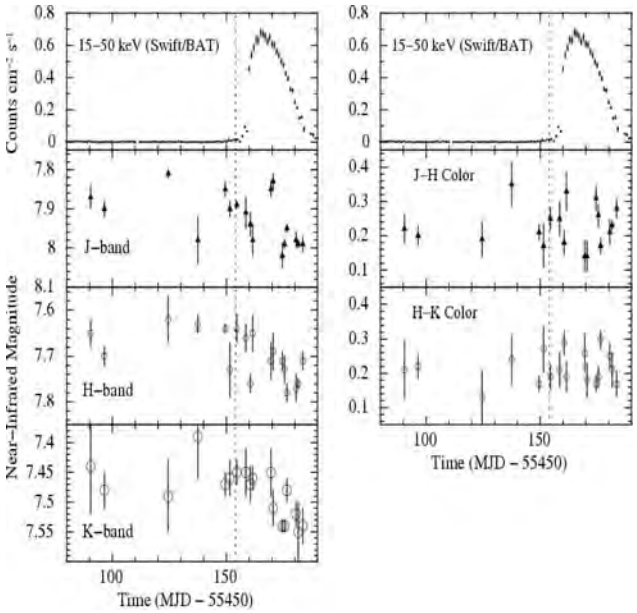

Figure 13: The Swift/BAT X-ray light curve (in 15-50 keV energy band; top panels) and the near-infrared JHK light curves (left panels) of the Be star in A0535+262/HDE 245770 binary system, covering the recent X-ray outburst in February-March, 2011. The second and third panels in right side show the J-H and H-K colors during the quiescent and outburst phase of the Be/X-ray binary system. The dotted line indicates the onset of the February-March, 2011 X-ray outburst.

(Sachindra Naik, B. Mathew, D. P. K. Banerjee, N. M. Ashok and Rajeev R. Jaiswal)

X-ray spectroscopy of the High Mass X-ray Binary Pulsar Centaurus X-3 over its binary orbit

Orbital phase dependent dipping activity in the X-ray binaries is believed to be caused by the obscuration of X-rays from the compact object by structures located in the outer regions of the disk particularly believed to be impact region of the accretion flow from the binary companion. Dipping in general leads to the hardening of the source spectrum because of the removal of the soft X-ray photons by photoelectric absorption. The observed properties during the dips viz. duration of the dip, depth of the dip, spectral behaviour of the object during the dip etc. show strong variation from dip to dip. The dipping behaviour repeats with the orbital period of the binary system. In the dipping low mass X-ray binary (LMXB) systems, the hardening of the energy spectrum during the dipping activities is often described by the "progressive covering" or "complex continuum" approach. This approach explains the spectral changes during the dipping intervals by the partial and progressive covering by an opaque neutral absorber. It is found that the dipping activities in the X-ray intensity are very common in LMXBs. However, these activities are rarely seen in the high mass X-ray binary (HMXB) systems. We have found such dipping activities in a HMXB pulsar Cen X-3.

Cen X-3 was the first binary pulsar to be discovered in X-rays. It is an eclipsing HMXB pulsar with a pulse period of ~4.8 s and an orbital period of ~2.1 days. The binary system consists of a neutron star with a mass of 1.21 +/- 0.21 solar-mass accompanied by an O 6-8 III supergiant star (V779~Cen) with a mass and radius of 20.5+/-0.7 solar-mass and 12 solar-radii, respectively. The distance to the binary system was earlier estimated to be ~8 kpc. The high luminosity of the X-ray source suggests that the predominant mode of accretion is via a disc, fed by incipient Roche-lobe overflow, although a strong stellar wind does emanate from the supergiant. The optical light curve supports the presence of an accretion disk, fed by Roche lobe overflow.

A comprehensive spectral analysis of the HMXB pulsar Cen X-3 was carried out using data from the Suzaku observatory covering nearly one orbital period. The light curve shows the presence of extended dips which are rarely seen in HMXBs (Figure 14).

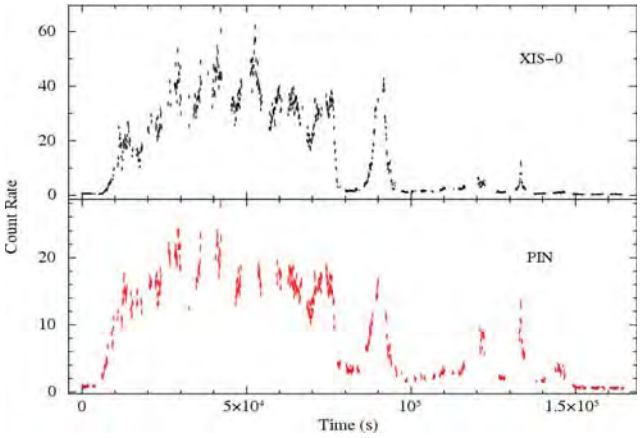

Figure 14: Light curves obtained from the Suzaku observation of the high mass X-ray binary pulsar Cen X-3 is shown here. Data from XIS-0 and HXD/PIN detectors are plotted here. The observation was carried out covering nearly entire orbit of the pulsar. The presence several dips in the light curve can be seen. The low count rate durations in the beginning (time < 1000 s) and end (time > 150000 s) show the eclipse of the pulsar by the optical companion.

These dips are seen up to as high as ~40 keV (Figure 15a & 15b). The pulsar spectra during the eclipse, out-of-eclipse, and dips are found to be well described by a partial covering power-law model with high energy cut-off and three Gaussian functions for 6.4 keV, 6.7 keV, and 6.97

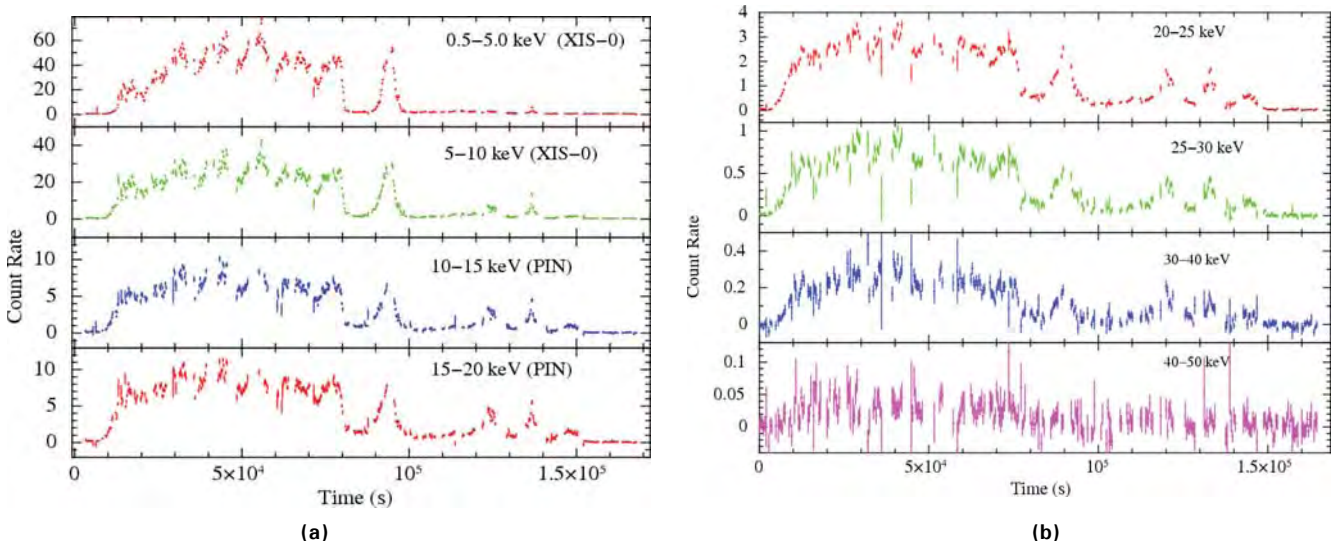

(a) (b)

Figure 15: Light curves at different energy bands obtained from the Suzaku observation of the high mass X-ray binary pulsar Cen X-3. Data from XIS-0 and HXD/PIN detectors are plotted here. The presence of dips in the light curves can be seen as high as up to ~ 40 keV.

keV iron emission lines. The dips in the light curve can be explained by the presence of an additional absorption component with high column density and covering fraction, the values of which are not significant during the rest of the orbital phases. The iron line parameters during the dips and eclipse are significantly different compared to those during the rest of the observation. During the dips, the iron line intensities are found to be lesser by a factor of 2-3 with significant increase in the line equivalent widths (Figure 16). However, the continuum flux at the corresponding orbital phase is estimated to be lesser by more than an order of magnitude. Similarities in the changes in the iron line flux and equivalent widths during the dips and eclipse segments suggests the dipping activity in Cen X-3 is caused by obscuration of the neutron star by dense matter, probably structures in the outer region of the accretion disk, as in case of dipping low mass X-ray binaries.

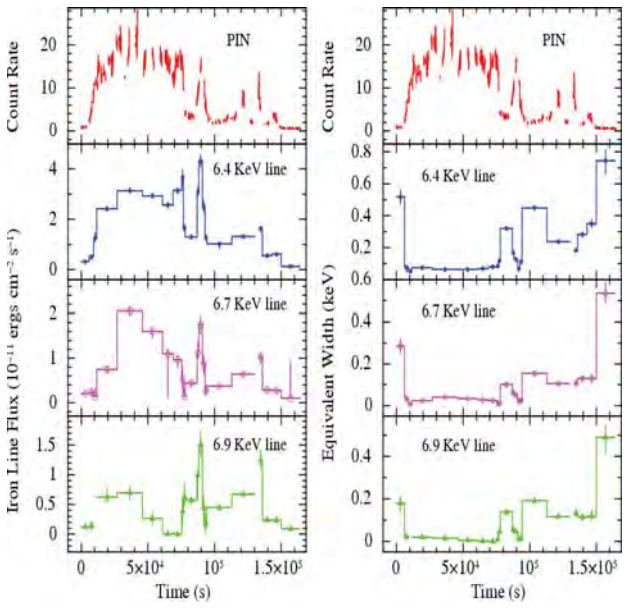

Figure 16: Iron emission line parameters obtained from the time resolved spectroscopy of Suzaku observation of Cen X-3 are shown. The top panels show HXD/PIN light curves with 100 s resolution. The bottom three panels in left side show the change in estimated line flux in 10^{-11} ergs cm^{-2} s^{-1} units where as the bottom three panels in right side show the variation in the equivalent widths for three iron emission lines during the entire observation.

This work was done in collaboration with Biswajit Paul of RRI, Bangalore.

(Sachindra Naik)

Energetic relationship among geo-effective solar eruptive phenomena

Major solar eruptive events viz. flares, coronal mass ejections (CMEs) and solar energetic particles (SEPs) influence the near-earth environment and are important constituents of space weather. Currently, the degree and mechanism of their influence on the space weather are not well understood, which, however, at the first instance, requires understanding of the energetic relationship among these explosive phenomena. In order to explore this aspect, we investigated 29 major solar flares (associated with a CME) observed by RHESSI in the declining phase of solar cycle 23. These solar eruptions were followed by geomagnetic storms with Dst index ranging between -30 and -400 nT. We performed the hard X-ray (HXR) spectral analysis of these flares to obtain non-thermal HXR spectral

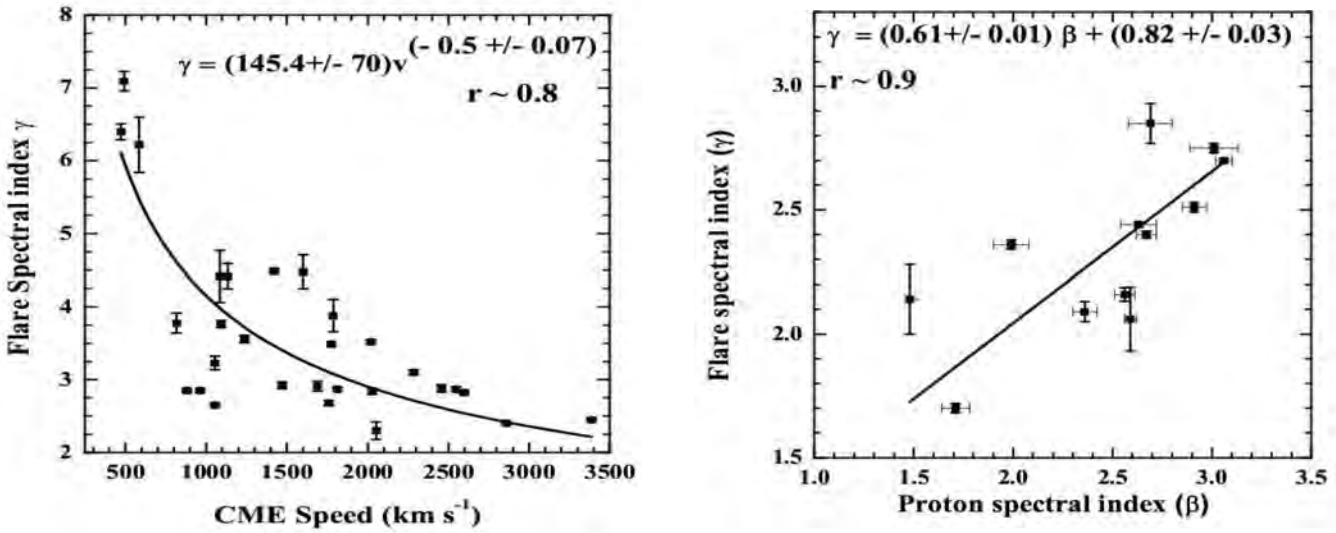

Figure 17: Left - Flare spectral index obtained from the fitted spectra for 29 flares is plotted as a function of the associated CME linear speed. The best fit is a power law relationship with r ~0.8. Right - Flare spectral index as a function of proton spectral index. The best linear fit reveals correlation coefficient of ~ 0.9.

index (γ) during the rise phase of the flare and compare with linear speed (v) of the CME observed by LASCO/ SOHO mission. We report a new relationship between v and (power law fit with r ~ 0.8) as shown in Figure 17 (left). Further, for 12 flares which were followed by SEP enhancement near Earth, we study the temporal evolution in the energy range 50-100 keV and proton spectral index (δ) of SEPs employing GOES proton data. This study reveals a new scaling law (r ~ 0.9) between the hardest X-ray flare spectrum and hardest proton spectrum near earth as shown in Figure 17 (right). Based on the results of this investigation we propose that potentially geoeffective flare and associated CME and SEP are connected with one another through a feedback mechanism, and should be regarded within the framework of a solar eruption. Owing to their space weather effects particularly on geospace, these new results will help to improve current understanding of Sun-Earth relationship.

This work was done in collaboration with Nipa J. Bhatt of C. U. Shah Science College, Ahmedabad.

(Rajamal Jain)

Is the precursor phase a cause to trigger the main phase energy release in solar flares?

X-ray emission in solar flares can be categorized in three phases viz. precursor, impulsive and gradual phase. The impulsive and gradual phases are very well studied however, the origin of the precursor phase emission is still not well understood owing to lack of high resolution as well as high S/N ratio observations. Further, due to interest in the search of driver of instability for main phase emission in flares, the study of the plasma parameters in the precursor is of utmost importance. Observations from current space missions enable one to undertake extensive studies of the precursor phase and relationship with the whole flare energetics. Therefore, we studied the underlying physical processes of energy release in precursor phase in 7 flare events. We employed X-ray observations from SOXS as well as RHESSI mission and EUV observations from TRACE as well as SDO/AIA missions.We define the precursor phase to be the emission observed in the energy <20 keV before the onset of the impulsive phase. We estimate the flare plasma parameters viz. temperature (T) and emission measure (EM) by processing the X-ray observations with

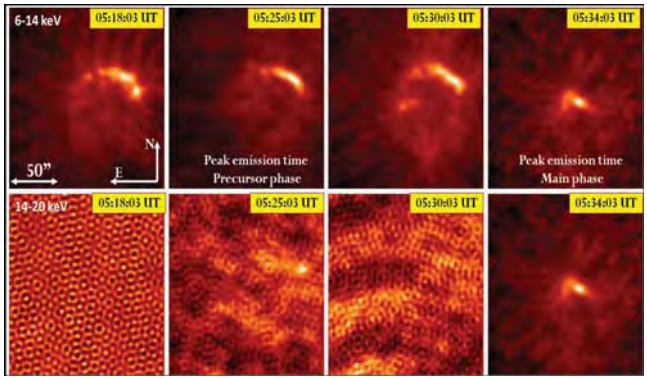

Figure 18: Time series of images observed in 6-14 and 14-20 keV X-ray energy band for the flare event of 26 Feb 2004 @ 05:18:03, 05:25:03, 05:30:03 and 05:34:03UT. The images correspond to time of commencement of precursor phase, peak emission during precursor phase, precursor to main phase transit and peak emission during main phase respectively. The co-spatial X-ray emission during the precursor and main phase may be noted.

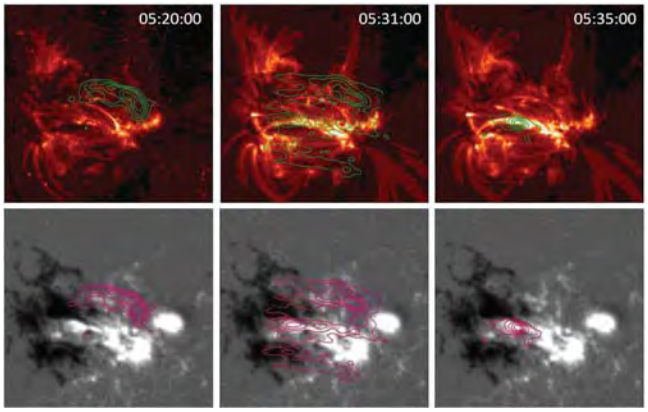

Figure 19: Time series of images observed in multi-wavelength for the flare event of 26 Feb 2004 @ 05:20, 05:31 and 05:35 UT correspond to time of peak emission during precursor phase, precursor to main phase transit and peak emission during main phase respectively. Top panel: Images observed in 171 Å from TRACE mission and processed by OCCULT (loop-tracing method) overlaid by contours of X-ray observation in 6-14 keV energy band from RHESSI. Bottom panel: Photospheric magnetic field observations from SOHO/MDI overlaid by contours of X-ray observation in 6-14 keV energy band from RHESSI.

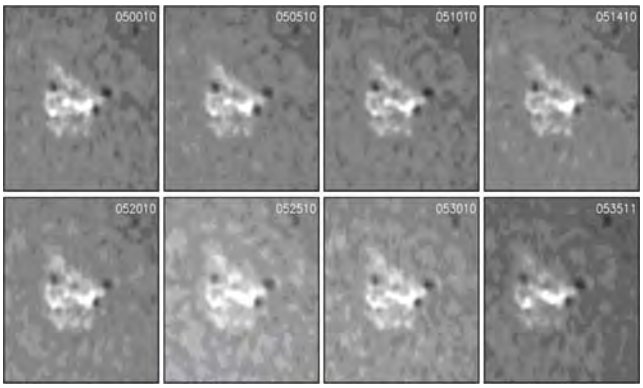

Figure 20: Time series of H-alpha images from Culgoora observatory for the flare event of 26 Feb 2004. It may be noted that no filament dynamics is seen over the whole duration of precursor and main phase emission.

the help of SolarSoft written in IDL. We estimate T and EM in precursor phase between 7-20 MK and 0.01-0.08 × 1049 cm^{-3} respectively. Further, we undertook the analysis of EUV observations from SDO/AIA mission in order to explore the changes in the loop topology. We also employ H-alpha emission observation from GONG project to visualize the filament dynamics and study the flux emergence, submergence, cancellation by employing the photospheric magnetic field observations from SDO/HMI mission. We report following findings: (1) isothermal plasma behavior in pre-flare phase, (2) the precursor phase emission is originated from low-altitude coronal loops, however, in co-spatial with the main phase energy release region (Figure 18), (3) loop-loop interaction appears to play the role of triggering the main phase emission (Figure 19), (4) No Filament dynamics and flux emergence or cancellation observed at the time of precursor as well as main phase (Figure 20).

This work was done in collaboration with Y. Hanaoka of National Astronomical Observatory of Japan, Mitaka, Tokyo, Japan.

(Arun K. Awasthi and Rajmal Jain)

Generalization of the Neupert effect over the Solar Flare Plasma Cooling

We investigate 10 M-class flares observed by the "Solar X-ray Spectrometer" (SOXS) onboard GSAT-2 Indian spacecraft to study the influence of the solar flare plasma cooling processes on the Neupert effect. It is widely known that energetic electrons responsible for the hard X-ray (HXR) emission by thick-target bremsstrahlung are the source of heating and thereby causing chromospheric evaporation seen in soft X-rays (SXR). A close relationship between the non-thermal and thermal time profiles was found, which is known as the Neupert effect. Accordingly, the time-derivative of thermal emission should mimic the non-thermal emission. This relationship, however, is strictly expected only for the asymptotic limit of very long cooling times while a physically more accurate model is necessary to generalize over finite cooling time.

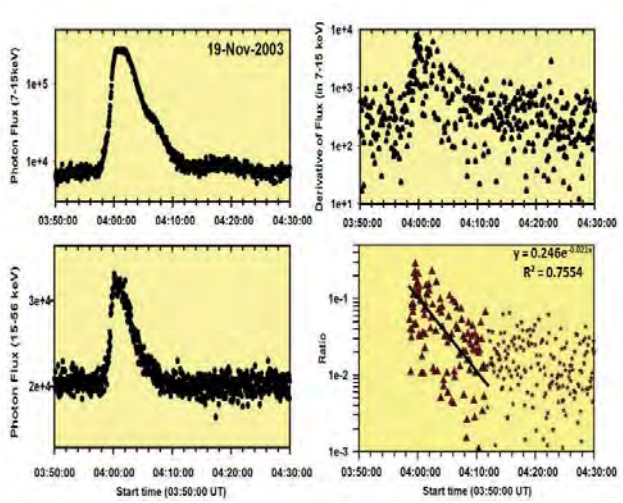

Figure 21: Top Panel: Light curve of Soft X-ray (SXR) Emission in 7-15 keV observed by SOXS mission and time derivative of SXR in the left and right panel respectively. Bottom Panel: Light curve of Hard X-ray (HXR) emission in 15-56keV and ratio obtained from derivative of SXR and HXR in the left and right panel respectively. It may be noted from the fitting obtained in the bottom right panel that the specified exponential decay (presumably referring to conduction cooling) fits well only the initial decay.

In this regard, we study the temporal evolution of X-ray emission observed by CZT detector of SOXS mission in 7-15 keV and 15-56 keV band representing the SXR and HXR emission respectively. We model the cooling as a function of time by estimating the ratio of time-derivative of SXR with the HXR flux. We found that the ratio is exponentially decaying in rise phase of the flare evolution, which, however, starts to rise after the peak emission in HXR. This changeover represents the swapping of underlying process of cooling of the plasma from conductive to radiative. We estimate the conduction cooling time scale for the events under investigation and found to be varying between 65 and 525 s (Figure 21). Further, we wish to model the second phase of cooling (referred as radiative cooling) with an exponential rising function (Figure 21). This study enables us to generalize the Neupert effect for finite cooling time and gives an idea about conductive and radiative cooling time scales.

(Arun Kumar Awasthi, Rajmal Jain)

X-ray Spectroscopy of Solar Flares: Modeling versus Observations

X-ray emission from a large variety of objects is mostly in continuum. Extracting the significant parameters from the X-ray continuum spectroscopic methods requires the detectors of sufficiently high spectral and temporal resolution. It is a technical challenge to meet these requirements. In the case of X-ray emission from solar flares it is more complex because the flux at low energies (below 20 keV) is extremely high while at higher energies (above 20 keV) it starves of photons. On the other hand extraordinary high flux from the X-ray emission lines coming from the high temperature corona (<5 keV) and during the flare (>5 keV) make the spectroscopy more and more complex. This restricts the application of one single detector in general and when one looks for high spectral resolution in particular.

The X-ray spectrum in the energy range 1-100 keV is composed of mainly three components: the 1-12 keV soft X-ray spectrum mainly due to multi-thermal temperatures; 12-25 keV emission mostly due to thermal plus non-thermal components, and >25 keV likely to be produced by non-thermal electrons. However, currently it is not known that what fraction of thermal and non-thermal bremsstrahlung contribute in the line emission below 10 keV and in the continuum during the flare emission and how this fraction vary with the magnitude of the flare? First, we model the X-ray emission from solar flares in the energy range 1-1000 keV (Figure 22) considering 3 temperature model and non-thermal bremsstrahlung. We compare the model results with observations from SOXS, GOES and RHESSI (Figure 23). It may be seen that performance of the Si detector of SOXS mission reveals better than RHESSI and GOES in lower energy band while in higher energy band RHESSI mission has better performance with reference to theoretical model.

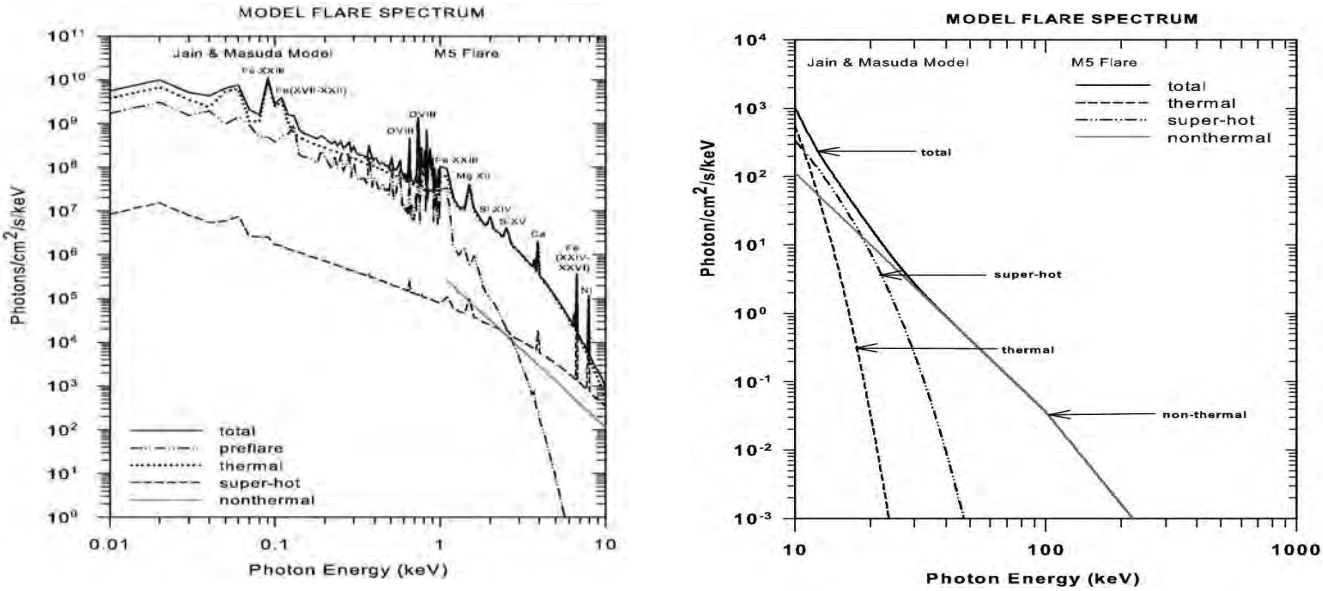

Figure 22: Simulation of full disk integrated X-ray photon emission spectrum from the Sun in the energy range 0.01-10 (left) and 10-1000 (right) keV for quiet and M5 solar flare conditions. The preflare background, thermal component, and superhot and non-thermal hard X-ray components of the solar flare are also shown by different lines. The solid thick line is total flux from all these assumptions (see text). It may be noted that iron and iron-nickel complex lines at 6.7 and 8 keV respectively appear only when flare occurs (left), and there is a break in energy from one to other spectrum (right).

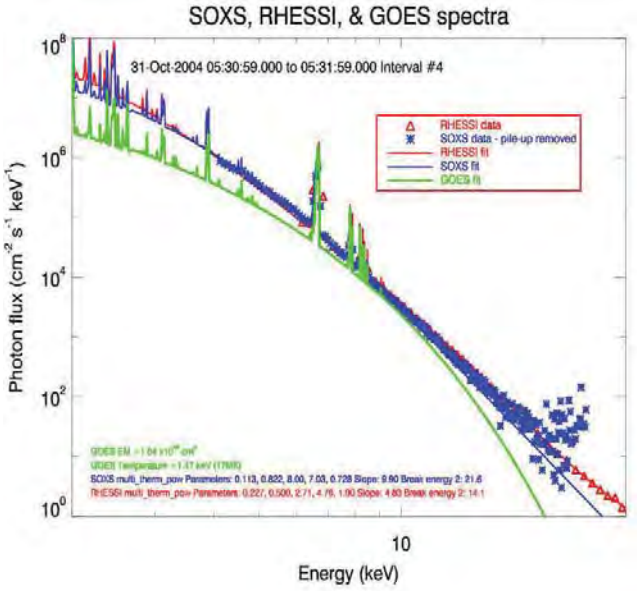

Figure 23: The X-ray photon spectra from flare of 31 October 2004 observed by SOXS, (blue), RHESSI (red) and GOES (green) missions. The count spectra are deconvoluted down to 2 keV energy to see the sensitivity of the detectors. It may be noted that SOXS reveals good sensitivity to line emission in soft X-ray emission while RHESSI in continuum above 10 keV. However, GOES spectra derived from two channels are neither sensitive to line nor to continuum.

This work was done in collaboration with Satoshi Masuda of Solar-Terrestrial Environment Laboratory, Nagoya University, Nagoya, Japan.

(Rajmal Jain)

Large peculiar motion of the solar system from the dipole anisotropy in sky brightness due to distant radio sources

We have determined our peculiar velocity relative to the frame of distant radio sources, by studying the anisotropy in the sky brightness from discrete radio sources, i.e., an integrated emission from discrete sources per unit solid angle. In past the angular variation in the temperature distribution of the Cosmic Microwave Background Radiation (CMBR) has been used for such a purpose. Our results give a direction of the velocity vector in agreement with the CMBR value, but the magnitude is ~ 4 times higher at a statistically significant (~ 3 sigma) level. A genuine difference between the two dipoles would imply anisotropic universe, with the anisotropy changing with the epoch. This would violate the cosmological principle where the isotropy of the universe is assumed for all epochs, and on which the whole modern cosmology is based upon.

(Ashok K. Singal)

Uniformity, Horizon problem, Flatness and the inflationary models of the Universe

It is shown that contrary to the prevalent view in the literature for the last thirty years or so, the conditions of uniformity, horizon problem, and the observed near-critical density (flatness) do not by themselves necessarily lead to the idea of the inflationary models of the Universe.

(Ashok K. Singal)

Some Null-Impedance Paradoxes in Electrical Circuit Theory

Three long standing null-impedance paradoxes in electrical circuit theory have been resolved. (i) Ideally one would want a battery to present zero internal resistance, so that there are no losses within the battery and that the voltage presented at its terminal is without any drop from its emf value. But we show that such a battery, even if somehow made, will be useless as it will not sustain any current in the outer circuit and that the internal resistance of a battery is unavoidable for its successful working as a source of current. (ii) In this famous paradox of two charged capacitors, energy conservation seems to be violated when some of the charges are transferred from one capacitor to the other, with a connecting wire having an identically zero resistance. We have shown that contrary to the prevalent belief, radiation does not play any role in resolving the paradox and that the paradox is successfully resolved only when one properly considers the not-so-apparent energy changes in the system. (iii) The energy disappearance in a lossless transmission line is a paradox because the line contains no resistance and yet its input impedance acts as a pure resistance. Driven by a sinusoidal source, it will absorb energy from the source at a constant rate. The question therefore arises as to what happens to this energy. The paradox is resolved if one considers the absence of a reflected wave in this case.

(Ashok K. Singal)

Phase-resolved spectroscopy of transient black hole candidate IGR J17091-3624 during 2011 outburst

Transient black hole binaries remain in quiescent state most of the time but their luminosity increases by orders of magnitude when they enter in outburst state. IGR J17091-3624 is a transient black hole candidate which showed outburst in January, 2011. It received a lot of attention recently due to peculiar 'heart-beat' type variability patterns exhibited by the source, in which quasi-periodic bursts are repeated over time scale as short as 5 seconds. So far, such variability behavior has been observed only in GRS

1915 + 105. IGR J17091-3624 has been found showing many other variability patterns as well. Observation of quasi-periodic bursts manifests an underlying quasi-periodic phenomenon taking place at timescales of few tens of seconds(Figure 24). In general, detailed study of such extreme variability can be very helpful in understanding the accretion processes very close to the black hole, however, for IGR J17091-3624 such study is not possible because basic system parameters (mass, distance, inclination etc.) are not known so far.

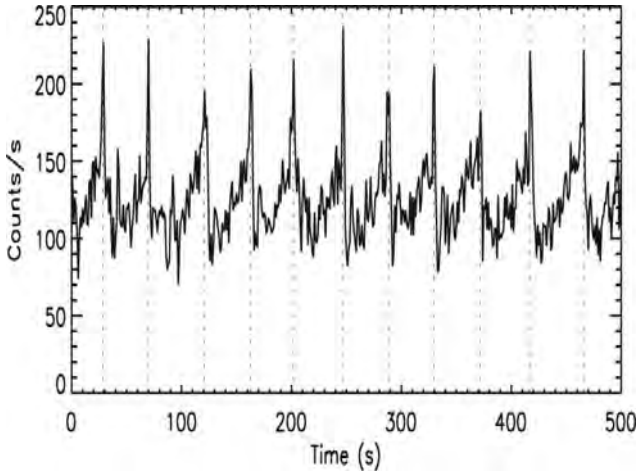

Figure 24: One second light curve of IGR J17091-3624 as observed by RXTE-PCA on 27 March, 2011. The bursts peak times (with quasi-period of 39 second) are marked with vertical lines and are used for generating 'psudo'-phase folded light curve.

Here we attempt to constrain some of the system parameters for this source with phase resolved X-ray spectroscopy simultaneous observation by RXTE and XMM-Newton during its 2011 outburst. RXTE light curve was showing nu-class behavior in this observation with burst period of about 39 seconds. Phase-resolved spectroscopy of bursts was done by dividing a burst into 64 phases and co-adding counts from respective phases of all bursts. The 64 phases were grouped into 5 phases before spectral fitting (Figure 25) and spectra of 5 phases were fitted simultaneously. We have found that IGR J17091-3624 is a high inclination binary with inclination angle greater than 40°. The 0.7-35 keV spectra can be fitted with 'canonical' model for black hole spectra consisting of only two components - accretion disk and power law (or its equivalent). Any other components, like Fe-K line or reflection from disk are not required for the fits which support high inclination of the binary. Strong correlation between source flux and disk temperature over the time scale of few tens of seconds was observed during individual burst profile. However, the inner disk radius was not found to vary significantly with phase of bursts unlike GRS1915 + 105 where the inner disk radius varies significantly during burst. Despite several similarities in variability patterns, the difference lies

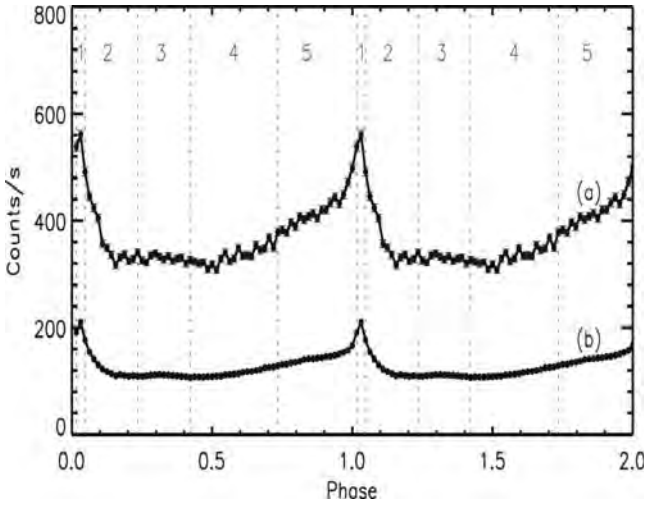

Figure 25: 'psudo'-phase folded light curve of IGR J17091-3624. Top curve is from XMM-Newton PN detector and bottom curve is from RXTE-PCA. The five period marked with vertical lines are used to obtain spectra for respective phases.

in their brightness. GRS 1915 + 105 is a very bright source whereas IGR J17091-3624 is a faint source. We have found that IGR J17091-3624 is a low spin black hole candidate having innermost stable orbit far away from central black hole in contrast to GRS 1915 + 105 which is a maximally rotating black hole ($a^* > 0.99$) with innermost stable orbit going very close to black hole. This explains the faintness of IGR J17091-3624 as compared to GRS 1915 + 105.

(Anjali Rao, S. V. Vadawale)

Investigating the feasibility of Compton X-ray polarimeter as a focal plane detector for hard X-ray optics

Most of the X-ray emitting objects are expected to show polarization signature due to the various physical processes occurring on in those sources. Accurate measurement of X-ray polarization can lead to a better understanding of the emission mechanism and the geometry at the close vicinity to the emitting region. X-rays polarization measurement, particularly at high energies, is very important as it can provide independent inputs to understand the non-thermal processes in X-ray sources such as binary black holes, rotation powered and accretion powered neutron stars, Blazars, Gamma Ray Bursts etc. Unfortunately, hard X-ray polarimetry is very difficult due to both – photon hungry nature of polarization measurement and very low sensitivity of hard X-ray detector. However, with the very recent availability of hard x-ray focusing (e.g. in the upcoming hard X-ray telescope NuStar), the sensitivity of the hard X-ray detector is expected to be enhanced greatly. In this context we are explore feasibility

of developing a hard X-ray polarimeter as a focal plane detector for hard X-ray optics in the energy range of 22 – 80 KeV

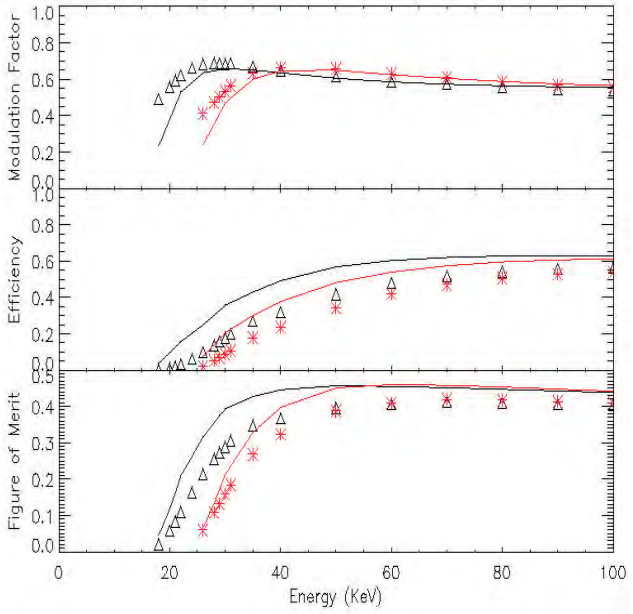

Figure 26: Modulation factor (μ), polarimeter efficiency (ε) and figure of merit ( ) as a function of energy. Black triangles and black solid line represent simulation and analytical results respectively for 1 KeV threshold. Red asterisks and red solid line represent the simulation and analytical results respectively for 2 KeV thresholds.

We have designed a focal plane hard X-ray polarimeter based on principle of Compton scattering. The geometry employs a thin plastic scatterer surrounded by a cylindrical array of CsI(Tl) detectors. We have carried out detailed Geant4 simulations to estimate the sensitivity of the polarimeter coupled with NuSTAR type of hard X-ray optics. The modulation factor and polarimetric efficiency estimated based on our simulations are shown in Figure 26 (with symbols). We have also carried out independent analytical estimation of these factors as shown by the continuous lines in Figure 26. Overall agreement between our simulations and analytical results confirms the validity of both, at the same time, the slight discrepancy, particularly at low energies and in efficiency, emphasizes the necessity of detail simulations, because it is very difficult to analytically analyze the real experimental geometry considering all minute details.

We plan to develop the X-ray polarimeter based on this design in near future. The first step is to determine the lowest possible detection threshold for the plastic scatterer which we plan to demonstrate during next few months

(Tanmoy Chattopadhyay, S. V. Vadawale)

Comparison of rotation estimates from various solar emissions

We have used disk integrated emissions as well as high resolution images of the Sun at various wave lengths. The disk integrated measurements include radio emissions at 2.8 GHz for a six solar cycles, multi frequency radio emissions for a limited period of 26 months, total solar irradiance measurements by VIRGO and SORCE. These have revealed many interesting aspect of solar rotation as a function of height above the photosphere as well as temporal variability. Recent data of SORCE is used for the period 2003-2011 to look for the rotational modulation on TSI. It is found that the rotational modulation varies from 9 – 42 % and it apparently varies in opposition of sunspot numbers. The derived sidereal rotation period varies from 22.5 to 30.5 days. The sufficiently high resolution and fairly regular observations at 17 GHz from the Nobeyama Radio Heliograph (NROH), soft X-ray by YOHKOH and extreme ultraviolet at 171 nm by SOHO were also used to learn about the differential rotation as a function of latitude. An interesting example for the comparison is shown in Figure 27. Here mages of all three type are analyzed using the flux modulation approach.

The comparison indicates that the rotation of the Sun is very complex. It changes both as a function of height above the photosphere as well as the latitude. At higher latitude the rotation period inferred by X-ray and EUV are comparable where as radio indicate higher rotation period. In the equatorial part of the Sun, radio and EUV estimates come closer where as X-ray estimates are much lower.

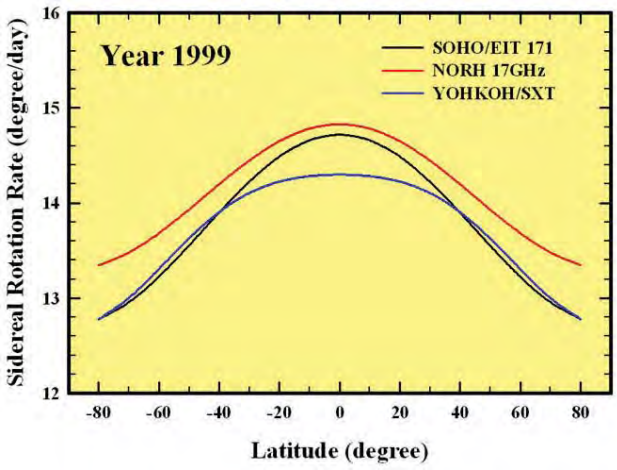

Figure 27: A comparison differential rotation during 1999.

This work is done in collaboration with Satish Chnadra of PPN PG College Kanpur.

(Hari Om Vats)

Temporal and spatial variability of solar X-ray flares

Solar flares are generally examined as individual events in great detail. The advent of spacecraft observations of flares in hard and soft X-rays has provided good and extensive data sets that are suited to statistical examination. We under took one such study using GOES X-ray flare observations. An occurrence statistics for three years 1993 – 1995 is shown in Figure 28.

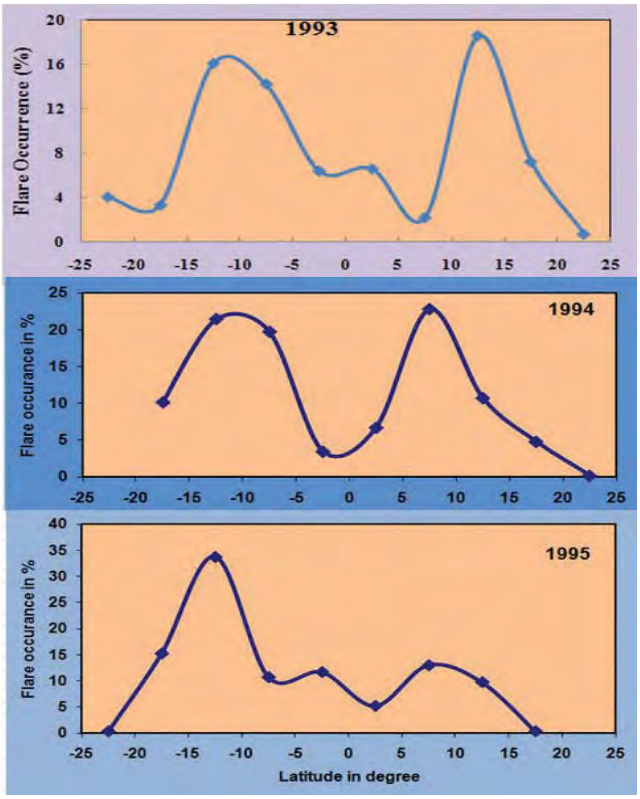

Figure 28: Occurrence statistics of solar X-ray flares for the years 1993 - 1995

In the period from 1993 – 2003 (almost one solar cycle) number flares varies from 129 in 1996 (solar minimum) to as much as 1418 flares in 2000 (solar maximum). The occurrence has two main peaks one in each hemisphere. As seen in the figure above the relative strength of the peaks have a temporal variability which could be due to the phase of solar activity. Further analysis will reveal this aspect more clearly. The long term distribution may have a systematic shift.

This work in being pursued in collaboration with Niraj Pandya of Tolani College of Arts and Science, Adipur, Gujarat.

(Hari Om Vats)

Infrared investigation of the circumstellar environment of a sample of post-AGB stars

Post-Asymptotic Giant Branch (PAGB) stars are rapidly evolving low and intermediate-mass stars (1-8 M) in the transition phase from the mass-losing AGB stars to the Planetary Nebulae (PNe) and are enshrouded by optically thick circumstellar matter that generally consists of molecular gas and dust. There exist a number of unresolved issues as to the physical processes that govern the evolution at these late stages. The chemistry of the circumstellar environment of these stars is highly dynamical due to the enrichment of the surface layers by the convective dredge-up process; initially oxygen-rich envelopes turning to carbon-rich. Polycyclic aromatic hydrocarbons (PAHs) are likely to form in such carbon-rich envelopes. PAH emission in the infrared ensues from the absorption of a UV photon by the molecule and is indicative of the evolution of the central star in to a hot core. We have undertaken an infrared photometric and spectroscopic investigation of a large sample of PAGB stars in order to understand their rapid evolution before emerging as PNe. The Spectral Energy Distributions (SEDs) were modelled for a sample of 72 stars (several of which are classified as proto-PNe) using the available archival data in the optical, near-, mid-, far-infrared regions. Our modelling shows that the circumstellar

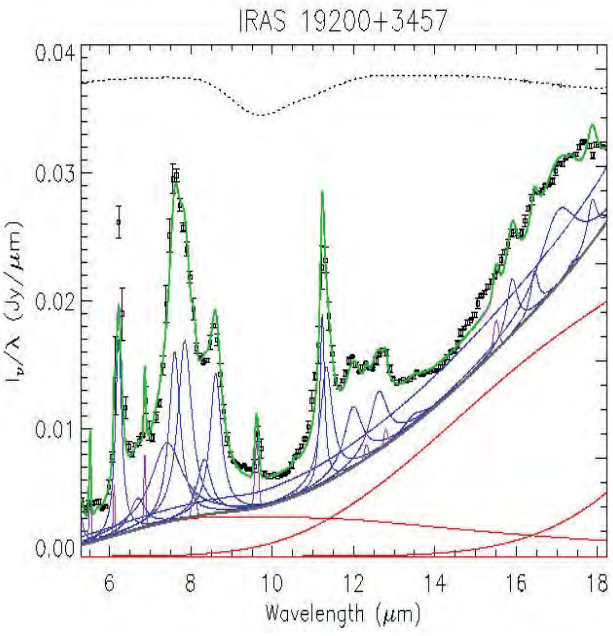

Figure 29: Shows IRS-SPITZER mid-infrared spectrum of the PAGB star IRAS 19200+3457 (black squares). Model composite spectrum is shown in green; and the individual PAH features are shown in blue curves. The violet and red curves are for atomic/ionic fine structure lines and continuum spectra respectively. The thick gray line represent the total (dust+stellar) continuum. The dotted line on the top represents extinction curve.

dust in PAGB stars is predominantly carbonaceous (either amorphous carbon or graphite grains or a combination of the two) which supports the fact that these stars are in an advanced stage of evolution. The mass-loss rates obtained from the model matches with those obtained from sub-mm observation. Dust shell inner radius and the mass loss rate show, as expected, an inverse relation with stellar temperature. The mid-infrared PAH emission features were studied using the archival data from Infra-Red Spectrograph (IRS) on board the Spitzer Space Telescope (SST). The mid-infrared emission features were modelled for obtaining the strengths of various features attributed to PAH molecules (Figure 29).

The dust temperatures obtained from the SED modelling matches with those derived from modelling of the spectra. From our study we find that the PAH molecules may be compact and neutral. Attributed to episodic mass-loss, spectral variability of various time scales is seen in a few PAGB stars from repeated near-infrared spectroscopic observations from Mt. Abu observatory.

(V. Venkata Raman and B.G. Anandarao)

Solar Physics

The research and development activities of the Udaipur Solar Observatory revolve around the central theme of solar activity and solar eruptive processes. Helioseismology is used as a tool to dig into the sub-surface origins of eruptions. Surface magnetic field is measured to monitor magnetic energy storage and evolution of the potential triggers of the eruptions. Above the surface, chromospheric and coronal phenomena are used to predict the geo-effectiveness of these eruptions. A combination of analyses of archived data, mathematical modeling and construction of sophisticated instruments is employed to achieve the desired goals.

Role of sunspot rotation on the activity of NOAA AR 11158

Activity of the sun is defined by eruptive events like coronal mass ejections (CMEs) and flares occurring in the active regions (ARs) consisting of groups of sunspots having positive and negative magnetic polarities. During the evolution of ARs, the sunspots exhibit proper as well as rotational motions, believed to be associated with the storage of energy by increasing the magnetic non-potentiality and eventual release in the form of observed eruptive events. Thus, by investigating the characteristic properties of the sunspots in the ARs helps in understanding the transient activity of the sun. We studied the rotating sunspots in AR 11158 and their possible role in the observed activity. Figure 30 (a) shows a huge coronal mass ejection (pointed by arrow) on 14 February, 2011.

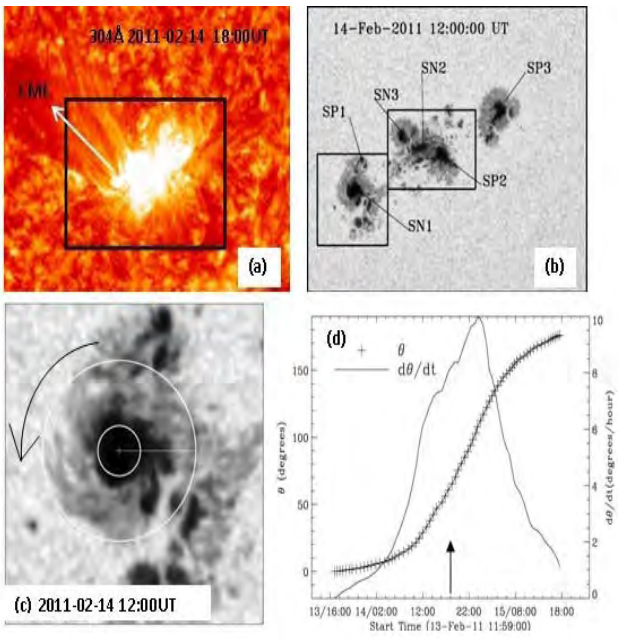

Figure 30 NOAA AR 11158 observed by - (a) Atmospehric Imaging Assembly (AIA) onboard Solar Dynamic Observatory (SDO) in 304Å channel showing the CME, pointed along the arrow (b) in continuum intensity with the labelled sunspots, SN1 and SP2, etc. (c) The expanded region around SN1 where sunspot centroid and annular region are marked by concentric circles. These were used to remap onto polar co-ordinate system. (d) The temporal profiles of feature displacement and angular velocity around the centroid.

The rectangular region of panel (a) is illustrated in panel (b) in continuum intensity observed by Heliosiesmic Magnetic Imager (HMI) on-board Solar Dynamics Observatory (SDO). We observed intrinsic rotation of sunspots SN1 and SP1 from animations of these observations. The sunspot SN1 is remapped to polar coordinate system to obtain information about the rotational parameters like angular distance (θ) and angular velocity (dθ/dt) with respect to time (panel c). Panel (d) shows the temporal profiles of these parameters. As indicated, the CME occurred around the time when dθ/dt reached a maximum. We estimated various physical parameters as the AR evolved with time and confirmed that rotational motions played a predominant role in increasing non-potentiality of magnetic structures by injecting helicity. This process increased the free energy available in the AR accounting for the observed transient activity.

This work was carried out in collaboration with Ram Ajor Maurya and J.-C. Chae of Seoul National university, South Korea.

(P. Vemareddy and Ashok Ambastha)

Spectral Line Profile Changes Associated with Energetic Solar Transients

Abnormal sign reversals in magnetic polarity and large enhancements in Doppler velocity have been observed during the impulsive phases of a few very energetic solar transients. One major concern in interpreting the observed results is whether these effects are related to the expected modification of spectral line profiles, employed in the measurement of photospheric magnetic/velocity fields, during the impulsive phase of energetic transients. In the absence of availability of spectral data during major solar events, inferences have been drawn so far based only on indirect evidences, such as, hard X-ray sources and white light flare kernels. The first X-class flare of 15 February, 2011 in NOAA AR 11158 provided a good opportunity to examine any flare induced changes in the line profile, and hence, in the measurements of velocity and magnetic fields. This event was observed by the recently launched Helioseimic and Magnetic Imagesr (HMI) onboard Solar Dynamics Observatory (SDO) which provides appropriate spectral data at six wavelength positions over the Fe I 6173 A line figure 31. We found spectral changes related to various Stokes' parameters during the peak phase of the flare. The thermodynamic change during the impulsive phase of the flare can drastically change the height of line formation due to the moderate perturbation of temperature and density. This can also occur as a result of the large

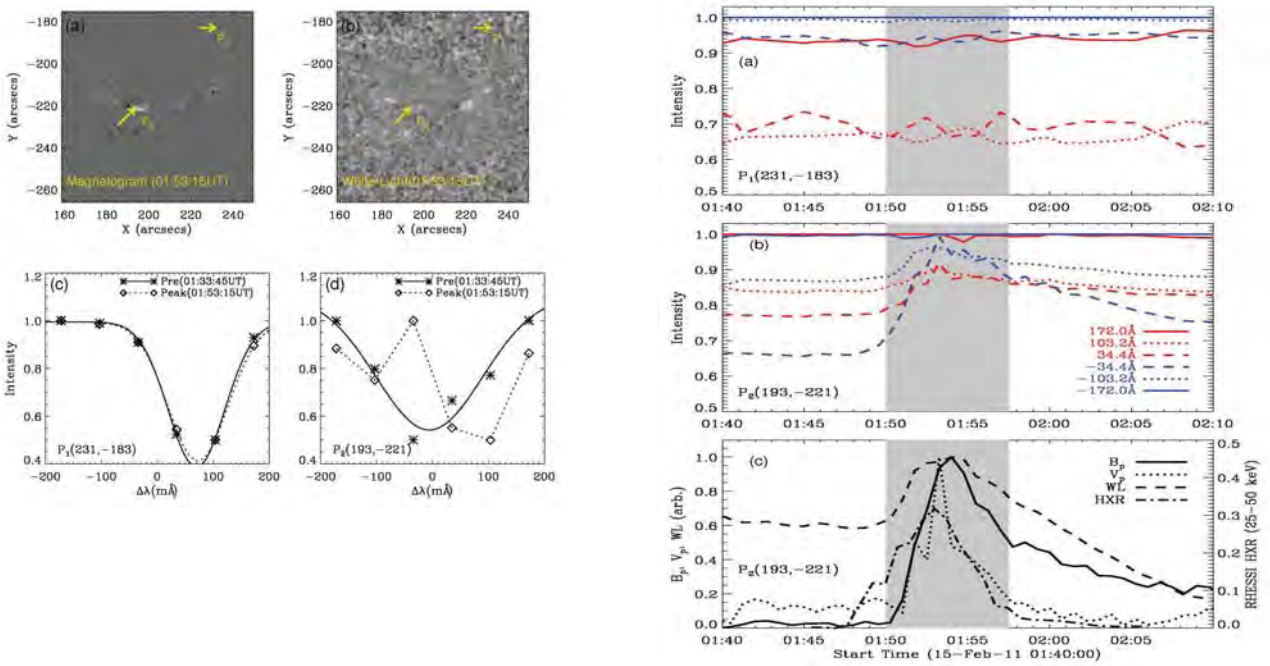

Figure 31. (Left column - Top row): Consecutive difference magnetogram (a) and white-light (b) images of the AR NOAA 11158 during peak phase (01:53:15 UT) of the flare. (Bottom row): Line profiles at quiet P1 (c) and transient P2 (d) locations marked by arrow heads in top panel. Fe I line profiles are plotted during pre (01:33:45 UT) and peak (01:53:15 UT) phases of the flare. (Right column) Panels (a-b) show temporal variations in the normalized line intensities at locations P1 and P2, respectively while panel (c) shows variations in the photospheric magnetic flux (Bp), Doppler velocity Vp, white light intensity (WL) and RHESSI HXR energy at the flare location P2.

increase of electron density as shown earlier by the non-LTE calculations of Ding (2002) for Ni I 6768 A line. The non-thermal excitation and ionization by the penetrating electrons can generate increased electron density which enhances the continuum opacity, thereby pushing the formation height of the line upwards. The precipitation of electrons and deposition of energy in the chromosphere, enhanced radiation in the hydrogen Paschen continuum gives rise to the line source function leading to an increase of the line core emission relative to the far wing and continuum. We thus suggest that the anomalous magnetic and Doppler changes observed during the energetic flare of 15 February 2011 were related to the Fe I line profile changes. Both thermal and non-thermal physical processes operating during the flare may contribute to the spectral profile changes at different stages of the flare evolution. Therefore, the observed magnetic/velocity transients are essentially the observational signatures of these physical processes, and do not correspond to any "real" changes in the magnetic (Doppler) field values.

This work was carried out in collaboration with Ram Ajor Maurya of Seoul National university, South Korea.

(Ashok Ambastha and P. Vemareddy)

Analysis of seismic sources observed in the active region NOAA 11158 during the X2.2 class flare on 15 February 2011

The solar active region NOAA 11158 produced a series of flares during its passage through the solar disk. The first major flare (of class X2.2) of the current solar cycle occurred in this active region on 15 February 2011 around 01.50 UT. We have analyzed the Dopplergrams observed by the HMI instrument on-board SDO to examine the seismic response of the solar photosphere corresponding to this flare. The HMI instrument provides high-quality Doppler images of the Sun at 0.5 arc-sec spatial resolution at a cadence of 45 sec. We identified several seismic sources in the AR during the flare. These seismic sources were located in the vicinity of flare ribbons as observed by Hinode in Ca II H wavelength (Figure 32 left). The seismic sources show enhanced upflows/downflows during the flare. Wavelet analysis of these locally enhanced velocity flows shows dominance in p-mode regime as well as high-frequency power during the flare (Figure 32 right). We have also analyzed the disk-integrated solar observations from GOLF during this period to study the flare related changes in the global velocity patterns in the Sun.

This work has been done in collaboration with Savita Mathur of High Altitude Observatory, Boulder, USA, and R. A. Garcia of Laboratoire AIM, CEA/DSM-CNRS, Universite Paris, IRFU/SAp, Centre de Saclay, Gif-sur- Yvette, France.

(A. Raja Bayanna, Brajesh Kumar, P. Venkatakrishnan, and Shibu K. Mathew)

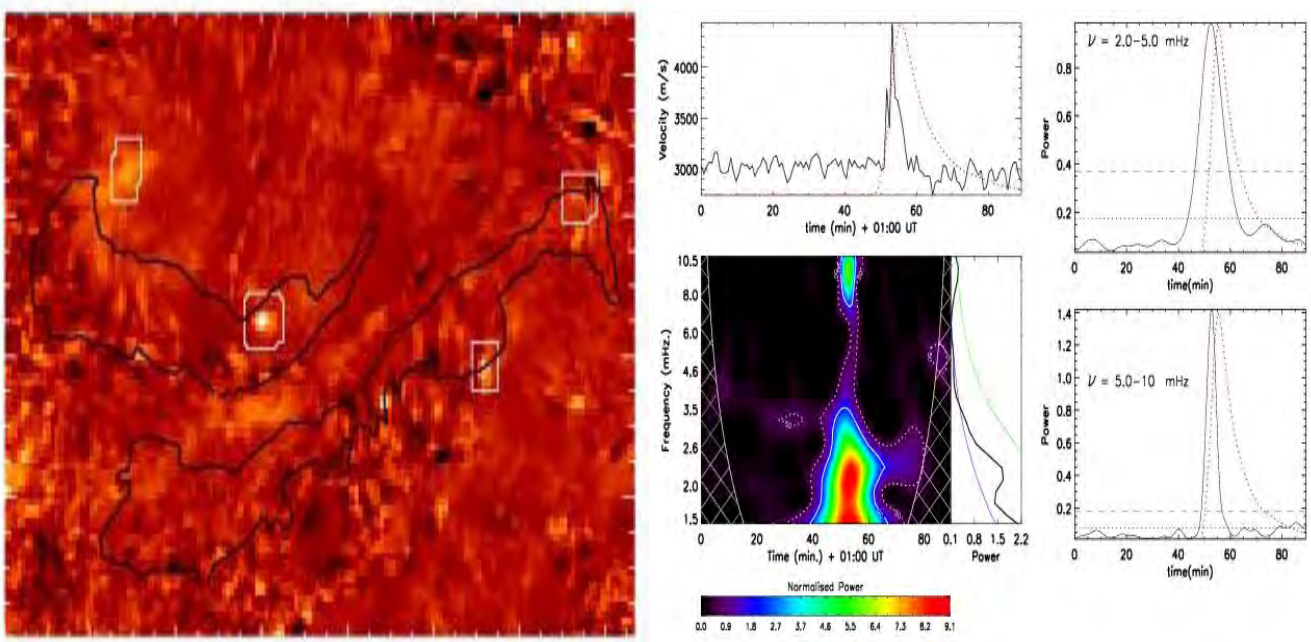

Figure 32. (left) The difference map of root mean square (rms) velocity in NOAA 11158 computed from the tracked HMI Dopplergrams taken before and during the flare. The white boxes show the identified seismic sources and the black contours show the location of Ca II H flare ribbons obtained by SOT instrument onboard Hinode spacecraft. (right) Wavelet analysis of a seismic source showing enhanced upflow during the flare. We observe enhanced power in the p-mode regime during the flare.

Analysis of flare-induced seismicity in the active region NOAA 10930 and related enhancement of global waves in the Sun

A major flare (of class X3.4) occurred on 13 December 2006 in the active region NOAA 10930 during the solar minimum of the activity cycle 23 and produced high-speed halo Coronal Mass Ejection (CME) and extremely energetic emissions This flare was well observed in high-energy and optical wavelengths by several ground- or space-based instruments, viz., GONG, *Hinode*, *GOES*, *RHESSI*, and Nobeyama Radio Polarimeters (NoRP). The energy released during large flares is believed to induce acoustic oscillations in the Sun. We have analyzed the line-of-sight velocity of this AR during the X3.4 flare using the GONG Dopplergrams along with the disk-integrated velocity observations by GOLF instrument onboard *SOHO* spacecraft to study any possible connection between the flare related changes in the local and global velocity oscillations. We have applied wavelet transform to the time series of the localized velocity oscillations as well as the global velocity oscillations spanning the flare event. The line-of-sight velocity shows significant enhancement in some localized sites of the penumbra of this active region during the flare (Figure 33). These sites are away from the flare location and the hard X-ray footpoints. The sudden enhancement in velocity seems to be caused by the Lorentz force driven by the "magnetic jerk" in the localized penumbral region. The evolution of local and global line-of-sight velocities during the flare was observed with GONG and GOLF. Application of wavelet analysis to these flare induced localized seismic signals show significant enhancement in the high-frequency domain ($5 < \nu < 8$ mHz) and a feeble enhancement in the *p*-mode oscillations ($2 < \nu < 5$ mHz) during the flare. On the other hand, the wavelet analysis of GOLF velocity data and the full-disk collapsed GONG velocity data spanning the flare event indicate significant post-flare enhancements in the high-frequency global velocity oscillations. We also found indications of a connection between the flare induced localized seismic signals and the excitation of global high-frequency oscillations.

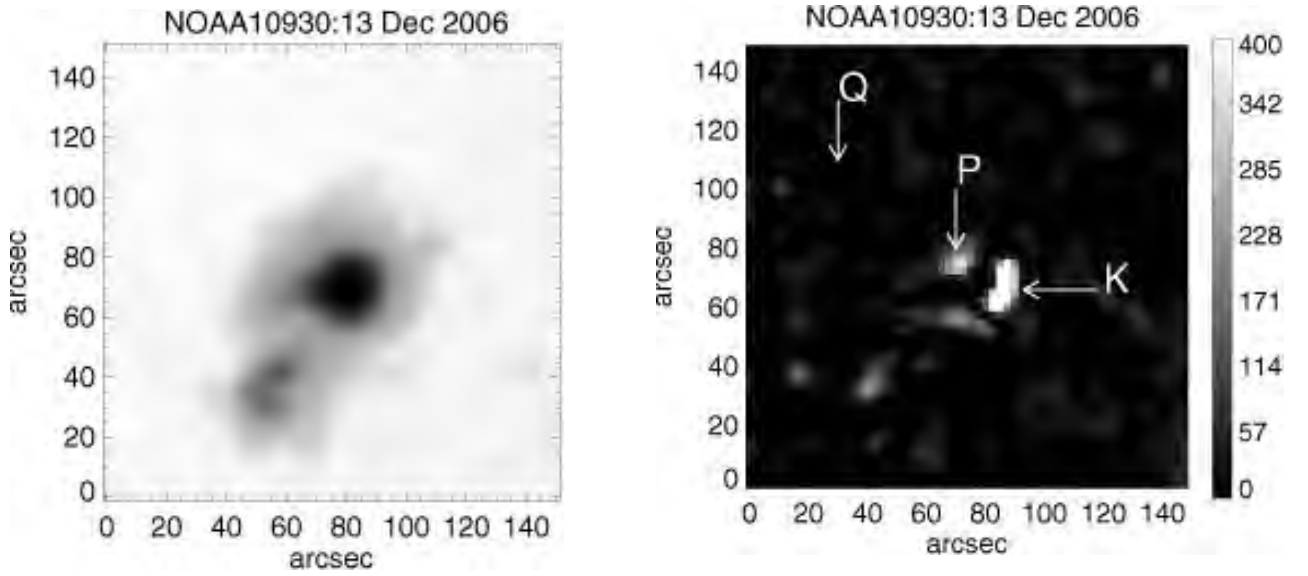

Figure 33. (left) Continuum intensity map of AR NOAA 10930 obtained by the GONG instrument on 13 December 2006 at 02:26 UT. (right) The corresponding grid shows the root mean square (rms) velocity map computed from the tracked GONG Dopplergrams for the period between 02:20 UT and 03:02 UT. The bright patchy region indicated by 'K' and 'P' show the locations of the suddenly enhanced velocity oscillations in the localized penumbral region of the active region. One of the quiet regions of the Sun is indicated by 'Q' in this image.

This work has been done in collaboration with Savita Mathur of High Altitude Observatory, Boulder, USA, and R. A. Garcia of Laboratoire AIM, CEA/DSM-CNRS, Universite Paris, IRFU/SAp, Centre de Saclay, Gif-sur-Yvette, France.

(Brajesh Kumar, P. Venkatakrishnan, and Sanjiv Kumar Tiwari)

Intense HXR emission and magnetic restructuring associated with an unusual impulsive flare: RHESSI and SDO observations

We have carried out a multi-wavelength investigation of a very impulsive M-class solar flare that occurred in AR NOAA 11302 on 26 September, 2011. Excellent set of high temporal and spatial resolution measurements obtained from different EUV/UV channels of Atmospheric Imaging Assembly (AIA) and Helioseismic and Magnetic Imager (HMI) onboard Solar Dynamics observatory (SDO) provide unique opportunity to understand the magnetic coupling of atmospheric layers of the Sun during the coronal energy release. The rise and main phase of the event was well observed by Reuven Ramaty High Energy Solar Spectroscopic Imager (RHESSI). The HMI magnetograms reveal emerging flux regions at the flaring location which developed at the flare onset. More interestingly, we find a rapid intrusion of magnetic flux of negative polarity into a larger region that is dominated by positive polarity. RHESSI light curves indicate a steep rise in the X-ray flux in all the HXR energy bands up to 100 keV, implying strong impulsive character of the flare. Moreover, we briefly observed a gamma ray source in 100-300 keV energy band images at the flare maximum which is rather unusual for such a confined flare. The synthesis of UV, EUV, and HXR images suggests that the majority of accelerated electrons, escaped from the primary energy release site, were injected in nearby loop systems, creating remote brightening in the form of ribbons and kernels (Figure 34). We propose a possible interpretation for this event in terms of solar flare models based on magnetic reconnection between interacting magnetic systems driven by emerging/ merging magnetic flux.

(Upendra Kumar Singh Kushwaha and Bhuwan Joshi)

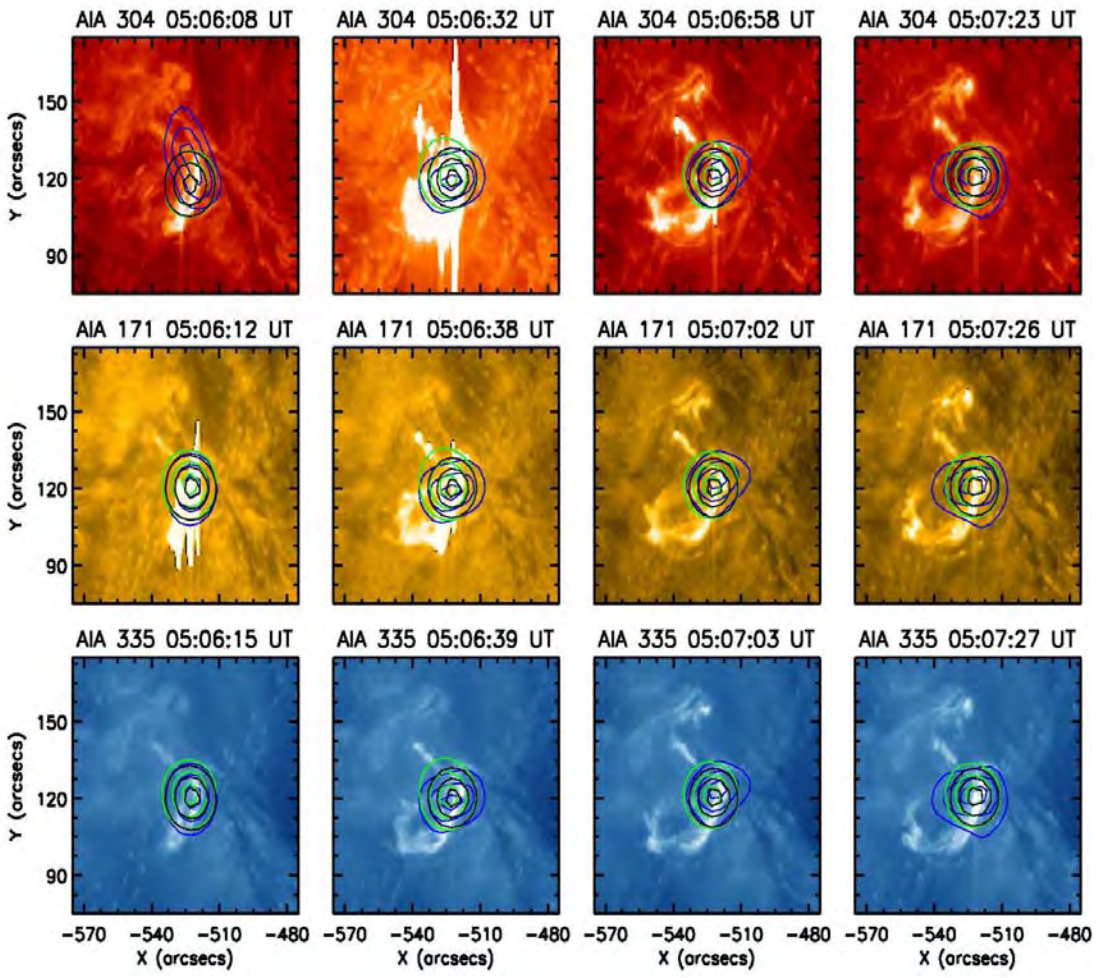

Figure 34. Multi-wavelength view of flaring region observed by SDO/AIA and RHESSI. The contours of RHESSI 'cleaned' images at different energy bands of 6-12 keV (black), 12-25 keV (green), and 50-100 keV (blue) are overlaid on AIA images. Contour levels are set as 60%, 80%, and 95% of peak flux for each image.

Evidence of magnetic reconnection during the extended X-ray precursor phase of an X-class solar flare

In order to understand the triggering mechanism of solar eruptions, it is essential to examine the pre-flare phase and probe small-scale, localized instances of energy release that may play important role in destabilizing the solar filaments leading to large-scale eruptions. With this motivation, we carried out a comprehensive multi-wavelength analysis of the pre-flare activity associated with an eruptive X-class solar flare which occurred in AR NOAA 10656 on 18 August 2004 near the west limb of the Sun. The soft X-ray light curves of GOES clearly indicate an extended and gradual precursor phase that lasted for about one hour. This precursor phase is characterized by three sub-peaks which are more pronounced in high energy GOES channel (0.5-4.0 Å). A comparison of time history of SXR profile with high temporal and spatial resolution TRACE EUV observations provides evidence of three localized events of energy release in the vicinity of a sub-filament region (Figure 35). During the whole pre-flare phase, the filament rises and undergoes morphological evolution as observed in EUV images. More intriguingly, RHESSI observations reveal a strong HXR source up to ~50-80 keV. The multi-wavelength signatures along with RHESSI X-ray spectra and available magnetic field measurements provide evidence that the discrete, confined events of energy release during the precursor phase correspond to the localized events of magnetic reconnection which act as a common trigger for the main flare and associated large-scale eruption.

(Bhuwan Joshi and Upendra Kumar Singh Kushwaha)

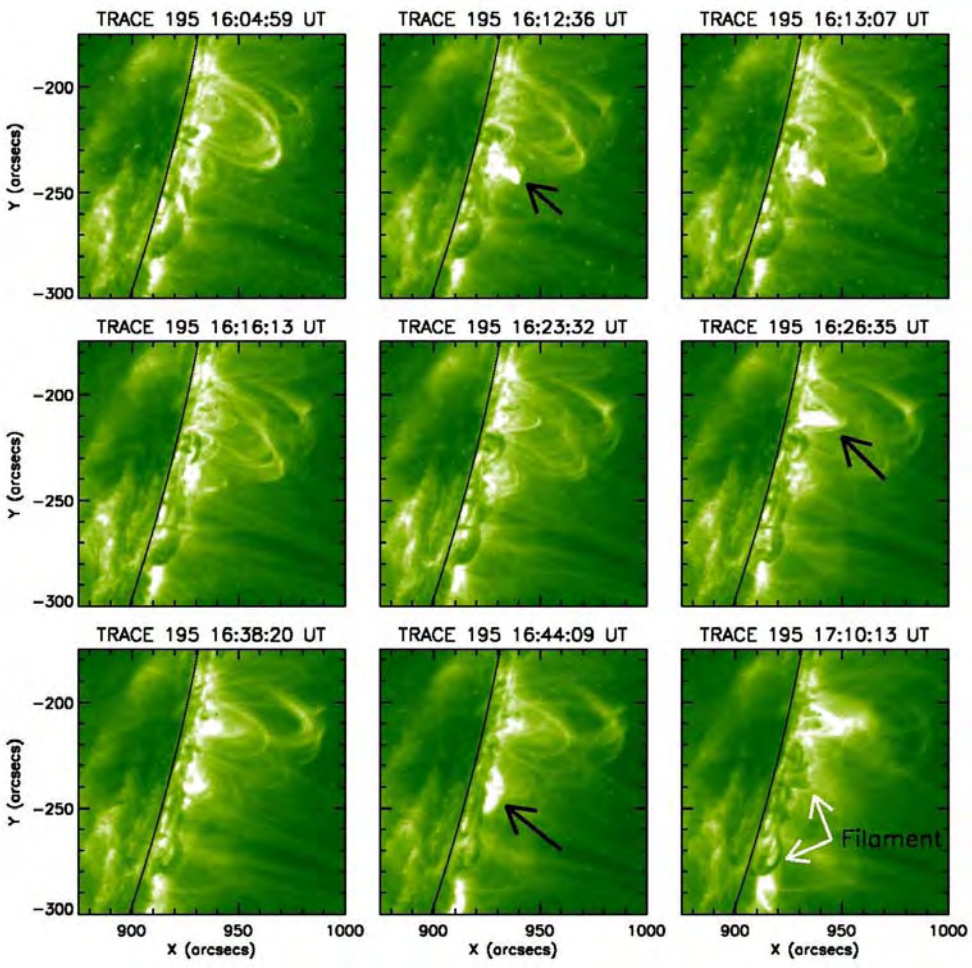

Figure 35. Sequence of TRACE 195 Å images showing three events of localized magnetic reconnection during the pre-flare phase in the form of confined flares (indicated by black arrows). The filament undergoes fast rise after the precursor events (indicated by white arrows in the last panel).

Rapid formation and disappearance of a filament barb

Barbs appear as feet of solar filament jutting from the side of the filament spine and anchored into the photosphere. In order to understand the role played by barbs in stability, activation and subsequently eruption, we carried out observations of filaments in May and August 2010 using the Dutch Open Telescope (DOT) situated at La Palma, Spain. Doppler images were recorded in H_α in a region about 110 x 110 arc sec^2 in area, at a cadence of 30 seconds. We analysed one such filament that showed an activated barb on 20 August, 2010 (Figure 36). The filament developed a new barb in 10 minutes which disappeared within the next 35 minutes. Such a rapid formation and disappearance of a filament barb is unusual, and has not been reported earlier. The offline image restoration technique of speckle reconstruction was applied to obtain diffraction limited images. Line-of-sight (LOS) velocity maps were constructed from the H_α Doppler images of the target filament. From this, we could observe flows in the filament spine moving towards the barb location prior to its formation, and flows in the barb towards the spine during its disappearance, with an approximate velocity of 10 km/s. The occurrence of these flows in proximity to the formation and disappearance of the barb suggests that they were responsible for the observed dynamics of the barb. The variation of magnetic flux in this duration as observed using HMI-SDO data supports the view that barbs are rooted in minor magnetic polarity. Our analysis shows that barbs can be short-lived and formation and disappearance of the barb was associated with cancellation of magnetic flux.

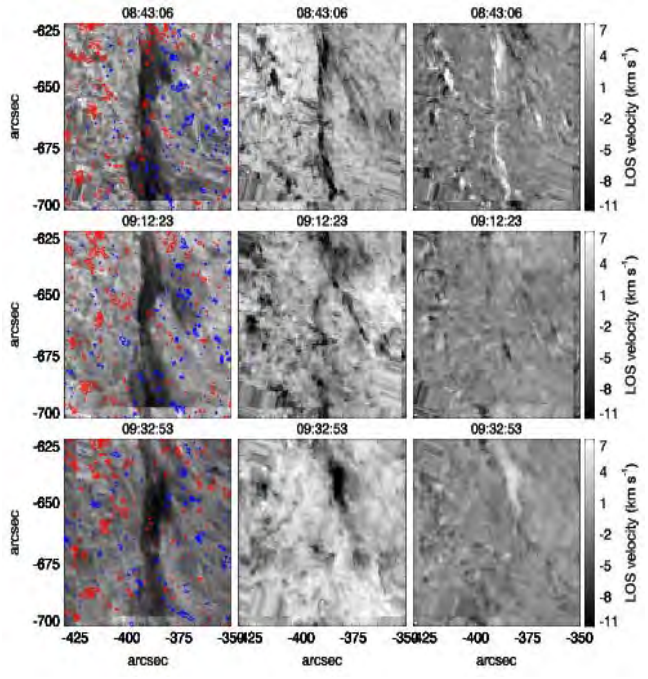

Figure 36: Time series of images used to study the filament barb on 2010 August 20. Left: Overlay of LOS magnetograms from HMI/SDO on H_α line centre images from DOT. Red indicates positive polarity, and blue indicates negative. Middle: Images in the blue wing of H_α Right: LOS velocity maps created from images in three line positions along the H_α line. All the axis coordinates are in terms of arc-sec from the Sun centre.

(Anand Joshi and Nandita Srivastava)

Tracking of CMEs in the inner heliosphere using J-maps:

The kinematics and dynamics of coronal mass ejections (CMEs) in interplanetary medium particularly along the Sun-Earth line is a topic of significant interest to solar terrestrial physics community. Though we have many statistical and empirical models to know the propagation profiles of CMEs in between the sun and earth but all these models are based on comparison of data taken at two points - near the sun as CME and near the earth as ICME. The identification of ICMEs near the earth is not straightforward because there is no single or combination of adequate signatures. Therefore, for a better understanding of these issues we plan to track the CMEs from near the sun to beyond 1 AU along the suitable position angle, particularly in the sun-earth line for geoeffective events. For this purpose, we

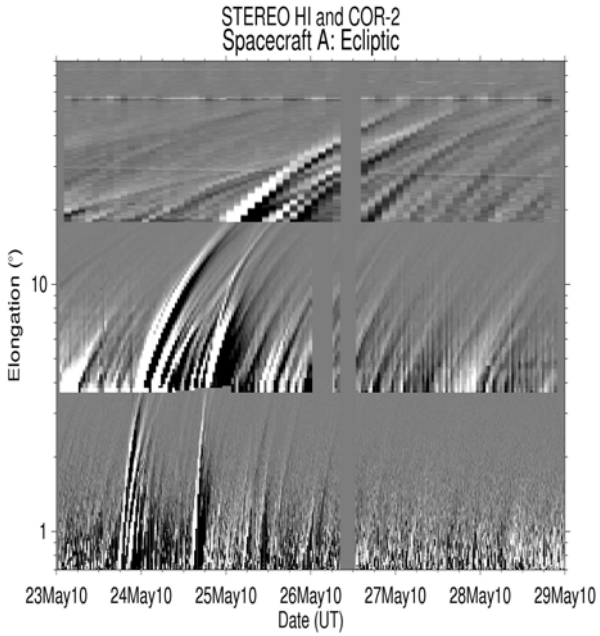

Figure 37: J-map constructed using running difference images from COR2, HI1 and HI2 instruments along the ecliptic plane for STEREO-A spacecraft. The y-axis shows the elongations angles plotted in logarithmic scale while the x-axis shows the time. Two features starting around 19:00 UT on 23 May 2010 and at 14:30 UT on 24 May, 2010 are coincident with the two CMEs and can be identified up to 50 degree elongation angles.

have used images from coronagraph COR2 and Heliospheric Imagers HI1 & HI2 instruments onboard STEREO. These instruments provide coverage over solar elongation angle from 0.7 to 88.7 degrees at the viewpoints of two spacecraft. To track the CMEs in the inner heliosphere, we constructed time elongation map (J-map) using the tools available in SECCHI software library distributed as part of the SolarSoft package. We constructed J-maps for the CMEs of 23-24 May 2010 as shown in Figure 37. The purpose of this study is to understand the propagation of CMEs, their arrival time, testing and also refining the existing models of CME propagation profiles. Our ongoing study will not only improve the understanding of evolution of CMEs in heliosphere but also of CME-CME interactions.

(Wageesh Mishra and Nandita Srivastava)

In-situ spacecraft observations of solar filament plasma at 1AU

Coronal Mass Ejections (CMEs) associated with solar filaments cause gigantic clouds of solar plasma to leave Sun into heliosphere, causing intense geomagnetic storms. In interplanetary medium, these structures maintain their three part similarity to CMEs and are termed as Interplanetary Coronal Mass Ejections (ICMEs). In rare cases, when sampled in-situ by spacecraft, the presence of dense, cold ejecta is observed in ICMEs which is believed to be associated with erupting filaments. This filament plasma retains its "frozen-in" compositional, magnetic and thermal properties and provides a unique way to investigate the environment of their origin. We studied two cases of observed filament plasma embedded in ICMEs; one related to a flare-associated eruptive filament (18 November, 2003) and other a quiescent filament eruption (1 August, 2010) at different phases of solar cycle by using plasma, magnetic and compositional parameters. Plasma properties such as low temperature, high proton and electron densities coincided with pressure balanced regions in magnetic clouds (Figure 38), along with compositional signatures such as depressed ion charge states, high ion and helium densities, and presence of He+ ions. These were used to locate filament plasma. In interplanetary medium, the magnetic cloud is identified by its high magnetic field strength, low plasma beta and changing elevation (θ) and azimuth (φ) angles. Depression in the magnitude of D_{ST} index gives the measure of associated geomagnetic storm. High proton and electron densities with low corresponding temperatures (shaded in yellow) indicate embedded filament plasma, within and outside magnetic cloud. The decreasing trend in bulk velocity (V) indicates the expansion of magnetic cloud. The studied ICMEs appear to have a mixture of cold and hot plasma with presence of He+ ions. The rarity of finding cold, low charge state ions at 1 AU as filament plasma suggests partial ionization of elements during transit through corona. The fact that filament material

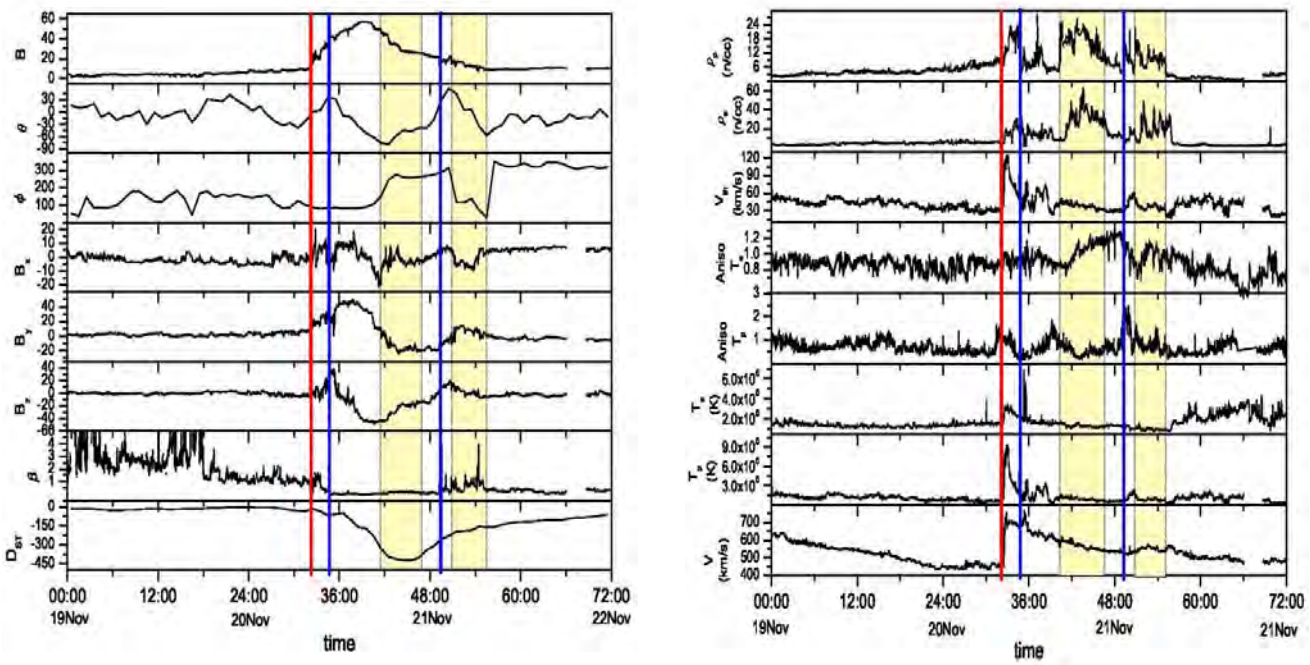

Figure 38. (Left panel) Interplanetary magnetic field parameters from November 19-22, 2003, obtained from Wind spacecraft and 1-hour averaged D_{ST} index. Red line indicates the shock while the region between blue lines is magnetic cloud resulting from 18 November 2003 CME. (Right panel) Proton and electron densities, proton thermal velocity (V_{th}), electron temperature anisotropy, proton temperature anisotropy, electron temperature (Te), proton temperature(Tp) and solar wind bulk velocity (V) obtained from Wind spacecraft.

is regularly observed in ICMEs at 1 AU but is not recognized as such because it is no longer distinguished as ionizationally cold.

This work was done in collaboration with Rahul Sharma, a student project trainee.

(Nandita Srivastava)

Evidence for Collapsing Fields in the Corona and Photosphere during the 2011 February 15 X2.2 Flare: SDO/AIA and HMI Observations

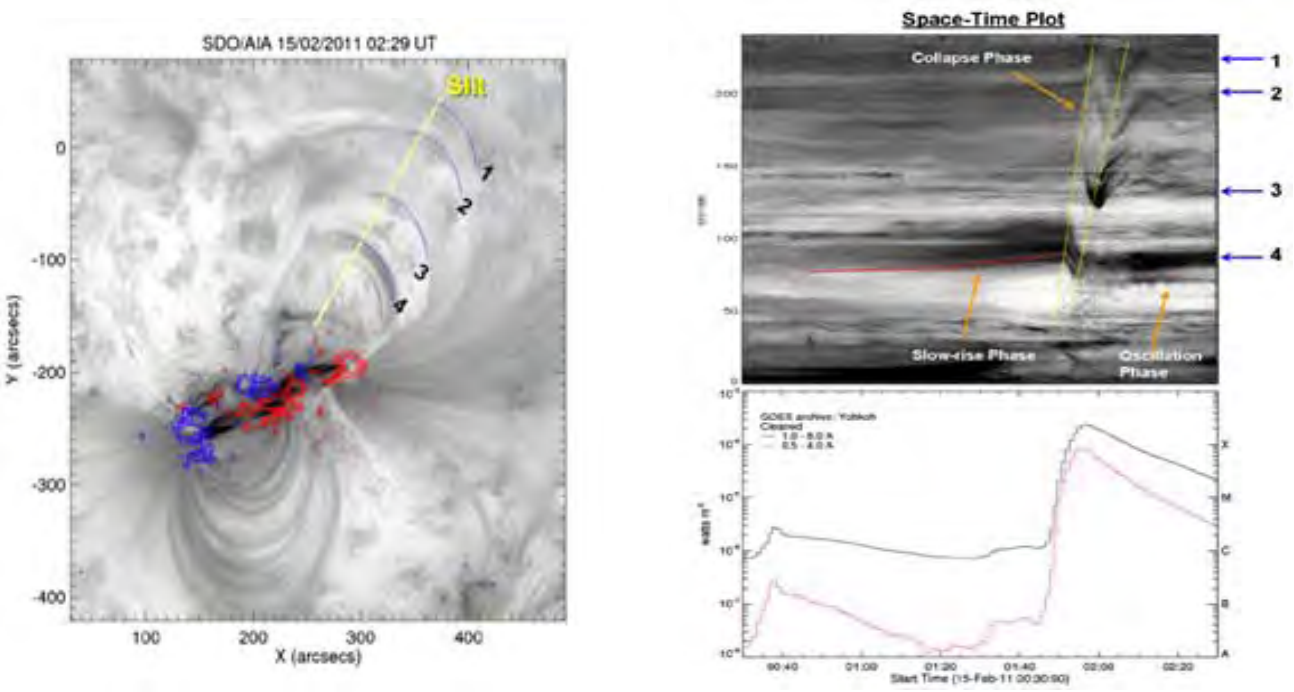

Figure 39. (Left) Inverted colour map of AR NOAA 11158 observed in Fe ix 171Å wavelength by the SDO/AIA instrument during 02:29 UT on 15 February, 2011. (Right) The space-time diagram corresponding to the slit. The positions corresponding to loops 1–4 are marked on the right side. The three phases of evolution are marked and indicated by arrows. The bottom panel shows the soft X-ray light curve observed by the GOES satellite.

We use high-resolution Solar Dynamics Observatory (SDO)/Atmospheric Imaging Assembly observations to study the evolution of the coronal loops in a flaring solar active region, NOAA 11158 (Figure 39, left). The loops marked 1–4 are studied for temporal evolution and are highlighted by blue curved line segments. The line contours at 500 and 1000 G levels of the longitudinal magnetic field observed by the SDO/HMI instrument are overlaid in blue (red) colors, representing negative (positive) polarity, respectively. The yellow line marks the position of the artificial slit that is placed to sample the dynamics of the apex of the loops. We identify three distinct phases of the coronal loop dynamics during this event: (1) slow-rise phase: slow rising motion of the loop-tops prior to the flare in response to the slow rise of the underlying flux rope; (2) collapse phase: sudden contraction of the loop-tops, with the lower loops collapsing earlier than the higher loops; and (3) oscillation phase: the loops exhibit global kink oscillations after the collapse phase at different periods, with the period decreasing with the decreasing height of the loops (Figure 39, right). The period of these loop oscillations is used to estimate the field strength in the coronal loops. Furthermore, we use SDO/Helioseismic and Magnetic Imager (HMI) observations to study the photospheric changes close to the polarity inversion line (PIL). The longitudinal magnetograms show a stepwise permanent decrease in the magnetic flux after the flare over a coherent patch along the PIL. We examined the HMI Stokes I,Q,U,V profiles over this patch and find that the Stokes-V signal systematically decreases while the Stokes-Q and U signals increase after the flare. These observations suggest that close to the PIL the field configuration became more horizontal after the flare. HMI vector magnetic field observations were used to quantify the changes in the field inclination angle which showed an inward collapse of the field lines toward the PIL by ~10 degrees. These observations are consistent with the "coronal implosion" scenario and its predictions about flare-related photospheric field changes.

(S. Gosain)

Rapid Disappearance of Penumbra-Like Features Near a Flaring Polarity Inversion Line: The Hinode Observations

We have studied the penumbra like features (PLFs) near a polarity inversion line (PIL) of a flaring region. The PIL is located at the moat boundary of AR NOAA 10960. The PLFs appear similar to sunspot penumbrae in morphology but occupy smaller area, about 6×10^7 km^2, and are not associated with sunspot or pore (Figure 40, left). We observed a rapid disappearance of the PLFs after a small C1.7 class flare, which occurred close to the PIL. The local correlation tracking (LCT) of these features shows presence of horizontal flows directed away from the end-points of the PLFs, similar to the radial outward flow found around regular sunspots, which is also known as the moat flow. Hard X-ray emission, coincident with the location of the PLFs, is found in RHESSI observations, suggesting a spatial correlation between the occurrence of the flare and decay of the PLFs. Vector magnetic field derived from the observations obtained by Hinode spectro-polarimeter SOT/SP instrument, before and after the flare, shows a significant change in the horizontal as well as the vertical component of the field, after the flare (Figure 40, right). The weakening of both the components of the magnetic field in the flare interval suggests that rapid cancellation and/or submergence of the magnetic field in PLFs occurred during the flare interval.

This work was carried out in collaboration of B. Ravindra, IIA

(S. Gosain)

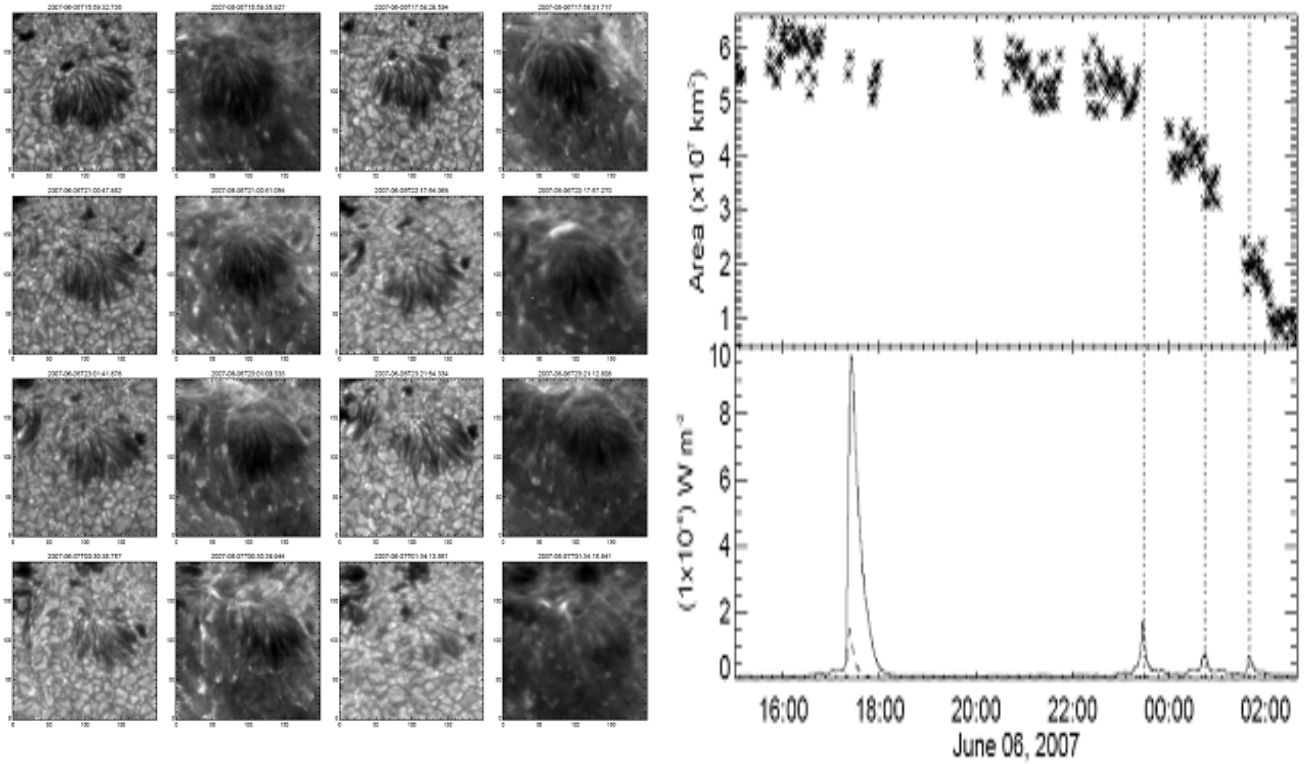

Figure 40. (Left) The temporal evolution of the PLFs is shown in sequence of G-band and Ca II H images alternatively. (Right) The temporal evolution of the area of PLFs is plotted along with GOES X-ray flux. The dotted vertical lines from left to right side represent the peak time of C1.7, B7.6 and B6.6 class flares respectively.

Analysis of a Fragmenting Sunspot using Hinode Observations

We employ high resolution filtergrams and polarimetric measurements from Hinode to follow the evolution of a sunspot for eight days starting on 28 June, 2007. The imaging data were corrected for intensity gradients, projection effects, and instrumental stray light prior to the analysis. The observations show the formation of a light bridge at one corner of the sunspot by a slow intrusion of neighbouring penumbral filaments. This divided the umbra into two individual umbral cores, the smaller of which gradually broke away from the parent sunspot nearly 2 days after the formation of the light bridge. Several aspects related to the evolution of the spot and its fragment were analyzed with the following main results: i) the intensity of the light bridge steeply increased from 0.28 to 0.7 I_QS in nearly 4 hr, followed by a gradual increase to quiet Sun (QS) values in 13 hr; ii) the increase in intensity was

accompanied by a large reduction in the field strength, with mean and minimum values of 900 and 300 G, respectively (Figure 41); iii) upflows, flanked by downflows, developed along the axis of the light bridge where the field was weakest; iv) the fragmentation was preceded by removal of the penumbra at the anchorage points of the light bridge and, after separation, the penumbra of the fragment decayed in about 34 hr; v) the penumbra in the parent regenerated when the inclination of the magnetic field at the penumbra-QS boundary became within 40 deg. from complete horizontal; vi) while the sunspot area exhibited a linear decay law, the decay rates varied during different phases of the evolution and similar trends were seen in the magnetic flux as well; vii) the fragment decayed much more rapidly following an exponential law; and viii) the fragment rotated around the parent umbra, with larger angular speeds prior to fragmentation. The significant weakening in field strength in the light bridge along with the presence of granulation is suggestive of strong convection in the sunspot which might have triggered the expulsion and fragmentation of the smaller spot. Although the presence of QS photospheric conditions in sunspot umbrae could be a necessary condition for fragmentation, it is not a sufficient one.

This work was done in collaboration with Luis R. Bellot Rubio of the Instituto de Astrofisica de Andalucia (CSIC), Apartado de Correos 3004, 18080 Granada, Spain, B. Ravindra of Indian Institute of Astrophysics, II Block, Koramangla, Bangalore - 560 034, India.

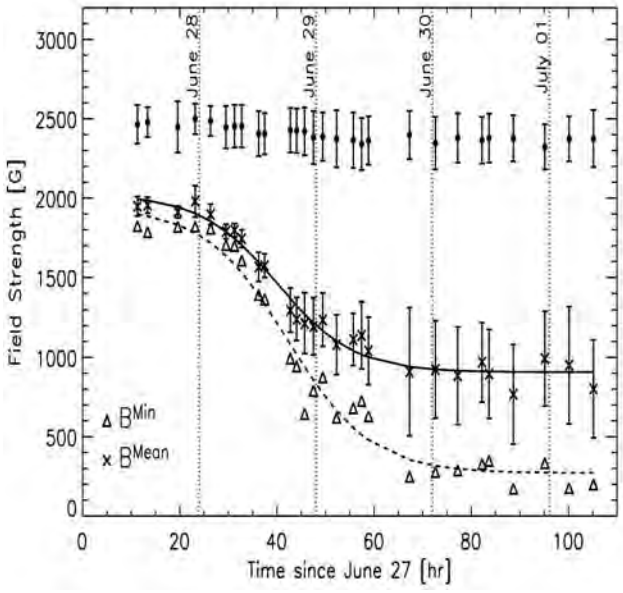

Figure 41 Evolution of field strength in the light bridge. The crosses and triangles represent the mean and minimum field strength of the region where the light bridge was formed. The vertical bars represent the rms fluctuations. The solid and dashed lines are Boltzmann sigmoid fits to the observed mean and minimum field strengths. The black circles correspond to the mean umbral field strength close to the LB.

(Rohan E. Louis, Shibu K. Mathew, A. Raja Bayanna and P. Venkatakrishnan)

Properties of Umbral Dots from Stray Light Corrected Hinode Filtergrams

High resolution blue continuum filtergrams from Hinode are employed to study the umbral fine structure of a regular unipolar sunspot. The removal of scattered light from the images increases the rms contrast by a factor of 1.45 on average. Figure 42 shows the improvement in image contrast and this renders identification of short filamentary structures resembling penumbrae that are well separated from the umbra-penumbra boundary and comprise of bright filaments/grains flanking dark filaments. Such fine structures were recently detected from ground based telescopes and have now been observed with Hinode. A multi-level tracking algorithm was used to identify umbral dots in both the uncorrected and corrected images which were subsequently tracked in time. The distribution of the values describing the photometric and geometric properties are more easily affected by the presence of stray light while it is less severe in the case of kinematic properties. Statistically, umbral dots exhibit a peak intensity, effective diameter, lifetime, horizontal speed and a trajectory length of 0.31 I_QS, 262 km, 10.3 min, 0.45 km/s and 283 km, respectively.

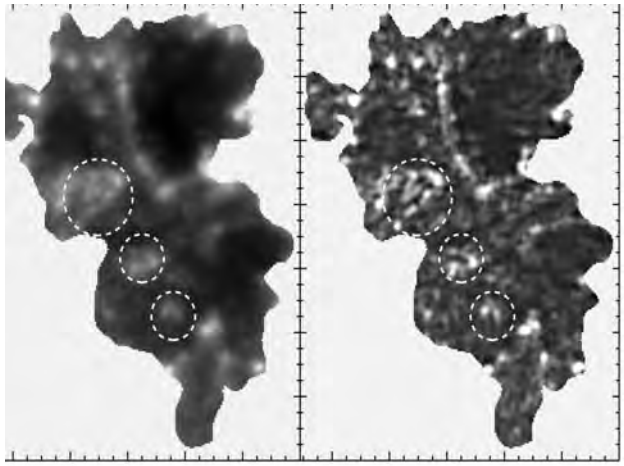

Figure 42. Improvement in image contrast after removal of stray light. (Left): Umbra before stray light correction. (Right): Stray light corrected image. Images in both the panels have been scaled identically. The white dashed circles enclose short filaments.

Umbral dots tend to appear and disappear from the same location on time scales of 45-50 min. Such sites are distributed evenly in the umbral region. The correction for scattered light in the Hinode filtergrams facilitates

photometry of umbral fine structure which can be related to results obtained from larger telescopes and numerical simulations.

This work was done in collaboration with Luis R. Bellot Rubio of the Instituto de Astrofisica de Andalucia (CSIC), Apartado de Correos 3004, 18080 Granada, Spain, Kiyoshi Ichimoto of Kwasan and Hida Observatories, Kyoto University, Yamashina-ku, Kyoto 607-8417, Japan, B. Ravindra of Indian Institute of Astrophysics, II Block, Koramangla, Bangalore - 560 034, India.

(Rohan E. Louis, Shibu K. Mathew and A. Raja Bayanna)

Numerical simulations of spontaneous current sheet formation in a superposed state of two linear force-free magnetic fields

We have carried out direct numerical simulation of an incompressible, viscid magnetofluid with infinite electrical conductivity with an objective to devise suitable initial value problems and explore the process of current sheet (CS) formation. We used an MHD version of the numerical model EULAG, originally developed to solve for geophysical flows. An interesting initial condition with observational significance is the magnetic field being a superposition of two linear force-free fields. The superposed B then supports a non-zero Lorentz force which eventually pushes the magnetic subvolumes to form CSs. For the simulations, we have used this superposed magnetic field and zero velocity as initial conditions. These numerical experiments are performed with 1283 uniform grid resolutions along with periodic boundary conditions. Figures 43 (a-b) illustrate the evolution of kinetic and magnetic energies for three different viscosities 0.004, 0.0055 and 0.0078 normalized to the initial total energy. The first peak in kinetic energy is formed as the initial acceleration of the magnetofluid by the non-zero Lorentz force gets arrested by viscosity. The magnetic energy shows a corresponding dip in magnitude. The onset of the second peak in kinetic

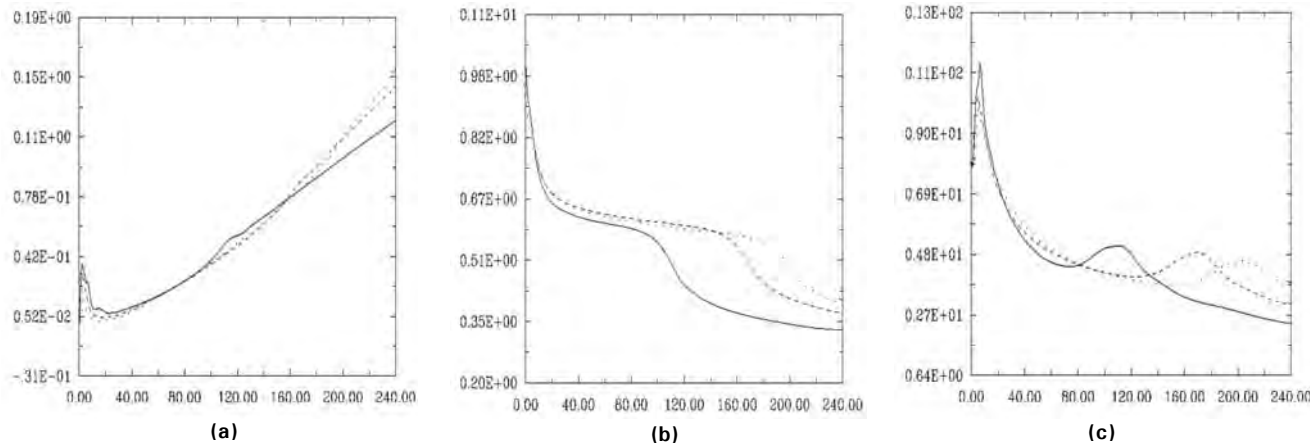

Figure 43. Temporal evolution of (a) normalized kinetic energy,(b) normalized magnetic energy and (c) normalized average current density for viscosities 0.004 (solid), 0.0055 (dashed) and 0.0078 (dotted).

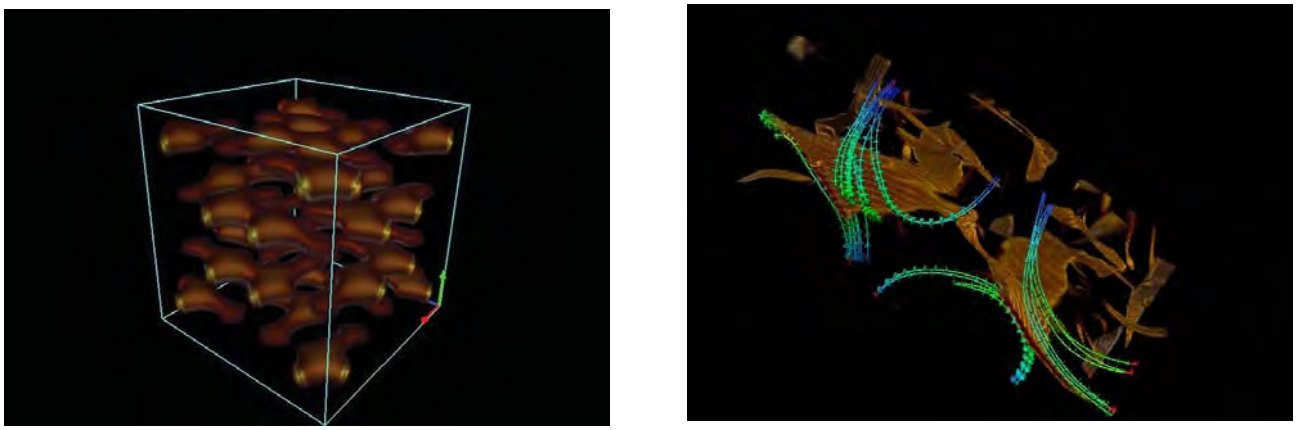

Figure 44. (Left) Direct volume rendering of current density at t = 0. (Right) Current sheets represented by surfaces and magnetic field lines across CSs at t = 100. The grid resolution is 128x128x128 and viscosity 0.004.

energy may be attributed to the formation of CSs by progressive pressing of magnetic subvolumes with oppositely directed field lines which eventually result in a numerically assisted reconnection. The second peak is formed as the accelerated magnetofluid is once again gets arrested by viscosity. The magnetofluid being more mobile for lesser viscosities, the second peaks in kinetic energies and the corresponding dips in magnetic energies are formed earlier in time for other viscosities as is evident. Figure (43c) depicts the history of average volume current density normalized to the initial total energy which reveals that the current density peaks up at almost the same time as the onset of the second peak in kinetic energy for relevant viscosities and hence strongly indicate the possibility of CS formation at t = 100. To further confirm this current sheet we have used a direct volume rendering of data for the volume current density as shown in Figure 44 for viscosity 0.004 which is distributed over a volume, and the expected CS at t = 100. It confirms the formation of CSs by showing the current density to be more localized in space in the form of surfaces with majority of magnetic field lines changing signs across them.

(Dinesh Kumar and Ramit Bhattacharyya)

Solar coronal loops as non force-free minimum energy relaxed states

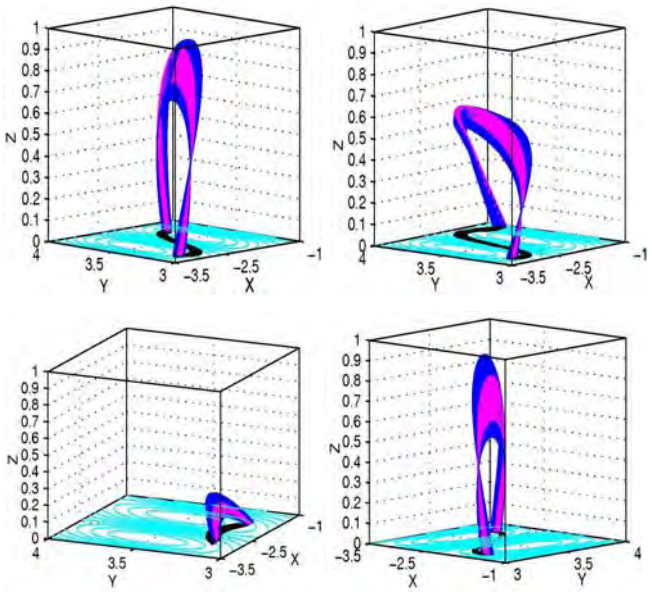

Figure 45. Three dimensional magnetic ribbons for (top left): a non force-free state with positive twist. (top right) force-free state with positive twist. The projections on the xy plane represent the forward sigmoidal structure. (bottom left) potential state with zero twist. (bottom right) a non force-free state with negative twist. The projection on the xy plane represents the backward sigmoidal structure.

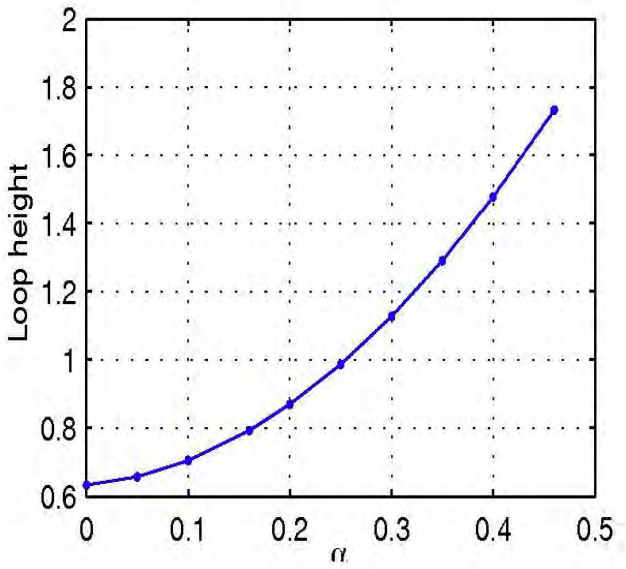

Figure 46. Loop height variation of non force-free states.

The tenuous, hot solar corona is characterized by million degree Kelvin temperature, ambient magnetic field of 10-15 Gauss and density - 10^7 m^{-3} , which renders the coronal gas as a near-ideal magnetofluid. The predominant structures seen in the corona are of the form of loops on the solar surface. The geometry of these loops along with their dynamics is believed to play a major role in various eruptive phenomena like the solar flares, CMEs and may also be responsible for coronal heating. We consider coronal loops as two-fluid minimum energy relaxed states with properly defined ion and electron generalized helicities as constraints. The corresponding Euler-Lagrange (EL) equations are of double curl in nature and couple flow to the magnetic field. Figure 45 (a-c) depict magnetic field lines for a non force-free, force-free and potential field, respectively, as solutions of the same EL equation obtained through the variational principle. These field lines are plotted in the form of magnetic ribbons for direct visualization of the twist. As expected, the magnetic ribbons corresponding to the potential field have zero twist. The projections of the non force-free and force-free ribbons on the x-y plane generate sigmoidal structures; further confirming the twisted nature of the field lines. Figure 45 (d) illustrates an example of non force-free state with the twist being negative in direction but the same in magnitude as in the ribbons of (a-c). The corresponding projections of magnetic ribbons on the x-y plane generate backward sigmoids confirming the opposite chirality of the field lines. It is also consistently found that the more non force-free loops attain larger heights as shown in figure 46 and is in qualitative agreement with the general notion that the upper corona is non force-free.

(Dinesh Kumar and Ramit Bhattacharyya)

The coronal magnetic field in linear force-free approximation

We have explored different topological features of magnetic field lines based on a linear force-free description with the objective to develop a proper boundary value problem (BVP) applicable to a half-infinite system like the hot solar corona having infinite electrical conductivity. The necessity of a proper formulation of the BVP arises from the fact that the magnetic energy for a half-bounded linear force-free field is known to diverge at infinity whereas the magnetic field remains finite. We present preliminary results for a pilot set of calculations where the linear force-free equation is solved in a spherical shell with an artificial magnetic flux surface (a surface tangential to magnetic field lines) posing as an outer boundary of the corona while base of the corona being represented by an unit sphere. The solutions are obtained in terms of spherical harmonics Ylm, in usual notations. Figure 47 (left) depicts the projections of an axisymmetric set of magnetic field lines characterized by $l=1$ and $m=0$ on the x-z plane on which the unit circle represents the projection of the unit sphere, with continuous and dotted lines being the positive and negative contours of the radial component of magnetic field. The obtained field lines are in general agreement with the observed global bipolar field of the Sun. More locally

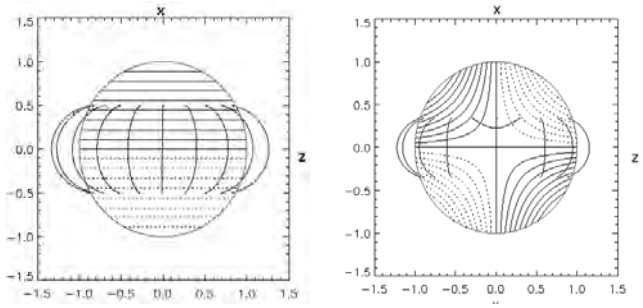

Figure 47. Projections on the x-z plane of (left) axisymmetric ($l=1$, $m=0$) bipolar magnetic field lines. (right) non axisymmetric ($l=2$, $m=1$) field lines.

structured field lines are obtained as we deviate from this axisymmetric configuration and allow for three dimensional field lines. Figure 47 (right) represents one such example for $l=2$ and $m=1$. The field lines are more localized in comparison to the axisymmetric case and qualitatively represent a more structured corona. Future work in this direction includes a parametric study of different topological features of field lines represented by higher order spherical harmonics and the replacement of the outer artificial boundary of the corona with a physical boundary.

This work was carried out in collaboration with Isha Bhattacharya, Udaipur.

(Ramit Bhattacharyya and P. Venkatakrishnan)

Making of sunspots catalogue from SOHO/MDI continuum images

Sunspots identification and characterization including location, area, lifetime, brightness, etc. are required for a quantitative study of the dependence of solar cycle on the above parameters. Continuum images for the solar cycle 23 and the initial stages of cycle 24 are available from SOHO/MDI, spanning from 1996-2011. These data sets were used for making a sunspot catalogue. First the data is pre-processed to remove limb darkening, stray-light and then flat-field correction is applied. After retrieving the corrected images, detection of sunspots were carried from each image. We have developed a new procedure for automatic detection of sunspots from full-disk continuum intensity images obtained from SOHO/MDI, which can also be applied on high resolution images from SDO/HMI. Our procedure is based on an active contour method using level set formulation. We implemented the "Selective Binary and Gaussian Filtering Regularized Level Set" method for sunspot detection. This method is computationally simple and fast. The algorithm is executed in two levels, initially for the detection of the umbra and then for the penumbra, with different parameter settings. The developed procedure can give all parameters of sunspots for example, location, centre of gravity, area, mean, minimum and maximum intensities of umbra and penumbra. Figure 48 shows an example of one of the images in which the automatic sunspot detection is executed. We are in the process of comparing our data catalogue, with similar ones compiled using other methods. This catalogue will used for our proposed study of solar cycle dependence on various sunspot parameters.

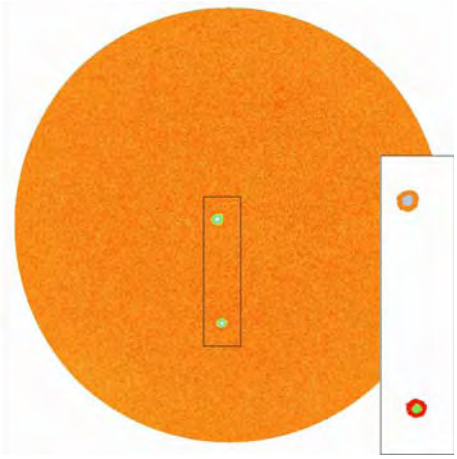

Figure 48 MDI full disk continuum image and the detected sunspot umbrae and penumbrae (inset) using the newly developed algorithm.

(Suruchi Goel and Shibu K. Mathew)

Hα Doppler Imager for Solar Observations

Filaments end their lifetime on the Sun in eruptions. However, the dynamics of such erupting filaments and the conditions leading to their eruptions are not well understood. Eruptions of solar filaments are known to be associated with coronal mass ejections (CMEs) which are important for space weather. A CME, if suitably directed, cause geomagnetic storm at the Earth. To address these issues, we have developed a new telescope named the Há Doppler Imager in the USO premises. This telescope would image the full solar disc at several positions along the Hα line required to determine Doppler or the line-of-sight velocities of the filaments. We can thus not only observe the changes in filament structure in the plane of sky from the Há line centre image, but also the flows within the filament during its activation stage. These observations will be useful in issuing forewarning of an erupting filament.

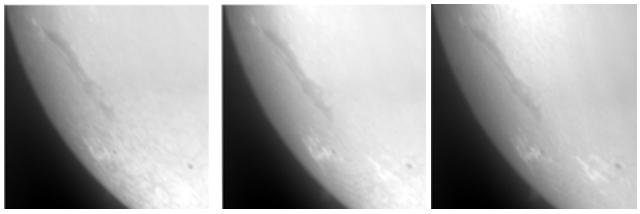

Figure 49: Hα images of a solar filament close to SE limb near NOAA 11354 in red wing (left), line centre (centre), and blue wing (right). The images in red and blue wings are separated from the line centre by 218 mÅ.

The main components of this telescope are a 0.2 Å passb and voltage-tunable Fabry-Pérot etalon (FP) and a 1 Å passband pre-filter. The FP and pre-filter are kept inside constant temperature ovens, as their refractive indices are sensitive to temperature. By applying suitable voltage to the FP, it can be tuned to any desired position along the Hα line. The calibration of the FP was carried out using a spectrograph set up in the optics laboratory of the Coudé telescope. We carried out sample observations from the telescope from September to November, 2011. Doppler scans were obtained by applying voltage to the FP. A filament observed on 18 November, 2010 is shown in red wing (left), line centre (centre), and blue wing (right) in Figure 49.

(Shibu K. Mathew, Anand D. Joshi, Nandita Srivastava and Sudhir K. Gupta)

A Narrow band imager for Multi-application Solar Telescope: Calibration of Fabry-Perot etalon

A narrow band imager is being developed for Multi-Application of Solar Telescope (MAST) for near simultaneous narrow band observations of the solar atmosphere at different heights. The heart of the system is two Fabry-Perot (FP) etalons working in tandem. The substrate of the etalons is made of Lithium Niobate electro-optic crystal, the electro-optic property of the crystal is the used for tuning the etalons for different wavelengths. Combining with two interference filters centred at 617.3 nm and 854.2 nm, the etalons are expected to give a spectral resolution of 54 mA (R = 114 k) and 104 mA (R = 82 k) at the above wavelengths, respectively. A littrow spectrograph was set up to calibrate the FP etalons. A f#15 beam from a Coude solar telescope of Diameter 15 cm is used to feed the spectrograph. A grating with 1200 lines/mm, blazed in second order with an effective diameter of 75mm gives a spectral resolution of 34 mA at 617.3 nm. The optical arrangement before the spectrograph slit (Figure 50) allows us to obtain both the channel spectrum and he solar spectrum simultaneously, making it easy to locate the channel spectrum with reference to the spectral line, and ascertain the wavelength tunability of the filter

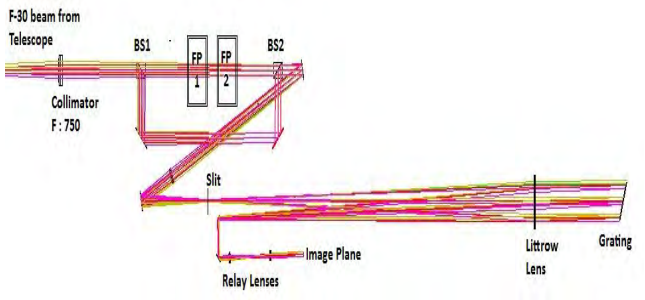

Figure 50: Schematic of the optical set-up used in calibration of the FP system. Transmitted beam from beam splitter (BS1) passes through the FP system, while the reflected beam by-passes the FP system via folding mirrors and then re-enters into main path through the second beam splitter (BS2). In the imaging plane both the solar spectrum and the channel spectrum are observed. FP1 and FP2 are calibrated separately and then used in tandem to obtain the maximum FSR and minimum FWHM.

during the application of voltage across the etalon wafer. Calibration of the FPs is planned for the two wavelengths. Free spectral range (FSR) obtained for FP1 and FP2 are 0.351 nm and 0.134 nm respectively, where as FSR of the FP1 and FP2 used in tandem is 0.667 nm. Voltage tuning rate of FP1 and FP2 are 0.0367 nm/kV and 0.0152 nm/kV respectively. Voltage tuning curves of FP1 and FP2 are shown in Figure 51. The results are in agreement with the theoretically predicted values. As it should be in the case of narrow-band imager, FP1 and FP2 were configured in tandem to scan across the 617.3 nm solar spectral line profile. Voltages to FP1 and FP2 are applied in such a way that the transmission peak in both the FPs coincide for each applied voltage steps. These steps are computed from the voltage tunability curves.

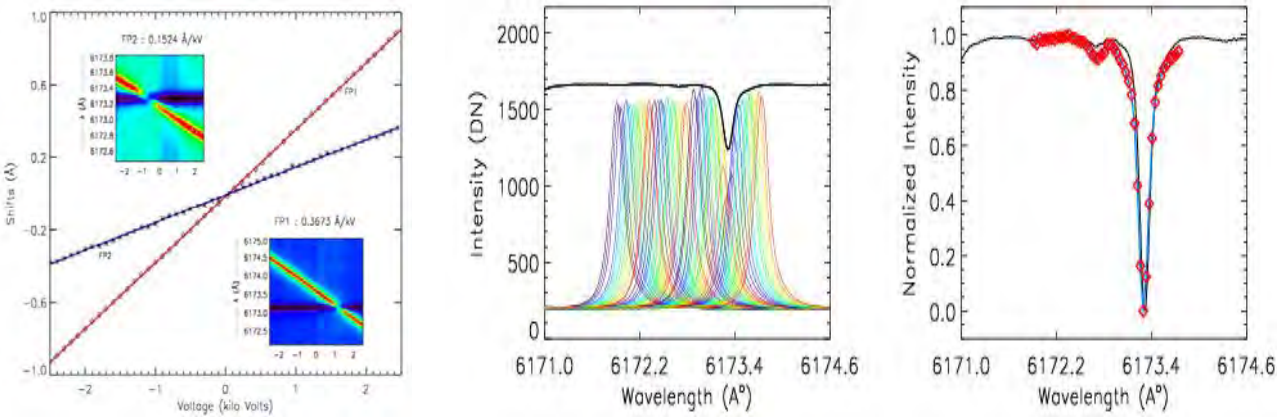

Figure 51. (Left) Voltage tuning curves of FP1 (red line with boxes) and FP2(blue line with asterisk) for wavelength 617.3 nm. Images in the bottom right corner and the top left corner, show the crossover of FP1 and FP2 channels across the line 617.3 nm solar spectral line, while applying voltages ranging from -2.5 kV to 2.5 kV, respectively. (Right) Line profile is scanned by FP1, FP channel at different voltages (colored lines) are over plotted on the spectral line (black solid line). Reconstructed line profile is shown on the right (red boxes) along with the original spectral line.

(A. Raja Bayanna, Shibu K Mathew, Rohan E Louis, Sudhir K. Gupta)

Planetary Sciences and PLANEX Program

The Planetary Sciences Division focuses on isotopic investigations of meteorites to understand processes and chronology of the early Solar System, and the nucleosynthesis and stellar environments at the birth of our Solar System. The PLANEX Program aims at the understanding of surface features and processes on Moon and Mars using remote sensing data from lunar and Mars missions. Another important objective of the PLANEX Program is to develop science payloads for planetary missions to Moon and Mars.

During the previous year, several new research programs have been initiated. One of these aims at a systematic geochemical investigation of water and volatile species in lunar apatite grains using the PRL NanoSIMS. Another investigation aims at identification of impactor signatures in Lonar crater glass using noble gas isotopes. Mo isotope composition of Permo-Triassic boundary sediments from Spiti Valley in Himalaya has been used to investigate redox conditions existing during the Permo-Triassic (P-T) boundary event. Analysing remote sensing data from Mars missions, ground based observations of asteroids and comets and laboratory studies of Mars analogues are the other important new initiatives. An account of these activities is summarised in this report.

Late irradiation scenario for production of short lived nuclides

In our continuing effort to understand the contributions of stellar nucleosynthesis and particle irradiation processes to the short lived radionuclides (SLRs) identified in the early solar system, we have taken up the study of ^{36}Cl ($t_{1/2}$ = 0.3 Myr) both by experimental and computational approaches.

Various irradiation models have been discussed for the production of short-lived nuclides present in the early Solar System. The major difference in the models discussed is the location where the production of SLNs is assumed to take place. Whereas one model deals with an astronomical setting of X point region of the X wind model located at ~0.06 AU, the other considers irradiation at 2-3 AU distance (asteroidal region) away from the Sun.

We have estimated the relative abundance of ^{36}Cl, ^{10}Be and ^{26}Al in the early solar system, due to SEP interaction with a hypothetical nebular material of sodalite composition at asteroidal distances. The $^{26}Al/^{27}Al$ value was constrained to be ~ 6×10^{-6} (as observed in the wadalite sample). The SEP flux is adjusted to match the observed initial $^{36}Cl/^{35}Cl$ ratio in wadalite ~2×10^{-5}, for all the irradiation durations. We assumed the Be concentration to be 100 ppm in sodalite. Figure 52 indicates the irradiation product relative to ^{36}Cl, and initial solar system for spectral exponent (γ) = 2 with the SEP power law [$dN/dE = kE^{-\gamma}$]. A flatter spectra (γ = 2) for SEP interacting with a sodalite composition target seems to give pretty consistent production of ^{26}Al as seen in grossular along with ^{36}Cl for shorter irradiation time scales. ^{10}Be is over produced for

any irradiation timescale due to high abundance of ^{16}O which is the main target for Be, and needs to be checked experimentally.

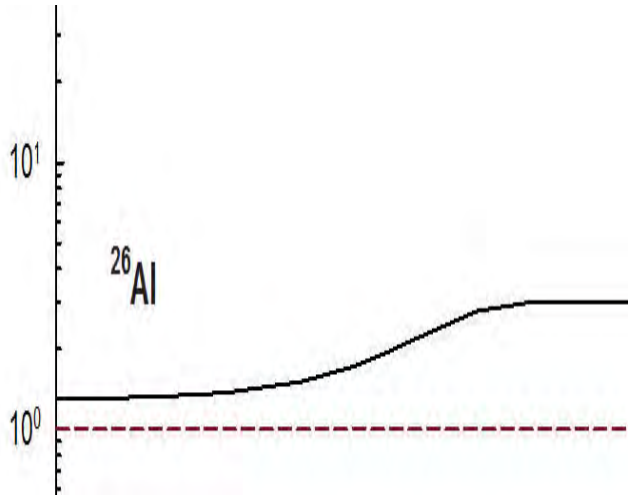

Figure 52. Ratio of calculated to measured solar system initial ratios of ^{36}Cl, ^{10}Be relative to their reference isotopes, by solar energetic particle (SEP) interactions plotted as a function of irradiation duration, and constrained by the observed $^{26}Al/^{27}Al$ found in wadalite. The irradiated objects were assumed to be of sodalite composition following a power-law distribution in size ($dn/dr \alpha r^{-4}$), with the spectral exponent of the SEP, $\gamma = 2$. The SEP fluence was adjusted to produce an initial $^{36}Cl/^{35}Cl$ ratio of 2×10^{-5} for all irradiation durations.

(K. K. Marhas)

Al-Mg systematics in CV CAIs

The systematics of the Mg isotopic composition of CAIs (calcium-, aluminum –rich inclusions), chondrules and Earth show that ^{26}Al was homogenously distributed (at ±10% level) in the early solar system, with a well established initial canonical value ($^{26}Al/^{27}Al \sim 5 \times 10^{-5}$). Thus, ^{26}Al is considered to be a reliable chronometer for dating processes in the early solar system. We have analysed the Al-Mg systematics in sixteen anorthite and melilite grains present in twenty four coarse grained CAIs using SIMS (Secondary Ion Mass Spectrometer). Eleven CAIs possess initial $^{26}Al/^{27}Al$ close to canonical value within error limits. The initial $^{26}Al/^{27}Al$ value in these CAIs indicates absence of any recrystallization since the incorporation of ^{26}Al in them. Based on Al-Mg systematics, the selected CAIs were further analysed for SLRs ^{7}Be and ^{10}Be, which are pure irradiation products. Presence of ^{7}Be and ^{10}Be in CAIs would provide an insight into the energetic environment of the proto-Sun during the formation of the Solar System.

(Y. Kadlag and K. K. Marhas)

Identification of impactor signatures in Lonar crater glass through noble gas isotopes

Identifying the impactor helps in the understanding of the crater formation process and possibly the nature, origin and flux of the impactor material. Earlier attempts have focused on siderophile elements (Co, Ni, PGEs) and Os and Cr isotopic ratios in the identification of the impactor. Here, we present the noble gas results from Lonar glasses to demonstrate the potential of noble gas isotopes as unmistakable tracers in the identification of meteoritic signatures in them. In this study, we have analysed 3 tektite like and one impactite like glasses from Lonar, for all the noble gases.

The noble gas isotopic compositions in the surface reservoir samples of Earth are expected to be a mixture of trapped (atmospheric) and in situ produced (radiogenic and nucleogenic) components. In addition, one might expect to find remnants of gases from the target material (depending on the degree of degassing), and in exceptional cases signatures of the impactor. So far there is no report of impactor noble gas isotopic signatures in impact glasses, and the present work is first such report. Meteorites have specific trapped ($^{40}Ar/^{36}Ar$), radiogenic ($^{129}Xe/^{132}Xe$) and cosmogenic ($^{21}Ne/^{22}Ne$) isotopic compositions that are radically different from terrestrial ratios, and cannot be mimicked by any known terrestrial processes. Our finding of these signatures could only be explained as due to the trapping of a solid piece of the impactor, which is either partially degassed or undegassed, in to the impact glass. The absolute excess of ^{129}Xe due to meteoritic contribution ranges from 0.02 to 2.0 (in 10^{-12} ccSTP/g glass sample) in the samples analysed here. It is possible to quantify the impactor material, with some reasonable assumptions, through the excess radiogenic ^{129}Xe, due to its better retention among the three meteorite specific isotopic excesses observed in the glasses, and we estimate up to about 2 wt. % meteorite matter in the glass with maximum observed ^{129}Xe excess.

(S.V.S. Murty and P.M. Ranjit Kumar)

Decoupling the nitrogen components in ilmenites from lunar meteorite Y983885

Moon is indigenously poor in volatiles, however lunar surface materials are rich in volatiles (noble gases and N). Due to the lack of atmosphere and global magnetic field, the lunar surface is directly exposed to solar wind (SW) as well as cosmic rays continuously. The solar wind is deposited on the surface of the material exposed on the Moon. Though noble gas amounts are accounted by solar

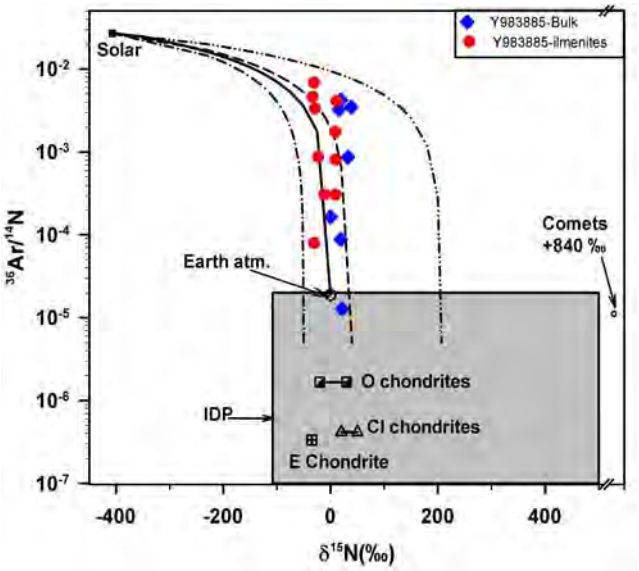

Figure 53: Correlation diagram between $^{36}Ar/^{14}N$ and $\delta^{15}N$. Grey colour box represents the range for IDPs. Values of Solar and ranges of Enstatite, CI Ordinary chondrites are also shown. Thick line represents the two component mixing between solar and Earth atmosphere. Dash-dot line is fit to one end of IDPs and solar, whereas dash-dot-dot line is fit to another end of IDPs and solar. The dashed line is the fit taken $\delta^{15}N = +40‰$ for IDPs.

wind source, N is over abundant by an order of magnitude. Also, nitrogen isotopic composition in lunar surface samples does not match SW value [$\delta^{15}N = -407$ ‰] and clearly indicates non-solar contributions. We have recently developed a laser heated gas extraction system, coupled to the multi-collector noble gas mass spectrometer, capable of analysing individual mineral grains of ~ 100 μm size simultaneous for N and noble gases. We have analysed individual ilmenite grains from lunar meteorite Y983885 to characterise the nature of the non-solar N found in lunar surface samples. Our data (Figure 53) reveals that nitrogen in these samples is a mixture of solar and a non-solar component with positive $\delta^{15}N$. In the plot of $^{36}Ar/^{14}N$ Vs. $\delta^{15}N$ the data fits better on the mixing trend between solar wind and IDPs, testifying them as the source of non-solar N.

(R.R. Mahajan and S.V.S. Murty)

Geochemical fractionation of elements between impact-melt and spherule from Lonar Crater, India

The Lonar crater (~570 ± 47 ka old), India, is one of the few known terrestrial asteroid impact craters that was excavated on basaltic target-rock and therefore comparable to those formed on the planets in the inner-solar system. The impact and impact-looking glasses occurring in and around the Lonar crater mainly fall under two fundamental petrographic classes: mm-sized impact-spherules and cm-sized (~≤1 to 30 cm) impact-melts that generally show a restricted occurrence outside the crater rim within the ejecta blanket. At the time of formation of impact-melt and spherules from the same target rock during the impact processes, geochemical fractionation occurs between these two glassy end products and it is imperative to understand the fractionation processes. The bulk of the glass appears as uniform brown, although some colourless and darker brown schlieren and partially melted mineral inclusions also occur (Figure 54a). Pyroxenes are mostly fractured due to shock while magnetite is the least affected mineral (Figure 54b). Spherules are mostly aerodynamic, spherical and often ellipsoidal in shape. Different sizes of spherules are considered to examine the chemical variation, e.g. few mm to up to 50 mm.

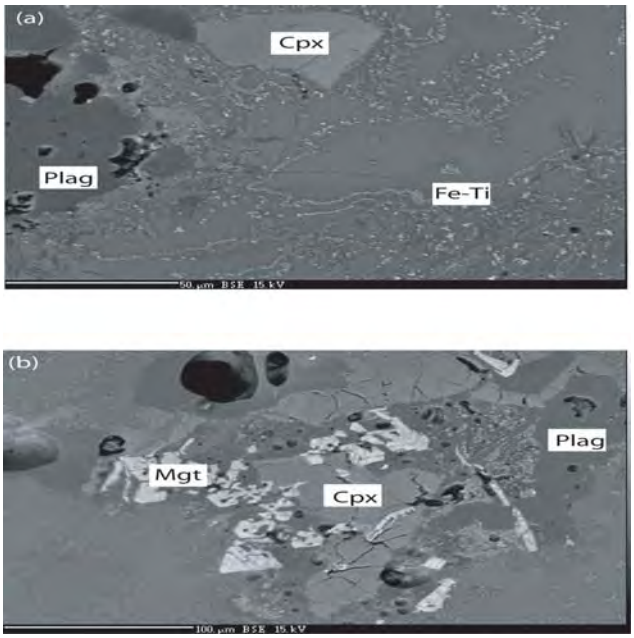

Figure 54 (a) BSE showing trains of titaniferous magnetite crystals in impact-melt rock (Impactite). Plag: plagioclase, Cpx: clinopyroxene, Fe-Ti: Fe-Ti oxides; (b) BSE showing plagioclase (dark grey, Plag), fractured clinopyroxene (light grey, Cpx) and magnetite (white, Mgt) in impact-melt rock (Impactite).

BSE images of the spherules look homogeneous, glassy, except in a few cases inclusion of plagioclase and magnetite are found. Based on petrography, i.e. presence of plagioclase melt, fractured pyroxene grains and undisturbed Fe-Ti oxides in shocked lonar basalt, it is ascertained that present impact-melt underwent third stage of shock metamorphism. In addition, the low total for Fe-Ti oxides of impact-melt suggests different stages of oxidation. Plagioclase-melts are relatively SiO_2 rich in the highest stage of shock metamorphism compared to unshocked

plagioclase. This is also supported by the mineral chemical data since plagioclase glasses display a higher proportion of SiO_2 (52-54 wt%) as compared to unshocked plagioclase (51 wt%). This process may also account for marginal enrichment of SiO_2 in lonar impactite. Differential elemental enrichment as reflected between core and rim of the spherule suggests geochemical fractionation.

(D. Ray)

Water in lunar apatites

The moon is thought to have indigenous water chemically bound to minerals within lunar rocks. Recent studies on lunar volcanic glasses and apatite [$Ca_5(PO_4)_3(F,Cl,OH)$] obtained limits on the indigenous volatile (CO_2, H_2O, F, S and Cl) contents of the most primitive basalts in the Moon. These works confirm minimum water contents of their lunar source region to range from 64 ppb to 5 ppm. The presence

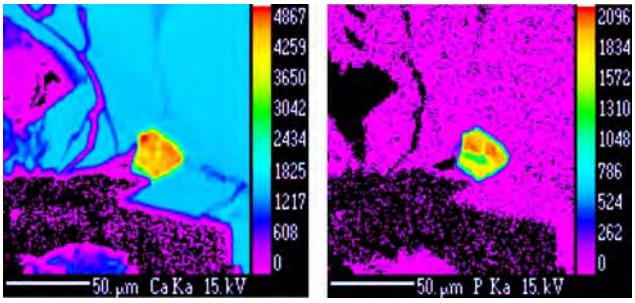

Figure 55: Calcium and Phosphorous X-ray images show the hot spots of apatite in Lunar basalt 15555,199.

of hydroxyl in a number of different types of lunar rocks indicates that water may be ubiquitous within the lunar interior, potentially as early as the time of lunar formation. Apatites are in the range of 5-50 μm in the mare basalt, 15555,199, occurring typically in association with Fe-rich olivine (fayalite), pyroxferroite, Fe-Ti oxide, Ba-rich feldspar and K-Si-rich glass. We have performed secondary electron imaging (SEM) and back-scattered electron imaging (BSE) to constrain the area of search for apatites by X-ray imaging (Figure 55). Major element analyses of the apatites has been carried out by wavelength dispersive spectrometers. Fluorine and chlorine concentrations are also measured by EPMA in differential mode. Water content is estimated to be 500 to 4500 ppm from stoichiometry, assuming that the F, Cl and OH together constitute an anionic site in apatite. A systematic geochemical investigation of volatile species, using state-of-the-art instrument NanoSIMS, of the observed apatite grains will be attempted from a range of selected lunar samples.

(A. Basu. Sarbadhikari and J. N. Goswami)

Radiation environment in the Earth-Moon space

The "Radiation Dose Monitor (RADOM)" payload on-board Chandrayaan-1 mission was switched on soon after launch and was operational till the end of the mission. This payload provided data on energetic particle environment in the earth-moon space including those for earth's radiation belts. Signature and intensity of proton and electron in the radiation belts, as well as energetic protons of solar and galactic in origin, could be well recognized in the data that also revealed effect of solar modulation of galactic cosmic rays. The maximum flux of electron and proton components in the radiation belt reached ~15000 and ~9600 particles cm^{-2} s^{-1}, respectively. The particle flux, en route to the moon, was rather low (~3 particles cm^{-2} s^{-1}) that decreased

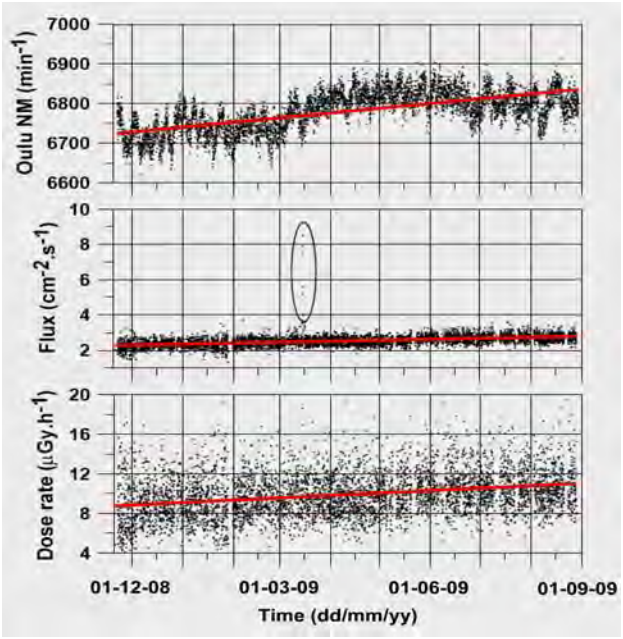

Figure 56. Data for radiation environment in lunar space during Chandrayaan-1 mission duration. The increasing trend in particle flux and dose rate suggests an increase in flux of galactic cosmic ray protons with time that is also supported by Oulu neutron monitor data (top panel). A short-term increase in intensity around mid-March, 2009, is related to a minor solar event.

to ~2.5 particles cm^{-2} s^{-1} at the final lunar orbit of 100 km reflecting shielding effect of the moon. A gradual increase in particle flux in lunar space as a function of time, over the mission duration (Figure 56), reflects effect of solar modulation in cosmic ray intensity. This is also supported by neutron monitor data for this period.

This study was carried out in collaboration with scientists from Bulgarian Academy of Sciences and ISRO Satellite Center, Bangalore.

(S. Vadawale, J. N. Goswami)

Observation of an asteroid occultation with the 50 cm telescope at Gurushikhar

Observation of asteroid occultation provides a direct measure of the size of the asteroid. An asteroid occultation happens when an asteroid moves in front of a background star and in the process reduces the photon flux received from the star. Since asteroids are small bodies, occultation events are relatively rare and the shadow has a very narrow path across the Earth. On 24 February 2012 the asteroid (247) Eukrate occulted a 11.3 mag star (TYC 0865-00418-1) in the constellation Virgo at 15:50 UT. At the time of the event the object was just rising in the east. Observations were carried out with the 50 cm telescope at Gurushikhar, Mt. Abu using an EMCCD camera with fast read out capability. In order to improve the signal to noise ratio, 5 frames of 200 ms were binned on the camera giving a timing resolution of 1 second. A thousand frames were acquired starting a few minutes before the expected time of the event. Initially the asteroid (mag 12.2) could be

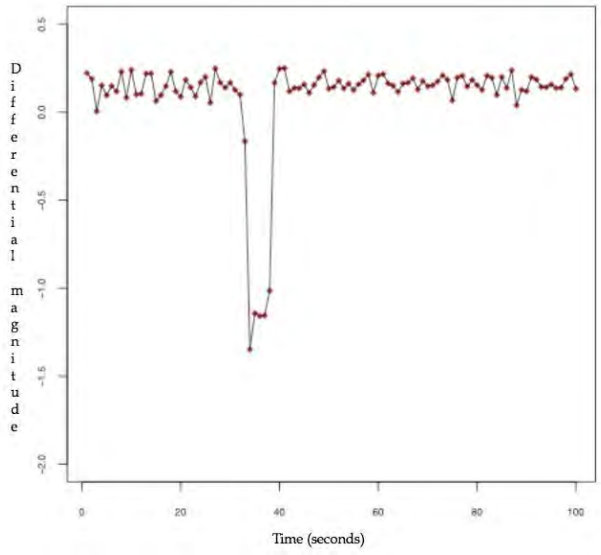

Figure 57: The light curve of the occultation event is shown here. The x-axis is labelled in seconds (only a subset of the light curve is shown here), and the y axis shows the differential photometry of the occulted star with an un-occulted comparison star in the same frame.

seen in the field next to the star and in the course of the 1000 frames it crossed the star. A drop of about 1.3 mag was seen for a duration of 9 sec. The light curve of the event is shown in Figure 57. The x-axis is labelled in seconds (only a subset of the light curve is shown here) and the y axis shows the differential photometry of the occulted star with an un-occulted comparison star in the same frame. From our results, we estimate the chord of the asteroid, as seen from Mt. Abu, to be 132 ± 15 km.

(S. Ganesh and A. Kalyaan)

Mo isotope composition and anoxic conditions at Permo-Triassic (P-T) boundary

The greatest mass extinction in the Phanerozoic (last 542 Myr) occurred at the time of the Permo-Triassic boundary around 251 Ma ago. To understand the cause of extinction, we studied the redox sensitive elements, S and Mo isotopes from the P-T section of Spiti valley of Himalaya, India. In Spiti valley, 1-10 cm of ferruginous band of sediments separates the Permian shale from the Triassic limestone. Analyses of redox sensitive elements such as As, Mo, As, Ni, Sb, Th, Mn and Fe show clear evidence of anoxia or euxinia. Study of stable isotopes of Mo has potential to distinguish between sulfidic deep water, suboxic and oxic conditions. Mo is the most redox sensitive and abundant transition metal in present day ocean. It enters the ocean through rivers (δ^{98}Mo ~ 0‰), and remains in the water in moderately unreactive MoO_4^{2-} form. Under the oxidizing marine conditions similar to present day, Mo from water column is slowly removed by incorporation into

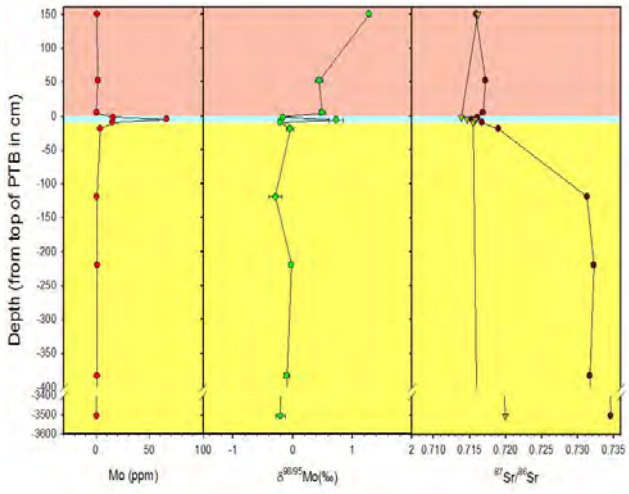

Figure 58: Mo abundance and $\delta^{98/95}$Mo of P-T section of Himalaya.

ferromanganese phases with preferential removal of lighter Mo isotopes (δ^{98}Mo ~-0.7‰). As a result, the sea water is enriched in heavier isotope (δ^{98}Mo ~ 2.3‰). However, in euxinic conditions with sulfidic deep water ($[H_2S] > 100\mu M$), Mo is quantitatively removed from the solution as MoS_4^{2-} without isotopic fractionation. Therefore Mo isotopic composition of sediments deposited under these conditions represents composition of water. Earlier studies argued prevalence of anoxic or euxinic condition during P-T transition, therefore the Mo isotope composition of sediments should represent the ocean Mo composition during the P-T boundary. Figure 58 shows a plot of Mo abundance and $\delta^{98/95}$Mo values as a function of depth for

the P-T boundary sediments. The enrichment of Mo abundance is accompanied by heavy isotope excursion upto δ^{98}Mo ~ 0.7±0.1‰. The physicochemical scenario which could produce such heavy Mo need to be worked out.

(V.K. Rai and A.D. Shukla)

Thermal stability of ESR signals in hydrothermal barites

Determination of the timescales of hydrothermal activity in the Southern Mariana trough has become important after the discovery of large hydrothermal plumes, with sudden changes in hydrothermal and volcanic activity in the sea floor. The long-term change of hydrothermal activities is also interesting in respect of ore formations. Electron Spin Resonance (ESR) dating of barites ($BaSO_4$) has been attempted in chimneys deposited from hydrothermal vents at the Archean site in the South Mariana spreading center and in the Okinawa Trough. A basic premise in ESR dating is that the decay of ESR signals is negligible for the dating age range under consideration. We have investigated the thermal stability and decay kinetics of SO_3^- centre in barites from chimneys deposited from hydrothermal vents in the Southern Mariana trough using isothermal and isochronal annealing experiments. The g-values observed in this study are 2.0034, 2.0022 and 1.9995. A combination of first and second order kinetics is required to explain the variation of the reciprocal ESR intensity with heating time. The Arrhenius plots of the decay rate constants give the activation energies of 1.0 - 1.3 eV. From the estimated decay rate constants at the sea bottom (3°C), the decay rate of the signal was calculated to be less than 2% for the period of 20 ka, suggesting the applicability of the ESR method for dating barites up to about twenty thousand years.

This work is done in collaboration with S. Toyoda of Okayama University of Sciences, Japan.

(D. Banerjee)

Gullies on the Moon: Evidence for dry-granular flows

Analysis of high-resolution images obtained by Terrain Mapping Camera (TMC) on board Chandrayaan-1 and the Lunar Reconnaissance Orbiter Camera (LROC) revealed landslides and gully formation on the interior wall of a 7 km crater emplaced in the Schrödinger basin on the far side of the Moon (Figure 59). The features occur on the steep upper wall of the crater where the slope is ~35 degrees. The gullies show a typical alcove-channel-fan morphology similar to the Martian gullies but with less conspicuous channels. Spectral reflectance data obtained

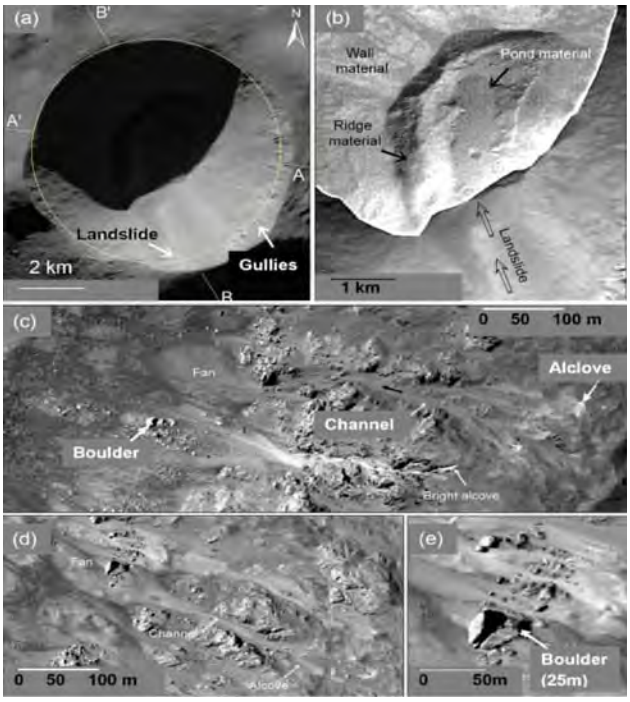

Figure59. (a) The Chandrayaan-1 Terrain Mapping Camera image of the ~7 km diameter near-circular fresh crater. The shadow-removed TMC image (b) reveals the presence of arcuate ridge and the pond material on the crater floor. (c) Distinct example of gullies, with bright alcove and channel and fan deposits. (d & e) Lobate fans formed at the base of bedrock-incised channels; the fan deposits also contain large rock fragments and boulders with maximum size of ~ 35 m.

by Chandrayaan-1 Hyperspectral Imager and Moon Mineralogy Mapper indicate that the gullies and landslides are of relatively recent origin. Absence of spectral features related to water or hydroxyl molecules suggest recent dry granular flows. Mass movements on the crater wall also led to the formation of arcuate ridges and ponding of fine-grained sediments on the crater floor. The gullies have an integrated alcove, channel, and fan morphology that begins in the upper crater walls. The landslides produced a smooth-surfaced pond of debris on the crater floor. Statistics of crater size distributions yielded formation time of ~30 Ma for the gullies and landslides and ~380 Ma for the host crater ~380. Although the lunar gullies appear similar to the gullies on Mars, they occur at steeper slopes than Mars and have poorly developed channels. The lunar gullies and landslides are the products of dry granular flows generated by seismic effects of one or multiple younger impacts that occurred at various parts of the Schrödinger basin.

This study was an Indo-US collaboration effort with the lead scientist from NGRI and contributions from NRSC, Hyderabad, and SAC, Ahmedabad.

(J. N. Goswami)

Remote Sensing data analyses from planetary missions

Topical Volcanism on the Far side of Moon

Unlike the dynamic Earth, which exhibits volcanic eruptions from time to time, it is generally believed that the Moon had a rather short extrusive phase due to reduction of heat producing radioactive elements, cooling and contraction. The major period extends from ~ 4 b.y. - 3 b.y. and the minor sporadic activities continued up to ~ 1 b.y. in certain regions. Here, high resolution reflectance datasets from Moon Mineralogy Mapper (M^3), Narrow Angle Camera (NAC) and Multi-band Imager (MI) onboard recent Moon missions Chandrayaan-1, Lunar Reconnaissance Orbiter and Kaguya respectively have been used to carry out detailed investigations of a conspicuous 60 sq km^2 resurfacing inside Lowell crater (12.9°S, 103.1°W), Orientale basin, on the far side of Moon, to understand its surface morphology and formation. The morphological and compositional studies have revealed that it would have formed as a result of recent volcanic activity in the region. Features characteristic of a volcanic terrain such as volcanic cone, lava pond, fresh flows, lava piles, collapse pits and pits with small central uplift etc. have been found. The unit is basaltic/gabbroic since its spectral reflectance signature shows distinct absorptions centred at ~ 1 and 2.2 μm indicating presence of high Ca-pyroxene in the unit. In comparison, the adjoining areas are composed of feldspathic, noritic and Mg-spinel dominant lithologies. Alternatively, it may be possible that this resurfacing with unique morphological features formed due to impact melts and debris flow from a small partially collapsed crater on the Lowell Crater rim which encountered a pre-existing dike. The unit lacks identifiable impact craters on its surface and exhibits high albedo possibly due to its extreme degree of freshness.

N. Srivastava and D. Kumar)

Origin of pyroclastic ring in the Orientale basin on Moon

Orientale basin, centred at 20°S 95°W is the youngest and the most well preserved multi-ring basin on the Moon. It is ~ 930 km in diameter and is located on the western limb of Moon. In contrast to the other multi-ring basins which are filled with basalts, the Orientale basin is only partially filled with basalts. Therefore, it clearly shows features essential for understanding the geology of multi-ring basins. Among the various formations inside the basin, a conspicuous low albedo ring is present in its southern portions (Figure 60). Its origin has implications to constraining the size of the transient cavity that formed during the Orientale impact event. We have used Moon Mineral Mapper (M^3), Kaguya and LROC-NAC data to carry

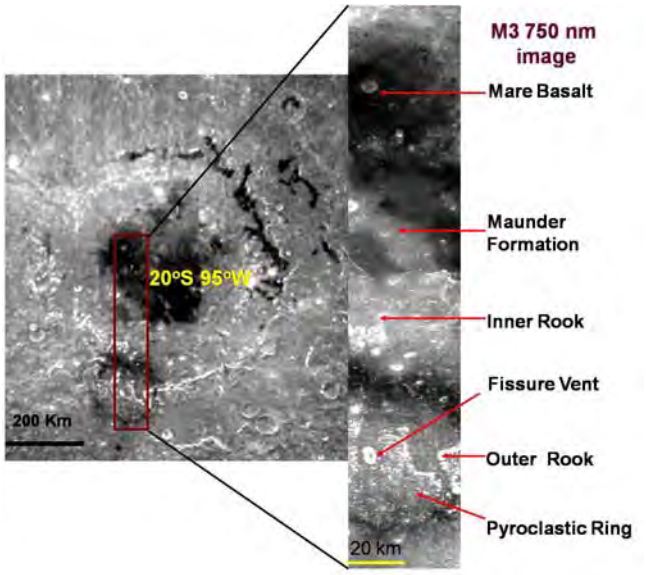

Figure 60: Clementine UVVIS mosaic of Orientale Basin showing the study area. M^3 750 nm data in the zoomed view shows the geological diversity in the region.

out high resolution spectral reflectance and morphological study of the ring and the adjoining areas to understand the geologic context and investigate the mode of formation of the ring. It has been found that the ring is highly space weathered; only fresh craters show presence of mafic components, the elongated vent at the centre has a depth of ~ 2.5 km, is noritic in composition and shows pyroclastics on its surface. Additionally, ~ 190 sq km melt sheet with mafic edges and an unusually mafic streak have also been identified within the ring structure. The findings are consistent with the single fissure theory for the formation of the Pyroclastic ring but understanding the origin of the melt pool with high Ca Pyroxene lining and unusually mafic streak within the ring is necessary to rule out the presence of a pre-Orientale basin in the region.

(N. Srivastava)

Crater Chronology of Copernican Craters

Crater chronology is an effective tool to determine the surface age of a given location of a planetary body using remote sensing technique. In particular, crater size frequency distribution and spatial density of craters can be ultilized for determining the age of lunar surfaces. We have used high resolution LROC-NAC data (spatial resolution ~ 1 m) to determine the ages of selected Copernican craters on the Moon such as Copernicus, and Lowell. Adequate regions of interest have been chosen in each case to minimize the errors due to endogenic and exogenic processes like magmatic flooding, ejecta

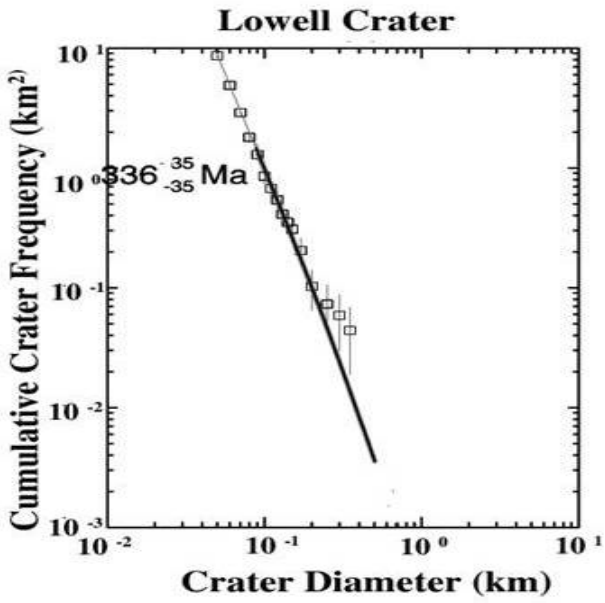

Figure 61: Crater Size Frequency Distribution for Lowell Crater.

blanketing, secondary cratering, superposition of craters, infilling and abrasion, mass wasting etc. which adversely affect the crater frequency. Further, to minimize the errors, only craters with diameter > 10 m have been counted.

The age for Copernicus crater have been estimated to be ~ 780 Ma, and is consistent with its expected age. The crater size frequency distribution for Lowell Craters is shown in Figure 61. The Lowell crater has been dated to be 336 ± 35 Million years old. The broader objective of this study is to date many such craters on Moon in order to subdivide the Copernican era spanning the last ~ 1 billion years., for a better understanding of recent events on the Moon.

(D. Kumar, K.N. Kusuma, N. Srivastava and S.V.S. Murty)

Geochemical and mineralogical analysis of Gruithuisen region on Moon using M³ and Diviner images

Three Gruithuisen domes, Gruithuisen Gamma (36.43N, 40.38W), Gruithuisen Delta (36.43N, 40.38W),and Gruithuisen NW (36.92°N, 40.86°W) located on the highland plateau edge off North Western border of the Imbrium basin are examples of non-mare domes on Moon. Till now, it has been speculated that these domes might be felsic in nature but there were no conclusive evidences. Study of such domes help in understanding the nature of silicic volcanism on Moon, which is rare and is significant in understanding lunar geology. Spectral information from the Moon Mineralogy Mapper (M³) onboard Chandrayaan-

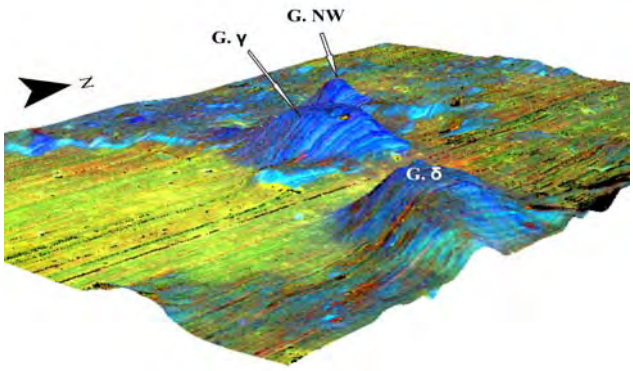

Figure 62: The result of integrated band depth analysis of the study area wrapped on the elevation model is shown. Colour composite of IBD was prepared by assigning red colour to 1000 nm IBD, green to 2000 nm IBD and blue to albedo of 1548 nm band. The Gruithuisen domes show deep blue colouration due to low 1000 nm and 2000 nm IBD values, which indicate lack of mafic minerals in these domes. The highland material also appears blue; but much paler than the domes (reduced blue colour) indicating presence of small amount of iron rich material. The mare basalts show greenish yellow colour due to the iron absorption of pyroxene minerals. The striping error in the M³ data has pronounced effect on the IBD, giving a striped appearance to the image.

1 and DIVINER Lunar Radiometer onboard LRO have been used for geochemical and mineralogical characterization of the Gruithuisen region on Moon along with morphometrical information from LOLA Digital elevation model. The apparent reflectance of M³ on global mode is used for 1) spectral characterization, 2) estimating the abundance of Ti and Fe using Lucey's method, and 3) discriminating non-mare region from mare regions by means of Minimum Noise Fraction (MNF) transform and Integrated Band Depth (IBD) parameters (Figure 62). Christensen frequency (CF) value derived from DIVINER data is used to delineate the silica saturated lithology from the undersataurated rocks as well as to delineate their spatial spread. Low values of FeO, TiO_2, and IBD indicate non-mare nature of the domes and highland material, also supplemented by CF values. The highland rocks represent signatures of sodic plagioclase, the end result of plagioclase crystallization from Lunar Magma Ocean. Compositional variations are observed among the domes. NW dome has highest silica concentration than the other two domes and in turn higher viscosity. It is most likely that the three domes tapped residual liquid from different locations of the residual magma chamber which is in constant mixing. The extrusion is probably a localized phenomenon, where urKREEP welled out along the zone of crustal weakness formed by Imbrium Impact. It is likely that ? dome has extruded over a larger time span than other two features.

(K.N. Kusuma, N. Sebastian and S.V.S. Murty)

Geomorphic investigation of recent debris flow features in Deuteronilus Mensae, Mars

Geomorphologic features within the fretted terrain on Mars resulting from the loss of contained ice in the near-surface have been observed. The presence of patterned lobate debris aprons (LDA) and linear valley fills (LVF) in the fretted terrain together with their topographic characteristics suggests creep deformation in the entire region. In this study we investigated the temporal characteristics of debris flow features in northern mid-latitude region of Mars. The study region is characterized by a compact arrangement of mesas that are centered at 44.5^0 N, 28.5^0 E in the Deuteronilus Mensae, Mars. The most prominent morphologic features observed from MRO-CTX image were mesas, LDAs, LVF, moraine ridges and depositions, mound and end-tail terrain, sublimation tills, and linear terrain Figure 63a. Apart from these observations, we account for the features on Mars akin to terrestrial glacier formation, wherein the two debris flow lobes initially in a different topographic regime diverge-converge to flow as a single lobe according to the local topography. Based on temporal observations of MEX HRSC images of 2005 and 2008, we also observed alterations in the geomorphology of debris flow features. The density of debris flow lineation marks from upstream to downstream region on the surface adjacent to the mesa in 2005 were found to get almost obliterated in 2008 resulting in formation of newer deposits in the downslope region (shown in colour in Figure 63b). The formations of newer deposits in the downslope region have been attributed to the debris-flow ridge fragmentation process, wherein the flow lines which were carrying the most degraded ice-rich materials were not able to get raised according to the topographic relief and were getting deposited in the region outside the flow ridge.

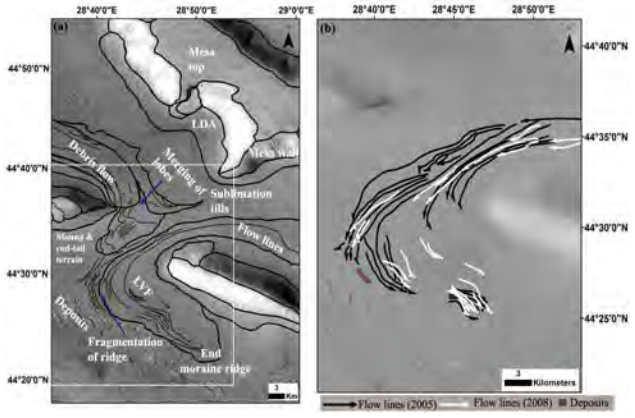

Figure 63 (a) Geomorphological map showing the surface land-forms in the study area. The white box marks the location of Figure (b) Expanded view present the changes in density of debris flow lines from 2005 to 2008. The obliteration of the debris flow lines from 2005-2008 results in formation of newer deposits in downstream region (shown in colour).

These observatious suggest that the ridges formed on the surface of fretted terrain may have undergone the fretting process during the time of flow of degraded apron materials. The results of this investigation significantly favor the presence of buried ice in the near surface which creeps to form morphologies similar to the terrestrial debris flow.

(R. K. Sinha and S.V.S. Murty)

Study of phyllosilicate-bearing terrestrial analogue of Mars

Phyllosilicates including serpentinites on Mars are mostly identified in ancient Noachian crust (~3.7 to 4.1 Ga) and attributed to the presence of liquid water at martian subsurface and therefore of great importance. Due to lack of in-situ mineralogical information on Mars (mostly available from orbital reconnaissance and a few SNC meteorites), studying new terrestrial analogues provide the best clue to assess formation condition of martian phyllosilicates. We have carried out a comparative mineralogical study of phyllosilicate-rich Rikhabhdev ultramafic suite, near Udaipur, Rajasthan, India. The ultramafic suites at Rikhabhdev are mainly emplaced concordantly along a lineament located on central part of

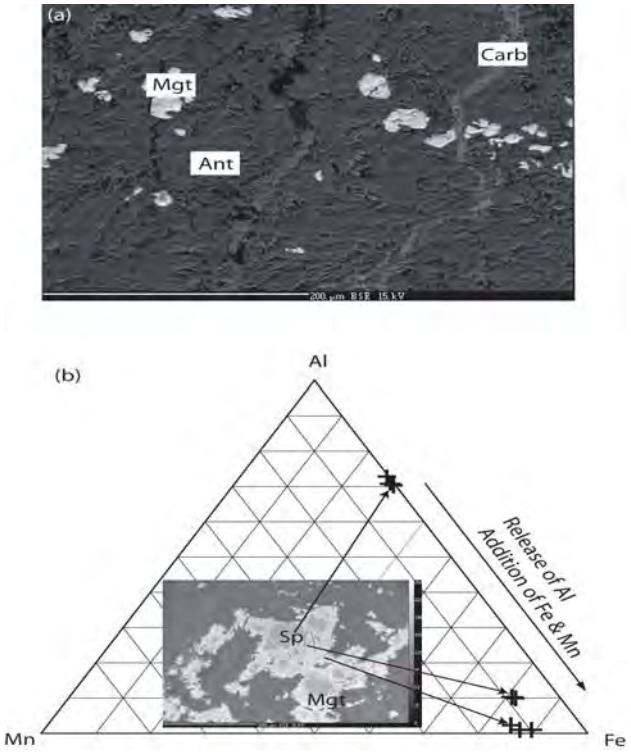

Figure 64 (a) Back scattered electron (BSE) images of Rikhabdeb serpentine (Antigorite, Ant), magnetite (Mgt) and late carbonate (Carb) vein; (b) BSE images to show spinel (Sp) alteration to secondary magnetite (Mgt) and elemental leaching and addition in Al-Mn-Fe ternary.

Udaipur group. The ultramafic rocks show evidences of extensive alteration to serpentine, chlorite, talc and Ca-Mg carbonates identified through XRD. Microtextural studies suggest two stage alteration processes: first stage corresponds to alteration of ultramafic to serpentinites followed by talc/tremolite and carbonate formation under low to medium grade greenschist facies condition (Figure 64a). Bulk serpentinisation prompted to modify the composition in terms of the Mg/Si ratio (Talc ~ 0.89; serpentinite ~ 1.22). Late stage carbonate veins and chromian spinel alteration with high MnO (up to 6.7 wt%) support prolonged hydrothermal alteration (Figure 64b). These particular mineral assemblages are locally similar with the orbital data as found in Nili Fossae, Mars. CRISM (Compact Reconnaissance Imaging Spectrometer for Mars) spectra show characteristic band positions at 2.1, 2.32 and 2.51 μm (Mg-serpentine), 2.31 and 2.51 μm (carbonate) and provide the best match. As Mg carbonates are a common association with serpentinite, it is presumed that Mg carbonate and talc at Nili Fossae region account for alteration of serpentinite. Thus, based on analogue study, we infer that ancient Mg-rich Martian crust underwent subsurface water-rock interaction resulting in the formation of Mg-rich phyllosilicates and carbonate. The mineralogical association of ancient Noachian crust at Nili Fossae typically suggests greenschist facies alteration (< 350°C).

(D. Ray and S.V.S. Murty)

Development and Characterization of Payloads for Space Missions

Development of APXS payload for Chandrayaan-2 rover

Alpha Particle X-ray Spectrometer (APXS) is a well proven instrument for quantitative in-situ elemental analysis of the planetary surfaces, and has been successfully used in Martian surface exploration. The objective of the Chandryaan-2 rover APXS is to obtain the chemical composition of the lunar soil/rock samples along the rover traverse. The working principle of APXS involves measuring the intensity of characteristic X-rays emitted from the sample due to alpha Particle Induced X-ray Emission (PIXE) and X-ray florescence (XRF) processes using suitable radioactive sources. In principle, it is possible to determine the concentration of elements from Na to Br, spanning the energy range of 0.9 to 16 keV. For our experiment, ^{244}Cm radioactive source has been chosen which emits both alpha particles (5.8 MeV) and X-rays (14.3 keV, 18.4 keV) respectively. APXS uses six alpha sources, each ~5 mCi activity, and a silicon drift detector (SDD) for X-ray detection.

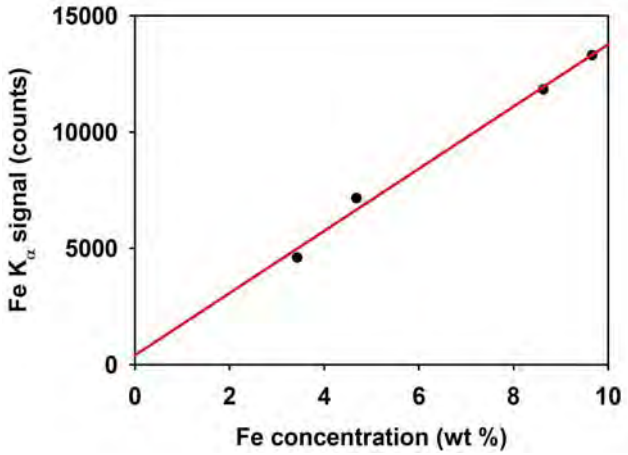

Figure 65: For a fixed geometry of source, sample and detector, several USGS standards were analysed. The above plot shows a linear correlation between Fe K_α signal and iron concentration, integration time is 3000 seconds.

The initial version of APXS instrument consisted of two packages, namely, APXS sensor head and APXS signal electronics with sensor head mounted on the robotic arm, and signal electronics mounted under the rover chassis inside the Warm Electronics Box (WEB). In the finalised configuration, subsequent to design review, robotic arm has been removed, and the APXS payload will be a single package mounted under the rover chassis inside the WEB at a height of ~ 18 cm from the lunar surface. The increase in the height of X ray detector from 3.5 cm (earlier configuration) to 18 cm from the lunar surface increases the integration time to about few hours. The temperature inside the WEB is maintained between -40°C to and 70°C using two thermal management units (TMU-Radioactive heating units). Mounting APXS payload inside the WEB has an advantage of payload surviving the low ambient temperatures of lunar nights, and enhancing the payload life. The detector and sources are protected from dust contamination using a shutter mechanism. The inner surface of the shutter will be coated with suitable target elements to serve as calibration targets.

The APXS payload assembly contains SDD, six alpha sources and front end electronic circuits such as preamplifier and shaper circuits and other interfaces with rover subsystems. The SDD module to be used in the experiment has 30 mm^2 active detector area with in-built peltier cooler and heat sink to maintain the detector at ≤ -35°C. The detector is covered with 8 m Be window which results in the low energy threshold of about 1 keV. The size of the APXS payload is 70 x 100 x 90 mm^3 (approx). The developed system has been thoroughly tested for its performance and provides energy resolution of ~150 eV at 5.9 keV which is comparable to the standard SDD based spectrometer systems when the detector is cooled

to -35°C. We also carried out the detection of X-ray fluorescence for some of the USGS standard samples having varied concentrations of Fe (~3 to 10 wt (%)) for the fixed detector, source to sample distances. We used a 1 mCi ^{241}Am X-ray source for this testing. Figure 65 shows a plot of signal (counts) vs Fe concentration. We observe a linear correlation between observed signal and Fe concentration over a Fe range of 3.5-9.5%. Presently, we are in the process of procuring qualified components for making qualification model, and subsequently the flight model of the APXS payload will be realized.

(M. Shanmugam, S.K. Goyal, B. Shah, A. Patel, Y.B. Acharya and S.V.S. Murty)

Solar X-ray monitor (XSM) on-board Chandrayaan-2 orbiter

The primary scientific objective of Solar X-ray Monitor is to provide real time measurement of solar X-ray spectrum for quantitative interpretation of the lunar X-ray fluorescence spectra measured by the CLASS experiment. XSM will accurately measure spectrum of solar X-rays in the energy range of 1- 20 keV with energy resolution ~200 eV @ 5.9 keV. This will be achieved by using state-of-the-art Silicon Drift Detector (SDD). SDD has a unique capability of maintaining high energy resolution at very high incident count rate (of the order of 10^5 counts per second) expected from solar X-rays, and XSM onboard Chandrayaan-2 will be the first experiment to use such detector for solar X-ray monitoring. Here we present the overall design of the XSM instrument as well as present development status.

XSM instrument will have two packages, XSM sensor package and XSM electronics package. The XSM sensor package houses SDD along with sensitive front-end electronics circuits. XSM uses SDD module with detector active area of ~30 mm^2. SDD module with 8 μm thick Be window provides low energy cut-off at 1 keV. The detector module will be covered with additional Al cap to reduce the detector aperture to ~0.2 mm^2. This cap will be kept at very close distance of < 0.2 mm from detector to achieve the detector field of view of ± 55°. The top and bottom side of the Al cap will be coated with suitable high-Z material of appropriate thickness to stop transmission of solar X-rays as well as the fluorescent X-rays due to Al cap.

One major challenge for XSM is to handle the extremely large variations in solar X-ray intensity which can range up to five orders of magnitude within few seconds. It is planned to include an active mechanism in the XSM sensor package in order to avoid saturation during very large solar flares while maintaining sensitivity for smaller flares. The XSM electronics will automatically detect occurrence of large flare and will activate a mechanism to bring in an additional Be filter of ~250 μm thickness to reduce count rate by temporarily increasing energy threshold to ~1.8 keV. This mechanism also includes onboard calibration

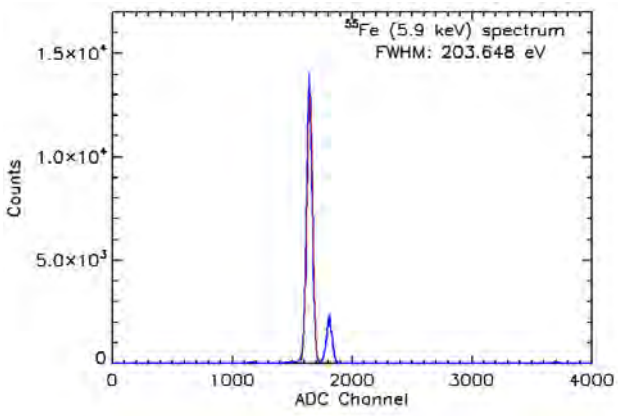

Figure 66: X-ray spectrum measured using a SDD based XSM for ^{55}Fe source. The FWHM for the 5.9 keV line is estimated to be ~204 eV.

using ^{55}Fe X-ray source. The sensor package will be mounted on an extended bracket outside the spacecraft.

XSM electronics package has ADC to convert analog signal to digital form with 10 bit resolution which is further processed by FPGA based digital electronics. The same FPGA will also be responsible for overall payload operation and control. This package will include all interfaces with spacecraft subsystems such as data handling (DH), TM/TC and power subsystem. Presently we have completed the laboratory model of the XSM payload. SDD detector is cooled to about -35°C by coupling the detector module on a 1mm thick Al wall enclosure. Developed XSM electronics has been tested for various peaking time constants, and observed that the energy resolution of ≤150 eV for the pulse peaking times > 2μs. We also observed that the energy resolution and peak position are largely unstable for higher pulse peaking times at higher input count rates compared to lower pulse peaking times (≤ 1μs). Based on these observations, we have selected 1 μs pulse peaking time for XSM which provides ~200 eV energy resolution at 5.9 keV with low energy threshold of 1 keV. The spectrum is shown in Figure 66. The system is also tested for count rates up to 40 K counts/s using available laboratory X-ray source. In order to further improve the performance at higher count rates, we have implemented parallelizable dead time in the event processing, which enables to select only clean events which are not affected by previous events for generating spectra. Presently, we are making qualification model of the payload and subsequently flight models will be made and delivered for integration for spacecraft.

(M. Shanmugam, S. Vadawale, Y.B. Acharya, S.K. Goyal, B. Shah and A. Patel)

Plasma and Current Experiment (PACE) for the first ISRO Mars Orbiter mission

The Plasma and Current Experiment (PACE) aims to probe the Martian atmosphere, and has been proposed for the first ISRO Mars Orbiter mission, likely to be launched during 2013. The PACE experiment proposes to study the escape processes of electrons and ions in the Martian atmosphere, and is very significant in context of the evolution of the Martian atmosphere. PACE is a plasma analyzer instrument and consists of Electron Spectrometer (ES) and Ion Mass Spectrometer (IMS). Figure 67 shows the design of PACE. Presently, the PACE instrument has been allocated mounting position on the +yaw deck of the spacecraft. The ES is composed of electrostatic analyzer (ESA) as charged particle (electrons) sensor, and MCP as the detector. It measures electrons of different energies in the dynamic range 1 eV to 30 keV. The IMS is composed of ESA, time-of-flight (TOF) unit and MCP to measure ions of different elements and energy. Both ES and IMS can measure particles arriving in the 360^0 azimuth direction with a angular resolution of 45^0 and energy resolution of about 10% of incident energy. The IMS and ES, however, require high voltage power supplies ranging from 1 kV to 15 kV. The bias supply, front-end electronics and processing electronics are required to drag the particle inside the sensor, to measure travel time in TOF and then process the data respectively. The block schematics of the instrument are shown in Figure 68.

The Front-end electronics (FEE) consists of multiple channels of pre-amplifier and leading edge discriminators to convert high speed, low voltage signal of MCP into precise time digital logic pulse. To realize flight model of FEE, AMPTEK A121 (pre-amp & discriminator) hybrid ICs will be used. For breadboard model development, BFR93A (6 GHz transistor) and AD8561 (fast comparator) based Constant-Fraction-Discriminator (CFD) channels are developed and characterized. We could achieve ~ 4 ns rise time LV-TTL logic pulse and ~3 ns time resolution for TOF. We also developed TI OPA847 (3.9 Ghz OP-AMP) and AD8561 based Leading-Edge discriminator channels and characterize. We could achieve ~3.8 ns rise time LV-TTL logic pulse and ~1 ns timing error for full dynamic range (-5 to -70 mV sub-nanosecond pulses). We also developed sub-nanosecond rise time pulser with FPGA to test our high speed FEE. Recently the PCBs of FEE for breadboard model are fabricated and electrical tests as well as functional tests with output from MCP have been successfully carried out. The satisfactory performance of pre-amplifier and leading edge discriminator have been successfully demonstrated. Furthermore, mechanical tasks are in an advanced stage.

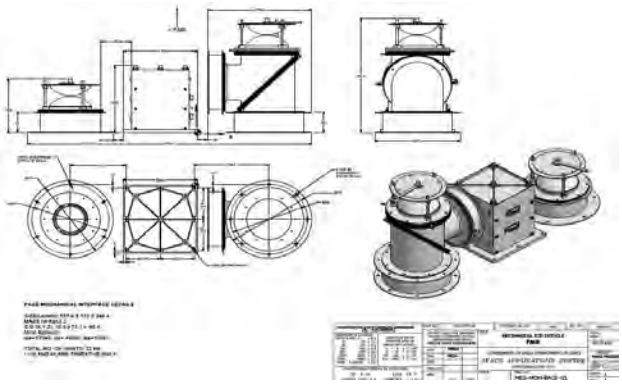

Figure 67: Schematics of electron spectrometer and ion mass spectrometer in PACE payload along with electronics package on spacecraft.

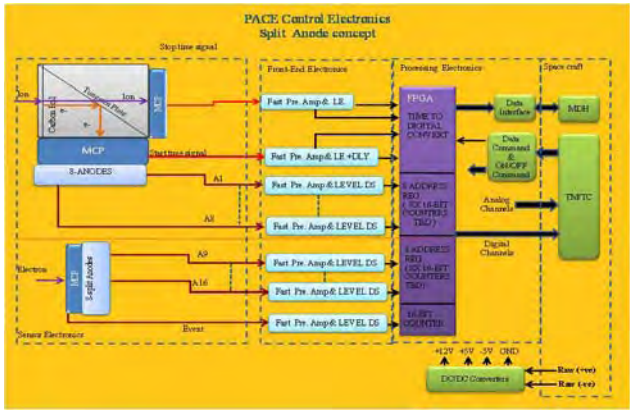

Figure 68: Block schematics of PACE control electronics.

The hardware fabrication of mechanical components of ES and IMS have been completed. Deposition of carbon foils on the nickel electroforms mesh mounts is in progress at SAC. The thermal tests of carbon foil has shown satisfactory performance for a temperature cycle of -100^0 to $+ 100^0$ C, expected in the Martian environment.

The mechanical design and fabrication are carried out in collaboration with A. R. Srinivas, R. Dev and D. Subramaniam of SAC, Ahmedabad.

(Rajmal Jain, Y. B. Acharya, A. B. Shah, Pranav Adhyaru, Jayesh Khunt, Ejaz Sheikh, Dhara Patel, G. P. Ubale, V. D. Patel)

Development of a $LaBr_3$:Ce Gamma Ray Spectrometer (GRS)

High energy (>100 keV) gamma ray spectroscopy is an important technique for remote sensing studies of chemical composition of planetary surfaces, and has been used to study surface composition of the Moon, Mars and Asteroids at various spatial resolutions. We are developing a $LaBr_3$:Ce gamma ray spectrometer for a future planetary mission. A 3 inch $LaBr_3$:Ce crystal was procured along with a 3.5

inch PMT and a preamplifier to check its suitability. We have checked the specifications of $LaBr_3$:Ce crystal using a pulse shaping amplifier, and an Ortec MCA card. Further amplification was provided by a pulse shaping amplifier whose coarse gain was set to 20 and fine gain to 0.5. The pulse shaping time was set to 2 μs. Pulses with a pulse height between 0 and 10 V were recorded with a Ortec multi channel analyser.

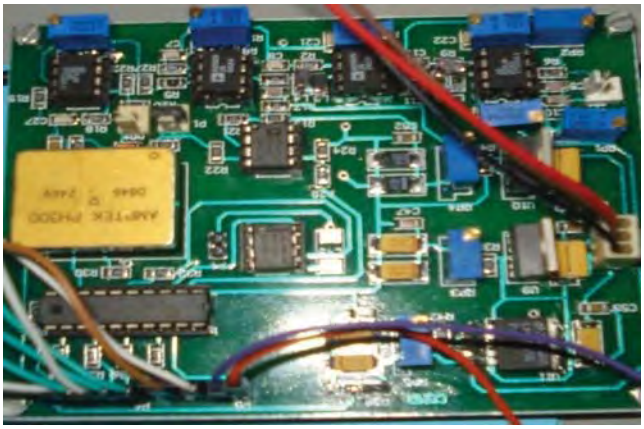

Figure 69: Bread-board model for GRS including shaping amplifier, peak detector and ADC subsystems.

After testing the performance of the detector, different individual subsystems including shaping amplifier, peak detection, analog to digital conversion and high voltage unit were developed. Once these modules were tested individually, we developed the bread board model for high voltage, and shaping amplifiers, peak detector and ADC (Figure 69). The $LaBr_3$:Ce detector requires a high voltage of 720 V DC. The bread board model of the high voltage is generated by using a toroidal transformer with a three stage voltage multiplication circuit. With the present design we are able to generate voltage from 600 V to 1100 V with 1 mA output current capacity. The shaping amplifier and peak detector were designed with hybrid components. Presently we are testing the detection with a shaping time 3 μs. This unit has been set to the gain of 10, and is used to change and amplify the pre-amplifier output to Gaussian shaped output. We have used a serial ADC of 12-bit resolution. The control signal for peak detector and ADC are being generated through FPGA program. The FPGA is converting 12 bits serial data into parallel data. This data is given to Data Acquisition Software developed in Labview. The development of the Labview based data acquisition software is in progress. At present with the data acquisition software we are able to get the counts from the bread-board model, and measure the different peaks using ^{22}Na source.

(D.K. Panda, S.K. Goyal, D. Banerjee and Y. B. Acharya)

Study of the nature of RF propagation on a lunar terrain based on recent datasets

Using WSN for a lunar mission involves many challenging aspects, an important one being communication between the nodes. Although the low dielectric permittivity nature of the lunar soil favours wireless communication, irregular terrain could be a bottleneck, particularly for specific regions on the Moon. Therefore it is necessary to assess the feasibility of using a large scale WSN for specific future targeted sites. We have carried out a feasibility study of using WSN for some important sites. A modified RF propagation model in conjunction with high resolution terrain data from recent missions has been used to estimate the nature of RF propagation on the lunar surface. Simulations have been carried out for various representative sites (highland, mare, craters etc.) of interest – for example, simulations have been carried out for Mare Imbrium (representative of a smooth terrain) and Tycho Crater (representative of rough terrain). Lunar terrain data for these sites have been taken from NASAs Lunar Reconnaissance Orbiter (LRO) – Lunar Orbiter Laser Altimeter (LOLA) instrument. Initial results show that WSN is feasible in sites even with rough terrain where a direct RF propagation path is not available. Study of RF communication scenario for a sensor network deployed on the above two sites of the Moon suggest, the RF losses are within tolerable limits. As shown in Figure 70 direct line of sight can exist between the nodes depending on their positions even when they are deployed in a rough terrain. These results may vary largely depending upon the local terrain and the positions of the sensor nodes. Such studies need to be carried out

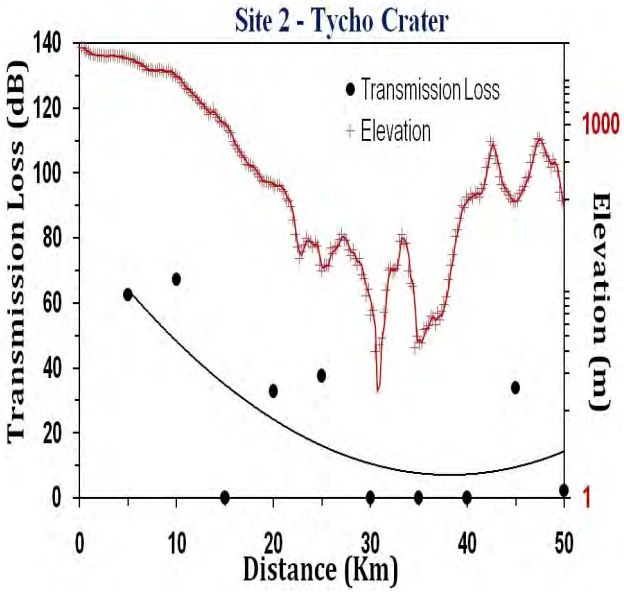

Figure 70: Results showing the nature of RF propagation between the deployed sensor nodes.

for maximum possible locations of the Moon to parameterise these values. These results should be further validated by means of field investigations, wherever possible. In short, this study shows that operating a large scale sensor network on the moon is not complex and is feasible if it is properly designed taking into account all the constraints.

(K. Durga Prasad and S.V.S. Murty)

Electromagnetic Characterization of lunar soil simulant

Electromagnetic (EM) characterization of the planetary analogues is useful for calibration of a sensor for future in-situ measurement on planetary surface and also for finding the depth of penetration of a RADAR signal. The higher depth of penetration helps in detecting the sub-surface features on a planetary surface. The EM characterization includes the study of permittivity, conductivity and magnetic permeability of the material under test. At lower frequency, this study may be carried out by the developed impedance sensor. The permittivity and the conductivity of the lunar soil simulant JSC-1A have been measured using the impedance sensor and the results are shown in Figure 71a and 71b respectively. The results are shown for dry sample, a sample with 2 % water and a sample with 5 % water. At higher frequency; the study may be carried out using a Vector Network Analyzer (VNA). The algorithms used for extracting the permittivity, conductivity and magnetic permeability of the sample have been developed for VNA based measurements.

(J. Pabari)

Effect of Electrode on Soil Property Measurement

While extracting the soil permittivity and conductivity, one needs to consider the electrical equivalent circuit of the soil to derive the soil properties. During the parameter extraction, there could be some effect of electrode resistance and stray capacitance on the measured properties. To check such effects, a simulation study has been carried out and a few soil electrical equivalent circuits have been compared. Typical simulation results obtained using the Mathematica software are shown in Figure 72a and 72b for permittivity and conductivity, respectively. The results show that as the stray capacitance is increased, the soil permittivity is

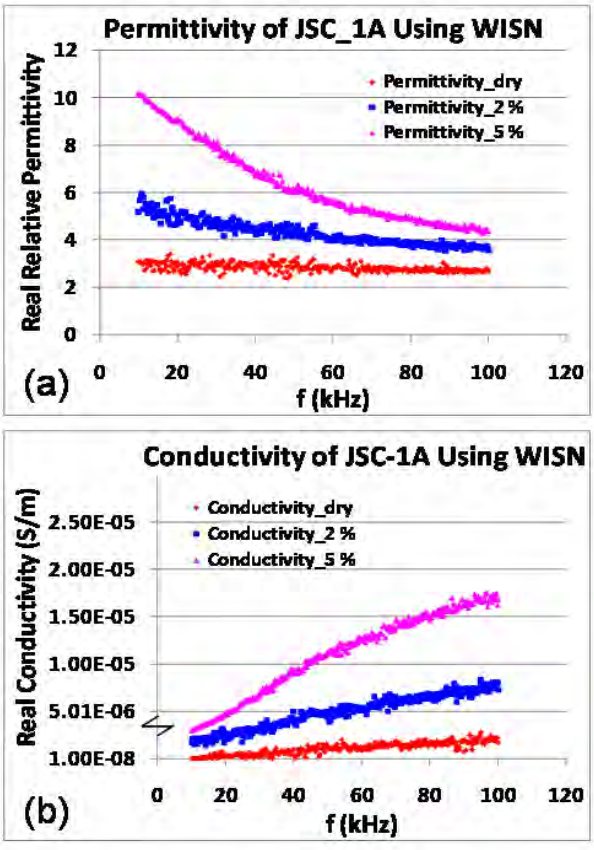

Figure 71 Measurements of (a) relative permittivity and (b) conductivity of JSC-1A, for various water contents

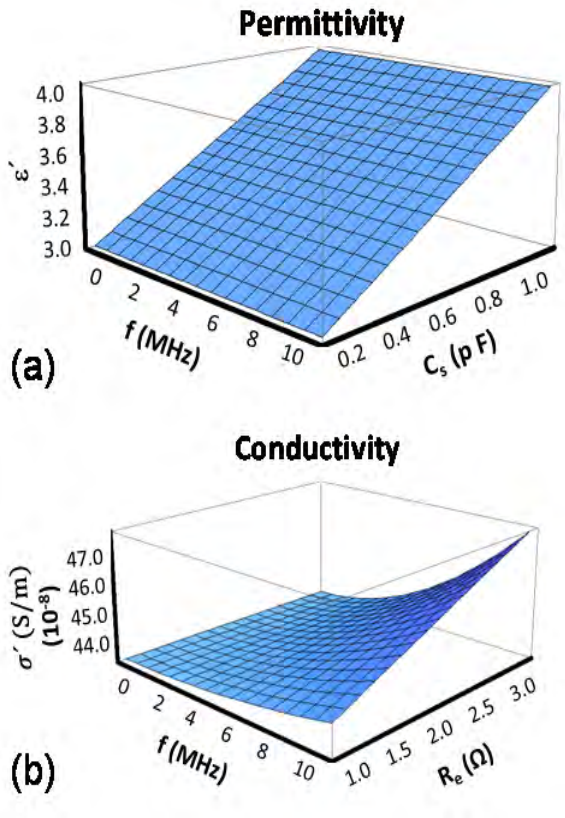

Figure 72: Results of simulations showing (a) relative permittivity as a function of stray capacitance, and (b) dependence of conductivity on electrode resistance.

increased moderately. Also, as the electrode resistance is increased, the soil conductivity is increased by a small amount.

(J. Pabari and Vijyeta Gohil)

Design, development and evaluation of an Ambient Light Sensing Node

Ambient light sensing at different wavelengths forms an important application of planetary surface exploration. Such tasks include real time and precise measurement of light in ambient conditions as well as in specific wavelengths. A Wireless Sensor Network is being developed as a tool for probing planetary surface/sub-surface characteristics. A highly optimized laboratory prototype of the sensor node has been developed earlier, and is currently undergoing survivability testing. In another parallel development, wireless sensor nodes using a different microcontroller and RF transceiver platforms have been designed. Although the targeted application of these nodes is to measure ambient light levels in a wide dynamic range, it has a provision for including other sensors. The prototype of the module using digital sensor with wireless capability is shown in Figure 73. The modules have been configured as a co-ordinator and end-devices and the ambient light intensities have been logged remotely. The performance of the modules has been evaluated by means of various experiments, both indoors and outdoors, including monitoring of Moon light. These sensor nodes can be deployed as an independent sensor network for probing the parameter of our interest (ambient light in this case). On the other hand, the individual modules can be a part of a heterogeneous sensor network thus providing a versatility of operation. The designed node weighs around 20 gms and measures around 4 x 3 x 2 cms.

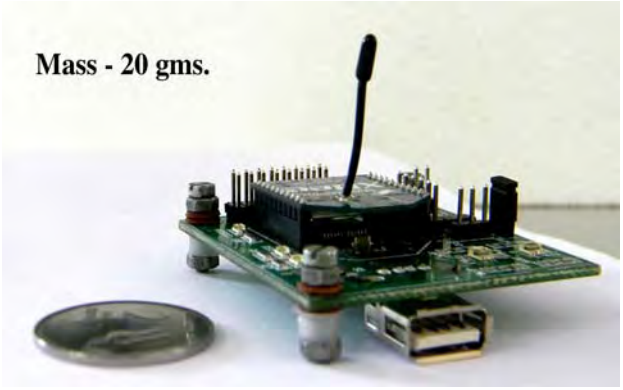

Figure 73: Prototype of an Ambient Light Sensing Node.

(K. Durga Prasad, A. Bhattacharya and S.V.S. Murty)

Space and Atmospheric Sciences Division

The research activities covered in Space and Atmospheric Sciences division pertain to the solar-terrestrial interactions, planetary atmospheres, dynamical processes in middle atmosphere and the climatic impacts due to natural and/or man-made sources in the lower atmosphere. Also, laboratory based simulation experiments relevant to near Earth environment are being pursued. Research investigations are carried out experimentally using the state-of-the-art instruments and substantiated with theoretical models.

Variability and sources of aerosol absorption over Bay of Bengal

Spatiotemporal variations in aerosol absorption properties were investigated over the Coastal, North, East and South Bay of Bengal (BoB) during winter using the spectral (370-950 nm) measurements of mass concentrations and absorption coefficients of black carbon (BC). Mass concentration of BC was higher over the North-BoB (4.1 μg m^{-3}) than the South (2.5 μg m^{-3}) (Figure 74). However, absorption Ångström exponents (α) derived from the spectral dependence of aerosol absorption coefficients, over the North and South-BoB were not significantly different. They were > 1.5 for more than 85% of the aerosol absorption spectra suggesting the dominant contribution from biomass burning (biofuel, crop waste open burning and forest fires) to the measured BC mass over the BoB. The amount of BC transported over the BoB was found to be higher during winter when compared to pre-monsoon and post-monsoon seasons. Mass concentrations of BC during 2008 were also higher than that of 1999, indicating an increase in the amount of BC aerosol emissions during the last decade.

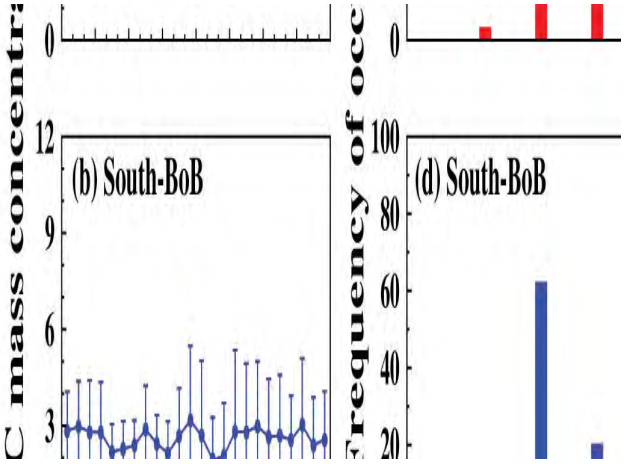

Figure 74: Diurnal variation of black carbon (BC) aerosol mass concentration over (a) North-Bay of Bengal (BoB) and (b) South-BoB. Vertical bars indicate $\pm 1\sigma$ variation from the mean in an hour. Frequency distribution of absorption Ångström exponent (α) derived from the spectral dependence of aerosol absorption coefficients in the 370-950 nm wavelength range over (c) North-BoB and (d) South-BoB.

(S. Kedia, S. Ramachandran, T.A. Rajesh, and R. Srivastava)

Differences in aerosol optical properties: External and core-shell mixing

Mineral/soil dust, insoluble organics, water soluble nitrates, sulfates & organics, black carbon, and sea salt are the dominant aerosol species that are present in the atmosphere. The presence of various aerosol species over a location produced by sources of local origin, and long range transport can give rise to different mixing states because of aging and interactions among different aerosol species. Assumptions regarding the mixing state of aerosol and its effect on aerosol optical properties can give rise to uncertainties in modeling their direct and indirect radiative effects. Aerosol optical properties for external and core-shell mixtures of various aerosol species at different relative humidity levels have been calculated. Mie calculations for core-shell were performed using the values of radii, refractive indices, and densities of aerosol species that act as core and shell, and the core-shell radius ratio. Absorption by combined aerosol was enhanced in core-shell mixture of absorbing and scattering aerosols when compared to their external mixture. Extinction coefficient, single scattering albedo (SSA), and asymmetry parameter were higher for external mixture when compared to BC (core)-water soluble aerosols (shell), and water soluble aerosols (core)-BC (shell) mixtures in the 0 to 90% relative humidity (RH) range. Asymmetry parameter for water soluble (core)-BC (shell) mixture was independent of RH as BC is hydrophobic. Aerosol optical depth (AOD) of core-shell mixtures increased at a higher rate when RH exceeded 70% in continental clean and urban aerosol models, whereas AOD remained the same when RH exceeded 50% for different mixing scenarios in maritime aerosol models. SSA for continental aerosols varied for core-shell mixing of water soluble (core)-shell (BC) when compared to their external mixture at different RH values, while SSA for maritime aerosols did not vary significantly owing to the dominance of sea salt aerosols. These results confirm that aerosol mixing can modify the optical characteristics of aerosols, and will prove useful in parameterizing the effect of core-shell versus external mixing of aerosols in global climate models.

(S. Ramachandran and R. Srivastava)

Mixing state of aerosols over Indo-Gangetic Plain: Impact on aerosol radiative forcing

Mixing state of aerosols over an urban (Kanpur) and a rural location (Gandhi College) in the Indo-Gangetic plain (IGP) was determined using the measured and modeled optical properties. Also, the impact of aerosol mixing state on radiative forcing was examined. The probable mixing states of aerosols over Kanpur and Gandhi College exhibit seasonal variations. Different fractions of black carbon (BC) and water soluble (WS) aerosols in core-shell mixing emerged as probable mixing state during winter, monsoon and post-monsoon over Kanpur, while insoluble-water soluble core-shell mixture was one of the probable mixing states in Gandhi College (Figure 75). Owing to the abundance of mineral dust (MD) over IGP during pre-monsoon, MD coated by BC emerges as the most probable mixing state. Top of the atmosphere (TOA) forcing changed from negative (winter) for external mixing to positive (pre-monsoon) over both the locations because of lower (<0.8) single scattering albedo in pre-monsoon. Surface aerosol forcing for probable mixing states during winter and pre-monsoon was similar over Gandhi College. In addition to significant seasonal variations, vertical profiles of aerosol heating rates show larger values for external mixture. Heating rate was larger (>1.5 K day^{-1}) near surface in the winter, while it was larger at a higher altitude of ~1 km during pre-monsoon due to the presence of elevated absorbing aerosol layer. Differences exist between the measured and model derived asymmetry parameter (*g*) because of the presence of non-spherical (dust) particles over the IGP. However, aerosol radiative forcing was found to be weakly sensitive to the variation in *g* due to higher (> 0.2) surface albedo. Regression analysis between model derived and measured aerosol radiative forcing yielded an

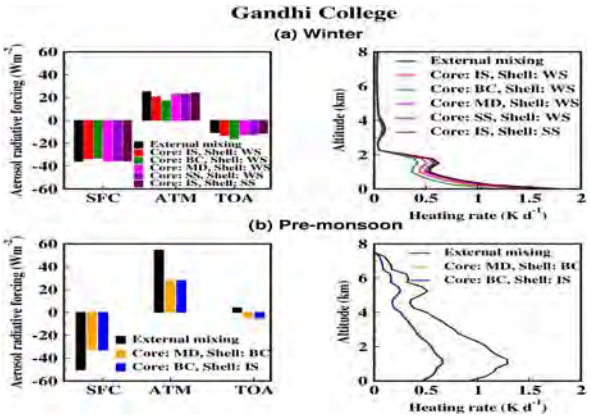

Figure 75: Aerosol radiative forcing at the surface (SFC), in the atmosphere (ATM) and at the top of the atmosphere (TOA) for external and different probable mixing states of aerosol species involving insoluble (IS), water soluble (WS), black carbon (BC), mineral dust (MD) and sea salt (SS) over Gandhi College during (a) winter and (b) pre-monsoon periods. Vertical profiles of aerosol heating rates (Kd^{-1}) for the resultant mixing states are also shown.

R^2 (square of correlation coefficient) > 0.92, thereby, confirming that the methodology adopted to retrieve aerosol optical properties and estimate forcing was robust. The modeling study revealed that aerosol mixing states can vary depending on the type and abundance of aerosol species over a given region.

(R. Srivastava and S. Ramachandran)

Trends in aerosol optical depths over different regions of India

Seasonal and annual mean trends in aerosol optical depths (AODs) for the last decade were derived using MODerate resolution Imaging Spectroradiometer (MODIS) (Level 2, 10 kmx10 km remote sensing) data for different locations in India. Annual mean AODs have increased by >40% during 2000-2009 in Jaipur, Hyderabad and Bengaluru. The increase in AODs over Hyderabad and Bengaluru, major high-tech cities, can be ascribed to the increase in urbanization. An increase in AODs over New Delhi where manmade aerosols are dominant can be attributed to an increase in the amount of aerosols from fossil fuel and biomass burning, while an increasing trend in AODs in the northeast, indicates an increase in the amount of aerosols produced from biomass burning and forest fires. AODs decreased in the high altitude sites of Shimla and Dehradun. AODs and wind speeds increased over Jaipur, while they decreased in Trivandrum during the last decade. An increase in wind speeds led to an increase in soil derived dust particles over Jaipur, an arid site, while a decrease in wind speeds over Trivandrum, contributed to a decrease in sea spray aerosols, thereby causing a decrease in AOD. Both AODs and rainfall have increased in the last decade over most study locations. These findings become important and useful in the context of regional and global climate change due to aerosols.

(S. Ramachandran, S. Kedia and R. Srivastava)

Seasonality in biomass burning and emissions of gaseous species in South and Southeast Asia

Emissions from South and Southeast Asia (S-SE Asia) region are significant source of atmospherically important gaseous and particulate species such as CO, oxides of nitrogen (NOx) and non-methane volatile organic compounds (NMVOCs), from both natural and anthropogenic sources. In addition to large uncertainty in the estimates of the emission inventory from biomass burning sources, these sources show variability that depend on seasons as the meteorology and agricultural practices are different in different seasons. The Along Track Scanning Radiometer (ATSR) fire count data at 3.7μm channel were used to investigate the trends and variability of major biomass burning sources over S-SE Asia. The burning activities are lowest during the summer monsoon and highest during the winter monsoon in the northern hemispheric parts of S-SE Asia. We have shown that the intensity of fires over Indonesia has been modulated by large scale climatic phenomena like ENSO (El Nino Southern Oscillations). The spatio-temporal patterns of CO, NOx, NMVOCs, have been analyzed using the Precursors of Ozone and related Tracers (POET) emission inventory for estimation of emissions due to biomass burning for the year 2001. Similar to the fire count data, the emissions of these species show bi-modal seasonality. From January-May, the biomass burning dominates in the northern hemispheric part of the S-SE Asia. From July-September the activities shift to the southern hemispheric parts where the emissions from Indonesian and Malaysian islands were the largest. The activities of biomass burning are the lowest during October-December period in S-SE Asia. Consistent with the fire count data, the highest emissions of all gaseous species occur in the month of April.

(L. K. Sahu and Varun Sheel)

Seasonal and diurnal variations of black carbon and organic carbon aerosols in Bangkok

Measurements of black carbon (BC) and organic carbon (OC) were conducted in Bangkok during 2007-2008. The daily concentrations of BC and OC varied in the ranges of 1-14 μg m^{-3} and 2-33 μg m^{-3}, respectively. Annual trends show strong seasonality with lower and higher concentrations during wet and dry seasons, respectively. In dry season, the averages of BC and OC were 5.3 ± 2.0 μg m^{-3} and 13.2 ± 5.8 μg m^{-3}. The flow of cleaner air and negligible biomass burning resulted in lowest concentrations of aerosols in the wet season. In addition to local anthropogenic emissions, transport of pollutants and biomass burning caused higher concentrations in the dry and hot seasons, respectively. In spite of extensive biomass burning in hot season, the moderate levels of 3.8 μg m^{-3} of BC and 11.0 μg m^{-3} of OC observed were due to the mixing with air from Pacific Ocean. Diurnal distributions of BC and OC exhibit peaks during the rush hours of traffic marked by minima in OC/BC ratio when the wind flow is stagnant (< 0.5 ms^{-1}). However, the concentrations of aerosols decrease with wind speed, the dependency varying with season due to the transport of air having different backgrounds of aerosols. The slope of ΔBC/ΔCO of 10.3 ng m^{-3} (ppbv)$^{-1}$ estimated for wet season represents the emission ratio from vehicular sources. The highest of ΔOC/ΔBC (3 μg (μg)$^{-1}$) in hot season was due to the predominant emissions from biomass burning.

This work is done in collaboration with Y. Kondo of University of Tokyo, Japan; Y. Miyazaki of Institute of Low Temperature Science, Hokkaido University, Sapporo, Japan and N.T. Kim Oanh and Prapat Pongkiatkul of Asian Institute of Technology, Bangkok, Thailand.

(L. K. Sahu)

Study of free tropospheric CO pollution episode over Indonesia using the Model of Ozone and Related chemical Tracers (MOZART-4)

Biomass burning events are a source of carbon monoxide (CO) which is one of the pollutants. One such intense event occurred over Indonesia in autumn of 2006. We study the impact of this event on the free tropospheric abundances of CO and ozone (O_3) using MOPITT (Measurement of Pollution In The Troposphere) observations, ozonesonde measurements, and the 3-D chemistry transport model MOZART. MOPITT observations showed an episode of enhanced CO in the free troposphere during this period over Indonesia region, which is reproduced well by MOZART (Figure 76). Using mass diagnostics of the model, it is seen that the convective activity enhanced the CO mixing ratio in the free troposphere by 100-250 ppbv whereas the role of chemistry is found to be negligible. The implication of the fire plume has been studied on the

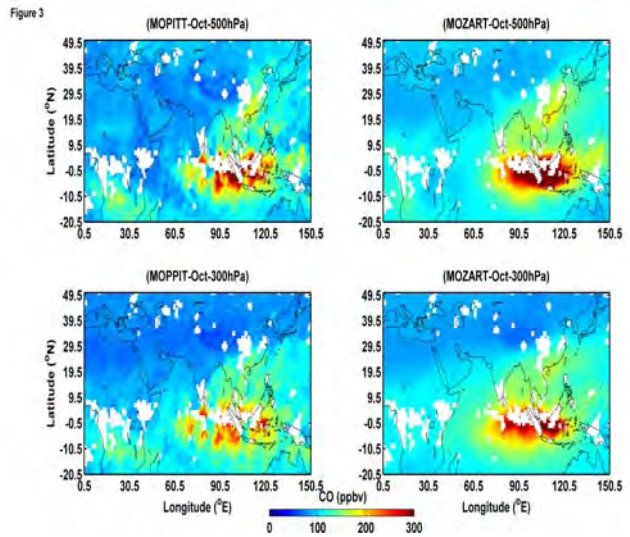

Figure 76: Comparision of CO distribution obtained from MOPITT instrument and MOZART simulation for October 2006 at 500 mb and 300 mb over the Indonesian region.

vertical distribution of O_3 over Kuala Lumpur. The tropospheric columnar ozone increased by 13-16 Dobson units during 2006 in comparison to Autumn 2005 and 2007 over this location. According to MOZART simulation, the maximum contribution to ozone enhancement comes from chemistry followed by convection. The model is run both with and without Indonesian biomass emissions. Comparison showed that as a result of the biomass burning event, there is an average increase in CO by 104 ± 56 ppbv and O_3 by 5 ± 1 ppbv from surface to 100 mb altitude range.

(Shuchita Srivastava and Varun Sheel)

Transport effects on the vertical distribution of ozone over Ahmedabad

Measurements of the vertical profiles of ozone have been made over Ahmedabad during July 2003 to June 2007 using balloon borne ozonesondes to study variability in its distribution. These balloon flights were made fortnightly and reached the ceiling heights of about 32 km. A particle dispersion model, FLEXPART, has been used to study transport from different regions over Ahmedabad for each profile for the entire troposphere at a height resolution of 200 m. The ozone profiles in the lower troposphere are mostly affected by transport from North India in the winter and from the Indian Ocean and the Arabian Sea during monsoon months. However, the ozone profiles in the middle and upper troposphere are affected by transport from as far as North Africa, Europe as well as North and South America during the winter season. Conspicuously, the ozone profiles in the upper troposphere during the monsoon season are affected by transport from the Central Asia.

This work has been carried out in collaboration with scientists from NOAA, Boulder, USA

(S. Lal)

Detection of a volcanic plume over Northern India

An event of high SO_2 loading over northern India due to long-range transport of SO_2 from a volcanic eruption inEthiopia was detected using observations from the Ozone Monitoring Instrument (OMI) onboard Aura satellite. Monthly averaged column SO_2 values over the Indo-Gangetic Plain (IGP) were observed to be in the range of 0.6-0.9 Dobson Unit (DU) during November 2008 as

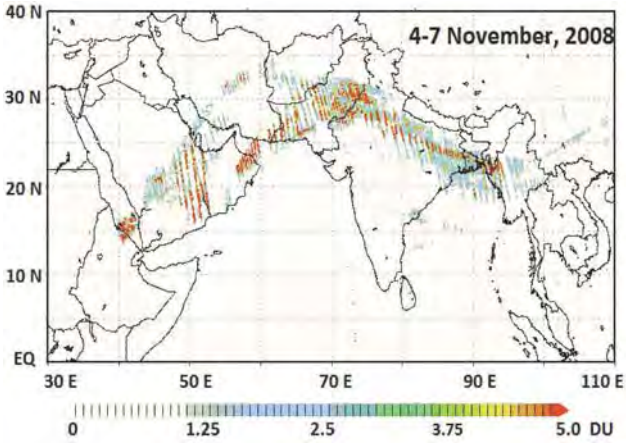

Figure 77: SO_2 column during 4-7 November 2008 as measured using the Ozone Monitoring Instrument (OMI) on board Aura satellite.

against the background levels of <0.3 DU. The columnar SO_2 loading are shown in Figure 77 during 4-7 November 2008. These values are higher by a factor of about 10 from the background levels at some of the places in the IGP. These enhanced SO_2 levels are not reflected in the satellite derived NO_2 or CO columns, indicating the effect of transport from a non-anthropogenic SO_2 source. Due to strong winds in the free troposphere, back-trajectory analysis revealed that SO_2 originated from the Dalaffilla volcanic eruption in Ethiopia during 4-6 November 2008. Since volcanic eruptions inject SO_2 directly into the free troposphere, where its lifetime is longer, it has greater potential to perturb atmospheric chemical and radiative properties compared to the surface level emissions.

This work has been carried out jointly with scientists from ARIES, Nainital and PNNL, USA.

(C. Mallik, S. Lal, and S. Venkataramani)

Airborne measurements of trace gases over Bay of Bengal during a winter month

Vishakhapatnam (17.72°N, 83.22°E), Chennai (12.99°N, 80.17°E), and Port Blair (11.64°N, 92.73°E). A comparative study of the distributions of these trace gases during all air sorties showed enhanced concentrations over east of Vishakhapatnam and south of Port Blair in comparison to over the north/north-east and west of Port Blair and east of Chennai (Figure 78). The back-trajectory analysis showed the outflow of highly polluted Indo-Gangetic Plain over east of Vishakhapatnam. Increasing trends from Chennai to Port Blair in mixing ratios of ozone (0.58 ppbv_deg^{-1}), CO (7.3 ppbv_deg^{-1}), ethane (62.3 pptv_deg^{-1}), and propane (13.9 ppbv_deg^{-1}) were noticed at 750 m indicating the advection of polluted air from eastern Bay of Bengal towards southern India. Air parcels sampled over south of Port Blair have passed through the region of intense biomass burning over South East Asian countries. A comparison of mixing ratios of these gases with previous ship based measurements indicates that degree of pollution is higher in transported continental air during the winter season.

(S. Srivastava, S. Lal, and S. Venkataramani)

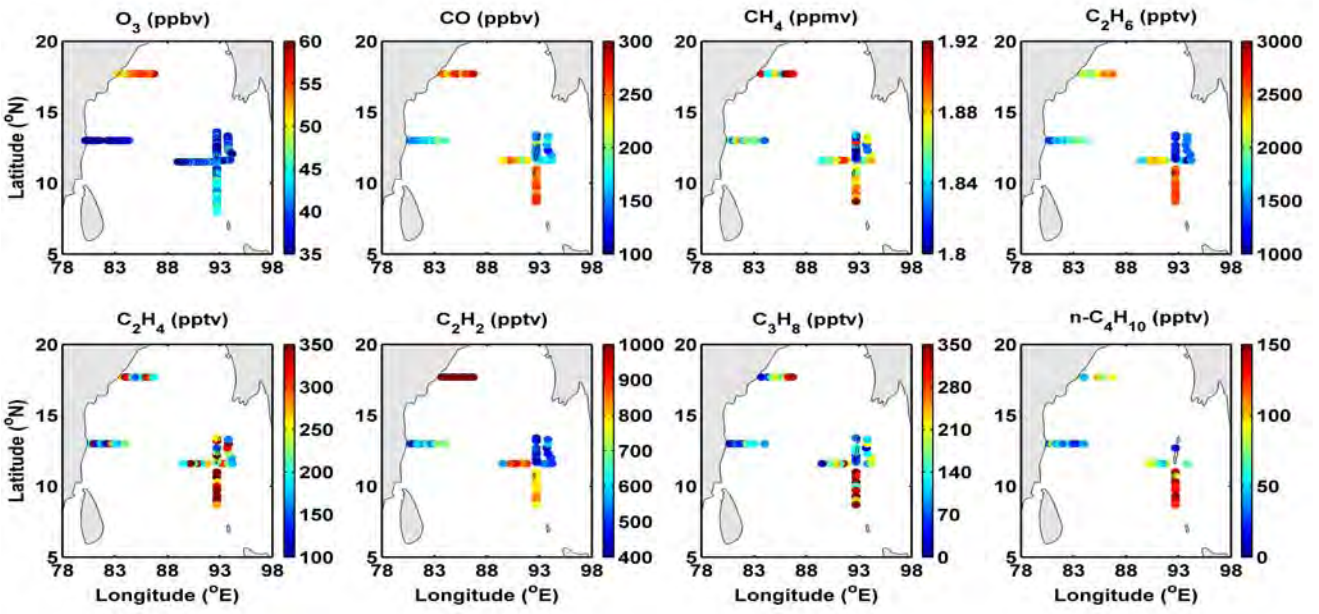

Figure 78: Distributions of various trace gases at 750 m altitude observed from air sorties conducted from Visakhapatnam, Chennai, and Port Blair during January 2009 as a part of the Winter phase of Integrated Campaign for Aerosols, gases and Radiation Budget (WICARB).

The Winter phase of the Integrated Campaign for Aerosol, gases and Radiation Budget (WICARB) was conducted during January 2009 over the marine region surrounding the Indian subcontinent. During this campaign, airborne measurements of O_3, CO, CH_4 and light non-methane hydrocarbons (NMHCs) were made over Bay of Bengal at 750 m and 1500 m altitude from the base locations at

Middle atmospheric thermal structure over sub-tropical and tropical Indian locations

Rayleigh Lidar observations during 1998-2001 over Mt. Abu and Gadanki have been used to study the structure of middle atmospheric temperature in the altitude region of 30-75 km. Nocturnal mean temperature profiles are utilized

to obtain average temperature profile for each month. Monthly mean profiles are further used to construct temperature climatology. Lidar observed temperatures are compared with those observed by Halogen Occultation Experiment (HALOE) on-board Upper Atmospheric Research Satellite (UARS), and the temperature structure by the models CIRA-86 and MSISE-90. Observed temperatures are in qualitative agreement with CIRA-86 and MSISE-90 models below 50 km, and the agreement is better during winter months. Significant differences of up to 10 K have been noted above 50 km. The temperature profiles are also compared with the equatorial model (based on rocket and balloon measurements) for the Indian region. Significant day to day variability is found, which is as high as $\pm$ 10 K at $\sim$70 km. The mean values of the stratopause height and temperature are found to be 48 km and 271 K, respectively. Seasonal variation shows equinoctial and summer maxima below 55 km, whereas above 70 km winter maximum with equinoctial minima are present. Comparative study of thermal structure over Gadanki, a tropical station, revealed significant differences (up to 10 K) in the thermal structure between tropical and sub-tropical locations. Observed differences are attributed to disparity in the dynamics and local processes over these regions.

This work is carried out in collaboration with NARL, Gadanki

(Som Sharma, S. Lal, H. Chandra, and Y. B. Acharya)

Characteristics of the intra-seasonal oscillations in the lower and middle atmosphere over Gadanki

Systematic measurements of zonal wind have been carried out using radiosonde over Gadanki (13.5°N, 79.2°E) during April 2006 to December 2009. These measurements are combined with the results obtained from TIMED Doppler Interferometer, European Center for Medium range Weather Forecasting (ECMWF) zonal wind data and Outgoing Longwave Radiation (OLR) data from tropics to address Intra-Seasonal Oscillations (ISO). There is an emphatic signature of ISO modulation by dominant annual oscillation in the zonal wind over lower troposphere and upper stratosphere. Periodogram analysis has revealed dominant oscillations in the periodicity range of 20-100 days. ISO amplitudes are significantly higher in the Mesosphere and Lower Thermosphere (MLT) region in comparison with that of the Troposphere and Stratosphere. ISO activity is found to be intermittent in the troposphere and consistent in MLT. Signature of the ISO is found to be insignificant in the stratosphere. Normally, there is good correlation between convection and zonal wind during all seasons within ISO scale of variability. Also mean latitudinal and longitudinal ISO amplitudes in OLR show common pattern of variability with higher activity during winter than over summer during certain times, which is affirmed by ECMWF filtered wind results. These findings indicate the presence of some complex mechanisms which alter the direct impact of convection on the tropical ISO during certain times.

This work is done in collaboration with M. Venkat Ratnam, National Atmospheric Research Laboratory and P. P. Batista, INPE, Brazil.

(A. Guharay and R. Sekar)

Multi-pattern nocturnal variation in the mesospheric OH and O_2 emissions

Based on the observed mesospheric OH and O_2 airglow emission intensities from a low latitude station (Maui :- 20.8°N and 156.2°W), representative mesospheric temperatures are derived. The variations in the intensities and the derived temperatures are then examined to decipher systematic patterns, if any. Characteristic downward phase propagations associated with the upward propagation of gravity waves are conspicuously seen on many cases. However, many cases are also identified wherein downward phase propagation is not evident in temperature and/or in the intensity data. On many occasions, the variations in temperatures and intensity at the two wavelengths are anti-correlated. In addition, the signature of the impact of wave propagation is evident in one emission and not in the other emission. Sometimes, both the emissions get affected by the wave propagation. These cases provide clues to the way that gravity waves affect the mesospheric temperature and dynamics.

This work is done in collaboration with M. J. Taylor, Center for Atmospheric and Space Sciences, Utah State University.

(A. Guharay and R. Sekar)

Balloon-borne investigations of wave dynamics

In order to investigate the wave dynamics in the less explored region of $\sim$110 km and its coupling to the upper atmospheric regions, a Balloon-borne Investigation of Regional-atmospheric Dynamics (BIRD) experiment was conducted on 08 March 2010 from Hyderabad, wherein daytime ultraviolet oxygen emission line intensities at 297.2 nm that emanate from around 110 km were obtained. Coordinated ground based radio and optical measurements were also carried out in a campaign mode. The results reveal both longitudinal and latitudinal wave features in these emissions. Scale sizes of these wave features were

found to be of 50 – 70 km with periodicities of 25 ± 5 minutes. Further, these structures seemed to be travelling eastward with speeds of 30 – 60 ms^{-1}.

Carried out as part of PRL – Boston University Collaboration with Supriya Chakrabarti

(D. Pallamraju, F. I. Laskar, R. P. Singh, and R. Narayanan)

Investigations on vertical coupling using multi-wavelength daytime optical emissions from low-latitudes

High-spectral resolution daytime optical emission measurements at multiple wavelengths over a large (140°) field-of-view were obtained simultaneously using the multi-wavelength high-resolution echelle spectrograph from a low-latitude location, Hyderabad. The three oxygen emission lines measured are 557.7 nm, 630.0 nm and 777.4 nm that emanate from around 130 km, 230 km and peak altitude of the F-region, respectively during daytime. Analysis of around 60 days of data obtained during January – April 2011 shows different wave features in different emissions (different altitudes), different diurnal patterns in consonance with the dynamics at that altitude, and latitudinal variations that reflect the effect of neutral- and electro-dynamics of the low-latitude region. Further, wave periodicities were obtained for all these emission variations. Larger periods (of > 2 hrs.) seem to be present on more number of days at higher heights (in 777.4 and 630.0 nm) as compared to those of the lower altitudes (in 557.7 nm). At all the heights, periodicities of smaller timescales (< 20 minutes) are found to be predominant away from the equator when compared to other directions. Also, 13 – 20 minute periods are seem to be present on almost all the days. Such simultaneous multiple wavelength emission measurements provide us with a means of comprehensive investigations of vertical coupling in the upper atmosphere.

Carried out as part of PRL – Jawaharlal Nehru Technological University, Hyderabad collaboration with T. Vijaya Lakshmi

(F. I. Laskar, D. Pallamraju, R. P. Singh, and R. Narayanan)

Enhancement in OI 630.0 nm dayglow emissions during geomagnetic storm event

Geomagnetic storms give rise to latitudinal and longitudinal gradients in temperatures and electron densities which result in the redistribution of energy and momentum across various latitudes. During one such event (Dst = -300 nT) ground-based optical daytime thermospheric measurements over a wide field-of-view indicated a steady propagation in the emission brightness from high- to low-latitudes. Latitudinal total electron content on that day showed an inter-hemispheric asymmetry, indicating a strong equatorward wind. However, no enhancement in electron density was observed. Forward modeling carried out using inputs by varying composition and temperature to the physics based photochemical model indicate that O/N_2 values of around 0.6 – 0.8 and a 30% enhancement in the neutral temperature are required to match with the observations. These values agree reasonably well with the Thermosphere Ionosphere Mesosphere Electrodynamical Coupled Model (TIMEGCM) calculations. Results such as these provide insights into the energy distribution in the upper atmosphere during space weather events.

This work is done in collaboration with Jeffrey Crowley ASTRA, USA and Stanley Solomon UCAR, USA

(D. Pallamraju)

Evidence for the polarity variation with altitude in the E-region vertical electric field over Thumba, India

An evidence for the variation in the polarity of the vertical electric field over the dip equatorial region (Thumba, 8.5°N, 77.5°E) is obtained using a unique set of rocket flight measurements. These measurements were carried out during a total solar eclipse that happened to be a geomagnetic storm day. The path of totality was 400 km north of Thumba. Spectral analysis of magnetometer observations at different stations revealed small scale fluctuations indicating passage of gravity waves in the E-region of the ionosphere over Thumba. A possible mechanism of alteration of polarity of the vertical electric field in terms of passage of gravity waves is discussed based on the first order analytical calculations. The origin of the gravity waves is likely to be due to solar eclipse and/or due to geomagnetic storm.

(R. Sekar, S. P. Gupta, and D. Chakrabarty)

Changes in the solar EUV flux (0.1-50 nm) during the deep minimum between solar cycle 23/24 and its impact on the low latitude ionosphere

Changes in the mean level of the EUV flux (0.1-50 nm) on the low latitude ionosphere during the deep minimum between solar cycles 23 and 24 are investigated. It is observed that the rate of decrease of the mean level of solar EUV flux during the declining phase of solar cycle

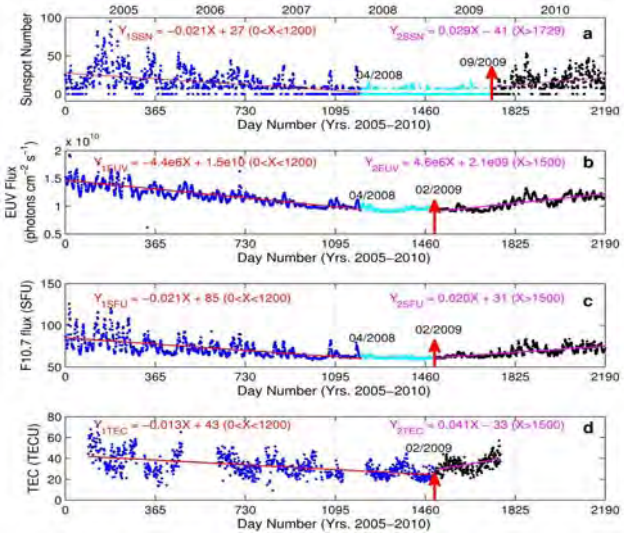

Figure 79: Variation of (a) daily sunspot number, (b) EUV flux, (c) F10.7 cm flux for the period 2005-2010 along with (d) the diurnal maximum TEC at Rajkot from 2005 to 2009. Separate linear regression lines are overlaid on the actual variations for the descending phase (red) of the solar cycle 23 and the beginning of the ascending phase of (pink) solar cycle 24. The cyan color in (a), (b) and (c) depict the interval when SSN, EUV flux and the F10.7 cm flux remain steadily low. The red arrow represents the onset of enhancements in the respective parameters in the solar cycle 24.

23 is comparable with the corresponding rate of increase during the ascending phase of solar cycle 24. However, the rate of increase of the mean TEC level over Rajkot (22.29°N, 70.74°E, 31.6°N dip angle) is found to be greater at the beginning of the solar cycle 24 compared to the rate of decrease during the declining phase of the solar cycle 23 (Figure 79). This anomalous behavior in TEC is attributed to the important roles played possibly by the residual (difference between annual averages) effects of the trans-equatorial wind and compositional changes over this time scale. It is verified that the inherent solar periodicity of around six months has no consistent causal connection with the semi-annual variation in TEC. A few spectral differences are also observed between the EUV flux and F10.7 cm (2800 MHz) flux. The annually averaged peak TEC value over Rajkot is found to be well-correlated (R = 0.98) with the corresponding annually-averaged F10.7 cm flux during 2005-2009. Statistical analyses also indicate that the time of occurrence of maximum TEC over Rajkot changes randomly during 2005-2009 indicating the possible role played by the processes related to the residual trans-equatorial wind over the years.

This work is done in collaboration with K. N. Iyer at Saurashtra University.

(D. Chakrabarty, Mala S. Bagiya, and Smitha V. Thampi)

Extreme changes in the in the equatorial- and low-latitude ionosphere during a space weather event

A case of drastic effects of an eastward prompt penetration and a subsequent westward overshielding electric field affecting the daytime equatorial ionosphere during a space weather event were investigated. The results showed that under the influence of the strong eastward prompt penetration electric fields the equatorial electrojet (EEJ) strength reached a value of 225 nT which is almost 7 times greater than the monthly quiet time mean at that time. This peak EEJ value exceeded the maximum observed values during the month for the entire solar cycle by more than 100 nT. Further, owing to an ensuing overshielding event that occurred during the main phase of the storm this unusually large EEJ showed a strong polarity reversal along with a weakening of the sporadic E-layer over the equator. The EEJ strength reduced from +225 nT to -120 nT resulting in a strong counter electrojet (CEJ) condition (Figure 80).

The latitudinal variation of the F-region electron density data over a large latitude range as observed from CHAMP satellite also revealed an ill-developed equatorial ionization anomaly over Indian sector due to this significant weakening

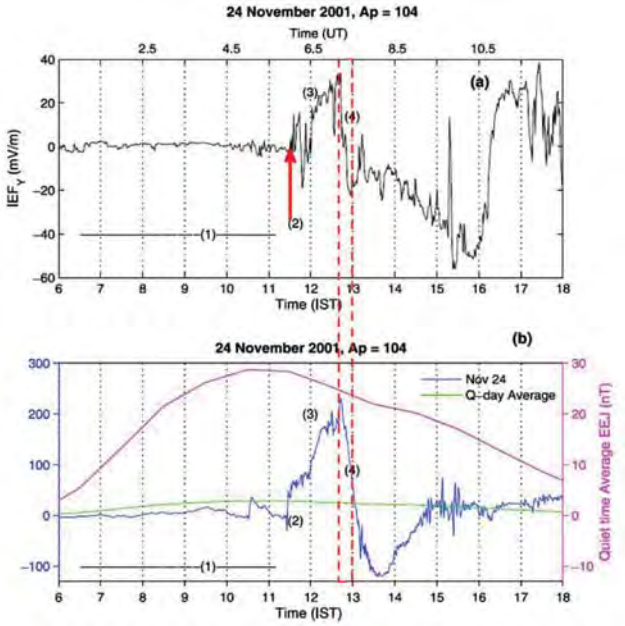

Figure 80: Variation of IEF$_Y$ on the space weather event day. The red arrow indicates the prompt penetration and the dotted rectangle indicates the overshielding event. The different phases of IEF$_Y$ variation are marked with numbers (1) to (4). (b) Variation of EEJ on the space weather event day, along with the quiet day variation for comparison. The quiet day mean values are plotted using hourly values, and they are plotted both on the same scale as that the storm day (left Y axis, quiet day mean is plotted with green color) and on an expanded scale (Right Y-axis, with pink color).

of the zonal electric field showing the significant degree to which the low latitude ionosphere can be affected by the interplanetary electric field (IEF).

This work is done in collaboration with K. G. Simi and S. R. Prabhakaran Nayar, University of Kerala, B. M. Pathan, Indian Institute of Geomagnetism and Tarun K. Pant, Space Physics Laboratory.

(Smitha V. Thampi and D. Chakrabarty)

Evolution of plasma bubbles observed using the CERTO beacon on board C/NOFS satellite

The ground-based reception of CERTO (Coherent Electromagnetic Radio Tomography) beacon signals from the C/NOFS (Communications/Navigation Outage Forecasting System) satellite, on 25 January 2009 showed the evolution of plasma bubbles. These observations are made from Bac Lieu, Vietnam (9.2°N, 105.6°E geographic, 1.7°N Mag. lat.). The ionosonde observations from Bac Lieu and Chumphon (10.7°N, 99.4°E, 3.3°N Mag. Lat.) show that there is a well developed Equatorial Spread F (ESF) at 105°E longitude whereas ESF was absent at 99° E longitude. Hence, the successive passes of C/NOFS reveal the evolutionary phases of plasma irregularities over 105° E longitude. The C/NOFS beacon reception also enabled observation of the corresponding VHF and UHF scintillations at their different phases of evolution, which provide a measure of the spectral evolution of irregularities. The spectral characteristics obtained from successive passes bring out the signatures of the cascading process of the plasma irregularities. This example shows the longitudinal variability of ESF during the deep solar minimum period.

This work is done in collaboration with M. Yamamoto, Kyoto University

(Smitha V. Thampi)

Evolutionary phases of equatorial spread F including L band scintillations and plumes in the context of GPS total electron content variability: A case study

The evolution of large scale (few kilometers), medium scale (few hundreds of meters), and small scale (meters) size plasma density irregularities in the post-sunset equatorial F region have been investigated from Indian longitudes using GPS total electron content (GTEC) variations. The ionograms and GTEC from a GPS receiver installed as a part of the GPS Aided Geo Augmentation Network (GAGAN) project for satellite based navigation are obtained from an equatorial station at Trivandrum (8.5°N, 76.91°E, 0.5°N Mag. Lat.). The residuals in GTEC obtained by subtracting the variations with the running mean in the GTEC are considered to represent the seed perturbations (P) for the plasma instability that results in the equatorial spread F (ESF) irregularities. The VHF radar at Gadanki (13.5°N, 79.17°E, 6.4°N Mag. Lat.) provided the small scale structures of ESF. The background thermospheric conditions that affect the growth of the plasma instability through ion-neutral collision frequency (V_{in}) are inferred using the F region base height (h'F). This (h'F) and the scale height for the neutral species at this altitude are used to estimate a growth factor (G). The present case-study reveals a close coupling between the background ionospheric conditions and the baseline perturbations in deciding the evolutionary phases of the ESF. It has been shown that although large scale size irregularities are formed without any constraints when the background ionospheric-thermospheric conditions are favorable, (in the presence of fluctuations in GTEC), the medium scale and small-scale irregularities show a remarkable similarity with the variations in the product of the perturbation (P) and growth (G) factors. Such clarity in the evolutionary pattern of different scale size irregularities are expected to pave way for a realistic forecasting of the phenomenon of ESF.

(Mala Bagiya and R. Sridharan)

Prediction of the occurrence pattern of L-band scintillations- a Reality

Ionospheric scintillations, whether they are in the VHF, UHF or L-band, are a hindrance to uninterrupted ground-satellite-ground communication links. Forecasting the occurrence of L-band scintillations has been a challenging task and this challenge has been tackled by evolving a simple/novel method using GPS-TEC data. A network of ground based GPS receivers has been established in India that provides round the clock data on TEC and scintillations in the L-band. For given background conditions, it has been shown that the fluctuations in the GPS-TEC truly represent the characteristic features of the perturbations that are responsible for the initiation of the plasma instability that finally culminates into the observed irregularities. The close linkage between the perturbation features and the evolutionary pattern of the scintillations enable us to forecast 'when', and 'for how long' the L-band scintillations would occur, in addition to their 'occurrence pattern'. The first of their kind of results take us a step closer towards operational forecasting of the L-band scintillations for real time navigational purposes.

This work is carried out in collaboration with S. Sunda at the Airports Authority of India

(R. Sridharan and Mala Bagiya)

Detection of sub-meter scale irregularities in nighttime E-region

Rocket-borne measurements on electron density were made over Trivandrum (8.5ºN, 76.9ºE) to study nighttime E-region plasma density irregularities. Irregularities with vertical scale sizes from a few km to 15 cm were detected during rocket's ascent and descent. Some of the important findings are: (i) horizontal gradients in electron density exist in 110 – 120 km region with horizontal scale size of at least 40 km, (ii) the horizontal distance over which the gradient drift instability operates is found to be at least 80 km, (iii) observed irregularities in regions of negative density gradient are suggested to be produced through the gradient drift instability (GDI) driven by vertical polarization electric field as well as by electric field produced through wind shears and those in positive gradient regions by wind driven GDI, (iv) largest irregularity amplitude (≈30%) were associated with steepest gradients and so were the presence of smallest vertical scale sizes (12 m to 15 cm), which were absent at other altitudes, (v) the spectral indices of irregularities was in the range of -2.2 ± 0.2 for large scales (few km > λ > 50 m), -3.25 ± 0.25 for medium scales (50 m > λ > 10 m), and -2.6 ± 0.1 for smaller scales (10 m > λ > 1 m), and (vi) irregularities in large and medium scales are expected to be produced directly through GDI and the small and sub-meter scales through non-linear GDI.

This work was done in collaboration with R. Pandey and Shweta Sharma of Mohanlal Sukhadia University, Udaipur

(H. S. S. Sinha and R. N. Misra)

Effects of a magnetic cloud simultaneously observed on the equatorial ionosphere in midday and midnight sectors

An impact of a magnetic cloud on the Earth's magnetosphere occurred at 1636 UT on 25 June 1998 associated with the sudden increase of the solar wind density, velocity and southward component of interplanetary magnetic field (IMF-Bz), which subsequently turned northward. During the positive phase of IMF-Bz, both the Auroral index (AE) and ring current index SYM-H remained steadily low indicating complete isolation of the Earth's magnetosphere from the solar wind and no significant changes were observed in the equatorial ionosphere. Subsequently, the southward turning permitted solar wind energy to penetrate the magnetosphere which caused a magnetic storm associated with strong auroral electrojet activity. Strong southward IMF-Bz corresponds to the dawn-dusk interplanetary electric field (eastward on the dayside and westward on the night side). The ionograms at Jicamarca (night side) showed strong spread-F and at Thumba (dayside) showed absence of equatorial type of sporadic-E, indicating dusk to dawn electric field. Thus, the observations point to electric field which is opposite in direction than what is expected by the prompt penetration of interplanetary electric field.

This work is done in collaboration with SPL, Thiruvananthapuram, IIG, Navi Mumbai and University of Massachusetts.

(R. G. Rastogi, H. Chandra, A. C. Das, and R. Sridharan)

Production and loss processes due to impact of galactic cosmic rays in the lower atmosphere of Mars

Understanding of the daytime lower ionosphere of Mars is limited due to lack of observations in this region. Production & loss rates and densities of electrons & 35 ions in the daytime lower atmosphere of Mars are calculated using energy loss method and continuity equation under the steady state chemical equilibrium condition. The primary ionization source in the model is taken as galactic cosmic rays. The chemical model couples the ion-neutral, electron-neutral, photodissociation of positive and negative ions, electron photo-detachment, ion-ion and ion-electron recombination processes through 101 chemical reactions. The model calculation of lower atmosphere of Mars suggests that maximum electron density of 0.5×10^2 cm^{-3} occurs at about 35 km due to high efficiency of electron attachment to O_x molecules, which implies that the concentrations of negative ions are higher than that of electrons below 35 km. Results show that out of all the processes included in the model, the most important process is the ion-neutral collisions wherein the reaction of $H_3O + (H_2O)_{2,3}$ with water and air molecules having the highest rates of $\sim 10^5$ cm^{-3} S^{-1}, making hydrated positive and negative ions as the most dominant ions with maximum densities of $\sim 10^3$ cm^{-3}. The ion-ion recombination, ion-electron recombination and photodissociation of positive ions are not very important processes, while electron-neutral collisions, electron-detachment of anions, and photodissociation of negative ions are significant only for a very few reactions.

(Varun Sheel and S. A. Haider)

Numerical simulation of the effects of a solar energetic particle event on the ionosphere of Mars

The ionospheric effect of solar energetic particle (SEP) event of 29 September, 1989 on Mars was investigated. The steady-state ionospheric model developed at PRL was used

to simulate vertical profiles of ion and electron densities. Due to this event electron density values exceeded 10^4 cm^{-3} in the 30-170 km range which is much larger than those typically observed in that altitude range. Ionosphere's total electron content was also increased by half of its subsolar value, which is capable of causing strong attenuation of radio waves. The simulated attenuation is 462 dB at 5 MHz, which demonstrates that SEP events can cause sufficient attenuation (> 13 dB) to explain the lack of surface reflections in some MARSIS topside radar sounder observations. A complementary generalized approach was also developed to the study of the ionospheric effects of SEP events. This approach predicts the threshold intensities at which a SEP event is likely to produce detectable change in electron density profiles and radio wave attenuation measurements. An event 100 times less intense than that on the 29 September, 1989 produces electron densities in excess of 3000 cm^{-3} at 80 km, which should be measurable by radio occultation observations and cause sufficient attenuation to eliminate MARSIS surface reflections. However, although enhancements in total electron content have been observed during SEP events, predicted magnitudes of enhancements in low altitude electron density were not confirmed by observations.

This work was done in collaboration with Paul Withers of Boston University

(Varun Sheel and S. A. Haider)

Meteor Showers on Mars

Meteor showers have been detected on Mars during summer and autumn seasons when comets 2007 P42 and 4015 Wilson-Harrington intersected the orbit of Mars on 21 January and 23 May 2005 from a close distance of 1.5 AU and 1.18 AU, respectively. The meteor shower of 21 January 2005 was observed at 77.7°N, 197.2°E and SZA of 74.3° during summer season (Ls = 147.4°). The meteor shower of 23 May 2005 was detected in autumn season at 65.1°N, 20.2° E and a SZA of 84.9° (Ls = 216.2°). The electron density profile measured by radio occultation experiment onboard Mars Global Surveyor on 21 January 2005 (Figure 81). It should be noted that 1435 electron density profiles of 1500 did not observe meteoric layers. The meteoric plasma layer is clearly distinct whenever it is visible in the lower atmosphere of Mars. This is not a permanent layer. We have reported earlier that D, E, and F peaks with concentrations of $7x10^1$ cm^{-3}, 2.4×10^4 cm^{-3}, and 8.4×10^4 cm^{-3} at altitude range of ~ 25-35, 100-112, and 125-135 km, respectively. The meteoric ablation produced fourth ionization peak ~ (1-2) x 10^4 cm^{-3} between D and E layers at altitude range ~ 80-105 km.

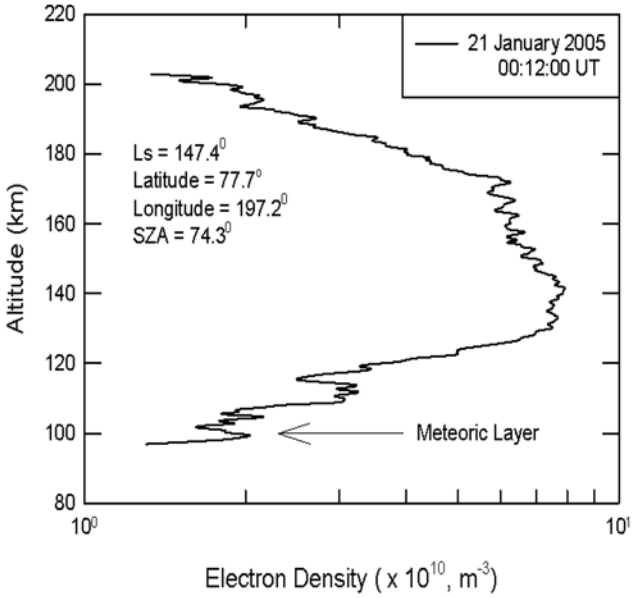

Figure 81: Electron density of Martian upper atmosphere obtained by MGS radio occultation data showing an ionization layer at around 100 km on 21 January 2005.

This work is carried out in collaboration with Mr. Bhavin Pandya, C.U. Shah College, Ahmedabad.

(S.A. Haider)

Response of solar X-ray flares in the Martian Ionosphere

Solar X-ray flux measured in the wavelength region of 1-8 Å onboard GOES 12 is considered as input to the Analytical Yield Spectrum and Total Electron Content (TEC) of the Martian ionosphere was calculated for several cases of solar flares. These TEC enhancements matched with the Mars Global Surveyor (MGS) observed ionospheric measurements with a time lag of around 4 minutes, which accounts for the time taken for the X-rays to travel from Earth to Mars. Further, on occasions, electron densities in the E region ionosphere increased by a factor of 2 during this period as measured by MGS. However, the calculated TEC values were very low on these days and thus, it is inferred that these enhancements observed were not produced as a result of ionization by solar X-rays and are probably due to shocks driven by CMEs.

This work is carried out in collaboration with K. N. Joshipura, S. P. University, Vallabh Vidyanagar, S .M. P Mckenna-Lawlor, National University of Ireland, Ireland, and C.D. Fry, Exploration Physics International Huntsville, USA.

(S.A. Haider and Rajmal Jain)

Core ionization leading to molecular fragmentation

Molecules may ionize and break-up when subjected to energetic charged particle impact. Removal of either valence or core electrons results in ionization. The two types of ionization mechanisms are expected to lead to different break-up pathways, which would be characterized by differences in the angular distributions of and energy sharing between the fragments. Core ionization may be directly distinguished from valence ionization by capturing the Auger electrons (which have well-defined energy) resulting from the electron cascade following core ionization. Ionization of molecules such as CO_2 and CO, subject to impact of fast highly charged ions is being studied. Efforts are underway to obtain an energy spectrum of electrons while simultaneously determining the mass and velocity spectra of the fragment ions. A set-up consisting of a cylindrical mirror analyzer for electrons and a time-of-flight based momentum imaging spectrometer for ions has been constructed and is being tested. Preliminary observations on CO_2 indicate that the branching ratios of various break-up fragments and their kinetic energies are different for core and valence ionization, as seen from the differences in the ion spectra observed in coincidence with Auger electrons and soft electrons.

This work is carried out in collaboration with C. P. Safvan at IUAC Delhi

(K. Saha, B. Bapat, and S. B. Banerjee)

Accessing potential energy functions of molecular di-cations

The process of creation and fragmentation of molecular ions from molecules is thought to occur in two steps: ionization of the neutral molecule (generally in its ground electronic) state resulting in an adiabatic transition to a molecular ion state, followed by separation of the nuclei, if the molecular state is unstable (lifetime $< 10^{-12}$ s). In an experiment one has control over the initial state of the molecule and the excitation agent, and the ionization–fragmentation pathway is estimated from the outcome of the process, viz. by identifying the fragments and measuring their kinematic parameters. This estimation is generally ambiguous, because a multitude of pathways could lead to near similar outcomes. The accuracy of the estimate is greatly enhanced if the potential energy functions of the intermediate molecular ion states can be computed. Measurements of the kinematics of break-up of doubly ionized molecular ions created by high energy electron-impact on small molecules (CO, N_2, H_2O) is being carried out. Computation of the potential energy functions of the molecular di-cations is performed using the molpro suite of programs. Various issues, such as evolution of the molecular di-cation state, adiabatic nature of the transition, etc. are being examined.

This work is carried out in collaboration with K. R. Shamsundar of IISER Mohali

(A Pandey and B Bapat)

Optical emission study of Carbon clusters formed in a laser vaporization cluster source

Optical emission spectroscopy methods are employed to study the process of clustering in a laser ablated graphite plume cooled by gas puffs from a pulsed valve. Synchronization between laser ablation and the pulsed gas puff was achieved by maximizing the emission intensities of C_2 Swan band identified in the emission spectrum from the cluster source. The vibrational temperature of Swan band is estimated for different gas fluences and also for different delays between laser ablation and gas puffing. The Swan band was numerically computed, and the vibrational temperature was estimated by matching the observed and computed spectra. It was observed that the vibrational temperature decreases with the amount of gas admitted to the ablation region.

(A. K. Saxena, Prashant Kumar, and K. P. Subramanian)

Determination of C_2 rotational and vibrational temperature of carbon plasma

The optical emission spectroscopy technique was applied to characterize the carbon cluster source based on ion sputtering on graphite, which was developed in the laboratory earlier. Evidence for clustering of sputtered material with argon and nitrogen as carrier gas was obtained by analyzing the C_2 Swan and the CN bands. The vibrational temperature of the Swan band was found to decrease with increase in carrier gas pressure, whereas, its emission intensity was found to increase with the discharge current in the cluster source. The estimated rotational temperature was found to be almost an order of magnitude less than the vibrational temperature. The plasma temperature in the source also was determined by calculating the excitation temperature of the argon carrier gas.

(Prashant Kumar, A. K. Saxena, and K. P. Subramanian)

Geosciences Division

The research activities of Geosciences Division focus on understanding of the origin and evolution of the planet Earth and its various components, with special emphasis on timescales and processes. The major areas of research of the division are: Solid Earth Geochemistry, Geomorphology and Tectonics, Paleoclimate and Paleoenvironmental studies, Hydrology, Aqueous Geochemistry, Oceanography and Paleoceanography, Biogeochemistry and Aerosol Chemistry. The methodologies followed center on the measurements of abundances of elements, activity of radioactive isotopes, ratios of radiogenic isotopes and light stable isotopes, and thermal/optical luminescence properties of materials using modern analytical tools.

IWIN National Programme

The National Programme on Isotope Fingerprinting of Waters of India (IWIN) crossed a milestone of 11,000 new isotope data ($\delta^{18}O$ and δD) generated exclusively at IWIN-IRMS laboratory at PRL. This has enabled isotopic characterization of different components of Indian Hydrological Cycle (i.e. vapour, rainwater, groundwater, river water and surface waters of Arabian Sea and Bay of Bengal) on a synoptic continental scale. Such isotopic characterization, essential to understand the interaction and exchange between these components, was not possible so far for want of data. Insights about various subtle processes in atmosphere, surface and subsurface components of hydrological cycle, which were not apparent until now, are now emerging from IWIN. The case of Indian Rivers is summarized in the following. The geographical distribution of seasonal contrast (max-min) in $\delta^{18}O$ and *d*-excess ($= \delta D - 8.\delta^{18}O$) of river water (Figure 82) reveal that over an annual cycle, the isotopic composition of river water can vary from as little as $\sim 1‰$ in both $\delta^{18}O$ and *d*-excess, to as large as $> 10‰$ in $\delta^{18}O$ and $> 30‰$ *in d*-excess. Four fluvial regions have been identified where different hydrological regimes prevail. These are: (i) Himalayan foothills and Gangetic plain, (ii) east coastal region $\sim 20°N$, (iii) southern tip of India, and (iv) west coastal region $\sim 20°N$. Hydro-meteorological processes responsible for the observed distribution are being examined in conjunction with corresponding isotopic signatures of groundwater and rain.

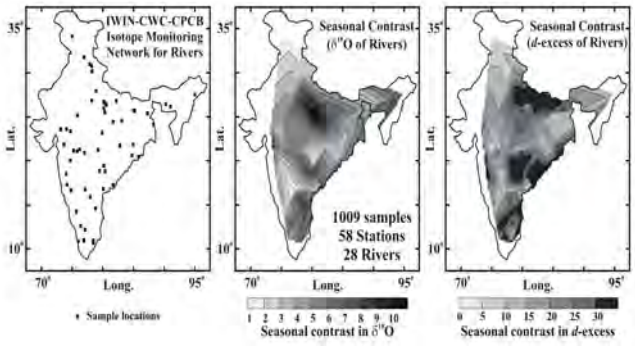

Figure 82: Geographical distribution of seasonal contrast (maximum - minimum) in $\delta^{18}O$ and d-excess ($= \delta D - 8.\delta^{18}O$) in Indian Rivers.

The characteristic features of four southern rivers (Cauvery, Godavari, Bharatapuza and Pennar) have been deciphered from the temporal variation in $\delta^{18}O$ of these rivers (Figure 83). The investigated rivers, whether east flowing or west flowing, have relatively lower $\delta^{18}O$ during SW summer monsoon months (JJAS). The west flowing Bharatapuza River has minimum lowering of $\delta^{18}O$ (only up to −4‰) during this period. The three east flowing rivers (Godavari, Cauvery and Pennar) have much lower $\delta^{18}O$ (up to −7‰) during SW summer monsoon months. Additionally, the three east flowing rivers also have variable extent of lowering of $\delta^{18}O$ during NE winter monsoon months (from middle of October to December). The Polavaram, Musiri, and Chennur stations, respectively on Godavari, Cauvery and Pennar Rivers, in southern Indian peninsula, dominated by NE Winter monsoon, have more pronounced lowering of $\delta^{18}O$ during corresponding winter months.

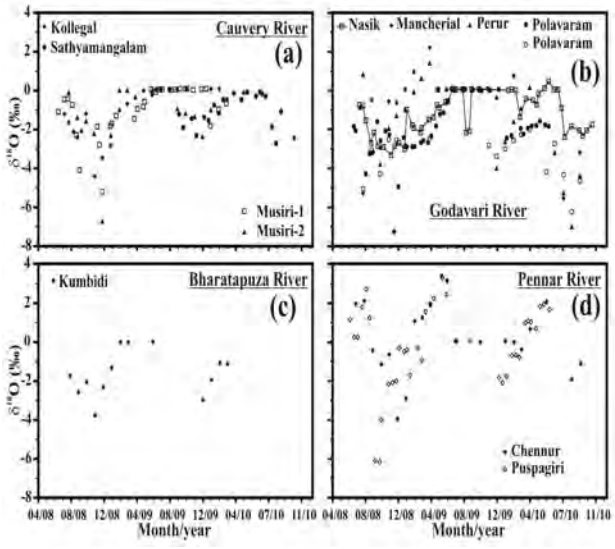

Figure 83: Temporal variation in $\delta^{18}O$ of Rivers (a) Cauvery, (b) Godavari, (c) Bharatapuza, and (d) Pennar.

Compared to four southern peninsular rivers, the Himalayan River Ganga has distinctly different isotopic character (Figure 84), both in terms of range of seasonal variation in $\delta^{18}O$ and its geographical variation among 9 stations being monitored under IWIN Programme. At Rishikesh, which is located farthest north among the 9 stations, the Ganga River has the lowest $\delta^{18}O$ values (< −10‰) throughout the year and vary in a narrow range from −10‰ to −13‰. These low $\delta^{18}O$ values can be ascribed to contribution largely from high altitude precipitation in upstream regions, and snow and glacial ice melt. Further downstream of Rishikesh, the Ganga River enters the plains where relative contribution of local precipitation at lower altitude and affluent groundwater is expected to increase which seems to be responsible for distinctly higher $\delta^{18}O$ values at all other downstream stations. The Ganga River exhibits distinct increase in $\delta^{18}O$ during dry pre-monsoon (March-May) months and decrease in $\delta^{18}O$ during SW summer monsoon (JJAS). The observed increase in $\delta^{18}O$ during dry pre-monsoon months may be related to considerable evaporation from flowing river and increased contribution of affluent groundwater discharge, originally derived from rainwater which normally undergoes evaporation prior to infiltrating. This is evident (Figure 83) from significant decrease in *d*-excess ($= \delta D - 8.\ \delta^{18}O$) of river water during pre-monsoon period. The *d*-excess is a useful isotopic parameter which can identify the effect of evaporation and/or change in primary vapor source for precipitation or condensation under condition of vapor supersaturated ambience.

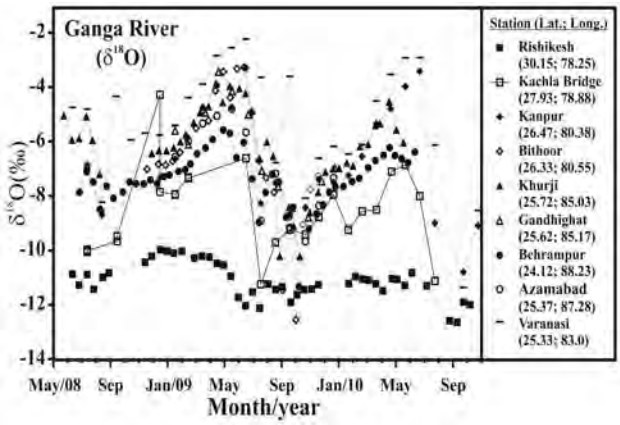

Figure 84: Temporal variation in $\delta^{18}O$ of Ganga River at 9 stations being monitored under IWIN Programme, in collaboration with CPCB and CWC.

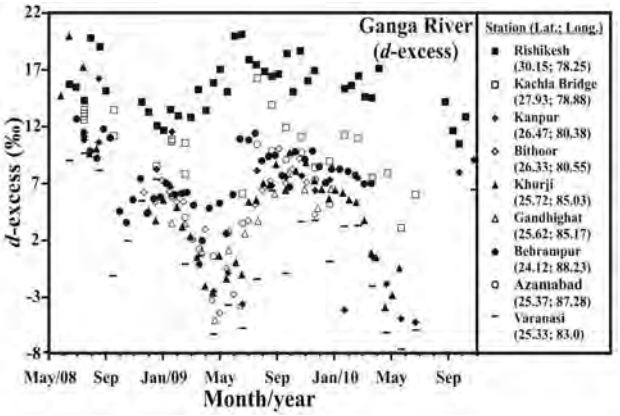

Figure 85: Temporal variation in d-excess of Himalayan River Ganga at 9 stations being monitored under IWIN Programme, in collaboration with CPCB and CWC.

Comparison of Figure 84 and Figure 85 reveals that higher $\delta^{18}O$ of Ganga River, during dry pre-monsoon months, corresponds to lower d-excess confirming the imprints of evaporation. It is seen (Figure 84 and Figure 85) that further

downstream from Rishikesh, the $\delta^{18}O$ increases and d-excess decreases progressively. The time series of d-excess of Ganga River (Figure 85) reveals that river water at Rishikesh has consistently higher d-excess (> ~12‰) throughout the year, compared to global average value for precipitation (10‰). The d-excess of Ganga River at Rishikesh increases up to ~20 ‰ during SW summer monsoon (JJAS). The constituent components of river discharge, namely, local precipitation (d-excess = ~11‰), groundwater around Rishikesh (d-excess = ~13‰) and snow-melt (d-excess = range ~15-25‰;) are not reported to have so high values that their fractional contribution can increase the d-excess of river water up to ~20 ‰, as observed. Therefore, it seems that there is possibly a source of water with considerably higher d-excess than known at present. Vapor deposition under supersaturated environment and kinetic fractionation effects during post depositional sublimation of ice can result in increased d-excess of ice and resultant melt. Comparison of these isotopic characteristics of rivers with those of rain and groundwater, in conjunction with hydrometric and meteorological parameters, has provided insights about region specific hydrological processes.

(R.D. Deshpande, Medha Dave, Rajlaxmi Singh, S.K. Gupta)

Stable O and H isotopes in rainwater during severe thunderstorms occurred in Assam

During the pre-monsoon season severe thunderstorms occur in some years over the Gangetic plains of India causing heavy rains and at times trail of destructions in its path. These move from Northwest to Southeast therefore called Nor'westers and locally 'Kal Baisakhi' as it occurs in Baisakh (pre-monsoon season) and causes huge economic losses. Isotopes in rainwater samples collected between 2009 and 2011 CE from Hailakandi, Assam, which includes 2010 CE (a Nor'westers year) show (Figure 86) wide range, from +0.7 to -13.8 ‰ in $\delta^{18}O$ values and from +12 to -98 ‰ in δD values. Using isotopic studies, satellite and re-analysis data it is found that strong evaporation and localised convection are associated with the elevated sea surface temperature in Bay of Bengal and therefore it could be the cause for the origin of the severe Thunderstorms. Additionally, this study also shows absence of any relationship between isotope and amount of rain (so called Amount Effect). A very low d-excess value (up to -26 ‰) was observed for the severe Thunderstorms and is attributed to the dominant contribution of the re-evaporated components from the major rivers and lowland areas. The Local Meteoric Water Line (LMWL) is indistinguishable from the GMWL (Figure 86) but is

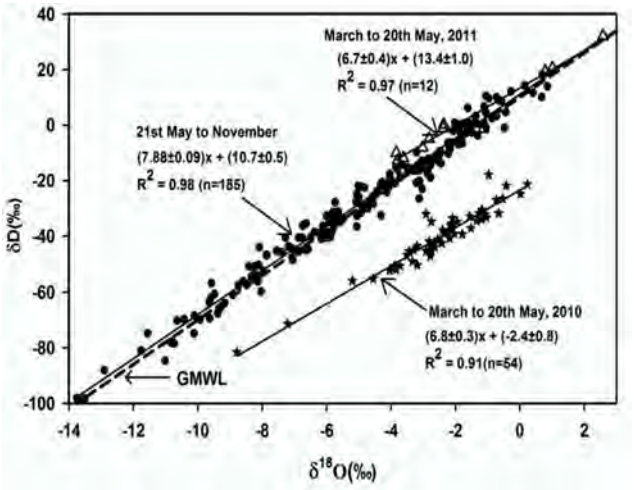

Figure 86: $\delta^{18}O$ and δD of rainwater collected from June, 2009 to July, 2011. During monsoon season (June to Oct) the local precipitation samples follow the GMWL (dotted line). During severe Thunderstorms in 2010 (star) the LMWL differs significantly from the GMWL.

significantly different from the Global Meteoric Water Line (GMWL) during severe Thunderstorms. Due to absence of any relationship between isotope and rain amount, attempt to reconstruct paleoclimate of the area would remain a challenging task.

(Amzad H. Laskar, R. A. Jani, R. Ramesh and M. G. Yadava)

Northern Indian Ocean as a source or sink of CO_2

The Arabian Sea and the Bay of Bengal in the northern Indian Ocean are characterized by contrasting oceanographic features resulting in distinct differences in

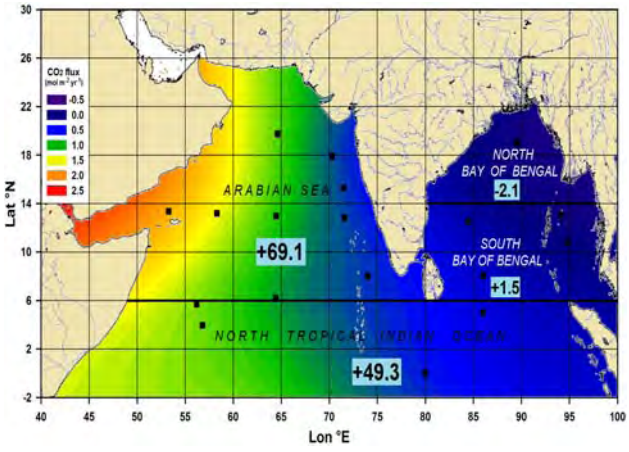

Figure 87: Contours of sea-air flux of CO_2 in the northern Indian Ocean. Net regional CO_2 fluxes (in $TgC.yr^{-1}$) are shown in the boxes for the four regions. Positive values of flux indicate net source (in the Arabian Sea and the North Tropical Indian Ocean), while negative flux indicates net sink (for the North Bay of Bengal).

their circulation pattern in the thermocline region and also in the magnitude and direction of the sea-air CO_2 fluxes. Radiocarbon has been used as a tracer to quantify air-sea exchange fluxes of CO_2 on decadal time scales. The small changes in bomb-^{14}C inventories, significant increase in the mean penetration depths and lowering of the surface $\Delta^{14}C$ values in the northern Indian Ocean indicate the temporal variation of bomb-^{14}C in two decades is mainly through downward transfer through mixing with deeper waters. The high bomb-^{14}C inventory at the equator can be attributed to lateral advection of ^{14}C-enriched waters from the Pacific Ocean through the Indonesian archipelago. Net sea-air flux of CO_2 estimated for the northern Indian Ocean between 0^0N and 25°N is $\sim 10^4 \pm 30$ TgC.yr^{-1}. The Bay of Bengal is a net sink of atmospheric CO_2 with an intake of $\sim 1 \pm 0.4$ TgC.yr^{-1}, while the Arabian Sea is a source of CO_2 releasing $\sim 69 \pm 21$ TgC.yr^{-1} (Figure 87).

This work was carried out along with K. Dutta, presently at University of Minnesota, Duluth, USA

(Ravi Bhushan)

Nitrogen and carbon dynamics in a tropical estuarine ecosystem

This is a new research program initiated with the aim to understand nitrogen (N) and carbon (C) dynamics in a tropical estuarine ecosystem. It is well known that nearly half of the world's population reside within 100 km of the coast leading to large scale pollutant discharge, including N and P. The estuarine ecosystems which process these high pollutant loads are deteriorating fast leading to ecological changes. The understanding of how these human-induced ecological changes affect the rates of biogeochemical processes in large estuaries is sparse.

The Cochin estuary is among the most vulnerable ecosystems in India due to increased anthropogenic activities. This estuary is connected to the Arabian Sea through two openings leading to transport of large amount of organic matter and nutrients to the coastal sea. During this program, we plan to conduct experiments on seasonal basis for measuring N and C transformation rates using stable isotope techniques. First field campaign for this study was successfully completed during April 2012 and sample analyses are underway. Particulate samples for N and C isotopic composition in suspended particulate matter are also being collected on monthly basis. We also plan to develop isotopic techniques for tracing the sources of nutrients (pollutants) to the estuary. Overall, the results of this study would provide us an insight into N and C turnover rates with respect to salinity and pollution gradient along with the pathways for origin and transformation of organic matter in the region.

This work is being done in collaboration with G. V. M. Gupta of Centre for Marine Living Resources and Ecology, Cochin.

(Sanjeev Kumar and Bhavya P.S.)

Climate induced changes in nitrogen cycling of coastal waters

Climate projection models predict increases in globally averaged mean sea surface temperature (SST) and precipitation over the 21st century. According to Indian Meteorological Department, the SST of equatorial central Indian Ocean has increased by 1.5°C in the last 50 years. Coastal Arabian Sea, due to its hydrographic settings, is also likely to experience increase in SST, higher freshwater runoff and decreased surface salinity. These conditions may alter nutrient cycling in coastal regions due to potential changes in phytoplankton community structure and their ability to assimilate nitrogen (N) and carbon (C).

Within this context, it is important to understand how climate-induced changes in SST and salinity may affect phytoplankton's potential to assimilate N and C. To assess this, we performed a large-scale mesocosm experiment with coastal seawater. During this experiment we manipulated temperature (28 and 31°C) and salinity (31 and 35) and performed tracer experiments to estimate carbon, nitrate, ammonium, and urea uptake rates under different conditions. Preliminary results obtained from this study indicate reduced N uptake rates under lower temperature and salinity conditions (28°C and 31). This suggests that the potential for biological N uptake in coastal regions around the world may hinge upon the combination of both temperature and salinity. Taken together, the final result of this experiment would help us to understand potential changes in N and C dynamics in the coastal regions under projected climatic conditions.

This work was done in collaboration with Anna Godhe of the University of Gothenburg, Sweden.

(Sanjeev Kumar, Bhavya P.S. and R. Ramesh)

Sea surface pCO_2 in the Indian Sector of the Southern Ocean during Austral summer of 2009

Southern Ocean plays a key role in removing carbon dioxide from the Earth's atmosphere by physical, chemical and biological processes. The present study attempts to

understand pCO_2 and its relationship with nutrients and biological production in the Indian sector of the Southern Ocean during the late austral summer of 2009 CE. The partial pressure of carbon dioxide (pCO_2) showed high spatio-temporal variability in the study area. The highest pCO_2 was recorded along the Polar Front (PF) on the two transects is attributed to low productivity in the PF. From 57°.30'E towards 48°E, the average sea surface pCO_2, chlorophyll and Total organic carbon (TOC) increased by 24 μatm, 0.3 mg/m3 and 3 μM, respectively, suggests that the physical processes are predominantly active along 48°E. Enhanced vertical mixing along 48°E supports with the corresponding increase in average NO_3, PO_4 and SiO_4 concentrations by 2 M, 0.4 μM and 1.7 μM, respectively. pCO2 and chlorophyll-a are negatively correlated along 57°.30'E, however, positively correlated along 48°E, which suggests that the biological processes control the pCO_2 along 57°.30'E. The average air-sea fluxes recorded were about −28 and −33 mmol $m^{-2}d^{-1}$, on TW and TE, respectively. A significant finding of this study is that although the Southern Ocean is a known sink of carbon dioxide, the vicinity of the Crozet Island, where oceanic fronts are known to merge, appears to act as a source of atmospheric CO_2. It is attributed that "The island mass effect" could also be a factor that generates elevated CO_2 in the vicinity of the study area. In the last one decade the oceanic pCO_2 increased at a rate 0.77 μatm /year in the region south of the Polar front; but is not associated with the Southern Annular Mode.

This work was done in collaboration with S. Shetye, M. Sudhakar, R. Mohan and S. Patil of NCAOR, Goa.

(A.H. Laskar and R. Ramesh)

Contribution of riverine dissolved inorganic nitrogen flux to new production in the coastal northern Indian Ocean – an assessment

Anthropogenic activities (such as deforestation and fertilizer use) have not only increased carbon dioxide (CO_2) in the Earth's atmosphere, but also nitrogen on the Earth's land surface. It is important to assess the sources and sinks of carbon and nitrogen as these two elements affect the Earth's climate significantly, and are coupled in some ways. The ocean is one of the major sinks of CO_2, and its efficiency of removing CO_2 by photosynthesis depends on the availability of nutrients (e.g., nitrogen, silicon, iron, and phosphorus) in the sunlit upper ocean. The ocean takes up CO_2 along with DIN (in a particular ratio known as *Redfield* Ratio, C:N:P:: 106:16:1) during photosynthesis in the photic zone (up to the depth at which the light intensity decreases to 1% of that at the surface) and the conversion rate of inorganic carbon to organic carbon is known as primary productivity. Part of this primary productivity which is supported by new nutrients (mainly nitrate), introduced from outside into the photic zone, is termed as new productivity. On an annual time scale it is approximately equal to the rate of export of organic matter to the deep from the upper ocean.

Primary productivity in the surface ocean is often limited due to the unavailability of nutrients such as nitrate, phosphate and iron. It is shown that the scarcity of nitrogen bearing nutrients (e.g., nitrate, nitrite, ammonia, urea and Dissolved Organic Nitrogen; DON) in coastal regions limits primary productivity while other nutrients are available. As a result of nitrogen limitation in the surface ocean, the riverine inorganic nitrogen flux is rapidly utilized in the coast itself. This enhances the importance of coastal ecosystems, as the coastal zone (depth < 200 m) occupies only ~7% of the total oceanic area and <0.5% of volume, but accounts for (i) ~18-33% of oceanic biological production (ii) ~80% of organic carbon burial (iii) ~90% of sedimentary mineralization (iv) >50% of sedimentary denitrification (v) ~50% of $CaCO_3$ deposition (vi) ~90% of the world's fish catch (vii) ~40% of the value of the world's ecosystem services and natural capital (viii) trapping the bulk of terrestrially-derived suspended matter, nutrients and other chemicals, including pollutants (ix) ~40% of the world population living within 100 km of the coastline (16 out of 23 mega cities); that makes the coastal regions extremely vulnerable to anthropogenic perturbations. Nutrients derived through rivers are partially responsible for all the above effects.

The northern Indian Ocean provides a unique opportunity to assess the impact of DIN fluxes through both larger and smaller rivers on new production. This oceanic basin is divided into two: the Arabian Sea, and Bay of Bengal. These regions are very different in many aspects; the eastern Arabian Sea receives relatively less water discharge (0.3×10^{12} m^3 yr^{-1}) relative to the Bay of Bengal from the rivers of subcontinental origin, while the western Arabian Sea is adjacent to the Arabian Desert. On the other hand, the Bay of Bengal receives a large amount of fresh water (1.6×10^{12} m^3 yr^{-1}, with prodigious amounts of dissolved nutrients) through rivers from the subcontinent. The Bay of Bengal offers a good opportunity to quantify the impacts of river discharge on new production, as some of the world's larger rivers debouch into this basin. Our study provides an analysis of DIN fluxes and its possible contribution to new production in the coastal northern Indian Ocean based on literature data. Most of the riverine DIN flux (~81% in the case of the Arabian Sea and 96% in the case of the Bay of Bengal) is not transported to the coastal ocean and is consumed on the course of the rivers

or in the estuaries. Coastal Bay of Bengal and Arabian Sea receive ~ 0.38 Tg N $year^{-1}$ (1 Tg = 10^{12} g) and ~ 0.06 Tg N $year^{-1}$, respectively, through rivers. A large variation in the contribution of DIN through river fluxes to new production is found in both these basins.

(R. Ramesh and A. Singh)

Reconstruction of Indian Summer Monsoon (ISM) during the last 11000 years, in Uttrakhand Himalaya

We have reconstructed a high resolution (centennial scale) monsoon variability using the lake sediments from Pinder river valley in the Uttrakhand Himalaya. The variation in the concentration of geochemical proxies in the lake sediment has been used as a surrogate for reconstructing the temporal changes in monsoon strength during the last 11000 years (Figure 88). High sedimentation rate (~100 cm/kyr) along with high concentration of geochemical proxies between 11000 year and 9400 year indicate strengthened Indian Summer Monsoon (ISM) resulting in increased catchment erosion. This event corresponds to the early Holocene strengthened monsoon in Indian sub-continent. This was followed by an abrupt decrease in the major and trace elements during 9400-9000 year implying weakening in the ISM intensity. This event is succeeded by overall improvement in ISM with fluctuation until around 6000 year. Following this, an appreciable decrease in the geochemical proxies after 6000 and 5000 year indicate declining ISM phase in the region. This event corresponds to the Mid Holocene aridity. The increase in geochemical proxies suggests improved ISM condition after 4000 year, which continued till 800 year with a minor reversal around 1200 year. The later part of this event corresponds to the Medieval Warm Period. After around 800 years, the geochemical data suggests a declining trend which seems to equate with the Little Ice age. Above observations accord well with the Total Solar Irradiance, thus, suggesting a close coupling between solar insolation and the ISM during the Holocene.

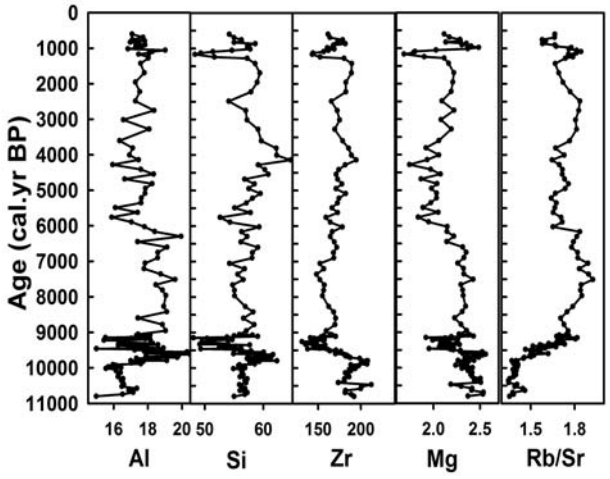

Figure 88: Major and trace element variations in the Benital Lake showing variations in catchment erosion and ISM intensity during the last 11kyr.

This work is done in collaboration with S. P. Sati and N. Rana of H.N.B. Garhwal University, Srinagar

(Ravi Bhushan, Anil D. Shukla and N. Juyal)

Ascertaining sediment sources in a proglacial lake during the marine isotopic stage

It has been suggested that during the Marine Isotopic Stage_2 (MIS^{-2}), there were periods of intense dust deposition both on the continent and sea. Particularly, there is evidence to suggest that during the global glacial maximum (~20 ka), there was increased dust transport across the globe. Therefore, the lakes that are located in the dust trajectories such (mid-latitude westerlies) would have received significant contribution from the extra basinal dust during their existence. One such lake located at the southern margin of the Tibetan plateau at Goting in the Dhauli Ganga basin was investigated in order to identify the endogenic (with in the lake catchment) to exogenic (outside the lake catchment) source of sediment. Towards this we used major and trace element geochemistry as the chemical composition of the lake sediments can be used effectively to identify the sources of the sediments and to understand the tectonic and climatic conditions prevailed during the lake sedimentation. Major and trace element composition of the lake sediment indicate that majority of the sediment deposited in Goting lake were derived from the local catchment lithology under the influence of physical weathering as indicated by low chemical index of alteration (CIA). The low chemical weathering is further supported by the close correspondence between Al_2O_3 and TiO_2 variability during the existence of the lake. Our data suggests that the sediment source was associated with the upper continental crustal type lithology (granodioritic) as indicated by the Al-K-Ca* + Na diagram, where majority of the sediments follow two parallel trends parallel to Ca* + Na-Al axis. Further few selected samples analyzed for trace and REEs suggests felsic to intermediate igneous lithology rocks on the chondrite normalized REE plot. Absence of exogenic source into the lake could be due either to the weak mid-latitude westerlies during the global glacial maximum or alternatively, the basin was shielded from the dust laded wind trajectories.

(A. D. Shukla and N. Juyal)

Pattern of Late Quaternary Glaciations in Indian Himalaya: current status

Glacier expansion is generally a response of lower temperature, but at high altitude it may be more sensitive to changes in moisture transport. It has been suggested that in humid regions, glaciers advanced due to changes in precipitation whereas in arid regions they are temperature driven. Although there is general agreement on the significance of monsoon strength and glacier response in Himalaya, the exact mechanisms, timing and geographical extent of monsoonal influence is still debated. We investigated the existing chronology (around 200 mostly exposure ages) obtained on the Quaternary glacial deposits in Indian Himalaya in order to assess the above suggestions.

The probability density distribution of the existing chronology obtained on sediments associated with glacier advances are biased towards periods of enhanced insolation/monsoon. This is further supported by the Guliya ice core data indicating periods of glacier expansions correspond to warm climatic intervals. In a monsoon dominated western and central Himalaya (Figure 89), it is reasonable to accept monsoon glacier relationship because in this part of the Himalaya, mass balance data indicate that snow accumulation and ablation occur during the summer. Hence the glaciation was asynchronous with the north hemisphere glaciations. However, in the mid-latitude westerly dominated northwestern Himalaya (Figure 90), it was expected that glaciers should have responded to enhanced westerlies (cold periods) thus should have been synchronous with the northern hemisphere glaciations.

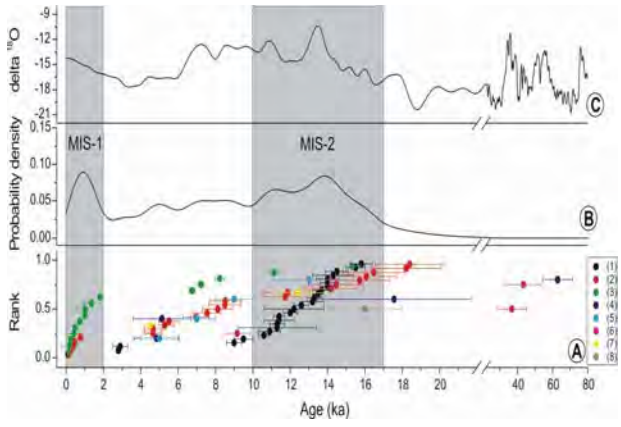

Figure 89: (A) Age distribution of the western and central Himalaya. (1) Owen et al 2001; (2) Scherler et al 2010; (3) Barnard et al 2004; (4) Sharma and Owen 1996; (5) Mehta et al 2012; (6) Owen et al 1997; (7) Nainwal et al 2007; (8) Pant et al 2006). Vertical dispersion of ages represents Rank (0-1), (B) Probability density plot of the published ages, (C) Oxygen isotopic record of Guliya Ice core. Enriched isotopic values indicate increase insolation and strengthen monsoon.

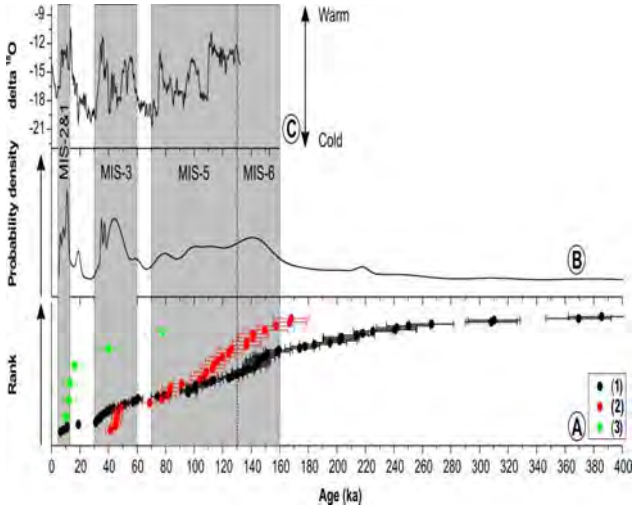

Figure 90: (A) Age distribution of the north western Himalaya. (1) Owen et al 2006; (2) Dortch et al 2010; (3) Taylor and Mitchell 2000). Vertical dispersion of ages represents Rank (0-1), (B) Probability density plot of the published ages, (C) Oxygen isotopic record of Guliya Ice core. Enriched isotopic values indicate increase insolation and strengthen monsoon.

Our study suggests that the existing data are too meager to ascertain the role of westerlies in modulating the late Quaternary glaciations in the northwestern Himalaya as also to unequivocally advocate the role of summer monsoon in glacier expansion during the late Quaternary. It is because of this, no meaningful inferences can be drawn in terms of quantifying the role of precipitation or the temperature changes in driving the glaciations in the Himalaya. Unless systematic mapping of the moraines located in different climatic zones should be carried out in the Himalayan region supported by stratigraphically constrained glacial events and combining them with multiple dating techniques, the existing interpretation that monsoon is the major driver of glcaition in Himalaya would remain speculative.

(S. Nawaz Ali and N. Juyal)

Significant are the mid-latitude westerlies in driving Nubra valley glaciations

In an effort to understand the role of mid-latitude westerlies in the expansion of glaciers particularly in the northwestern Himalaya, a preliminary field investigation was carried out in the Nubra valley. It is believed that Nubra valley owe its evolution to the contribution made by the Siachin and its tributary glaciers during the Quaternary which are fed by the mid-latitude westerlies. Therefore paleoglaciation study in this valley provides an opportunity to test the hypothesis that whether the entire Himalayan glaciers advanced and retreated asynchronously with that of the Northern

Hemisphere thus emphasizing the role of ISM or were there specific geographical regions that responded to the changes in the intensity of westerlies.

Nubra valley is located in the Trans Himalaya and spans the Central Karakoram and Ladhak range in the extreme northwest of India and the relics of past glaciation are preserved in the forms well defined ridges of lateral moraines which provide an opportunity to reconstruct the extent of glaciation during the late Quaternary. The preliminary chronology obtained on the recessional moraines collected between the Siachin glacier snout and the confluence of Nubra-Shyok rivers at Tirit indicate that the recessional moraine proximal to the Siachin glacier snout (near OP Baba shrine) are dated between 0.52 ± 0.04 ka to 0.94 ± 0.1 ka. The two lateral moraines viz. at Sasoma ($\sim$35 km downstream of Siachin snout) is dated to 24.0 ± 2.0 ka. Whereas the farthest located two lateral moraines $\sim$90 km away from the snout at Tirith is dated to 24.4 ± 2.0 ka and 18.2 ± 1.1 ka respectively. In terms of climate variability, it can be suggested Nubra valley was extensively glaciated during the Last Glacial Maximum (LGM) so much so that the Siachin glacier descended up to Tirit a distance of around 90 km from the present day snout. This would imply that Nubra valley glaciers responded in accordance with the Northern Hemisphere glaciations during the LGM thus emphasize the role of the mid-latitude westerlies in glacial advancement in the northwestern Himalaya.

This study was carried out in collaboration with Yogesh.C. Nagar, A. Ganjoo and P.K. Staywali of Snow and Avalanche Study Establishment (SASE), Manali.

(N. Juyal)

Increasing aridity over the past 223 years in the Nepal Himalaya inferred from a tree-ring $\delta^{18}O$ chronology

A tree-ring $\delta^{18}O$ chronology of Abies spectabilis from the Nepal Himalaya was established to study hydroclimate in the summer monsoon season over the past 223 years (AD 1778–2000). Response function analysis with ambient climatic records revealed that tree-ring $\delta^{18}O$ was primarily controlled by the amount of rainfall during the monsoon season (June–September). Since tree-ring $\delta^{18}O$ was simultaneously correlated with temperature, drought history in the monsoon season was reconstructed by calibrating against the Palmer Drought Severity Index (PDSI). Our reconstruction that accounts for 33.7% of the PDSI variance (Figure 91) shows a decreasing trend of moisture over the past two centuries, and is consistent with reduction

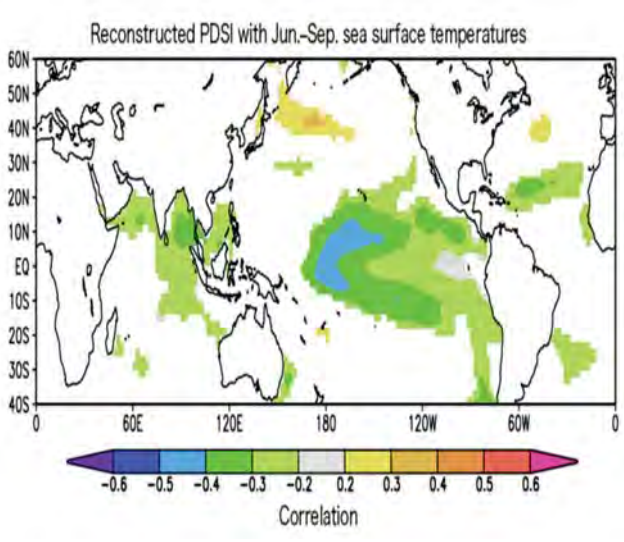

Figure 91: Spatial correlation field comparing the reconstructed PDSI with SSTs (ERSST v3) for the period of 1901–2000. This figure was generated using KNMI climate Explorer (http://climexp.knmi.nl/).

in monsoon precipitation recorded in Himalayan ice-core records. Spatial correlation analysis with global sea surface temperatures suggests that the tropical oceans play a role in modulating hydroclimate in the Nepal Himalaya. Our reconstructed PDSI shows a negative correlation with sea surface temperature (SST) over most of the tropical Pacific and Indian Ocean, in particular the central Pacific (Figure 91), suggesting that the tropical oceans play a role in modulating hydroclimate in the Himalaya. In fact, a modeling study indicates that a weakening trend of monsoon precipitation found in northern India and eastern Tibetan Plateau over the latter half of the 20th century can result from an increase in SST over the tropical Pacific and Indian Ocean. When coupled with the fact that a consistent warming over the last two centuries was found in a coral-based reconstruction of large-scale tropical SSTs, the SST forcing can explain the overall decrease trend in our reconstructed PDSI. It should be noted, however, that other proxy records from lower altitudes indicate a strengthening of the monsoon winds and precipitation. It is indicated that north–south differences of monsoon intensity are attributed to a southward shift in the overall position of the monsoon trough. The present study suggests that elevated SST over the tropical oceans may be responsible for the increased north–south differences over the couple of centuries.

This work was done in collaboration with Masaki Sano (Japan), M. S. Sheshshayee (UAS) and R. Sukumar (IISc)

(R. Ramesh)

Variations in O and C isotopic compositions in speleothems from Andaman Islands and their potential for paleomonsoon reconstruction

The Indian monsoon activity, coinciding with the Inter Tropical Convective Zone (ITCZ), progresses from the southern Indian Ocean during boreal summer and withdraws toward the south in winter. Islands situated to the south of India receive therefore the first and last showers of monsoon, and speleothems in such islands need to be explored for their potential to reconstruct past monsoon activity. Stable carbon and oxygen isotopic compositions ($\delta^{13}C$ and $\delta^{18}O$) of a stalagmite collected from the Baratang island of Andamans, along with new data on $\delta^{18}O$ of modern monsoon precipitation (May to July 2010 CE) were used to understand: (i) whether these samples are amenable to dating using ^{14}C; (ii) Whether their oxygen isotopes indicate precipitation under isotopic equilibrium; (iii) if (i) and (ii) above are true, whether we reconstruct monsoon activity during the past millennia? We find that $\delta^{18}O$ of speleothem does show evidence for precipitation under isotopic equilibrium, while dating by ^{14}C shows inversions due to varying contributions from dead carbon. The summer monsoon over the Andaman Islands was similar to the present a few millennia ago; the southwest monsoon was the main source of annual precipitation (Figure 92).

This work was carried out in collaboration with Geological Survey of India, Kolkata and the University of Hyderabad.

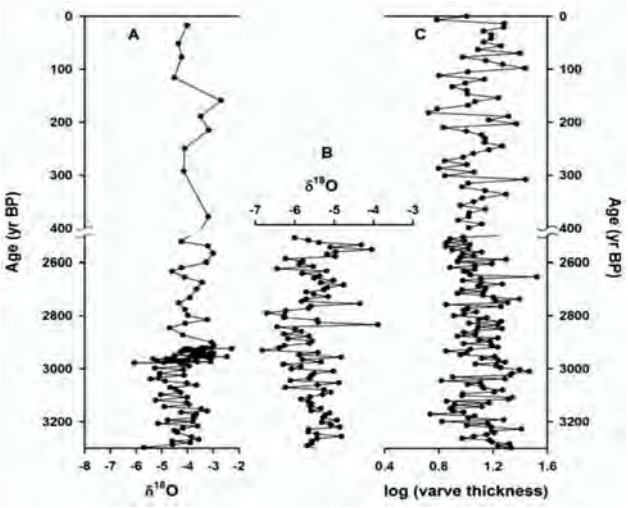

Figure 92 : Comparison between different records: (A) stalactite $\delta^{18}O$ from the Gupteswar cave, Central India (B) $\delta^{18}O$ variation in stalagmite from Baratang (this study). (C) varve thickness variation from sediment core from northern Arabian Sea.

(Amzad H. Laskar, R. A. Jani, R. Ramesh and M. G. Yadava)

Rhenium in Indian Rivers: Sources, fluxes and contribution to oceanic budget

Dissolved and particulate Rhenium (Re) has been studied extensively in the Himalayan and the Peninsular Indian rivers from their origin to final outflow before falling into the Bay of Bengal and the Arabian Sea. The large data set on Re from these rivers draining through variety of lithologies in various geological settings e.g. the Himalaya, Deccan, Vindhyan and the shield areas in the Indian Peninsula provide not only a better understanding about its geochemistry but also constrain its sources and fluxes to the Bay of Bengal and the Arabian Sea. Dissolved Re in the Himalayan and the Peninsular Indian rivers shows large variability; ranges from 1.4 to 72.7 pmol/kg with mean 7.8 pmol/kg and 0.5 to 122 pmol/kg with mean 15 pmol/kg, respectively. The major sources of Re to the Himalayan rivers is black shales whereas that to the east flowing Deccan river is basalt. Some of the rivers having very high Re concentration indicate significant influence of anthropogenic Re inputs to these rivers. Natural and anthropogenic Re supply by these rivers have been delineated. The Peninsular rivers supply 14640 mol anthropogenic Re annually which is ~70% of the total Re supplied of the Indian rivers and 3.4% of the global river. The Himalayan and the Peninsular rivers supply 5854 and 15742 mol/year to the Arabian Sea and the Bay of Bengal. They together supply ~21600 mol Re annually which corresponds to ~5% of the total global riverine supply to the oceans.

(Waliur Rahaman, Anil Dutt Shukla and Sunil Kumar Singh)

$^{87}Sr/^{86}Sr$ and major ion composition of rainwater of Ahmedabad, India: Sources of base cations

Rainwater samples from Ahmedabad are analysed for their chemical composition and Sr isotopic ratio. Dominance of Ca in the cation budget indicates its importance in the acid neutralization whereas SO_4 and NO_3 dominate the anion budget. Na and Cl show very good correlation with ratio similar to the seawater ratio, implying their marine origin. Non sea salt Ca and Mg vary from 99% to 99.6% and 25% to 89% of the measured Ca and Mg respectively whereas non sea salt component of SO_4 and HCO_3 contribute 84.3% to 98.9% and 99.1% to 99.9% respectively. Sr concentrations in these rainwaters vary from 32 to 191 nM and $^{87}Sr/^{86}Sr$ from 0.70878 to 0.71027. Sr concentration shows a very good correlation with the non sea salt component of Ca and Mg indicating their continental sources and having similar provenances. Carbonates and basalts seem to contribute significantly to

dissolved base cations of the rainwaters. The basalts from Deccan region, which is isotopically indistinguishable from the African basalts and the sediments from the Ganga plain (which is originated from the Himalayan lithologies) could be potential dust sources for this particular site. The sources of dissolved base cations deduced from Sr isotope composition of the rainwaters are consistent with wind back trajectory data obtained from NOAA HYSPLIT model.

(Jayati Chatterjee and Sunil Kumar Singh)

Spatial distribution of dissolved neodymium and εNd in the Bay of Bengal: Role of particulate matter and mixing of water masses

The concentrations and isotope composition of dissolved Nd have been measured in the water column along 87°E transect in the Bay of Bengal to investigate the effect of water mass mixing and Nd release from particulate matter in determining these properties. The concentration of Nd in surface waters of the BoB shows a North-South decreasing non-linear trend (~ 46 to ~ 22 pmol/kg) with salinity, whereas its depth profiles typically show a high value in surface waters, a minimum (~ 15 to ~ 23 pmol/kg) in shallow subsurface (~ 50-200 m) followed by a gradual increase with depth (Figure 93). The Nd concentration (~ 20 to ~35 pmol/kg) in depth interval ~ 100-2000 m of the BoB waters is generally higher than that in nearby oceanic basins. The ε_{Nd} of the northern BoB waters ~ -15 ± 1 (Figure 94) overlaps with the values of dissolved and particulate phases of the Ganga-Brahmaputra (G-B) Rivers, but less radiogenic than those reported for other regions of global oceans, except the Baffin Bay and the North Atlantic Subpolar Gyre. The abundance and distribution of dissolved Nd and its unradiogenic isotope composition suggests that the dominant source of Nd in the BoB is the dissolved and/or particulate phase of the G-B river system.

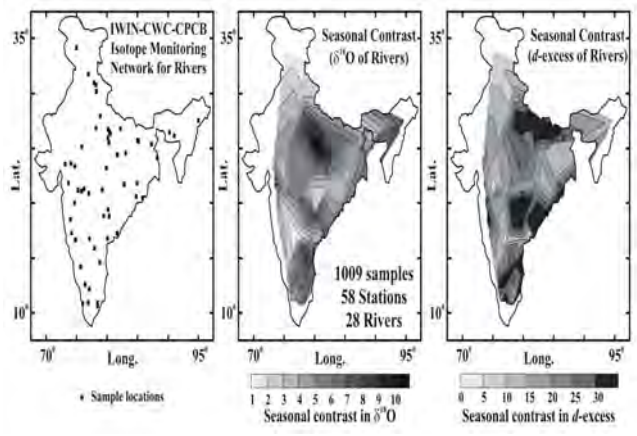

Figure 93: Dissolved Nd in the Bay of Bengal

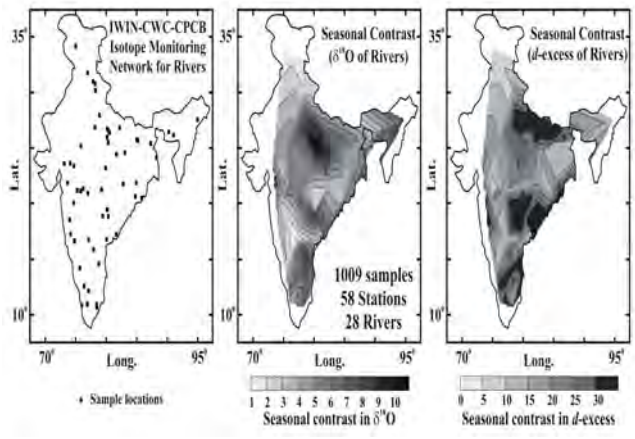

Figure 94: ε_{Nd} in water columns of the Bay of Bengal

The ε_{Nd} values in the BoB show greater variation in the upper water column (Figure 92) with more radiogenic values ~ -8 in surface waters of the southernmost profile (~6°N), which decreases to -15 in the northernmost profile (~ 20°N). This latitudinal trend is most likely a result of the variation in mixing proportion between the Indonesian Throughflow surface waters (IW) and the G-B river water. The former's signature is clearly discernible in surface waters of the two southernmost profiles, (~ 6°N and ~ 8.5°N). Attempts to balance the Nd budget in the water column, based on an inversion model, suggest that in addition to water masses other source(s) is required, the strength of which is estimated to vary from 1% to 65 % of measured Nd concentration. The calculations also show that ε_{Nd} of this additional source(s) has to be in the range of ~ -16 ± 2, typical of G-B river sediments. These observations coupled with the North-South distribution of dissolved Nd and ε_{Nd} indicate that this additional source is released from particulate phases supplied by the G-B river system. The calculations also bring out the presence of "hot-spots" of Nd release (Excess Nd) near the sediment-water interface in the northern slope of the bay indicating supply of Nd from continental margin sediments. This study underscores the significant role of dissolved/particulate Nd from the Ganga-Brhamputra river system in contributing to the dissolved Nd budget of the global ocean.

(Ravi Bhushan, Vineet Goswami, Satinder Pal Singh, Vinai Kumar Rai and Sunil Kumar Singh)

Temporal variation in $^{187}Os/^{188}Os$ of the Arabian Seawater

To obtain a reliable and high resolution record of marine $^{187}Os/^{188}Os$ form the Arabian Sea, sediments from a core in the south-eastern Arabian Sea (SS3101G; 6.0°N, 74.0°E) have been analyzed. The results display significant variation in $^{187}Os/^{188}Os$ of marine Os record from the Arabian Sea

during last 29 ka. The $^{187}Os/^{188}Os$ of seawater in the most recent sample has a value of 1.04 ± 0.01, close to the Os isotopic composition of present day seawater (1.06 ± 0.01). The Os isotopic composition of the Arabian seawater varies in phase with that of the global ocean since last 29 ka except during the Last Glacial Maxima (LGM). During LGM, $^{187}Os/^{188}Os$ deviates from the trend set by the global ocean and shows an excursion towards higher $^{187}Os/^{188}Os$. In addition, Os concentrations of the leachable fraction and Re contents of bulk sediments from the Arabian Sea are higher during the LGM. Higher concentrations of Re and Os in the sediments deposited during LGM indicate higher degree of anoxicity at the sediment water interface during LGM. This could be due to reduction in the oxygen content in the bottom water during LGM. Lower oxygen content in the bottom water of the Arabian Sea could have been caused by the reduced transport of polar waters (North Atlantic Deep water, NADW) into the Arabian Sea. Deviation of Os isotope composition of Arabian Seawater from the global oceanic trend and higher concentration of Re and Os during LGM, thus, indicate the reduced supply of NADW to the Arabian Sea during LGM, resulting in partial isolation of the Arabian Sea from rest of the oceans during the LGM.

(Ravi Bhushan, Vineet Goswami and Sunil Kumar Singh)

Sr and Nd isotopes in sediments from the Irrawaddy continental shelf, northern Andaman Sea

Sr and Nd concentrations and their isotope compositions have been analysed in silicate fraction of Irrawadi continental shelf sediments along with sediments of Irrawaddy and Salween rivers to track sources of sediments and their deposition patterns. $^{87}Sr/^{86}Sr$ and ε_{Nd} of shelf sediments display ranges from 0.712245 to 0.742183 and -17.3 to -9.3 respectively. The two major rivers Irrawaddy and Salween supply sediments with $^{87}Sr/^{86}Sr$, 0.7167 and 0.7314, and ε_{Nd}, -9.1 and -15 respectively to the shelf region of northern Andaman Sea. Spatial distribution of the sediments in the shelf region indicates that Irrawaddy river is the major supplier of sediments to the shelf with subordinate contribution from the Salween river. Sediments deposition pattern in the shelf region of the northern Andaman Sea depends on the amount of sediments supplied by these two rivers and the surface current dynamics in this region.

This work is being done in collaboration with V. Ramaswamy, NIO, Goa.

(Damodar Rao Karri, Vinai Kumar Rai, Sunil Kumar Singh)

Infrared Stimulated luminescence in Natural Feldspars

On account of its high luminescence sensitivity and high saturation dose, infrared stimulated feldspar luminescence has attracted considerable attention for geochronometric application, so as to extend the dating range range achievable using quartz. A major bottleneck in this effort has been the presence of a-thermal loss of luminescence signal due to quantum mechanical tunnelling effects leading to an underestimation of ages. Currently considerable effort is underway to understand and model the luminescence process and the athermal fading so that appropriate correction factors/measurement protocols are developed for robust age estimations. Toward this we analyzed the infra-red stimulated luminescence (IRSL) decay curve, using compressed hyperbolic function (Becquerel function), to derive some insight into the physical process leading to IRSL curve has more physical information about the system, i.e., feldspar. The current understanding of the IRSL process invokes the presence of bad tail states and charge hopping between these states, facilitated by temperature and the impurity distance. We examined the nature of IRSL decay rate under several measurement temperatures.

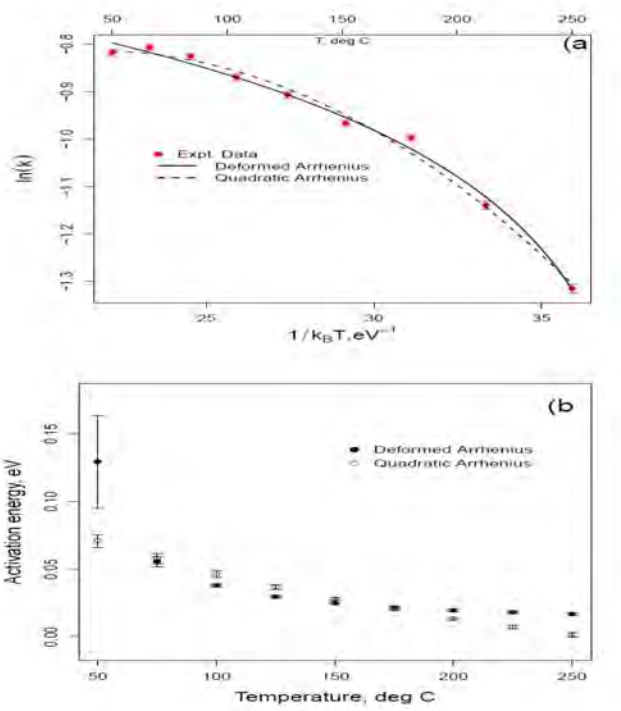

Figure 95 (a) Fitting of temperature dependent decay rate (k) using deformed Arrhenius plot and (b) the obtained temperature dependent thermal activation energy. Decay rates (k) were the expectation values of the probability distribution function of decay rates obtained by the Laplace Transform of the fitted compressed hyperbolic function to the cw-IRSL experimental data at various stimulation temperatures.

The temperature dependent decay rate of the IRSL curves followed non- Arrhenius kinetics (Figure 95a). This non-Arrhenius kinetics data set were analyzed by both quadratic Arrhenius plot and deformed Arrhenius plot and this indicated a thermal activation energy that was temperature dependent (Figure 95b). Further, time-resolved IRSL (TR-IRSL) where the IR stimulation was pulsed use analyzed to derive analytical functions to describe the TR-IRSL during both ON and OFF times. We also calculated the relaxation rate using the numerically convoluted curve using LED function (step function) and relaxation functions such as stretched exponential and Becquerel relaxation functions. This was the first such analysis where both ON and OFF time data was analyzed using relaxation functions. Figure 96 shows the TR-IRSL data of feldspar fitted with newly derived analytical functions for ON and OFF time and numerically convoluted function for ON + OFF time data for 5 ON times starting from 10 to 50 μs. The OFF time was always kept as 100 μs.

Analysis of TR-IRSL of feldspar (FL1) using compressed hyperbolic function. LEDIR (thin line) is the stimulation of IR photons during ON and OFF times, measured by the back scattered IR photons from an empty disc. IRF (thick line) stands for instantaneous response function where in this figure above, it describe the TR-IRSL both during ON and OFF time data. ON (hyphened line) and OFF (dotted line) describe the ON and OFF time data using derived analytical functions respectively.

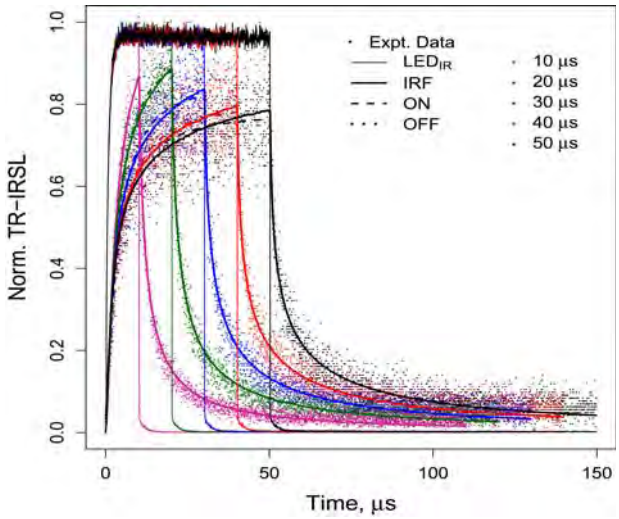

Figure 96: Analysis of TR-IRSL of feldspar (FL1) using compressed hyperbolic function. LEDIR (thin line) is the stimulation of IR photons during ON and OFF times, measured by the back scattered IR photons from an empty disc. IRF (thick line) stands for instantaneous response function where in this figure above, it describe the TR-IRSL both during ON and OFF time data. ON (hyphened line) and OFF (dotted line) describe the ON and OFF time data using derived analytical functions respectively.

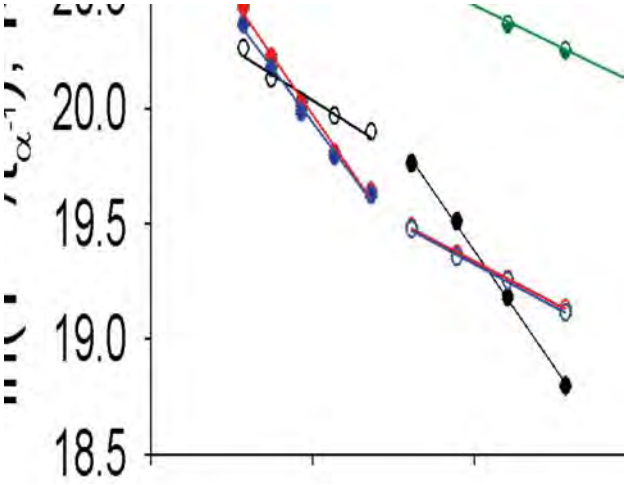

Figure 97: Analysis of the temperature dependent hopping time using variable range hopping (VRH) theory. T is the stimulation temperature which was varied from 50 to 250°C with an interval of 25°C. In the analysis, the density of states (DOS) was assumed to vary in a quadratic manner with energy i.e., N(E) $\propto\{ \mu$ (E-EA)2}. Parameter ta^{-1} is the hopping time derived from TR-IRSL OFF time data. Data shown in filled circles were explained by variable range hopping (VRH) theory and others could not be explained by VRH.

Analysis of the OFF time data set of four feldspar samples (FL1, FL2_1, FL2_2 and FL3) using Smoluchowski's equation gave the electron hopping times that were compatible with the analyses of the data with variable range hopping mechanism (Figure 97). Following these the calculation of the hopping length, hopping energy and diffusion constant helped us to understand the width and density of states of the band-tail states. The above studies help visualize chare dynamics during a normal IRSL (cw-IRSL) and TR-IRSL. And will eventually help isolate the least fading IRSL signals.

A part of this work was done with V. Pagonis, McDaniel College, Westminster, Madison, USA

(P. Morthekai, R. H. Biswas and A. K. Singhvi)

Luminescence dating of Red Dune sands (Teri sands)

A program on optically stimulated luminescence dating of red dunes of near coastal regions of South India was initiated to develop an event chronology for their evolution. In the dating effort, some of the methodological issues related to the timing and the effect of reddening on optical bleachability of red sand, the wind regimes and the sand supply through time. Tropical Climate of the region is expected to play a role in the dune reddening process. OSL dating of the samples at a locality Muttom

(8°8′03"N, 77°19′08"E) samples shows red dune sand aggraded between 21-11 ka and suggest larger sand supply from exposed shelf exposed due to lower sea levels. Modern ages of samples from the upper part of this sequence suggest a recent local reworking of sand unit. Microliths occur within the dune bodies and suggest occupation of microlithic culture in South India as early as 21ka and is consistent with the age of similar occurrence in Sri Lanka during ~25ka.

This work was done in collaboration with Prof. P. Serlathan, Cochin University

(L. Allapat and A.K.Singhvi)

OSL dating of aeolian sand sequences in the Thar Desert, Rajasthan

Large succession of sediments accumulated in the desert regions around the world has been useful to reconstruct the palaeo-climate of Quaternary. The calcretes are valuable palaeoclimatic indicators as during the wetter span of climate, the soil stabilization allows calcium carbonate to leach and subsequently get precipitated at depth. OSL dating of quartz samples from two deep sections in western and central Thar at Chamu (26°, 40′ 35" N; 72° 35′ 33.5" E) indicated ages of a 55ka and 110ka. These confirmed our earlier age assignments and the attest to fact that the Thar Desert formed due to geological and atmospheric processes. Samples from a ~9m profile at Pabupura section (27° 23 54N; 72° 43 22"E) in central- western Thar gave OSL ages between ~120 - 7 ka with periods of aeolian aggradations at 120-95 ka, 71-55 ka 3 7ka, 27 ka and 13-7 ka. Presence of calcretes indicated periods of wetter climate with seasonality and the date are being interpreted in terms of regional climatic record, given that this mimics other records in Thar.

This work was done in collaboration with R.P. Dhir, former Director, Central Arid Zone Research Institute, Jodhpur

(L. Allapat and A.K. Singhvi)

Thermal history of meteorites: studies on individual chondrules

Plagioclase Feldspar is the major luminescent mineral in chondritic meteorites. Parameters of its thermoluminescence glow peaks viz. peak temperature (Tm), peak widths (FWHM), ratios of the intensity of high temperature (HT) to low temperature peak (LT), sensitivity (TL/dose/mass) inform on the degree of crystallinity of the mineral. A longstanding yet unresolved problem in meteorite feldspar is to establish the correlation between quantum mechanical athermal fading and structural state. Inter meteorite comparison can address this issue but large variability in their thermal metamorphism obscures this. We therefore used intra meteorite approach and examined individual chondrules with the premise that thermal metamorphism history of all the chondrules are similar but the formation environment (temperature and cooling duration) of different chondrules are different and hence have different degree of crystallinity. Individual chondrules were separated using a freeze-thaw technique from single parent body (Dhajala meteorite). Results show large variation in Tm (155-229°C), FWHM (80-210°C) and HT/LT (0.07-0.47) (Figure 98a) and suggest that chondrules within a parent body had different crystallization environment and hence different crystallinity. Measured athermal fading qualitatively suggest that fading initially increases as the crystal goes from a low temperature form to high temperature form where the then fading rate drops to nearly zero, i.e. the high temperature form of feldspar crystal shows least fading (Figure 98b and 98c). Further studies on thermal annealing of chondrules at different temperature to convert low temperature form to high temperature form of the crystal are underway to possibly estimate the thermal environment during chondrule formation.

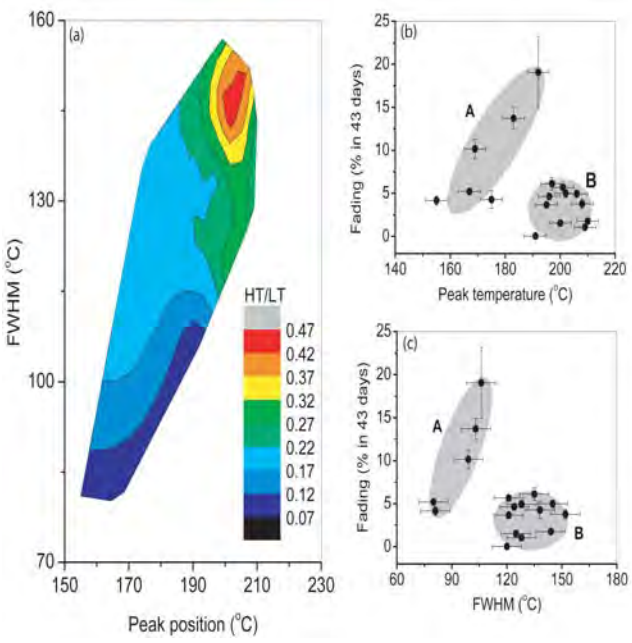

Figure 98: (a) Contour plot of peak temperature, FWHM and HT/LT of 20 individual chondrules of Dhajala meteorite, (b) variations of athermal fading rate with TL peak temperature, (c) variations of athermal fading rate with FWHM

(R.H. Biswas and A.K. Singhvi)

Radiocarbon and stable carbon isotopes in Soils from Northeast India

Understanding the mechanistic controls over the fate, transport, and turnover times of organic carbon in soils is important because it is a significant carbon reservoir with a potential role in the global carbon budget. To understand dynamics of soil organic carbon (SOC), factors governing the turnover time of SOC in two soil profiles from Assam, North-East India, one from Bakrihawar, an agricultural land and the other from Chandipur, a virgin hilly area were investigated (Figure 99). Due to the fluvial nature of the sediments, the agricultural site has higher clay content and SOC. A 'peak' like highest $\delta^{13}C$ value in both the profiles is

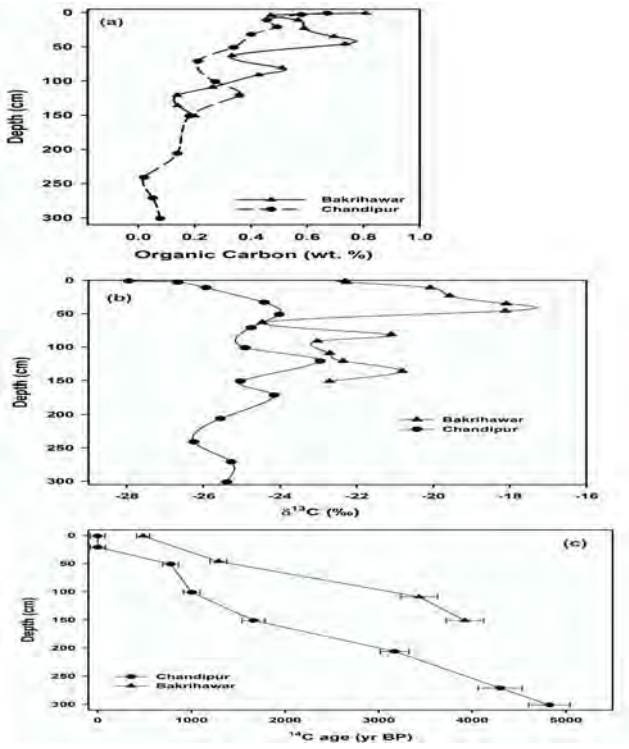

Figure 99: Depth profiles of organic carbon contents (a), $\delta^{13}C$ (b) and radiocarbon ages in the two soil sections.

observed. This was explained as due to the chromatographic-like effect in the soils; i.e., the clay with a complex binding with the old metabolized organic matter (due to microbial decomposition it has higher $\delta^{13}C$ values relative to surface vegetation) does not get rejuvenated with the fresh organic matter (from the surface having the $\delta^{13}C$ value of the contemporary vegetation) which eventually percolates further into deeper layers with a lesser clay content. Using the residual ^{14}C content, it is found that the turnover time of organic carbon, depends strongly on the particle size distribution, especially the clay content.

(Amzad H. Laskar, R. Ramesh and M. G. Yadava)

Origin of fluids in mud volcanoes of Andaman accretionary prism: implications for fluid migration in forearcs

Extensive mud volcanism on the Andaman accretionary prism is driven by tectonic activity, along extensive fault network, caused by the convergence of the Indian plate and the Burmese micro plate. These mud volcanoes are the least studied amongst all such structures present on subduction zone forearcs. In an effort to characterize the ejecta, and to understand their origin and implications for the forearc processes we have studied the mineralogy of mud matrix, chemistry of water, and isotopic composition of gases expelled by the mud volcanoes of middle and north Andaman Islands. Our study reveals that the gases have the deepest origin (15-25 km), followed by water (4 to 5 km) and mud matrix (< 2 km). The modes of $\delta^{13}C$ distribution for methane (> -42‰), ethane (> -27‰) and CO_2 (< -3‰) indicate their thermogenic origin, with TOC and N of associated mud suggesting marine organic matter as their source. The waters ejected at these mud volcanoes are much fresher (Cl = 45 to 135 mM) than seawater and their $\delta^{18}O$ (-0.2 to 2.6‰) and δD (-24 to -14‰) isotopic compositions fall well below the global meteoric water line. Lowering of K at the expense of Na in these waters has been attributed to smectite to illite conversion, which in turn hints at freshening of sediment pore water (ancient seawater) by water released by dehydration of clays. The latter is conclusively proven by our modelling efforts to explain the stable isotopic variations using a simple water-rock interaction model, which indicates that waters from dehydrating clays cause the observed isotopic shifts in pore waters. Such an origin for mud waters also explains their high contents of Sr and Ba and supports the idea that water plays an important role in the transfer of elements out of the slab in a forearc environment. The $^{87}Sr/^{86}Sr$ of mud waters (~0.707) suggests that clays of the slab are predominantly derived from the altered oceanic crust. The solid ejecta from mud volcanoes carry clasts from the underlying rock formations and the mud matrix is composed of quartz, plagioclase, calcite and serpentinite, apart from clay minerals, all derived from the slab.

(J.S. Ray, Alok Kumar, D.K. Rao, A.K. Sudheer, R.D. Deshpande, N. Awasthi and R. Bhushan)

Origin of breccia in mud volcanoes of the Andaman accretionary prism

Mud volcanoes at convergent margins are important pathways through which clay minerals and fluids, collectively known as mud breccia, derived from deep within the forearcs, are ejected at the surface, opening an important window to the processes within subduction

zones. In spite of the fact that the mud breccia is the only detachable part of a subducting slab at shallow depths, its origin and impact on the composition of the arc magmas remains largely unknown. In an attempt to understand its importance in the mantle recycling of crustal materials, we have carried out a detailed mineralogical, geochemical and isotopic study of mud breccia ejected from the mud volcanoes of the Andaman accretionary prism. Our study reveals that the smectite-chlorite-kaolinite-illite rich matrix of mud breccia is derived from the subducting slab that carries > 33 kyr old trench sediments. Geochemistry and Sr-Nd-Pb isotopic ratios of mud breccia indicate that it contains materials derived from both the altered oceanic crust and accompanying sediments, with the former contributing the most (>75%). Our results show that the mud matrix, unlike the accompanying fluids, is an efficient carrier of Rb, Ba, Th and light rare-earth elements, and possibly acts as the main agent for metasomatism of the mantle wedge. We also infer that the depletions of Nb and Ta observed in arc lavas are not generated by their retention in the slab. Mixing models using Nd-Pb isotopic ratios suggest that the arc lavas at the Andaman subduction zone are contaminated up to 4% by the slab derived material, an estimate that is higher than generally expected.

(J.S. Ray, Alok Kumar, N. Awasthi and A.D. Shukla)

Chronology of major terrace forming events in the Andaman Islands during the last 40 kyrs

Major earthquakes that trigger tsunamis are great natural hazards. The devastations caused by the December 26, 2004 Sumatran earthquake, and the March 11, 2011 Japan earthquake, and associated tsunamis will remain in our memories for a long time. Such events reaffirm the need for studying the cause and effects of large earthquakes of the past to prepare the world better for the future. In such an effort, to understand the pattern of earthquakes and their effects on the geomorphic evolution we have studied deformation history in Andaman and Nicobar Islands, located in one of the most active convergent margins of the world. Focusing on tectonically formed coastal terraces and determining the timing of their formation from the exposed dead corals, we have been able to reconstruct the history of major earthquakes in these islands for the last 40 kyr. Our results in conjunction with the existing radiocarbon age data from coastal terraces of these islands appear to suggest that the frequency of major earthquakes (M > 7) in the region has increased during the last 9 kyr. In confirmation with some earlier work, we find evidences for a major earthquake and a tsunami between 500-600 yr BP and possibly 4 others during 6-9 cal kyr BP. Our results also indicate that there has been a continuous subsidence of the south Andaman Islands.

(N. Awasthi, J.S. Ray, A.H. Laskar, M.G. Yadava)

Temporal trends in atmospheric $PM_{2.5}$, PM_{10}, EC, OC, WSOC and optical properties in the Indo-Gangetic Plain

The first simultaneous measurements and analytical data on atmospheric concentrations of $PM_{2.5}$, PM_{10}, inorganic constituents, carbonaceous species, and their optical properties (aerosol optical depth: AOD; absorption coefficient: b_{abs}; mass absorption efficiency: σ_{abs} and single scattering albedo: SSA) from an urban site (Kanpur) in the Indo-Gangetic Plain are documented in this study. Significantly high aerosol mass concentration (>100 μg m^{-3}) and AOD (>0.3) are seen as a characteristic feature throughout the sampling period, from October 2008 to April 2009. The temporal variability in the mass fractions of carbonaceous species (EC, OC and WSOC) is pronounced during October-January when emissions from biomass burning are dominant and OC is a major constituent (~30 %) of $PM_{2.5}$ mass. The WSOC/OC ratio varies from 0.21 to 0.65, suggesting significant contribution from secondary organic aerosols (SOAs). The mass fraction of SO_4^{2-} in $PM_{2.5}$ (Av: 12.5%) exceeds that of NO_3^- and NH_4^+. Aerosol absorption coefficient (@ 678 nm) decreases from 90 Mm^{-1} (in December) to 20 Mm^{-1} (in April), and a linear regression analysis of the data for b_{abs} and EC (n = 54) provides a measure of the mass absorption efficiency of EC (9.6 m^2g^{-1}). In contrast, scattering coefficient (@678 nm) increases from 98 Mm^{-1} (in January) to 1056 Mm^{-1} (in April) and average mass scattering efficiency of 3.0 ± 0.9 m^2g^{-1} is obtained for PM_{10} samples. The highest b_{scat} was associated with the dust storm event (17 April, 2009) over northern Iraq, eastern Syria, and southern Turkey; thus, resulting in high SSA (0.93 ± 0.02) during March-

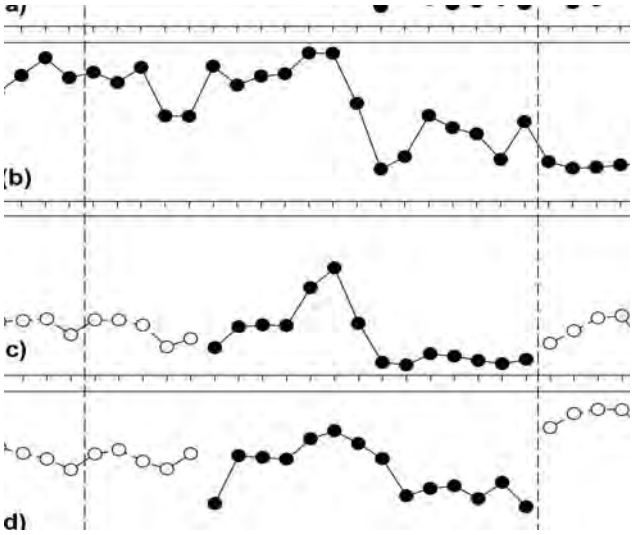

Figure 100: Temporal variation in optical properties of PM_{10} collected during Oct 2008 – April 2009; (a) Aerosol Optical Depth (@500 nm), (b) absorption coefficient (b_{abs}), (c) scattering coefficient (b_{scat}) and (d) single scattering albedo (SSA). Data shown by open circles represent extrapolated SSA (@678 nm), using mass scattering efficiency of 3.0 m^2 g^{-1}.

April compared to 0.82 ± 0.04 in October-February (Figure 100). These results have implications to large temporal variability in the atmospheric radiative forcing due to aerosols over Northern India.

This work was done in collaboration with S.N. Tripathi, IIT, Kanpur

(Kirpa Ram and M.M. Sarin)

Atmospheric ^{210}Pb, ^{210}Po and ^{210}Po/^{210}Pb activity ratio in urban aerosols: Impact of biomass burning emissions

Atmospheric ^{210}Pb, ^{210}Po and their activity ratio (^{210}Po/^{210}Pb) have been studied for two years (January 2007-April 2009) from an urban site (Kanpur: 26.5°N and 80.3°E) in the Indo-Gangetic Plain. The average activities of ^{210}Pb and ^{210}Po center on 1.8 mBq m^{-3} (range: 0.5-4.8 mBq m^{-3} for n = 99) and 0.094 mBq m^{-3} (n = 21, range: 0.002 to 0.28 mBq m^{-3}), respectively. The temporal variability in the activity of ^{210}Pb is significantly pronounced, with relatively high levels during October-November and December-February; a trend similar to that observed for the carbonaceous species (OC, EC). The high aerosol abundance coinciding with the biomass burning emissions (agricultural-waste burning) during October-November and stagnant boundary layer in the wintertime (December-February) is the dominant factor for this temporal trend. The preliminary data suggest that biomass burning emissions also contribute to the atmospheric ^{210}Po activity during the wintertime, as evident from large variability in the ^{210}Po/^{210}Pb activity ratio (range: 0.02 to 0.23) at the urban site. These results have implications to the model based activity levels of ^{210}Pb and ^{210}Po from in-situ decay of the parent nuclide (^{222}Rn) for the given latitude.

(Kirpa Ram and M.M. Sarin)

Secondary inorganic aerosols during wintertime fog and haze over urban sites in the Indo-Gangetic Plain

The chemical composition of total suspended particulate (TSP) matter and secondary aerosol formation was studied during wintertime fog and haze events from urban sites (Allahabad and Hisar) in the Indo-Gangetic Plain. The atmospheric abundances of elemental carbon (EC), organic carbon (OC), water-soluble OC (WSOC) suggest that organic matter is a major component of TSP, followed by concentrations of sulphate and nitrate under varying meteorological conditions. The concentrations of EC, OC and WSOC show nearly 30% increase during fog and haze events at Allahabad and a marginal increase at Hisar; whereas inorganic constituents (NH_4^+, NO_3^- and SO_4^{2-}) are 2-3 times higher than those during clear days at both the locations. The sulphur and nitrogen oxidation rates (SOR and NOR) also exhibit significant increase suggesting possible enhancement of secondary formation of SO_4^{2-} and NO_3^- during fog and haze events. A significant correlation between NH_4^+–SO_4^{2-} ($R^2 = 0.66$, n = 61) and NH_4^+/SO_4^{2-} equivalent ratio ≥ 1 during fog-haze conditions suggest near-complete neutralization of sulphuric acid by ammonia. In contrast, NH_4^+/SO_4^{2-} equivalent ratios are less than 1 during normal days suggesting NH_3^- deficient environment and the possible association of SO_4^{2-} with mineral dust for neutralization. Secondary inorganic aerosol formation and their hygroscopic growth can have significant impact on atmospheric chemistry, air-quality and visibility impairment during fog-haze events over Northern India.

(Kirpa Ram, M.M. Sarin, A.K. Sudheer and R. Rengarajan)

Chemical Characterization of atmospheric outflow from the Indo-Gangetic Plain

The atmospheric outflow from the Indo-Gangetic Plain (IGP) is a dominant source of pollutants entering the marine atmospheric boundary layer (MABL) of the Bay of Bengal during the wintertime (December-February) and spring intermonsoon (March-April). A systematic study on the chemical composition of fine mode ($PM_{2.5}$) aerosols has been carried out from Kharagpur (22.3° N; 87.2° E), a sampling site representing the integrated downwind transport of pollutants from the IGP. The air mass back trajectories (AMBTs) also suggest the transport of chemical constituents from the upwind source regions. The composition of water-soluble inorganic constituents (ΣWSIC) for $PM_{2.5}$ in the IGP-outflow has been compared with our reported data from the MABL of Bay of Bengal (Figure 101). The contribution of nss-SO_4^{2-} and NH_4^+ to ΣWSIC is quite similar in the IGP-outflow and over the North Bay of Bengal. However, the contribution of nss-K^+ and NO_3^- to ΣWSIC are relatively low over the Bay of Bengal. It is noteworthy that total contribution of all anthropogenic constituents (nss-SO_4^{2-}, NO_3^-, NH_4^+ and nss-K^+) to ΣWSIC in the IGP-outflow and over Bay of Bengal are close to 98%, suggesting their common source and dominant impact on the MABL.

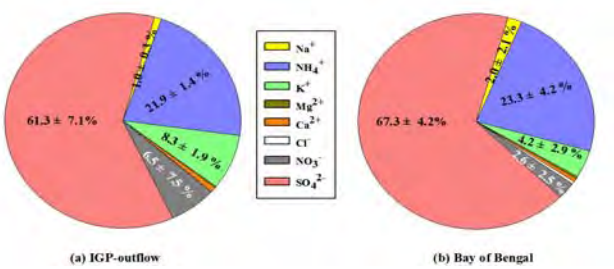

Figure 101: A comparison of data on water-soluble inorganic constituents for $PM_{2.5}$ in (a) IGP-outflow (at Kharagpur) and (b) Bay of Bengal

In contrast, contribution of mineral dust and organic matter to the total $PM_{2.5}$ mass show a decreasing trend from IGP outflow to the North Bay of Bengal. This can be explained in terms of variability in the sources (and their source strength) and/or size-sorting of the particulate matter during the long-range transport.

For this study, logistic help for sampling was provided by A. Sarkar & T. K. Dalai of IIT-Kharagpur

(B. Srinivas, M.M. Sarin and R. Rengarajan)

Impact of Biomass Burning Emissions in the Indo-Gangetic Plain

A large stretch of the Indo-Gangetic Plain (IGP) experiences heavy fog and haze conditions on an annual- and seasonal-basis. The emissions of pollutants from large-scale biomass burning and fossil-fuel combustion, coupled with the prevailing meteorological conditions are the possible causes for deterioration in the regional air-quality. However, atmospheric chemistry and mixing of carbonaceous aerosols with other chemical species has lead to diverging views on the emission sources within the Indo-Gangetic Plain. It is, thus, important to document the spatio-temporal variability in the chemical composition of aerosols through ground-based measurements. Dominance of biomass burning emissions in the IGP has been studied by assessing the relative abundances of OC/EC, WSOC/OC, ΣPAHs/EC and PAHs isomer ratios from a sampling site at Patiala (30.2^{0}N; 76.3^{0}E; 250 m amsl) in the Northern India. Field-campaigns were conducted (during October 08-May 09 and October 10-May 11) to assess relative impact of biomass burning emissions vis-à-vis fossil-fuel combustion sources. Our comprehensive study documents characteristic differences in the mass fractions of OC and EC associated with the paddy-residue burning (during October-November) and wheat-residue burning (during April-May). The ΣPAHs/EC ratios are significantly higher from the paddy-residue burning. The cross-plot of PAHs shows distinct difference in isomer ratios from agricultural-waste burning emissions vis-à-vis fossil-fuel combustion.

Logistic help for sample collection at Punjabi University – Patiala was provided by Darshan Singh

(Prashant Rajput and M.M. Sarin)

Atmospheric mineral dust and trace metals over urban environment in western India during winter

Trace metal concentrations in $PM_{2.5}$ and PM_{10} are studied from Ahmedabad. During winter, concentrations of Zn, Cd and Pb are in the range of 16.5-290, 0.1-5.4, 28-1023 ng m^{-3} in $PM_{2.5}$ and 38-459, 0.21-8.4, 48-1223 ng m^{-3} in PM_{10} respectively. Enrichment Factor (EF) analysis with respect to Al showed significant enrichment of elements

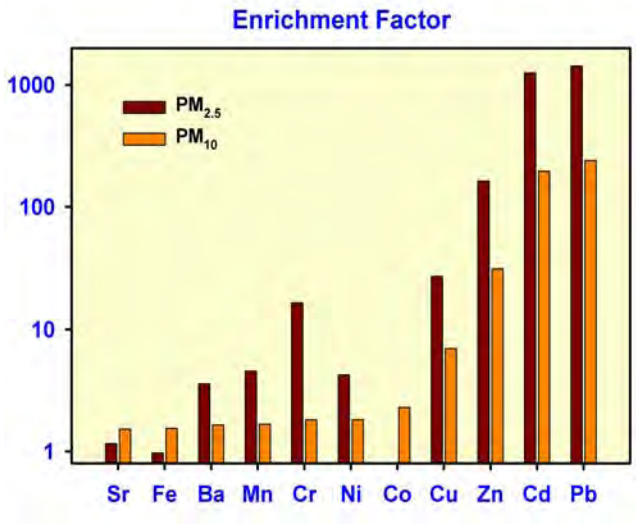

Figure 102: Enrichment factors using the metal concentrations during winter at Ahmedabad.

like Cd, Pb, Zn and Cu in fine mode particles suggesting their strong anthropogenic contribution (Figure 102). About 43% of PM_{10} mass is constituted by mineral dust and dominant fraction (~88%) of the same exists in coarse fraction with a characteristic Fe/Al ratio of 0.53. Ca/Al ratio is ~1.1 in PM_{10} and ~0.8 in $PM_{2.5}$ indicating that aerosol over this region is rich in Ca minerals compared to average upper continental crust. Positive Matrix Factorization (PMF) analysis using trace metal and major components reveals five sources for $PM_{2.5}$ and 6 sources for PM_{10}. PMF results suggest anthropogenic sources contribute ~80% and 40-50% of the $PM_{2.5}$ and PM_{10} mass respectively. Incineration/industrial emission, biomass burning, vehicular emissions and re-suspended/long range transported dust are the other prominent sources identified. These source contributions exhibit large temporal variability during winter as the sampling location is influenced by air masses from different source regions.

(R. Rengarajan and A. K. Sudheer)

Effect of ambient relative humidity on Secondary organic aerosol formation over an urban environment

Organic aerosol, a major component of atmospheric aerosol, emitted from both natural and anthropogenic sources can be primary as well as secondary in nature. Estimates of secondary organic aerosol (SOA) production based on biogenic and anthropogenic volatile organic compound (VOC) precursor fluxes suggest that their dominance over primary component, but large discrepancies exist in these estimates and the inconsistencies are attributed to the poor understanding of SOA formation mechanisms from the precursors and controlling factors. The variation of secondary organic carbon (SOC) with relative humidity (RH) over an urban environment has been investigated in this study.

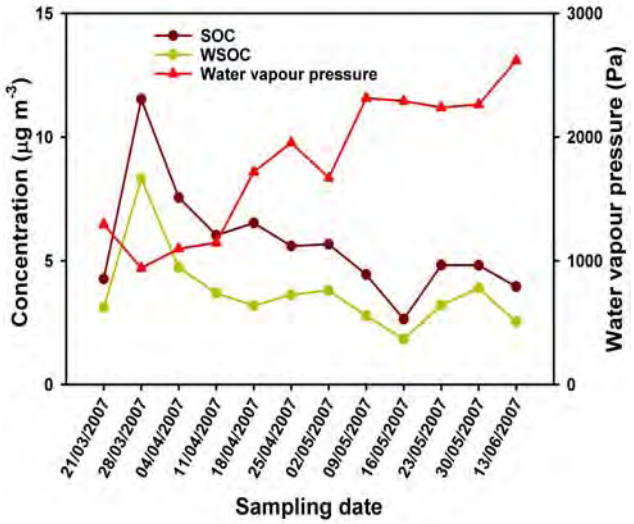

Figure 103: Water vapor pressure shows significant correlation with SOC and WSOC concentrations.

$PM_{2.5}$ and PM_{10} samples (particles with aerodynamic diameter < 2.5 and 10 μm respectively) collected from Ahmedabad during March-July, 2007 were analysed for OC, EC, water soluble organic carbon (WSOC), water-soluble ionic species and crustal elements like Fe, Al. SOC was estimated based on EC-tracer method assuming minimum OC/EC as the primary ratio. Significant fraction of SOC is expected to be a major water-soluble component. In $PM_{2.5}$, WSOC/OC ratio varied from 0.34 to 0.57 and on an average, WSOC constitutes 47% of the total OC during the study period. SOC and WSOC exhibit significant negative correlation with water vapour (Figure 103) which provides the direct evidence for the SOA formation inhibited by the increase in RH. This relation is prominent in fine particles during day time where the secondary production of organic matter is expected to be high compared to coarse particles. These results suggest that SOA formation at this site is not favoured by ambient water vapour which is contrary to the laboratory and field observations reported earlier. Based on gas-aerosol equilibrium partitioning of semi-volatile organic compounds along with water vapour an opposite trend is expected. This difference can be attributed to significant role of heterogeneous oxidation of VOCs on mineral aerosol where adsorption of precursors will be controlled by presence of water vapour in ambient air. Such dependence is observed only in those days when the aerosol liquid water content (calculated by gas aerosol equilibrium model ISORROPIA-II) is absent. Hence RH dependence of SOA formation cannot be represented similar for entire RH range especially in presence of significant amount of mineral dust in ambient air to estimate SOA formation in regional scale.

(R. Rengarajan and A. K. Sudheer)

Diurnal variation in water-soluble ionic species in $PM_{2.5}$ during post-monsoon and winter over Ahmedabad

Understanding sources, formation, transformation and transport of atmospheric aerosol is crucial to assess their environmental impact both on regional and global scales. Studies on time-resolved aerosol chemical composition revealing the extent of variability are essential to understand the above atmospheric processes occurring in a time scale of few hours. Towards this, near real-time measurement of water-soluble ionic species (NH_4^+, K^+, Na^+, Ca_2^+, Mg_2^+, Cl^-, NO_3^-, SO_4^{2-}) in $PM_{2.5}$ was carried out at Ahmedabad during post-monsoon (September–October 2011) and winter (December 2011- January 2012) seasons using Ambient Ion Monitor (URG 9000D), installed in PRL during September 2011. The technique involves aerosol collection using a steam jet collector and subsequent online analysis of aqueous solution for ionic species with a time resolution of one hour using two ion chromatographs. Interfering gas phase constituents like SO_2, NO_x, NH_3, HCl and HNO_3 were removed using parallel plate diffusion denuders connected upstream of steam jet collector. These gaseous constituents were also measured by ion chromatographs in series after oxidation with H_2O_2. Since this technique provides crucial information on particle composition as well as related gaseous components with a high time resolution, it is ideal for studying the atmospheric processes involving inorganic aerosol.

Part of the results obtained from Ahmedabad during post-monsoon and winter are presented in Figure 104. These constituents exhibit distinct diurnal cycle due to changes in emission intensities, formation and transformation processes and boundary layer heights. Most of the constituents exhibit a minimum concentration level during afternoon hours and maximum during night; a trend

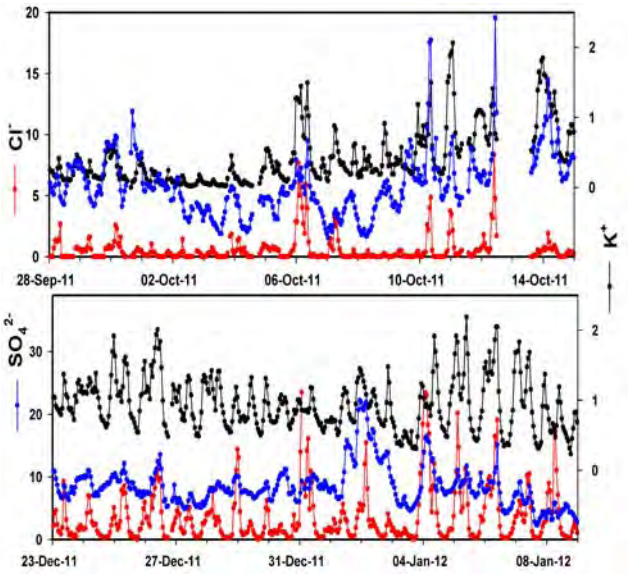

Figure 104: Daily variation of water-soluble constituents (SO_4^{2-}, Cl^- and K^+) during post-monsoon and winter at Ahmedabad. Concentrations are in μg m^{-3}.

typically produced by difference in boundary layer heights. This feature is more pronounced during winter compared to post monsoon season. For example, K^+, tracer for biomass burning emission, exhibits maxima both at 09:00 and 22:00 LT during post monsoon; morning peak is shifted systematically to 10:00 LT during winter which may be explained by fumigation effect getting delayed by change in sunrise time. Hence the observed concentrations can be considered as background levels in this urban location and not influenced significantly by the local emission changes. Ca_2^+, a typical indicator for dust sources, exhibits a night time maximum at 20:00 LT. During winter, Cl^- shows a diurnal pattern similar to that of K^+ during winter time. Cl^- generally believed to be associated with Na^+ and sea-salt origin but this data indicates its association with K^+ and no correlation with Na^+. SO_2 and NO_x oxidation ratios do not show a general diurnal trend during the observation period indicating major formation pathways for SO_4^{2-} and NO_3^- other than photochemical oxidation during day time.

(A.K. Sudheer, R. Rengarajan, S. K. Singh, R. Bhushan, M. Y. Aslam, Dipjyoti Deka)

Characteristics of ambient aerosols over the source region of atmospheric haze in Indo-Gangetic Plane

In recent years, a haze layer in the atmosphere has been observed almost perennially over northern India (Indo-Gangetic Plane (IGP)) due to increasing airborne emissions over this region from the variety of biomass and fossil fuel burning sources. These sources produce both inorganic as well as organic aerosols. However, the relative contribution of different sources to ambient aerosols (mainly organics) and their characteristics on diurnal to seasonal scales are far from understood. Towards this, daytime and nighttime pair sampling of particulate matter smaller than 2.5 μm ($PM_{2.5}$) on pre-combusted tissuquartz filter using high volume air sampler has been initiated over Patiala, Punjab. The location of this site can be considered as the representative of source region of atmospheric haze in IGP. A few batches of the collected samples have been analyzed for $PM_{2.5}$ mass, acid-soluble inorganic components, and carbonaceous aerosols (elemental carbon (EC) and organic carbon (OC)). Preliminary results showed significant diurnal trends in $PM_{2.5}$ mass and carbonaceous aerosols with the night-time concentrations often noticeably higher than the daytime concentrations during paddy residue burning period (October-November). Carbonaceous aerosols appeared to be the major contributor to $PM_{2.5}$ mass over study region.

(Neeraj Rastogi and M. M. Sarin)

Identification of source for excess methane in marine atmosphere over Arabian coast

Systematic air sampling has been done on board 'Sagar Pachmi' in the coastal region of Arabian Sea along the cruise track from Cochin to Goa during November 2010 to find the source for excess methane in marine atmosphere over Arabian Sea. Ambient air was collected into a 10L SS cylinders at 7bar pressure from a height of ~5 meters above Sea surface at different latitude intervals. The carbon isotopic composition ($\delta^{13}C$) in these samples was measured using dual inlet IRMS after methane is converted in to CO_2. Methane concentrations in all these samples vary from 1880 to 1943 ppbv where as its $\delta^{13}C$ values vary in a narrow range of -44.9 to -46.5‰. The CH_4 concentrations are more than that of tropospheric values (1754 ppbV) over the coastal waters of Arabian Sea from Kanyakumari to Mumbai during the month of November-December from 2003-2007 (Figure 105). It is estimated that an excess methane of ~ 6 – 9.5% in these samples. In general, it is believed that CH_4 concentrations in marine atmosphere are related to emissions from the Arabian Sea due to upwelling which brings methane rich water to the surface. The excess methane in these samples is either from surface waters or wind flown from land surface to sampling location. Our data suggests that excess methane must have come from land to Ocean surface since the wind direction is NE in three samples. In these cases, there is an increase of CH_4

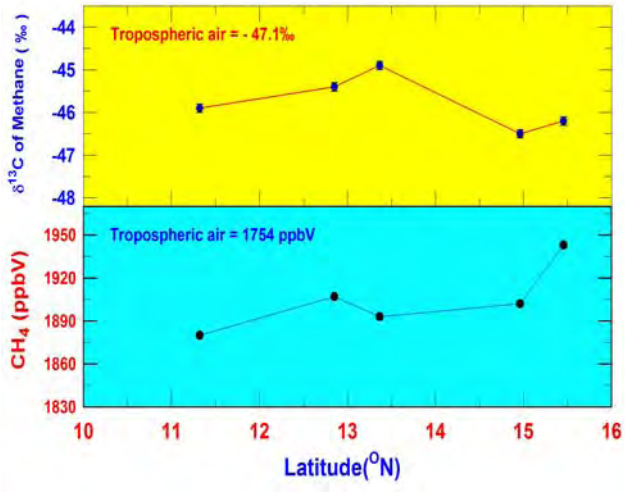

Figure 105: Latitudinal distributions of (top panel) CH_4 (ppbV) concentration and (bottom panel) $\delta^{13}C$ (‰) of Methane from the atmospheric air samples collected along the cruise track.

concentrations with increasing wind speed. This also indicates that CH_4 emissions must have come from land surface. The values of $\delta^{13}C$ of CH_4 in these samples are enriched compared to that of from tropospheric value (-47.1‰) which indicates that the excess methane is thermogenic type. Based on simple mass balance equation for two component mixing, the $\delta^{13}C$ of the source for each sample calculated separately, using the difference with estimated background values of both concentration and isotopic composition. They are in the range of -39.5 to -30.5‰ and confirm the source for excess methane in these samples is thermogenic type.

(D.K. Rao and R.A. Jani)

Theoretical Physics

The activities of the Theory Division involve the modeling of elementary and complex systems with a view of explaining the experimental results and making predictions for forthcoming experiments. The specific areas explored are particle and astroparticle physics, atomic and nuclear physics, non-linear dynamics and complex systems and lasers and optics. Highlights of some of these activities are given below.

Desynchronization bifurcation of coupled nonlinear dynamical systems

When two Rössler systems are coupled they first show a bifurcation to a synchronization state as the coupling strength increases beyond a critical value. As the coupling strength in increased further there is a desynchronization bifurcation at a second critical coupling strength. We analyze this desynchronization bifurcation in the coupled Rössler oscillators. After the bifurcation the coupled oscillators move away from each other with a square root dependence on the parameter. We define System Transverse Lyapunov Exponents (STLE) and in the desynchronized state one is positive while the other is negative. We give a simple model of coupled integrable systems with quadratic nonlinearity that shows a similar phenomenon. We conclude that the desynchronization is a pitchfork bifurcation of the transverse manifold. Cubic nonlinearity also shows the bifurcation but in this case the system transverse Lyapunov exponents are both negative.

(S. Acharyya and R. E. Amritkar)

Amplitude death in complex networks induced by environment:

Among the emergent phenomena in coupled systems, the suppression of dynamics or amplitude death is often a useful control mechanism for stabilizing systems to steady states. We present an interesting phenomenon in which the collective dynamics of coupled systems is quenched due to interaction with an environment or external agency. For this, we model the average effect of the environment by an over-damped oscillator which is kept alive with feedback from the subunits. We find that while the coupling among the units can give rise to synchronizing tendency, the coupling through an environment has a tendency to drive the systems to a state where the sum of the variables is small. The combined effect of these two tendencies is to lead the coupled systems to the state of amplitude death.

This work was done in collaboration with V. Reshmi and G. Ambika from IISER, Pune.

(R. E. Amritkar)

Extreme events on complex networks:

We study the extreme events taking place on complex networks. The transport on networks is modelled using random walks and we compute the probability for the

occurrence and recurrence of extreme events on the network. We show that the nodes with smaller number of links are more prone to extreme events than the ones with larger number of links. We obtain analytical estimates and verify them with numerical simulations. They are shown to be robust even when random walkers follow shortest path on the network. The results suggest a revision of design principles and can be used as an input for designing the nodes of a network so as to smoothly handle an extreme event.

This work was done in collaboration with M. S. Santhanam from IISER, Pune

(Vimal Kishore and R. E. Amritkar)

Collective excitations of a binary condensate in an axially symmetric trap

A Bose-Einstein condensate (BEC) is an interacting quantum many-body system. As such, one of its most important features is its collective excitation. A key parameter in the collective excitation of a binary BEC is the coupling between the two components. Depending on the relative strength of the intra- and inter-component interactions, a binary BEC can have a rich variety of structures. In this work, we consider a special case where no inter-phase boundaries are present.

We show that in the Thomas-Fermi approximation, all the collective excitations of a pure binary-phase Bose-Einstein condensate (BEC) in a spherically or axially symmetric trap can be obtained from those of a single-component condensate by a simple scaling. Furthermore, several accidental degeneracies will appear in the spectrum due solely to the interaction between the two components of the binary condensate. We identify them and find conditions for their occurrence.

(J. Banerji)

Subtle is the method of ordinary least squares

Most of us came to know about the method of least squares while trying to fit a curve through a set of data points. The parameters of the curve are obtained by solving a set of equations (called the normal equations). Although widely used, this approach is not foolproof and, in some cases, it can even give results that are plain wrong! This happens due to some subtleties that are often overlooked by the user. We demonstrate, by means of a simple numerical example, what can go wrong and how to fix them. Using only elementary matrix algebra, we introduce (and show the importance of) singular value decomposition, discrete Picard condition, Tikhonov regularisation, the L-curve and the L-curve criterion in addressing the subtle points of this method so that stable and reliable results are obtained in the end.

(J. Banerji)

Self-healing property of optical ring lattice

The superposition of two LG beams with different radial and azimuthal indices, but having the same waist position and waist parameter, generates interesting light structures. In literature, these structures have been called by various names such as composite vortex beam, Ferris wheel, spiral beams, and linear azimuthons. They show diffraction broadening with some of them showing a rotational dynamics as well. These beams preserve their shape-like Gaussian beams. However, it has not been observed that these structures can reconstruct themselves after perturbation.

We generate experimentally optical ring lattice structures by superposing two coaxial Laguerre–Gaussian modes with common waist position and waist parameter. To study the self-healing property, we have perturbed the shape of the ring lattice by blocking a portion and observed that the original structure reconstructs itself after some distance. We have studied the reconstruction of both bright and dark ring lattice. Although these structures are not diffraction-free, they show self-healing property. This self-reconstruction of the ring lattice can be understood by looking into the transverse energy flow at different z planes. The experimental results are verified by the numerical simulations.

(Pravin Vaity and R. P. Singh)

Generation of quadrupoles through instability of dark rings in photorefractive media

The optical dark ring beam forms ring dark soliton while propagating through Kerr media which is a special class of the dark solitons. The concept of ring dark soliton has also been studied in Bose-Einstein condensates (BEC) where it splits into cluster of vortex pairs.

In the present work, instead of Kerr media we have taken photovoltaic photorefractive (PR) media with defocusing nonlinearity. It is observed that the dark ring undergoes a modulation instability called snake instability as it propagates through the PR media. Unlike forming a dark soliton in case of Kerr media, this instability leads to

formation of quadrupole that remains stable while propagating through the PR media. The experimental results could be taken as a consequence of modulational instability during beam propagation that is revealed through the numerical analysis.

(Pravin Vaity and R. P. Singh)

Entanglement of a quantum optical elliptic vortex

Entanglement is fundamental in determining the usefulness of a quantum state in quantum information protocols. Entangled states play a central role in quantum key distribution, superdense coding, quantum teleportation, and quantum error correction, which cannot be realized classically.

For a vortex, orbital angular momentum (OAM) follows the same numbers as vorticity or topological charge of the vortex, i.e. an optical vortex of topological charge m, carries an OAM of m' per photon. Although, the OAM is quantized in case of an optical vortex, most of its studies as well as applications belong to the classical domain. We calculate the entanglement of a generalized elliptical vortex formed by quantized radiation field, using Wigner quasiprobability distribution function. We find a critical squeezing parameter above which the entanglement is less for higher vorticity that is counter intuitive.

(Abir Bandyopadhyay and Shashi Prabhakar and R. P. Singh)

Hanbury Brown and Twiss- type experiments with optical vortices

In the 1950s, Robert Hanbury Brown and Richard Q. Twiss performed a series of intensity correlation experiments to measure the correlation between intensity fluctuations in the light beams from different sources of light. The objective of these experiments was to calculate the size of radio stars through the coherence of the observed radiation measured with an intensity correlation experiment. Later, the concept of the measurement of intensity correlation function heralded the birth of modern quantum optics. Although the original Hanbury Brown and Twiss (HBT) experiments were conducted half a century ago, these experiments still carry their importance in many branches of science.

We have performed famous HBT type experiments with optical vortices. Though the intensity correlation for vortices are found to be similar to that of the TEM00 mode of the He-Ne laser used to generate the vortices, an interesting difference is observed when they are scattered through a rotating ground glass plate. For smaller time delays, correlations for vortices follow the same pattern as the scattered Gaussian beam of light except that the vortices decay faster and the rate of decay depends on the order of the vortex. For longer time delays, however, the intensity correlation curves for vortices are found to be modulated and this modulation becomes more prominent as the order of the vortex is increased. This seemingly counter-intuitive observation is supported by exact analytical results.

(Ashok Kumar, J. Banerji and R. P. Singh)

Investigation of local structural properties of self-assembled photonic crystals by optical diffraction

Three-dimensional (3-D) colloidal photonic crystals (PhCs) contain finite number of closed packed layers such that each layer has hexagonally close packed colloidal spheres of size comparable with optical wavelength. These crystals show a unique property of photonic stop band, for which a certain range of wavelengths at a particular angle satisfies Bragg's diffraction condition and cannot propagate through the crystal along that direction. The PhCs have tremendous applications due to its stop band property, such as control of spontaneous emission and localization of light.

An experimental investigation of optical diffraction in three-dimensional self-assembled PhCs is presented to find out their structural information. The crystals are synthesized using polystyrene colloidal particles of four different sphere diameters and diffraction is studied under three different wavelength illuminations. The differences in the relative intensities of diffracted spots indicate the twin FCC lattice arrangement of the crystals. This is confirmed by monitoring the variation in intensity of diffracted beam with respect to the incident angles. Moreover, the diffraction angle vs. the incidence angle plot provides us with an estimate of the colloidal sphere diameter also.

(Sunita Kedia and Ashok Kumar and R. P. Singh)

Coreless vortex dipoles and trapped droplets in phase-separated binary condensates

Vortex dipoles are generated when an obstacle moves through a superfluid above a critical speed. In case of phase-separated binary condensates, with appropriate interaction parameters in pan-cake shaped traps, we show that coreless vortex dipoles are created when a Gaussian obstacle beam traverses across them above a critical speed. As the obstacle passes through the inner component, it carries along a droplet of the outer component. Using

Thomas-Fermi approximation, we show that phase-separated binary condensates can either support vortices with empty or filled cores.

This work is done in collaboration with P. Muruganandam, Bharathidasan University, Tirruchirapalli.

(S. Gautam and D. Angom)

Frequency-modulation-mode-locked optical parametric oscillator

Like lasers, optical parametric oscillators (OPOs) are versatile sources of coherent optical radiation

Based on nonlinear optical processes in crystals, OPOs generate tunable radiation for spectral regions inaccessible to conventional lasers. Since the nonlinear optical processes are parametric in nature (no involvement of atomic energy levels unlike lasers), the OPOs have instantaneous gain. As a result, OPOs cannot be mode-locked to generate ultra-short pulses. We demonstrate a novel technique for the generation of mode-locked pulses from a continuous-wave (cw) OPO. The technique is based on the deployment of a phase modulator in combination with an antiresonant ring interferometer internal to a cw OPO, simultaneously providing spectral broadening and phase-to amplitude feedback modulation. With the phase modulator activated and the cavity length synchronized, a stable train of 800 ps pulses is generated at a repetition rate of 160 MHz. Using single-pass second harmonic generation (SHG) of the OPO output, we observe a four times enhancement in SHG compared with cw operation, confirming the real achievement of energy concentration as a result of mode-locked operation. The technique may be further combined with passive mode-locking methods to produce pulses of shorter duration.

This work was done in collaboration with Majid Ebrahim-Zadeh and his group from the Institute of Photonic Sciences, Barcelona.

(G K Samanta)

High-efficiency, multi-crystal, single-pass, continuous-wave second harmonic generation

Despite the golden jubilee of laser invention we are still struggling to develop green laser which has great demand due to its wide range of applications in many fields of science and technology. Due to the absence of suitable laser gain materials for the green spectral range, green lasers are realized by second harmonic generation (SHG) of 1μm lasers. The simplest way of green source development relies on single-pass SHG of high power lasers in nonlinear crystals. However, the attainment of high SHG conversion efficiencies in cw regime is challenging, due to the low available nonlinear gain. While SHG efficiency and power can be increased with higher input power as well as longer crystal length, however, the thermal effects arising from the absorption of input and generated radiation over longer crystal length reduce overall SHG efficiency and power. Although significantly higher SHG power and efficiency can be accessible at high input powers, at the lower pump power regime both SHG power and efficiency are of major concern. We have demonstrated a simple and compact implementation for single-pass SHG of cw laser radiation, based on a cascaded multi-crystal scheme, that can provide conversion efficiency as high as 56% in the low-power as well as the high-power regime, providing 5.6 W of green output for 10 W and 13 W of green output for 25.1 W of input pump power. We have also studied different schemes including double-crystal and single-crystal and their different performances. We also studied the thermal effects of all the schemes which have included measurements of temperature acceptance bandwidth and rate of change of phase-matching temperature with fundamental power.

This work was done in collaboration with Majid Ebrahim-Zadeh and his group from the Institute of Photonic Sciences, Barcelona.

(G K Samanta)

High Energy Emissions from Young Stellar Objects

The problem of X-ray emissions from young stellar objects (YSO) has been revisited. These emissions are detected by many X-ray missions that are providing important information about their properties. However, their emission processes are not fully understood. We propose a new model for the generation of emissions from a YSO on the basis of a simple interaction between the YSO and its surrounding circumstellar accretion disc containing neutral gas and charged dust. It is also assumed that the YSO has a weak dipole type magnetic field and its lines are threaded into the circumstellar disc. Considering the motion of ions and charged dust particles in presence of of neutral gas, we show that the sheared dust-neutral gas velocities can lead to a current along the direction of ambient magnetic field. Magnitude of this current can become large and is capable of generating an electric field along the magnetic field lines. With the help of two free parameters of the model it is shown how the particles can gain energy up to MeV range and above, which can produce high energy radiations from the YSO.

(A.C. Das and Ashok Ambastha)

Hilbert space representation of Hamilton-Jacobi flow and quantum mechanics

Following Dirac's conjectural comments that a solution of the Hamilton-Jacobi equation–the principal function–represents a 'family' of solutions and that the family corresponds in classical mechanics to a state of motion in quantum mechanics, we develop an equation which describes what we term as the "Hamilton-Jacobi flow" to describe the dynamical evolution of the 'family'. The evolution takes place along the characteristics of the Hamilton-Jacobi equation. A Hilbert space representation of the flow is then constructed, and it is shown to yield a generalized set of equations of the Schrodinger form. Having been obtained from the Hamilton-Jacobi flow, these equations then together represent the dynamics of the 'family' as contained in the latter flow. Interestingly, one of them with the lowest mode number n = 1 can be identified as the quantum mechanical Schrödinger equation, while the modes with the large mode numbers n!1 are seen to describe classical mechanics in the spirit of the WKBJ limit. This then represents a covering formalism for classical and quantum mechanics. More importantly, the formalism also predicts the existence of new modes of non-classical behaviour corresponding the modes n = 2, 3, 4, the observational implications of which are discussed.

(R.K.Varma)

Macro-quantization of the guiding centre of charged particles in a magnetic

The review presented here describes the results of investigations on charged particle dynamics in a magnetic field carried out over a number of years. The studies have unraveled the existence of some very surprising and unusual phenomena. Though existing on the macro-scale, they are found to be of quantum origin, and are thereby not covered by the Lorentz equation, which has been regarded conventionally as the descriptor of electrodynamic phenomena on the macro-scale. These novel phenomena have been found to be attributed to the 'quantum modulation' of the de Broglie wave along the magnetic field. This is brought about through the scattering induced transition across Landau levels leading to the modulation of the plane wave state along the field as a result of the entanglement between the parallel and perpendicular degree of freedom. These findings were motivated by the predictions of a formalism developed by the author and include such unusual phenomena as (i) macro-scale matter wave interference effects, and (ii) the detection of curl-free vector potential also on the macro-scale, both attributed to quantum modulation which is a matter wave on the macro-scale. The formalism is thus described as 'macro-quantization of guiding center motion'.

(R.K.Varma)

From hunches to surprises—discovering macro-scale quantum phenomena in charged particle dynamics in a magnetic field

The account presented in the following pages describes how, an intuitive guess–a hunch-in relation to a system of charged particles in a magnetic field-pursued over four decades, has led to the discovery of an entirely new set of phenomena, which could not have been conceived in view of the prevailing conceptions. They pertain to the existence of quantized residence times in an adiabatic magnetic trap, and more surprisingly, the existence of macro-scale matter wave interference effects, with an The independent matter wave length. Even more spectacularly, they include the observation of a curl-free vector potential on the macro-scale as against its micro-scale detection 'a la Aharonov-Bohm. Though on the macro-scale, these results cannot be understood in terms of the Lorentz equation which is known to govern the dynamics on the macro-scale. They have, in fact, been shown to be of quantum origin and are found to be attributed to the quantum modulation of the de Broglie wave, and hence could not have been covered by the Lorentz equation. All these phenomena are seen to run counter to the well entrenched canonical perception that matter wave interference effects and the vector potential observation–the Aharonov-Bohm effect–pertain only to the micro-scale. The unusual phenomena so discovered constitute a complete surprise as they are entirely unexpected under the canonical view and appear to upturn the latter.

(R.K.Varma)

The macro-scale curl-free vector potential observation in charged particle dynamics in a magnetic field—and a new, quantum modulated state of the electron

The recently reported curl-free vector potential observation [R. K. Varma, S. B. Banerjee, A.Ambastha, Eur. Phys. J. D 66, 38 (2012)] in relation to a system of charged particles in a magnetic field, point to the existence of a new state of the electron–a quantum modulated state–which arises through a scattering induced transition across Landau levels. This quantum modulated state has been shown to account for some very unusual effects on the macro-scale, which are distinct from the ones, which can be understood in terms of a 'classical electron'. They are also distinct from the ones which can be understood in terms of a 'quantum electron' on the micro-scale characterized by the Planck quantum. They are found to represent matter wave behaviour on the macro-scale, and thereby bear a quantum signature, but on the macro-scale. The manner in which this new state representing quantum dynamics on the macro-scale

differs from the state representing the quantum electron on the micro-scale, is analyzed here in relation to the curl-free vector potential observation on the two scales–the Aharonov-Bohm effect on the micro-scale, and the recently reported one on the macro-scale. This helps clarify the nature of the latter, as contrasted with the former, and lead in the process to an understanding of the nature of this new–quantum modulated state.

(R.K.Varma)

Superluminal Neutrinos

Recently the OPERA collaboration, Gran Sasso, Italy, reported that the neutrinos from the SPS facility at CERN, Geneva, Switzerland, had apparently travelled there faster than light. This result is highly intriguing and challenges the Einstein's special theory of relativity. In an attempt to understand this result, several new concepts have been put forward. A general phenomenological analysis of the constraints coming from the pion decay poses stringent restrictions on all these models. Only the conservation of energy and momentum have been used to obtain these constraints. This analysis could be further extended to study the cosmic ray muon spectrum in the light of the OPERA result, which in turn, provides the strongest bound on the possibility of violation of special relativity.

This work has been done in collaboration with R. Cowsik of the Washington University in St. Louis, USA and S. Nussinov of the Chapman University, California, USA.

(U. Sarkar)

Baryogenesis and the Neutron-Antineutron oscillations

The unification of the strong and weak forces implies proton decay, and hence, baryon number violation in nature. Although this baryon number violation could generate a baryon asymmetry of the universe explaining why there are more matter in the universe compared to antimatter, a mechanism known as the baryogenesis, before the electroweak phase transition this baryon asymmetry would have been erased by the sphaleron transitions. A new mechanism of baryogenesis has thus been proposed, in which the baryon number violation required for baryogenesis comes from the neutron-antineutron oscillations. The model predicts new physics in the TeV scale, which could be detected in the ongoing experiment at LHC.

This work has been done in collaboration with P. Gu of Max-Planck Institute, Heidelberg, Germany.

(U. Sarkar)

Probing anomalous tbW couplings in single-top production using top polarization at the LHC

A study is carried out of the sensitivity of the Large Hadron Collider (LHC) to anomalous tbW couplings in single-top production in association with a W boson, followed by semileptonic decay of the top. Top polarization and the effects of these anomalous couplings to it at two centre-of-mass (cm) energies of 7 TeV and 14 TeV are calculated. As a measure of top polarization, various laboratory frame distributions of its decay products are proposed, viz., lepton angular and energy distributions and b-quark angular distributions, without requiring reconstruction of the rest frame of the top. The effect of anomalous couplings on these distributions is studied. Certain asymmetries are constructed to study the sensitivity of these distributions to anomalous tbW couplings. It is found that 1σ limits on real and imaginary parts of the dominant anomalous tensor coupling which may be obtained by utilizing these asymmetries at the LHC with cm energy of 14 TeV and an integrated luminosity of 10 fb^{-1} will be significantly better than the expectations from direct measurements of cross sections and some other variables at the LHC and over an order of magnitude better than the indirect limits.

(S.D. Rindani and P. Sharma)

CP violation in tbW couplings at the LHC

Obtaining an understanding of the mechanism of CP violation is of great importance. Anomalous CP-violating tbW effective couplings that might arise from new physics are studied in a model-independent fashion in the context of the process $pp \to tW^+X$ and the conjugate anti-top production process, followed by semileptonic decay of top and anti-top. These processes have a dependence on effective tbW couplings both in the production process as well as in the decay of the top or anti-top. Several CP-violating asymmetries constructed out of variables in the two processes, including top and anti-top polarization, and energy and azimuthal angles of the decay particle, are proposed for study at the Large Hadron Collider (LHC). It is shown that it is feasible to probe a certain CP-violating combination of anomalous couplings at the per cent level at the LHC for centre-of-mass energy 14 TeV and an integrated luminosity of 10 fb^{-1}.

(S. D. Rindani and P. Sharma)

Detection of long range fifth forces from the precession of satellite based spin-polarized bodies

Gauge fields which couple to the lepton or baryon (or some linear combination) charges give rise to composition dependent long range forces. Constrains on long-range leptonic forces have been put from the lunar ranging experiment. We show that by measuring the precession of the spin of a gyroscope with spin-polarized electrons in a satellite based orbit of the earth, one can put bounds on the leptonic long range which is three orders of magnitude more stringent than the one obtained from lunar ranging experiments.

This work was done in collaboration with A.R. Prasanna and G. Lambiase from University of Salerno, Italy.

(S.Mohanty, A.R.Prasanna and G.Lambiase)

Energy level statistics of interacting trapped bosons

It is a well established fact that statistical properties of energy level spectra are the most efficient tool to characterize non-integrable quantum systems. Large number of interacting many fermion systems such as atoms, nuclei, mesoscopic systems etc. have been investigated in the past. There is now interest in the study of statistical properties and spectral fluctuations in interacting many boson systems. Specially, there is interest in weakly interacting trapped bosons in the context of Bose-Einstein condensation (BEC) as their energy spectrum shows a transition from the collective to single particle nature with the increase in the number of levels. However this has received less attention as it is believed that the system may exhibit Poisson like fluctuations due to the existence of external harmonic trap. We have computed numerically, using a method developed by Kolkata group, the energy levels of the zero-temperature many-boson systems (with boson number changing from 3 to 5000) which are weakly interacting through the van der Waals potential and are in the 3D confined harmonic potential. We have studied the nearest neighbour spacing distribution (NNSD) and the spectral rigidity by unfolding the spectrum. It is found that increase in number of energy levels for repulsive BEC induces a transition from "a Wigner like form displaying level repulsion to Poisson distribution" for NNSD. For repulsive interaction, the lower levels are correlated and manifest level repulsion. For intermediate levels NNSD shows mixed statistic which clearly signifies the existence of two energy scales: external trap and inter-atomic interaction. For very high levels the trapping potential dominates, generating Poisson distribution. In addition, power spectrum of the energy levels showed $1/f^{\alpha}$ noise with $1 \leq \alpha \leq 2$ and this is one of the few known realistic examples showing this feature. Finally, for small boson systems spacing distribution shows Shrielman peak which arises due to large number of quasi-degenerate states.

This work was done in collaboration with Barnali Chakrabarti of Lady Brabourne College, Kolkata.

(V.K.B. Kota)

Thermodynamic region in interacting boson systems: results from bosonic embedded ensembles

One plus two-body embedded Gaussian orthogonal ensemble of random matrices for spinless bosons [BEGOE $(1+2)$] was known, as shown by PRL group in the past, to exhibit Poisson to GOE transition in level fluctuations and Breit-Wigner to Gaussian transition in strength functions as the strength (l) of the interaction is increased from zero λ is in units of average single particle level spacing). The chaos markers for these two transitions are λ_c and λ_F respectively with $0 < \lambda_c < \lambda_F$. Then a question is: if we increase λ further from F, will there be a region where thermodynamic principles can be applied. With recent interest in "Thermodynamics of Finite Quantum Systems", this question has become important. In the past there was a simple model study using two interacting bosons but there is no study yet using many boson systems to address this question. This year, PRL group has investigated this using BEGOE $(1+2)$ as this is a generic model for isolated finite interacting many boson systems. Using different definitions, temperature and similarly entropy are calculated as a function of λ for a 100 member BEGOE $(1+2)$ with 10 bosons $(m=10)$ in five single particle levels $(N=5)$. It is found that in a region $\lambda \sim \lambda_t$, $\lambda_t >> \lambda_F$ different definitions of temperature give essentially same values and the same happens with different definitions of entropy; (m,N) dependence of λ_t also has been derived. Thus, in general interacting boson systems, just as fermion systems, exhibit in the dense limit (with $m >> N$) a thermodynamic region.

This work was done in collaboration with N.D. Chavda of M.S. University of Baroda.

(V.K.B. Kota)

Bosonic embedded ensembles with spin one (p) bosons: BEGOE (2)-p

Numerical matrix construction and group theoretical methods for deriving analytical results, developed last year by PRL group for BEGOE$(1+2)$-F for two species boson systems has been extended this year to boson systems

consisting of bosons carrying angular momentum unity (p bosons) with the Hamiltonians preserving many-boson angular momentum [called BEGOE(1 + 2)-p]. In the space of this ensemble, there will be two different pairing algebras [unlike only one type of pairing for BEGOE (1 + 2)-F] as discussed before, by PRL group, in the context of IBM-3 model of atomic nuclei. Preliminary calculations are carried out for eigen value densities (found to follow Gaussian form) and level fluctuations. This ensemble is being investigated to understand general structures generated by IBM-3 model of atomic nuclei and in addition, the ensemble is also being explored for applications to spinor BEC.

This work was done in collaboration with N.D. Chavda of M.S. University of Baroda.

(V.K.B. Kota and Manan Vyas)

Lorentz invariant dark-spinor and inflation

We have investigated the possibility of the inflation driven by a Lorentz invariant non-standard spinor(NSS) field. As these spinors are having dominant interaction via gravitational field only, they are considered as Dark Spinors. We study how these dark-spinors can drive the inflation and investigate the cosmological (scalar) perturbations generated by them. Though the dark-spinors obey a Klein-Gordon like equation, the underlying theory of the cosmological perturbations is far more complex than the theories which are using a canonical scalar field. For example the sound speed of the perturbations is not a constant but varies with time. We find that in order to explain the observed value of the spectral-index one must have upper bound on the values of the background NSS-field. The tensor to scalar ratio remains as small as that in the case of canonical scalar field driven inflation because the correction to tensor spectrum due to NSS is required to be very small. In addition we discuss the relationship of results with previous results obtained by using the Lorentz invariance violating theories.

(A. Basak and J. Bhatt)

Tensor operators and B → V V, V T polarization puzzle

The V-A structure of the weak interactions predicts that the longitudinal fraction is order unity while the data show significant deviation from such an expectation for the penguin dominated B → Vector-Vector (V V) modes. This is referred to as the polarization puzzle and has attracted a lot of attention, including the possibility of this being due to new physics. The situation is further complicated by the opposite behaviour of B → Vector-Tensor (V T) modes which are expected to behave very similar to the corresponding B → V V modes. Any explanation of B → V V polarization puzzle must address the B → V T modes simultaneously. Within the standard model, it is possible that higher order hadronic effects reduce the tension with the data. We explore the possibility whether presence of tensor operators can resolve the polarization results in penguin dominated B → V V, V T modes.

(Namit Mahajan)

Quantum electrodynamics with twisted photons

Recently it has been demonstrated that twisted photons i.e. photons with orbital angular momentum can be realized in the laboratory, with the possibility of creating twisted electrons as well. While this is all very interesting, the field theory of such states is not fully developed. We intend to consider elementary processes in quantum electrodynamics with such twisted photons in order to understand the subtle features that may be inherent to such a construction.

(Namit Mahajan)

Axial anomaly, magnetic field and photon production in heavy ions

It is expected that large magnetic fields are present in the early phases of heavy ion collisions. This can lead to photon production due to the U(1) axial anomaly wherein the pions (pseudoscalars) get converted into thermal photons. The pseudoscalar correlator at finite temperature and density is known to show an enhancement and therefore it is expected that the photon yield via this mechanism may be significant. We explore this possibility in detail.

(Namit Mahajan)

Flat directions and gravitino production in SUSY models

Flat directions in supersymmetric models can get large vacuum expectation values in the early Universe which leads to a large mass for gauge bosons and gauginos. We point out that this can then result in enhanced gravitino production because the cross-section for the production of helicity ½ states of the gravitino is proportional to the square of the gaugino masses. We consider gravitino production after inflation in such a scenario and find that the abundance in some cases can be much larger than the upper bound on the gravitino abundance from cosmological constraints unless the flat direction has a very small vacuum expectation value when it commences oscillating.

(Raghavan Rangarajan and Anjishnu Sarkar)

Kinetic and chemical equilibrium of the Universe and gravitino production

Flat directions in generic supersymmetric theories can change the thermal history of the Universe. A novel scenario has been proposed earlier where the vacuum expectation value of the flat directions induces large masses to all the gauge bosons and gauginos. This delays the thermalization of the Universe after inflation and solves the gravitino problem. We have reanalysed this scenario including certain aspects not considered earlier and shown that the gravitino problem is actually not solved for certain initial values of the flat direction vacuum expectation value. In fact the large gaugino mass can lead to enhanced gravitino production.

(Raghavan Rangarajan and Anjishnu Sarkar)

Neutrinoless Double Beta Decay in TeV scale Left-Right Symmetric Model

We studied in detail neutrinoless double beta decay in left-right symmetric models with right-handed gauge bosons at TeV scale which is within the presently accessible reach of colliders. We discuss the different diagrams that can contribute to this process and identify the dominant ones for the case where the right-handed neutrino is also at the TeV scale. We calculate the contribution to the effective mass governing neutrinoless double beta decay assuming type-I, and type-II dominance and discuss what are the changes in the effective mass due to the additional contributions. We also discuss the effect of the recent Daya-Bay and RENO measurements on 1-3 leptonic mixing angle on the effective mass in different scenarios.

This work was done in collaboration with Sudhanwa Patra from IOP, Bhuvneswar.

(Joydeep Chakrabortty, Srubabati Goswami and H. Zeen Devi)

Neutrino mass hierarchy and octant determination with atmospheric neutrinos

The recent 5.2-sigma discovery of nonzero 1-3 mixing angle by the Daya Bay experiment, and the concurrent indication that this angle is relatively large, significantly impacts existing experiments and the planning of future detectors.

In particular, large detectors will be sensitive to matter effects on the oscillations of atmospheric neutrinos. This renders them capable of addressing, without assistance from beam experiments, the nature of the neutrino mass hierarchy and the octant of the 2-3 mixing angle. We show that a 50 kT Liquid Argon atmospheric neutrino detector can determine both the hierarchy and the octant with high significance in moderate exposure times.

This work was done in collaboration with Vernon Barger of University of Wisconsin, Madison, Danny Marfatia of Kansas University, Raj Gandhi and Pomita Ghoshal from Harish-Chandra Research Institute, Allahabad, Suprabh Prakash, Sushant K. Raut and S Uma Sankar Indian Institute of Technology, Mumbai.

(Srubabati Goswami)

Optimization of the baseline and the parent muon energy for a low energy neutrino factory

We discuss the optimal setup for a low energy neutrino factory in order to achieve a 5 sigma-discovery of the third leptonic mixing angle, nonzero CP phase , and the mass hierarchy. We explore parent muon energies in the range 5—16 GeV, and baselines in the range 500—5000 km. We present the results in terms of the reach in the 1-3 mixing angle, emphasizing the dependence of the optimal baseline on the true value of the CP phase. We show that the sensitivity of a given setup typically increases with parent muon energy, reaching saturation for higher energies. The saturation energy is larger for longer baselines; we present an estimate of this dependence. In the light of the recent indications of a large 1-3 mixing angle, we also determine how these preferences would change. In such a case, the baselines of the order of 2500 km (1500 km) may be expected to lead to hierarchy determination (CP phase discovery) with the minimum exposure.

This work was done in collaboration with Amol Dighe from Tata Institute of Fundamental research and Shamayita Ray of Cornell University.

(Srubabati Goswami)

Mass scale determination of elementary particles at the hadron collider

In the presence of invisible particles (say, dark matter particles) is a challenging task at any hadron collider (like LHC), especially, when we expect most of the signatures originating from the new physics beyond the Standard Model (BSM) contain two or more invisible particles. So far several mass-measurement variables were proposed with their own limitations for determination of new physics masses indirectly or at list to have some form of correlation between masses in the decay chain. We demonstrate that many of these variables are quite closely related in a unified manner once two key ingredients of these variables ('Transversification' and 'Projection') are well defined and classified. This work demonstrate (i) a better understanding of how collider mass variables fit together, (ii) an

appreciation of how these variables could be generalized to search for things more complicated than supersymmetry, (iii) will depart with an aversion to thoughtless or naive use of the so-called transverse methods of any of the popular computer Lorentz-vector libraries, and (iv) will take care in their subsequent papers to be explicit about which of the 61 identified variants of the ''transverse mass'' they are employing.

This work was done in collaboration with A. J. Barr (Oxford, UK), T. J. Khoo, C. G. Lester (Cambridge, UK), K. C. Kong (University of Kansas, USA) K. Matchev, M. Park (University of Florida, USA).

(Partha Konar)

The variable

This was originally proposed as a model-independent, global and fully inclusive measure of the new physics mass scale in missing energy events at hadron colliders. In the present work we advertize two improved variants of this variable, which overcome the problem from underlying events which is inevitable part of hadron collider like LHC. We demonstrated that the variable at the RECO level, in terms of the reconstructed objects in the event, the effects from the underlying event are significantly diminished and the nice correlation between the peak in the distribution and the new physics mass scale is restored.

These works are done in collaboration with K. C. Kong (University of Kansas, USA) K. Matchev and M. Park (University of Florida, USA).

(Partha Konar)

Asymptotic methods for Rydberg transitions

Quantum mechanical expressions of several important physical quantities like the hydrogen dipole matrix elements, line strength and form factors for several excitation processes have long been available in the literature in terms of the terminating hypergeometric functions but calculations from these expressions generally present serious numerical problems for large principal quantum numbers n and n'. Determination of asymptotic and other appropriate approximations of these quantities for large n and n' has for long been posing challenges. We discuss a recent method that transforms the terminating hypergeometric functions into the Jacobi polynomials and exploits the properties of the Jacobi polynomials to provide a solution to the problem of the evaluation of these physical quantities. A noteworthy result of this method is that he exploitation of the recurrence relation of the Jacobi polynomials permits exact numerical calculations for various Rydberg processes for so large $n, n' \sim 2000$ for which computation was usually not possible earlier.

Another noteworthy outcome is that the method readily leads to a strikingly accurate expression of a Rydberg matrix element between nearby Rydberg states in terms of the Bessel functions, called a NRS-formula, which also helps to solve, without any recourse to classical and semi classical arguments, a long standing problem of how to consistently derive the formula of classical mechanics obtained earlier by invoking the correspondence principle. The numerical results from the exact and approximate formulae of various quantum matrix elements presented in the article are so extensive that they reveal how various formulae including those of the correspondence principle convergence to their respective exact quantum expressions. Also, for numerical and analytical study of various matrix elements involving states lying near the continuum threshold, which have posed problems earlier, simpler quantum expressions are presented. The quantum expressions presented in the article provide nearly complete solutions over the hydrogenic bound-state spectrum for the calculation of several physical quantities like the radial dipole matrix element, line strength and form factors for transitions between arbitrary s states and between arbitrary circular states.

(D.P.Dewangan)

Strong CP violation and chiral symmetry breaking in quark matter.

We investigate chiral symmetry breaking and strong CP violation effects in the phase diagram of strongly interacting matter. We demonstrate the effect of strong CP violating terms on the phase structure at finite temperature and densities in a 3-flavor Nambu-Jona-Lasinio (NJL) model including the Kobayashi-Maskawa-t'Hooft (KMT) determinant term. This is investigated using an explicit structure for the ground state in terms of quark-antiquark condensates for both in the scalar and the pseudoscalar channels. CP restoring transition with temperature at zero baryon density is found to be a second order transition at $\theta = \pi$ while the same at finite chemical potential and small temperature turns out to be a first order transition. Within the model, the tri-critical point turns out to be (Tc, μc) (273,94) MeV at $\theta = \pi$ for such a transition.

This work was done in collaboration with Amruta Mishra from IIT, Delhi.

(Bhaswar Chatterjee and Hiranmaya Mishra)

Strong magnetic field and strong CP violation

The largest magnetic field in the universe can possibly be produced in off central heavy ion collisions at LHC. We study here the effect of magnetic field on the phase structure of hot and dense quark matter. We discuss the phase diagram of hot and dense matter in presence of strong magnetic field and its possible consequences regarding the order of the phase transition. The possibility of local CP violating phases is being studied within the NambuJona Lasinio model for the quark matter along with a CP violating t'Hooft determinant term.

This work was done in collaboration with Amruta Mishra from IIT, Delhi.

(Bhaswar Chatterjee and Hiranmaya Mishra)

Bulk and shear viscosities of hadronic matter

Viscos effect play an important role in the hydrodynamic evolution of the matter produced in heavy ion collision experiments. In the present work we estimate the bulk and shear viscosities of hadron gas at finite temperature and baryon densities. Low energy theorems of QCD are being used to estimate the same. This will be of relevance for the planned heavy ion collision experiments at FAIR in Germany, Beam Energy Scan at RHIC, Brookheaven and NICA at Dubna.

(Guruprasad Das and Hiranmaya Mishra)

Transport properties of quark matter

We investigate the transport properties of relativistic fluid composed of constituent quarks at finite temperature and density. In particular, we focus on the shear and bulk viscosities and study their behavior near chiral phase transition. Actual calculations are performed within a Polykov loop extended through the Nambu–Jona-Lasinio Lagrangian. The transport coefficients are calculated within kinetic theory under relaxation time approximation including in-medium modification of quasi-particles dispersion relations.

(Paramita Deb and Hiranmaya Mishra)

Vacuum stability of the Higgs potential

The behaviour of the Higgs coupling under renormalization group running provides a important criterion for testing new physics. The constraints on Type-1 and Type III see-saw neutrino mass models from the Higgs potential stability criterion have been studied. There are implications of the RG running of Higgs coupling in Inflation with the Higgs field which are being pursued.

(Subhendra Mohanty, Moumita Das, Joydeep Chakrabortty, Gaurav Tomar)

Higgs mass and Dark matter in Supersymmetry

The minimal models of supersymmetry which give the observed Higgs mass are severely constrained as they require an unnatural fine-tuning of parameters. In addition SUSY models are required to provide a viable dark matter candidate which which has become difficult to achieve in the minimal models. Non-minimal models of SUSY with extended Higgs sector or non-universal parameters (like gaugino masses) at the GUT scale have been studied with a motivation of explaining the observed Higgs mass and at the same time provide a viable dark matter candidate.

This work was done in collaboration with D.P. Roy from HBCSE, Mumbai

(Subhendra Mohanty, Soumya Rao, Tanushree Basu)

t-b-tau unification in the proposed minimal supersymmetric SO(10) models

The t-b-tau unification with positive Higgs mass parameter mu in the minimal supersymmetric standard model prefers "just so" Higgs splitting and a light gluino < 500 GeV which appears to be ruled out by the recent LHC searches. We reanalyze constraints on soft supersymmetry breaking parameters in this scenario allowing independent splittings among s quarks and Higgs doublets at the grand unification scale and show that it is possible to obtain t-b-tau unification and satisfy experimental constraints on gluino mass without raising supersymmetry breaking scale to very high value $\sim$ 20 TeV. We discuss the origin of independent s quark and Higgs splittings in realistic SO(10) models. Just so Higgs splitting can be induced without significantly affecting the t-b-tau unification in the proposed minimal supersymmetric SO(10) models . This splitting arises in the presence of non-universal boundary conditions from mixing between 10 and other Higgs fields. Similarly, if additional matter fields are introduced then their mixing with the matter multiplet 16 is shown to generate the s quark splitting required to raise the gluino mass within the t-b-tau unified models with positive mu.

(Anjan S. Joshipura and Ketan M. Patel)

New limit for the EDM of an electron

The electric dipole moment (EDM) enhancement factor of atomic Tl is of considerable interest as it has been used in determining the most accurate limit on the electron EDM to date. However, its value varies from -179 to -1041 in different approximations. In view of the large uncertainties associated with many of these calculations, we have performed an accurate calculation employing the relativistic coupled-cluster theory and obtain 466, which in combination with the most accurate measurement of Tl EDM yields a new limit for the electron EDM as $|d_e| < 2 \times 10^{-27}$ e-cm.

This work is done in collaboration with H. S. Nataraj (Tohoku University, Japan), B. P. Das (IIA, Bangalore) and D. Mukherjee (IACS, Kolkata)

(B. K. Sahoo)

Lifetimes, transition probabilities and branching ratios of atomic states in Indium

Accurate results for various transition properties of the first six low-lying excited states of indium are reported. The calculations were performed using the relativistic coupled-cluster method in the framework of the singles, doubles, and partial triples approximation. The lifetime of the $[4p6]5s^2\ 5p_{3/2}$ state in this atom is reported for the first time in the literature. Accuracies of the results for the lifetimes, transition probabilities and branching ratios of other states are improved significantly which can guide now the experimentalists to observe them in the right direction.

This work has been carried out in collaboration with B. P. Das from IIA, Bangalore.

(B. K. Sahoo)

Parity nonconservation in ytterbium ion

By considering parity nonconservation (PNC) effect in the singly ionized ytterbium (Yb^+) arising from the neutral current weak interaction, we have calculated the PNC induced electric dipole transition amplitude and the properties associated with it. These results are given within the accuracies of 5%; the improvement of this result is possible. It, therefore, appears that this ion is a promising candidate for testing the standard model of particle physics and our reported results will be useful if the proposed experiment to measure PNC in Yb^+ at Los Alamos National Laboratory is going to be successful.

This work is carried out in collaboration with B. P. Das from IIA, Bangalore.

(B. K. Sahoo)

Search for a permanent electric-dipole moment using atomic Indium

We have proposed indium as a possible candidate for observing the permanent electric dipole moment (EDM) arising from the violations of parity (P) and time-reversal (T) symmetries. This atom has been laser cooled and therefore the measurement of its EDM has the potential of improving on the current best EDM limit for a paramagnetic atom, which comes from thallium. We report the results of our calculations of the EDM enhancement factor due to the electron EDM and the ratio of the atomic EDM to the electron-nucleus scalar-pseudoscalar (S-PS) interaction coupling constant in Indium. It might be possible to get new limits for the electron EDM and the S-PS CP-violating coupling constant by combining the results of our calculations with the measured value of the EDM of Indium when it is available.

This work is carried out in collaboration with R. Pandey and B. P. Das from IIA, Bangalore.

(B. K. Sahoo)

Sc III Spectral Properties of Astrophysical Interest

Transition properties such as oscillator strengths, transition rates, branching ratios and lifetimes of many low-lying states in the doubly ionized scandium (Sc III) are reported. A relativistic method in the coupled-cluster framework has been employed to incorporate the electron correlation effects due to the Coulomb interaction to all orders by considering all possible singly and doubly excited electronic configurations conjointly with the leading order triply excited configurations in a perturbative approach. Present results are compared with the previously reported results for the transition lines of astrophysical interest. In addition, some of the transition properties and lifetimes of a few low-lying states are given for the first time. The role of the correlation effects in the evaluation of the transition strengths are described concisely.

This work is done in collaboration with C. Li from WIPM, Wuhan, China

(D. K. Nandy, Yashpal Singh and B. K. Sahoo)

Multipolar blackbody radiation shifts for single-ion clocks

Appraising the projected 10^{-18} fractional uncertainty in the optical frequency standards using singly ionized ions, we have estimated the blackbody radiation (BBR) shifts due to the magnetic dipole (M1) and electric quadrupole (E2) multipoles of the applied external electromagnetic field. Multipolar scalar polarizabilities are determined for the singly ionized calcium (Ca^+) and strontium (Sr^+) ions. It is shown that the estimated shifts are large enough and may be a prerequisite for the frequency standards to achieve the foreseen 10^{-18} precision goal.

This work is carried out in collaboration of B. Arora from IISER, Mohali

(D. K. Nandy and B. K. Sahoo)

PUBLICATIONS

Publications in Journals

Astronomy and Astrophysics

1. Baug, Tapas and Chandrasekhar, T., 2012, *"Near-infrared angular diameters of a few asymptotic giant branch variables by lunar occultations"*, Mon. Not. R. Astron. Soc., v. 419, p. 866-872.

2. Bisoi, S.K., Chandra, C.H.I., Sirothia, S. K., and Janardhan P., 2011, *"Deep GMRT 150 MHz Observations of the DEEP2 fields: Searching for High Red-shift Radio Galaxies Revisited"*, J. Astrophysics and Astronomy, v. 32, p. 613-614.

3. Chandra, S., Baliyan, K.S., Ganesh, S., Joshi, U.C., 2011, *"Rapid Optical Variability in Blazar S5 0716+71 During 2010 March"*, ApJ, v. 731, p. 118-123.

4. Chandra, S., Baliyan, K.S., Ganesh, S., and Joshi, U.C., 2012, *"Optical Polarimetry of the Blazar CGRaBS J0211+1051 from Mount Abu Infrared Observatory"*, ApJ., v. 746, p. 92-96.

5. Chesneau, O., Meilland, A., Banerjee, D. P. K., Bouquin, Le, J.B., McAlister, H., Millour, F., Ridgway, S.T., Spang, A., Brummelaar, T.T., Wittkowski, M., Ashok, N.M., and 11 co-authors, 2011, *"The 2011 outburst of the recurrent nova T Pyxidis. Evidence for a face-on bipolar ejection"*, Mon. Not. R. Astron. Soc. Letters, v. 534, p. L11-L15.

6. Dewangan, L.K., and Anandarao, B.G., 2011 *"Infrared photometric study of the massive star forming region S235 using Spitzer-Infrared Array Camera and JHK Observations"*, Mon. Not. R. Astron. Soc. Letters, v. 414, p. 1526-1544.

7. Jain, R., Awasthi, A. K., Chandel, B., Lokesh; B., Hanaoka, Y.; and Kiplinger, A. L., 2011, *"Probing the Role of Magnetic-Field Variations in NOAA AR 8038 in Producing a Solar Flare and CME on 12 May 1997"*, Solar Physics, v. 271, Issue 1-2, p. 57-74.

8. Janardhan, P., Bisoi, S.K., Ananthakrishnan, S., Tokumaru, M., and Fujiki, K., 2011, *"The prelude to the deep minimum between solar Cycles 23 and 24: Interplanetary Scintillation signatures in the inner heliosphere"*, Geophys. Res. Lett., v. 38, p. L20108 (1-5).

9. Joshi, V.H., Ashok, N.M., and Banerjee, D.P.K., 2011, *"A study of the near-infrared modulation at spin and orbital periods in the intermediate polar WX Pyx"*, BASI, v. 39, p. 259-275.

10. Mathew, B., Banerjee, D.P.K., Ashok, N.M., Subramaniam, A., Bhavya, B., and Joshi, V., 2012, *"Studies of a possible new Herbig Ae/Be star in the open cluster NGC 7380"*, RAA, v. 12, p. 167-176.

11. Naik, S., Mathew, B., Banerjee, D.P.K., Ashok, N.M., and Jaiswal, R.R., 2012, *"Near-infrared observations of the Be/X-ray binary A0535+262"*, RAA, v. 12, p. 177-186.

12. Naik, S., Paul, B. and Zulfikar, A., 2011, *"X-ray spectroscopy of the High Mass X-ray Binary Pulsar Centaurus X-3 over its binary orbit"*, The Astrophysical Journal, v. 737, p. 79-87.

13. Raj, Ashish, Ashok, N.M., and Banerjee, D.P.K., 2011, *"Nova V5579 Sgr 2008: near-infrared studies during maximum and the early decline phase"*, Mon. Not. R. Astron. Soc. Letters, v. 415, p. 3455-3461.

14. Raju, K.P., Chandrasekhar, T., and Ashok, N.M., 2011, *"The analysis of Coronal Green Line Profiles : Evidence of Excess Blue Shifts"*, The Astrophysical Journal, v. 736, p. 164-170.

15. Redaelli, M., Kepler, S.O., Costa, J.E.S., et al. including Baliyan, K.S., Vats, H.O., 2011, *"The pulsations of PG 1351+489"*, Mon. Not. R. Astron. Soc., v. 415, p. 1220–1227.

16. Singal, A.K., 2011, *"A first principles derivation of the electromagnetic fields of a point charge in arbitrary motion"*, Am. J. Phys., v. 79, p. 1036-1041.

17. Singal, A.K., 2011, *"Large peculiar motion of the solar system from the dipole anisotropy in sky brightness due to distant radio sources"*, Astrophys. J. Lett., v. 742, p. 23-26.

Solar Physics

18. Bayanna, A.R., Mathew, S.K., Sankarasubramanian, K., Venkatakrishnan, P., Singh, J., and Prasad, B.R., 2011, *"Issues with External Occultation of a Coronagraph"*, Experimental Astron. , v. 29, p. 145-153.

19. Gosain, S., 2012, *"Evidence for Collapsing Fields in Corona and Photosphere during the 15 February 2011 X2.2 Flare: SDO AIA and HMI Observations"*, ApJ, v. 749, p. 85-94.

20. Gosain, S., Mathew, S. K. and Venkatakrishnan, P., 2011, *"Acoustic Power Absorption and its Relation to Vector Magnetic Field of a Sunspot"*, Solar Phys., v. 268, p. 335-348.

21. Joshi, A.D., and Srivastava, N., 2011, *"Acceleration of Coronal Mass Ejections from three-dimensional reconstruction of STEREO Images"*, ApJ, v. 739, p. 8-20.

22. Joshi, B., Veronig, A.M., Lee, J., Bong, S.C., Tiwari, S.K., and Cho, K.S., 2011, *"Pre-flare Activity and Magnetic Reconnection during the Evolutionary Stages of Energy Release in a Solar Eruptive Flare"*, ApJ, v. 743, p. 195-207.

23. Kumar, B., Venkatakrishnan, P., Mathur, S., Tiwari, S.K., and Garcia, R.A. 2011, *"On the Flare-Induced Seismicity in the Active Region NOAA 10930 and Related Enhancement of Global Waves in the Sun"*, ApJ, v. 743, p. 29-37.

24. Kumar, D. and Bhattacharyya, R., 2011, *"Solar Coronal Loops as Non Force-Free Minimum Energy Relaxed State"*, Phys. Plasmas, v. 18, p. 084506 (1-4).

25. Maurya, R.A., Vemareddy, P., and Ambastha, A., 2012, *"Velocity and Magnetic Transients Driven by the X2.2 White-Light Flare of 2011 February 15 in NOAA 11158"*, Ap J, v. 747, p.134-145.

26. Mierla, M., Inhester, B., Rodriguez, L., Gissot, S., Zhukov, A., and Srivastava, N., 2011, *"On 3D Reconstruction of CMEs II Longitudinal Width Analysis of 31 August 2007 Event"*, J. Atmos. Sol. Terres. Phys., v. 73, p. 1166-1172.

27. Panasenco, O., Martin, S.F., Joshi, A.D., and Srivastava, N., 2011, *"Rolling Motion in Erupting Prominences Observed by STEREO"*, J. Atmos. Solar Terr. Phys., v. 73, p.1129-1137.

28. Ravindra, B., Venkatakrishnan, P., Tiwari, S.K. and Bhattacharyya, R., 2011, *"Evolution of Currents of Opposite Signs in the Flare-Productive Solar Active Region NOAA 10930"*, ApJ, v. 740, p. 19-25.

29. Schmieder, B., Démoulin, P., Pariat, E., Török, T., Molodij, G., Mandrini, C.H., Dasso, S., Chandra, R., Uddin, W., Kumar, P., Manoharan, P.K., Venkatakrishnan, P. and Srivastava, N., 2011, *"Actors of the Main Activity in Large Complex*

Centres during the 23 Solar Cycle Maximum", Adv. Space Res., v. 47, p. 2081-2091.

30. Srivastava, N., Mierla, M., and Rodriguez, L., 2011, *"On Three Dimensional Aspects of CMEs, Their Source Regions and Interplanetary Manifestations"*, J. Atmos. Sol. Terres. Phys., v. 73, p. 1077-1081.

31. Vemareddy, P., Maurya, R. A., and Ambastha, A., 2012, *"Filament Eruption in NOAA 11093 Leading to a Two-Ribbon M1 Class Flare and CME"*, Solar Phys., v. 277, p. 337-354.

Planetary Sciences & PLANEX Program

32. Asagoe, M., Toyoda, S., Voinche, P., Falguères, C., Tissoux, H., Suzuki, T., and Banerjee, D., 2011, *"ESR dating of tephra with dose recovery test for impurity centers in quartz"*, Quaternary International, v. 246, p. 118-123.

33. Basu, S.A., Goodrich, C.A., Liu, Y., Day, J.M.D., and Taylor L.A., 2011, *"Evidence for heterogeneous enriched shergottite mantle sources in Mars from olivine-hosted melt inclusions in Larkman Nunatak 06319"*, Geochim. Cosmochim. Acta, v. 75, p. 6803–6820.

34. Dachev, T.P., Tomov, B.T., Matviichuk, Yu.N., Dimitrov, P.S., Vadawale, S.V., Goswami, J.N., de Angelis, G., and Girish, V., 2011, *"An overview of RADOM results for earth and moon radiation environment on Chandrayaan-1 satellite"*, Adv. Space Res., v. 48, p. 779-791.

35. Kumar, S.P., Kumar, S.A., Keerthi, V., Goswami, J.N., Krishna, G.B., and Kumar, K.A.S., 2011 *"Chandrayaan-1 observation of distant secondary craters of Copernicus exhibiting central mound morphology: Evidence for low velocity clustered impacts on the Moon, Planet"*, Space Sci., v. 59, p. 870-879.

36. Kusuma, K.N., Sebastian, N., and Murty S.V.S., 2012, *"Geochemical and mineralogical analysis of Gruithuisen region on Moon using M^3 and DIVINER images"*, Planet. Space Sci., v. 67, p. 46-56.

37. Maibam, B., Goswami, J.N., and Srinivasan, R., 2011, *"Pb-Pb zircon ages of Archaean metasediments and gneisses from the Dharwar craton, Southern India: Implications for the antiquity of the eastern Dharwar craton"*, Jour. Earth Sys. Sci., v. 120, p. 643-661.

38. Niyogi, A., Pati1, J.K., Patel, S.C., Panda, D.K., and Patil, S.K., 2011, *"Anthropogenic and impact spherules: Morphological similarity and chemical distinction – A case study from India and its implications"*, J. Earth Syst. Sci., v. 120, p. 1041–1054.

39. Pabari, J.P., Acharya, Y.B., Desai, U.B., and Merchant, S. N., 2012, *"Development of impedance based miniaturized wireless water ice sensor for future planetary applications"*, IEEE Transactions on Instrumentation and Measurement, v. 61, p. 521-529.

40. Ray, D., Rajan, S., and Ravindra, R., 2012, *"Role of subducting component and sub arc mantle in arc petrogenesis: Andaman volcanic arc"*, Current Science, v. 102, p. 605-609.

41. Sato, F., Toyoda, S., Banerjee, D., and Ishibashi, J., 2011, *"Thermal stability of ESR signals in hydrothermal barites"*, Radiation Measurements, v. 46, p. 866-870.

42. Senthil Kumar, P., Senthil Kumar, A., Keerthi, V., Goswami, J.N., Gopala Krishna B., and Kiran Kumar, A.S., 2011, *"Chandrayaan-1 observation of distant secondary craters of Copernicus exhibiting central mound morphology: Evidence for low velocity clustered impacts on the moon",* Planet. Sp. Sci. v. 59, p. 870-879.

43. Shanmugam, M., Acharya, Y.B., Mishra, V., Patel, P.N., and Goyal, S.K., 2012, *"A compact X-ray spectrometer using Silicon Drift Detector"*, Sensors & Transducers Journal, v. 138, p. 22-34.

44. Shanmugam, M., Vadawale, S., Acharya, Y.B., Mishra, V., Patel, P.N., and Goyal, S.K., 2012, *"Design and performance evaluation of SDD based X-ray spectrometer for future planetary exploration"*, Radiation Measurements, v. 47, p. 375-382.

45. Vadawale, S.V., Goswami, J.N., Dachev, T.P., Tomov, B.T., and Girish, V., 2011, *"Radiation Environment in Earth-Moon space: Results from RADOM experiment onboard Chandrayaan-1"*, Adv. Geosciences, v. 25, p. 121-132.

46. Weider, S.Z., Kellett, B.J., Swinyard, B.M., Crawford, I.A., Joy, K.H., Grande, M., Howe, C.J., Huovelin, J., Narendranath, S., Alha, L., Anand, M., Athiray, P.S., Bhandari, N., Carter, J.A., Cook, A.C., d'Uston, L.C., Fernandes, V.A., Gasnault, O., Goswami, J.N., Gow, J.P.D., Holland, A.D., Koschny, D., Lawrence, D.J., Maddison, B.J., Maurice, S., McKay, D.J., Okada, T., Pieters, C., Rothery, D.A., Russell, S.S., Shrivastava, A., Smith, D.R., and Wieczorek, M., 2012, *"The Chandrayaan-1 X-ray Spectrometer: First results"*, Planet Sp. Sci., v. 60, p. 217-228.

Space and Atmospheric Sciences

47. Bagiya, M. S., and Sridharan, R., 2011, *"Evolutionary Phases of Equatorial Spread-F (ESF) including L-band scintillations and plumes in the context of GPS-TEC variability - a case study"*, J. Geophys. Res., v. 116, p. A10304 (1-12).

48. Bapat, B., and Kushawaha, R.K., 2011, *"Similarities in Kinetic Energy Distributions of Associative Fragments during Dissociative Ionization of Organic Molecules"*, J. Korean Phys. Soc., v. 59, p. 2905-2909.

49. Cherian, R., Venkataraman, C., Ramachandran, S., Quaas, J., and Kedia, S., 2012, *"Examination of aerosol distributions and radiative effects over the Bay of Bengal and the Arabian Sea region during ICARB using satellite data and a general circulation model"*, Atmos. Chem. Phys., v. 12, p. 1287-1305.

50. Das, U., Pan C.J., and Sinha, H.S.S., 2011, *"Effects of Solar Cycle Variations on Oxygen Green Line Emission Rate over Kiso, Japan"*, Earth Planets Space, v. 63, p. 941-948.

51. Guharay, A., and Sekar, R., 2011, *"Seasonal Characteristics of gravity waves in the middle atmosphere over Gadanki using Rayleigh Lidar observations"*, J. Atmos. Sol-Terr. Phys., v. 73, p. 1762-1770.

52. Guharay, A., and Sekar, R., 2012, *"Signature of latitudinal coupling during a major sudden stratospheric warming in the tropics"*, J. Atmos. Sol-Terr. Phys., v. 75-76, p. 122-126.

53. Guharay, A., Sekar, R., M.Venkat Ratnam, Batista, P.P., 2012, *"Characteristics of the intraseasonal oscillations in the lower and middle atmosphere over Gadanki"*, J. Atmos. Sol-Terr. Phys., v. 77, p. 167–173.

54. Jana, M.R., Ghosh, P.N., Bapat, B., Kushawaha, R.K., Saha, K., Prajapati, I.A., and Safvan, C.P., 2011, *"Ion-induced triple fragmentation of CO_2^{3+} into $C^+ + O^+ + O^+$"*, Phys. Rev., v. A84, p. 062715 (1-5).

55. Kedia, S., and Ramachandran, S., 2011, *"Seasonal variations in aerosol characteristics over an urban location and a remote site in western India"*, Atmos. Env., v. 45, p. 2120-2128.

56. Kondo, Y., Matsui, H., Moteki, N., Sahu, L., Takegawa, N., Kajino, M., Zhao, Y., Cubison, M.J., Jimenez, J.L., Vay, S., Diskin, G., Anderson, B., Wisthaler, A., Mikoviny, T., Fuelberg, H.E., Blake, D.R., Huey, G., Weinheimer, A.J., Knapp, D.J., and Brune, W.H., 2011, *"Emissions of black carbon, organic, and inorganic aerosols from biomass burning in North America and Asia in 2008"*, J. Geophys. Res., v. 116, p. D08204 (1-25).

57. Lal, S., Sahu, L.K., Venkataramani, S., and Mallik, C., 2012, *"Light non-methane hydrocarbons at two sites in the Indo-Gangetic Plain"*, J. Environ. Monit., v. 14, p. 1159-1166.

58. Mallik, C., and Lal, S., 2011, *"Changing long-term trends in tropospheric temperature over two megacities in the Indo-Gangetic Plain"*, Curr. Sci., v. 101, p. 637-644.

59. Manju, G., Sridharan, R., Sreelatha, P., Ravindran, S., Haridas, M., Pant, T.K., Kumar, P.P., Thampi, R.S., N. Naik, N., Mridula, N., Jose, L., Sumod, S.G., 2012, *"A Novel probe for in-situ Electron density and Neutral Wind (ENWi) measurements in the near Earth space"*, J. Atmos. Sol-Terr. Physics, v. 74, p. 81-86.

60. Matsui, H., Kondo, K., Moteki, N., Takegawa, N., Sahu, L.K., Koike, M., Zhao, Y., Fuelberg, H.F., Sessions, W.R., Diskin, G., Anderson, B.E., Blake, D.R., Wisthaler, A., Cubison, M.J., J. L. and Jimenez, 2011, *"Accumulation-mode aerosol number concentrations in the Arctic during the ARCTAS aircraft campaign: Long-range transport of polluted and clean air from the Asian continent"*, J. Geophys. Res., v. 116, p. D20217 (1-14).

61. McNaughton, C.S., Clarke, A.D., Freitag, S., Kapustin, V.N., Kondo, Y., Moteki, N., Sahu, L., Takegawa, N., J. P. Schwarz, J.P., Spackman, J.R., Watts, L., Diskin, G., Podolske, J., Holloway, J.S., Wisthaler, A., Mikoviny, T., Gouw, J. de., Warneke, C., Jimenez, J., Cubison, M., Howell, S.G., Middlebrook, A., Bahreini, R., Anderson, B.E., Winstead, E., Thornhill, K.L., Lack, D., Cozic, J., and Brock, C.A., 2011, *"Absorbing aerosol in the troposphere of the Western Arctic during the 2008 ARCTAS/ARCPAC airborne field campaigns"*, Atmos. Chem. Phys., v. 11, p. 7561-7582.

62. Pallamraju, D., Chakrabarti, S., and Solomon, S., 2011, *"On deriving auroral particle fluxes in the daytime using combined ground-based optical and radar measurements"*, J. Geophys. Res., v. 116, p. A04309 (1-7).

63. Pallamraju, D., Lu, G., and Lin, C., 2012, *"An overview of the special issue on the Atmospheric Coupling Processes in the Sun-Earth System",* J. Atmos. Sol-Terr. Phys., v. 75–76, p. 1-4.

64. Ramachandran, S., and Kedia, S., 2011, *"Aerosol radiative effects over an urban location and a remote site in western India: Seasonal variability"*, Atmos. Environ. v. 45, p. 7415-7422.

65. Ramachandran, S., Kedia, S., and Srivastava, R., 2012, *"Aerosol optical depth trends over different regions of India"*, Atmos. Environ., v. 49, p. 338-347.

66. Rao, P.B., Beig, G., Dabas, R.S., Ramkumar, G., Gurubaran, S., Rao, K.G., Manoharan, P.K., Patra, A.K., Ravindran, S., Pant, T.K., Venkat Ratnam, M., Chakravarty, S.C., and Sridharan, R., 2012, *"An Overview of CAWSES-India Program with Emphasis to Equatorial Atmospheric Coupling Processes"*, J. Atmos. Sol.-Terr. Phys., v. 75 - 76, p. 98-114.

67. Rastogi, R.G., Chandra, H., Trivedi, N.B., and Doumbya, V., 2011, *"Equatorial electrojet in the South Atlantic anomaly region"*, J. Earth Syst. Sci., v. 120, p. 301-310.

68. Reddy, B.S.K., Reddy, L.S.S., Cao, J.J., Kumar, K.R., G. Balakrishnaiah, G., Gopal, K.R., Reddy, R.R., Narasimhulu, K., and Lal, S., 2011, *"Simultaneous measurements of surface ozone at two sites over the Southern Asia: A comparative study",* Aerosol and Air Quality Res., v. 11, p. 895-902.

69. Sahu, L.K., Kondo, Y., Miyazaki, Y., Pongkiatkul, P., and Kim Oanh, N.T., 2011, *"Seasonal and diurnal variations of black carbon and organic carbon aerosols in Bangkok"*, J. Geophys. Res., v. 116, p. D15302 (1-14).

70. Sahu, L.K., Lal, S., and Venkataramani, S., 2011, *"Seasonality in the latitudinal distributions of NMHCs over Bay of Bengal"*, Atmos. Environ., v. 45, p. 2356-2366.

71. Sahu, L.K., Lal, S., Thouret, V., and Smit, H.G., 2011, *"Climatology of tropospheric ozone and water vapour over Chennai: a study based on MOZAIC measurements over India"*, Int. J. Climatology, v. 31, p. 920–936.

72. Schaufelberger, A., Wurz, P., Barabash, S., Wieser, M., Futaana, Y., Holmstrom, M., Bhardwaj, A., Dhanya, M.B., Sridharan, R., and Asamura, K., 2011, *"Scattering function for energetic neutral hydrogen atoms off the lunar surface"*, Geophys. Res. Lett., v. 32, p. L22202 (1-6).

73. Sekar, R., Chakrabarty, D., and Pallamraju, D., 2012, *"Optical signature of shear in the zonal plasma flow with a tilted structure associated with equatorial Spread F during a space weather event"*, J. Atmos. Sol-Terr. Phys., v. 75-76, p. 57-63.

74. Shinozuka, Y., Redemann, J., Livingston, J.M., Russell, P.B., Clarke, A.D., Howell, S.G., Freitag, S., O'Neill, N.T., Reid, E.A., Johnson, R., Ramachandran, S., McNaughton, C.S., Kapustin, V.N., Brekhovskikh, V., Holben, B.N., and McArthur, L.J.B., 2011, *"Airborne observation of aerosol optical depth during ARCTAS: vertical profiles, inter-comparison and fine-mode fraction"*, Atmos. Chem. Phys., v. 11, p. 3673-3688.

75. Simi, K.G., Thampi, S.V., Chakrabarty, D., Pathan, B.M., Nayar, S.R.P., and Pant, T.K., 2012, *"Extreme changes in the equatorial electrojet under the influence of interplanetary electric field and the associated modification in the low-latitude F-region plasma distribution",* J. Geophys. Res., v. 117, p. A03331 (1-11). [AGU Editors Choice: "Space Weather", April, 2012]

76. Sinha, H.S.S., Pandey, R., Sharma, S., and Misra, R.N., 2012, *"Nighttime E region plasma irregularities over an equatorial station Trivandrum"*, J. Atmos. Sol.-Terr. Phys. v. 73, p. 2444 – 2452.

77. Srivastava, R., Ramachandran, S., Rajesh, T.A., and Kedia, S., 2011, *"Aerosol radiative forcing deduced from observations and models over an urban location and sensitivity to single scattering albedo"*, Atmos. Environ., v. 45, p. 6163 – 6171.

78. Srivastava, S., Lal S., Venkataramani, S., Gupta, S., and Acharya, Y.B., 2011, *"Vertical distribution of ozone in the lower troposphere over the Bay of Bengal and the Arabian Sea during ICARB-2006: Effects of continental outflow"*, J. Geophys. Res., v. 116, p. D13301 (1-13).

79. Srivastava, S., Lal S., Venkataramani, S., Gupta, S., and Sheel, V., 2012, *"Surface distributions of O_3, CO and hydrocarbons over the Bay of Bengal and the Arabian Sea during pre-monsoon season"*, Atmos. Env., v. 47, p. 459-467.

80. Srivastava, S., Lal, S., Naja, M., Venkataramani, S., and Gupta, S., 2012, *"Influences of regional polution and long range transport to western India: Analysis of ozonesonde data"*, Atmos. Env., v. 47, p. 174-182.

81. Sunder, Raman, R., Ramachandran, S., and Kedia, S., 2011, *"A methodology to estimate source-specific aerosol radiative forcing"*, J. Aerosol Sci., v. 42, p. 305-320.

82. Thampi, S.V., Yamamoto, M., Lin, C., and Liu, H., 2011, *"Comparison of FORMOSAT-3/COSMIC radio occultation measurements with radio tomography"*, Radio Sci., v.46, p. RS3001 (1-11). [AGU Editors Choice: "Space Weather", June, 2011]

83. Tsunoda, R.T., Yamamoto, M., Tsugawa, T., Hoang, T.L., Tulasi Ram, S., Thampi, S.V., Chau, H.D., and Nagatsuma, T., 2011, *"On seeding, large-scale wave structure, equatorial spread F, and scintillations over Vietnam"*, Geophys. Res. Lett., v. 38, p. L20102 (1-5).

84. Tulasi Ram, S., Yamamoto, M., Tsunoda, R.T., Thampi, S.V., and Gurubaran, S., 2012, *"On the application of differential phase measurements to study the zonal large scale wave structure (LSWS) in the ionospheric electron content"*, Radio Sci., v. 47, p. RS2001 (1-10). [AGU Editors Choice: "Space Weather", March, 2012]

85. Verma, R.L., Kondo, Y., Oshima, N., Matsui, H., Kita, K., Sahu, L.K., Kato, S., Kajii, Y., Takami, A., and Miyakawa, T., 2011, *"Seasonal variations of the transport of black carbon and carbon monoxide from the Asian continent to the western Pacific in the boundary layer"*, J. Geophys. Res., v. 116, p. D21307 (1-22).

Geosciences

86. Amatullah, H., North, M.L., Akhtar, U.S., Rastogi, N., Urch, B., Silverman, F.S., Chow, C.W., Evans, G.J., and Scott, J.A., 2012, *"Comparative Cardiopulmonary Effects of Size-Fractionated Airborne Particulate Matter"*, Inhalation Toxicology, v. 24 (3), p. 161-171, doi: 10.3109/08958378.2011.650235.

87. Laskar, A.H., Raghav, S., Yadava, M.G., Jani, R.A., Narayana, A.C., and Ramesh, R., 2011, *"Potential of stable carbon and oxygen isotope variations of speleothems from Andaman Islands, India, for paleomonsoon reconstruction"*, Journal of Geological Research Volume 2011 (2011), Article ID 272971 (1-7).

88. Beukema, S.P., Krishnamurthy, R.V., Juyal, N., Basavaiah, N., and Singhvi, A.K., 2011, *"Monsoon variability and chemical weathering during the late Pleistocene in the Goriganga basin, higher central Himalaya"*, Quaternary Research, v. 75, p. 597-604.

89. Chamyal, L.S., Malasse, A.D., Maurya, D.M., Raj, R., Juyal, N., Bhndari, S., Pant, R.K., and Gaillard, C., 2011, *"Discovery of a robust fossil Homo Sapiens in India (Orsang River valley, Lower Narmada basin, Gujarat); possible continuity with Asian Homo erectus"*, Acta Anthropologica Sinica, v. 30, p. 167-191.

90. Chauhan, N., and Singhvi, A.K., 2011, *"Distribution in SAR paleodoses due to spatial heterogeniety of natural beta dose"*, Geochronometria, v. 38, p. 190-198.

91. Gandhi, N., Singh, A., Prakash, S., Ramesh, R., Raman, M., Sheshshayee, M.S., and Shetye, S., 2011, *"First direct measurements of N2 fixation during a Trichodesmium bloom in the eastern Arabian Sea"*, Global Biogeochem, Cycles 25, GB4014, doi:10.1029/2010GB003970.

92. Glennie, K.W., Fryberger, S.C., Hern, C., Lancaster, N., Teller, J.T., Pandey, V.P., and Singhvi, A.K., 2011, *"Geological importance of luminescence dates in Oman and the Emirates, An overview"*, Geochronometria, v. 38, p. 259-271.

93. Goswami, V., Singh, S.K., and Bhushan, R., 2012, *"Dissolved redox sensitive elements, Re, U and Mo in intense denitrification zone of the Arabian Sea"*, Chemical Geology v. 291, p. 256–268.

94. Goswami, V., Singh, S.K., Bhushan, R., and Rai, V.K., 2012, *"Temporal variations in 87Sr/86Sr and μNd in sediments of the southeastern Arabian Sea: Impact of monsoon and surface water circulation"*, Geochem. Geophys. Geosyst., v. 13, Q01001, doi:10.1029/2011GC003802.

95. Hunter, K.A., Liss, P.S., Surapipith, V., Dentener, F., Duce, R., Kanakidou, M., Kubilay, N., Mahowald, N., Okin, G., Sarin, M.M., Tegen, I., Uematsu, M., and Zhu, T.T., 2011, *"Impacts of anthropogenic SOx, NOx and NH3 on acidification of coastal waters and shipping lanes"*, Geophy. Res. Lett. v. 38, p. 1-6, L13602, doi:10.1029/2011GL047720.

96. Jayangondaperumal, R., Murari, M.K., Subramaniyam, P., and Singhvi, A.K., 2012, *"Luminescence Dating of Teri Red Sands in SE coast India: Implications for environmental change and dune reddening"*, Quaternary Research, v. 77, p.468-481.

97. Kirpa, R., and Sarin, M.M., 2012, *"^{210}Pb, ^{210}Po and ^{210}Po/^{210}Pb activity ratio in urban aerosols: Temporalvariability and impact of biomass burning emission"*, Tellus-b, v. 64, p.1-11, doi:10.3042/tellusb.v64io.1751.

98. Kirpa, R., Sarin, M.M., and Tripathi, S.N., 2012, *"Temporal trends in atmospheric PM2.5, PM10, Elemental Carbon, Organic Carbon, Water-soluble Organic Carbon and optical properties. Impact of biomass burnig emissions in the Indo-Gangetic Plain"*, Environ. Sci Technol, p.686-695.

99. Kumar, A., Sudheer, A.K., Goswami, V., and Bhushan, R., 2012, *"Influence of continental outflow on aerosol chemical characteristics over the Arabian Sea during winter"*, Atmospheric Environment, v. 50, p. 182-191. doi:10.1016/ j.atmosenv. 2011.12.040.

100. Kumar, S., Finlay, J.C., and Sterner, R.W., 2011, *"Stable isotopic composition of suspended particulate matter in Lake Superior: Implications for nutrient cycling and organic matter transformation"*, Biogeochemistry, v. 103, p. 1-14, doi: 10.1007/s10533-010-9441-6.

101. Lupker, M., France, Lanord, C., Galy, V., Lavé, J., Gaillardet, J., Gajurel, A.P., Guilmette, C., Rahman, M., Singh, S.K., and Sinha, R., 2012, *"Predominant floodplain over mountain weathering of Himalayan sediments (Ganga basin)"*, Geochimica et Cosmochimica Acta, v. 84, p. 410-432.

102. Maurya, A.S., Shah, M., Deshpande, R.D., Bhardwaj, R.M., Prasad, A., and Gupta, S.K., 2011, *"Hydrograph separation and precipitation source identification using stable water isotopes and conductivity: River Ganga at Himalayan foothills"*, v. 25, p. 1521-1530.

103. McWhinney, R.D., Rastogi, N., Urch, B., Silverman, F., Brook, J., R., Evans, G.J., Abbatt, J.P.D., 2012, *"Characterization of the University of Toronto Concentrated Aerosol Particle Exposure Facility (CAPEF) - Effects on fine and ultrafine non-refractory aerosol composition"*, Aerosol Science and Technology v. 46, p. 697-707, doi:10.1080/02786826.2012.656769.

104. Morthekai, P., Jain, M., Cunha, P.P., Azevedo J., and Singhvi, A.K., 2011, *"An attempt to correct for the fading in million year old basaltic rocks"*, Geochronometria, v. 38, p. 223-230.

105. Morthekai, P., Thomas, J., Pandian, M.S., Balaram V., and Singhvi, A.K., 2012, *"Variable range hopping mechanism in band-tail states of K-feldspars – a time resolved IRSL study"*, Radiation Measurements, v. 47, p. 1-7.

106. Nair, R.R., Vijaya, C.S., Murari, M.K., Buynevich, I., Srinivasan, P., Murthy, S.G.N., Vijayalakshmi, C.S., Trivedi, D., Kandpal, S.C., Hussain, S.M., and Singhvi, A.K., 2011, *"Subsurface signatures and timing of extreme wave events along the southeast Indian coast"*, J. Earth Sys. Sci. v. 120, p. 873-883.

107. Okin, G.S., Baker, A.R., Tegen, I., Mahowald, N.M., Dentener, F.J., Duce, R.A., Galloway, J.N., Hunter, K., Kanakidou, M., Kubilay, N., Prospero, J.M., Sarin, M.M., Surapipith, V., Uematsu, M., and Zhu,

T., 2011, *"Impacts of atmospheric nutrient deposition on marine productivity: roles of nitrogen, phosphorus, and iron"*, Global Biogeochemical cycles, v. 25, p. 1-10, doi:10.1029/2010GB003858.

108. Rahaman, W., and Singh, S.K., 2012, *"Sr and $^{87}Sr/^{86}Sr$ in estuaries of western India: Impact of submarine groundwater discharge"*, Geochimica et Cosmochimica Acta, v. 85, p. 275-288.

109. Rajput, P., Sarin, M.M., and Rengarajan, R., 2011, *"High-precision GC-MS analysis of atmospheric Polycyclic Aromatic Hydrocarbons (PAHs) and isomer ratios from biomass burning emissions"*, Journal of Environmental Protection, v. 2, p. 445-453.

110. Rajput, P., Sarin, M.M., Rengarajan, R., and Singh, D., 2011, *"Atmospheric polycyclic aromatic hydrocarbons (PAHs) from post-harvest biomass burning emissions in the Indo-Gangetic Plain: Isomer ratios and temporal trends"*, Atmos. Environ., v. 45, p. 6732-6740.

111. Ramesh, R., 2011, "*Nitrogen and the North East Arabian Sea",* Geography and You, v. 11, Issue 67, p. 16-20.

112. Ramesh, R., Mangave, S.R., Lekshmy, P.R., Laskar, A.H., Yadava, H.G., and Jani, R.A., 2012, *"Comment on -Tracing the sources of water using stable isotopes: first results along the Mangalore-Udupi region, south-west coast of India"*, Rapid Commun. Mass Spectrum, v. 26, p. 874-875, doi:10.1002/rcm.6174.

113. Ramesh, R., Tiwari, M., and Singh, A., 2011, *"High-resolution monsoon records since Last Glacial Maximum: a comparison of marine and terrestrial paleo-archives from South Asia"*, Journal of Geological Research, Volume, Article ID 765248 (1-12).

114. Rastogi, N., McWhinney, R.D., Akhtar, U.S., Fila, M., Urch, B., Abbatt, J.P.D., Brook, J.R., Silverman, F., and Evans, G.J., 2012, *"Physical characterization of the University of Toronto coarse, fine, and ultrafine high-volume particle concentrator systems"*, Aerosol Science and Technology, v. 46, p. 1015-1024, doi:10.1080/02786826.2012.686674.

115. Rastogi, N., Zhang, X., Edgerton, E.S., Ingall, E., and Weber, R.J., 2011, *"Filterable water-soluble organic nitrogen in fine particles over the southeastern USA during summer"*, Atmospheric Environment, v.45, p. 6040-6047, doi: 10.1016/j.atmosenv.2011.07.045.

116. Ray, J.S, Mahoney, J.J., Duncan, R.A., Ray, J., Wessel, P., and Naar, D., 2012, *"Chronology and geochemistry of lavas from the Nazca Ridge and Easter Seamount Chain: a ~30 Myr hotspot record"*, Journal of Petrology, v. 53, p.1417-1448.

117. Rengarajan, R., Sarin, M.M., and Sudheer, A.K., 2011, *"Wintertime $PM_{2.5}$ and PM_{10} carbonaceous and inorganic constituents from urban site in western India"*, Atmos. Res., v. 102, p. 420-431.

118. Sano, M., Ramesh, R., Sheshshayee, M.S., and Sukumar, R., 2011, *"Increasing aridity during the past 223 years in the Nepal Himalaya inferred from a tree-ring $\delta^{18}O$ chronology"*, The Holocene, doi: 10.1177/0959683611430338.

119. Sarin, M.M., Kumar, A., Srinivas, B., Sudheer, A.K. and Rastogi, N., 2011, *"Anthropogenic sulphate aerosols and large Cl-deficit in marine atmospheric boundary layer of tropical Bay of Bengal"*, Jour. Atmos. Chem. v 66, p.1-10; doi:10.1007/s10874.

120. Sastry, M.D., Gaonkar, M., Nagar, Y.C., Mane, S.N., Desai, S.N., Bagla, H., Ramachandran, K.T., and Singhvi, A.K., 2011, *"Optically Stimulated luminescence (OSL) and laser excited photoluminescence of electron beam treated (EBT) diamonds: radiation sensitization and tissue equivalent dosimetry"*, Diamond and Related Materials, v. 20, p. 1095-1102.

121. Shetye, S., Sudhakar, M., Ramesh, R., Mohan, R., Patil, S., and Laskar, A.H., 2011, *"Sea surface pCO_2 in the Indian Sector of the Southern Ocean during Austral summer of 2009",* Adv. Geosci., v. 25, p. 50-60.

122. Singh, A., and Ramesh, R., 2011, *"Contribution of Riverine Dissolved Inorganic Nitrogen Flux to New Production in the Coastal Northern Indian Ocean: An Assessment"*, International Journal of Oceanography, v. 2011, Article ID 983561 (1-7), doi: 10.1155/2011/983561.

123. Singh, A., Gandhi, N., and Ramesh, R., 2012, *"Contribution of atmospheric nitrogen deposition to new production in the nitrogen limited photic zone of the northern Indian Ocean"*, Journal of Geophysical Research – Oceans, v. 117, p. 1-11, C06004; doi:10.1029/2011JC007737,2012.

124. Singhvi, A.K., Stokes, S., Chauhan, N., Nagar, Y.C., and Jaiswal, M., 2011, *"Changes in Natural OSL sensitivity during single aliquot regeneration procedure and their implications for equivalent dose determination"*, Geochronometria, v. 38, p. 231-241.

125. Srinivas, B., Kumar, A., Sarin, M.M., and Sudheer, A.K., 2011, *"Impact of continental outflow on chemistry of atmospheric aerosols over tropical Bay of Bengal"*, Atmos. Chem. Phys. Discuss., v 11, p. 20667-20711, doi:10.5194/acpd-11-1-2011.

126. Srinivas, B., Sarin M.M., and Kumar, A., 2011, *"Impact of anthropogenic sources on aerosol iron solubility over the Bay of Bengal and the Arabian Sea"*, Biogeochemistry, p. 1-12, doi: 10.1007/s10533-011-9680-1.

127. Srinivas, B., Sarin, M.M. and Sarma V.V.S.S., 2011, *"Atmospheric dry deposition of inorganic and organic nitrogen to the Bay of Bengal: Impact of continental outflow"*, Marine Chemistry, v 127, p.170-179.

128. Sudhakar, M., and Ramesh, R., 2012, *"Possible future directions for oceanographic research in India"*, International Journal of Research in Chemistry and Environment, v. 2, Issue 1, p. 314-315.

129. Thirumalai, K., Singh, A., and Ramesh, R., 2011, *"A MATLAB™ code to perform weighted linear regression with (correlated or uncorrelated) errors in bivariate data"*, J. Geol. Soc. Ind., v. 77, p. 377-380.

130. Tyagi, A.K., Shukla, A.D., Bhushan, R., Thakker, P.S., Thakkar, M.G., and Juyal, N., 2012, *"Mid-Holocene sedimentation and landscape evolution in the western Great rann of Kachchh, India"*, Geomorphology, v. 151-152, p. 89-98.

131. van de Flierdt, Tina, Pahnke Katharina Amakawa Hiroshi, Andersson P., Basak Chandranath, Coles Barry, Colin Christophe, Crocket Kirsty, Martin, F., Norbert, F., Goldstein Steven L., Goswami, V., Haley Brian A., Hathorne Ed C., Hemming Sidney R., Henderson Gideon M., Jeandel Catherine, Jones Kevin, Kreissig Katharina, Lacan Francois, Lambelet Myriam, Martin Ellen E., Newkirk Derrick R., Obata Haijme, Pena Leopoldo, Piotrowski Alexander M., Pradoux Catherine, Scher Howie D., Schöberg Hans, Singh, S.K., Stichel Torben, Tazoe Hirofumi, Vance Derek, and Yang Jingjing, 2012, *"GEOTRACES intercalibration of neodymium isotopes and rare earth element concentrations in seawater and suspended particles – Part 1: reproducibility of results for the international intercomparison"*, Limnology and Oceanography: Methods, v. 10, p. 234-251.

132. Weinman, B., Yoo K., and Singhvi, A.K., 2011, *"Chemical-weathering rates of aquifers and the mixing of soils: The role of Optical Dating in quantifying near surface processes on Earth and their time scales"*, Current Science, v. 101, p. 1136-1140.

Theoretical Physics

133. Acharyya, A., and Amritkar, R.E., 2011, *"Desynchronization bifurcation of coupled nonlinear dynamical systems"*, Chaos, v. 21, p. 023113 (6).

134. Ambika, G., and Amritkar, R.E., 2011, *"Delay or anticipatory synchronization in one-way coupled systems using variable delay with reset"*, Pramana, v. 77, p. 891-904.

135. Ambika, G., and Amritkar, R.E., 2011, *"Synchronizing time delay systems using variable delay in coupling"*, Chaos, Solutions and Fractals, v. 44, p.1035-1042.

136. Ananthanarayan, B., Garg, S.K., Patra, M., and Rindani, S.D., 2012, *"Isolating CP-violating γZZ coupling in $e^+e^- \rightarrow gZ$ with transverse beam polarizations"*, Phys. Rev. D., v. 85, p. 034006 (1-11).

137. Arora, B., Nandy, D.K., and Sahoo, B.K., 2012, *"Multipolar Black Body Radiation Shifts for the Single Ion Clocks"*, Phys. Rev. A., v. 85, p. 012506 (1-10).

138. Bandyopadhyay, A., Prabhakar, S., and Singh, R.P., 2011, *"Entanglement of a quantum optical elliptic vortex"*, Phys. Lett. A., v. 375, p. 1926.

139. Banerji, J., 2011, *"Collective excitations of a binary condensate in an axially symmetric trap"*, Asian Journal of Physics, v. 20, p. 203-207.

140. Banerji, J., 2011, *"The method of (not so) ordinary least squares: what can go wrong and how to fix them"*, Contemporary Physics, v. 52, p.181-195.

141. Barr, A.J., Khoo, T.J., Konar, P., Kong, K., Lester, C.G., and Matchev, K.T., and Park, M., 2011, *"*Guide to *Transverse projections and mass-constraining variables"*, Phys. Rev. D., v. 84, p. 095031 (1-44).

142. Basak, A. and Bhatt, J., 2011, *"Lorentz invariant dark-spinor and inflation"*, JCAP, v.06-011, p.1-17.

143. Bhatt, J.R., Mishra, H., and Sreekanth, V., 2011, *"Shear viscosity, cavitation and hydrodynamics at LHC"*, Phys. Lett. B., v. 704, p. 486-489.

144. Bhatt, J.R., Mishra, H., and Sreekanth, V., 2012, *"Cavitation and thermal dilepton production in QGP"*, Nucl. Phys. A., v. 875, p. 181-196.

145. Chakrabortty, J., Goswami, S., and Raychaudhuri, A., 2011, *"An SO(10) model with adjoint fermions for double seesaw neutrino masses"*, Phys. Lett. B., v. 698, p. 265-270.

146. Chatterjee, B., Mishra, H., and Mishra, A., 2011, *"Vacuum structure and chiral symmetry breaking in strong magnetic fields for hot and dense quark matter"*, Phys. Rev. D., v. 84, p. 014016 (1-17).

147. Choudhury, D., Godbole, R.M., Rindani, S.D., and Saha, P., 2011, *"Top polarization, forward-backward asymmetry and new physics"*, Phys. Rev. D., v. 84, p. 014023 (1-13).

148. Choudhury, D., Mahajan, N., Patra, S., and Sarkar, U., 2012, *"Radiative Leptogenesis at the TeV scale"*, Journal of Cosmology and Astroparticle Physics, v. 4, p. 017 (1-13).

149. Cowsik, R., Nussinov, S., and Sarkar, U., 2011, *"Superluminal Neutrinos at OPERA Confront pion decay kinematics"*, Phys. Rev. Lett., v. 107, p. 251801 (1-4).

150. Das, A.C., and Ambastha, A., 2012, *"High Energy Emissions from Young Stellar Objects"*, J. Astrophys. Astro., v. 33, p.1-8.

151. Esteban Martin, A., Samanta, G.K., Kumar, S.C., Devi, K., and Ebrahim Zadeh, M., 2012, *"Frequency-modulation-mode-locked optical parametric oscillator"*, Opt. Lett., v. 37, p. 115-117.

152. Gautam, S., Muruganandam, P., and Angom, D., 2012, *"Coreless vortex dipoles and trapped roplets in phase-separated binary condensates"*, J. Phys. B., v. 45, p.055303 (8).

153. Ghosh, K., Mukhopadhyaya, B., and Sarkar, U., 2011, *"Signals of an invisibly decaying Higgs in a scalar dark matter scenario: a study for the Large Hadron Collider"*, Phys. Rev. D., v. 84, p. 015017 (1-9).

154. Godbole, R.M., Hangst, C., Muhlleitner, M., Rindani, S.D., and Sharma, P., 2011, *"Model-independent analysis of Higgs spin and CP properties in the process* $e^+e^- \to tt\varphi$*"* Eur. Phys. J. C., v. 71, p. 1681 (1-19).

155. Gu, P., and Sarkar, U., 2011, *"Baryogenesis and neutron-antineutron oscillation at TeV"*, Phys. Lett. B., v. 705, p. 170-173.

156. Gupta, S., Joshipura, A.S., and Patel, K.,M., 2012, *"Minimal extension of tri-bimaximal mixing and generalized* Z_2 *X* Z_2 *symmetries",* Phys. Rev. D., v. 85, p. 031903 (1-6).

157. Huitu, K., Rai, S.K., Rao, K., Rindani, S.D., and Sharma, P., 2011, *"Probing top charged-Higgs production using top polarization at the Large Hadron Collider"*, JHEP, v. 4, p. 026 (1-19).

158. Joshipura, A. S., and Patel, K.M., 2011, *"Fermion Masses in SO(10) Models",* Phys. Rev. D., v. 83, p. 095002 (1-17).

159. Joshipura, A.S., and Patel, K.M., 2011, *"Viability of the exact tri-bimaximal mixing at M_{GUT} in SO(10)",* Journ. of High Energy Physics., v. 1109, p.137 (1-1 7).

160. Kishore, V., Santhanam, M.S., and Amritkar, R.E., 2011, *"Extreme Events on Complex Networks"*, Phys. Rev. Lett., v. 106, p. 188701 (4).

161. Konar, P., Kong, K., Matchev, K.T., Park M., *"RECO level and subsystem : Improved global inclusive variables for measuring the new physics mass scale in missing* E_T *events at hadron colliders"*, JHEP, v. 1106, p. 041 (1-35).

162. Kota, V.K.B., Relano, A., Retamosa, J. and Vyas, M., 2011, *"Thermalization in the Two-Body Random Ensemble"*, J. Stat. Mech., P10028 (1-22).

163. Kumar, A., Prabhakar, S., Vaity, P., and Singh, R.P., 2011, *"Information content of optical vortex fields"*, Opt. Lett., v. 36, p.1161-1163.

164. Kumar, A., Vaity, P., Banerji, J., and Singh, R.P., 2011, *"Making an optical vortex and its copies using a single spatial light modulator''*, Phys. Lett. A., v. 375, p. 3634-3640.

165. Kumar, S.C., Samanta, G.K., Devi, K., and Ebrahim Zadeh, M., 2011, *"High-efficiency, multi-crystal, single-pass, continuous-wave second harmonic generation"*, Opt. Express, v. 19, p. 11152-11169.

166. Kumar, S.C., Samanta, G.K., Devi, K., Sanguinetti, S., and Ebrahim Zadeh, M., 2012, *"Single-frequency, high-power, continuous-wave fiber-laser-pumped Ti:sapphire laser"*, App. Opt., v. 51, p. 15-20.

167. Lambiase G., Mishra, H., and Mohanty, S., 2012, *"Dark energy from Neutrinos and Standard Model Higgs potential",* Astroparticle Physics, v. 35, p. 629-633.

168. Lambiase, G., and Mohanty, S., 2011, *"Leptogenesis by curvature coupling of heavy neutrinos"*, Phys. Rev. D., v. 84, p. 023509 (1-6).

169. Ma, E., and Sarkar, U., 2012, *"Scalar neutrino as asymmetric dark matter: Radiative neutrino mass and leptogenesis"*, Phys. Rev. D., v. 85, p. 075015 (1-4).

170. Mishra, H., Mohanty, S., and Nautiyal, A., 2012, *"Warm natural inflation"*, Phys. Lett. B., v. 710, p. 245-250.

171. Mohanty, S., and Das, M., 2012, *"Magnetic field generation in Higgs inflation model"*, Int. J. Mod. Phys., A., v. 27, p. 1250040 (1-11).

172. Mohanty, S., Rao, S., and Roy, D.P., 2012, *"Relic density and PAMELA events in a heavy wino dark matter model with Sommerfeld effect"*, Int. J. Mod. Phys. A., v. 27, p. 1250025 (1-20).

173. Morisi, S., Patel, K.M., and Peinado, E., 2011, *"Model for T2K indication with maximal atmospheric angle and tri-maximal solar angle"*, Phys. Rev. D., v. 84, p. 053002 (1-6).

174. Nandy, D.K., Singh, Y., Sahoo, B.K., and Li, C., 2011, *"Sc III Spectral properties of astrophysical Interest"*, J. Phys. B., v. 44, p. 225701(1-11).

175. Nataraj, H.S., Sahoo, B.K., Das, B.P., and Mukherjee, D., 2011, *"A Reappraisal of the Electric Dipole Moment Enhancement Factor for Thallium"*, Phys. Rev. Lett., v. 106, p. 200403 (1-4).

176. Navinder, S. and Paul, B., 2011, *"Electronic energy transfer in model photosynthetic systems: Markovian vs. non-Markovian dynamics"*, Faraday Disc, v. 53, p. 41-50.

177. Navinder, S., 2012, *"Phase controllable dynamical localization of a quantum particle in a driven optical lattice"*, Phys. Lett. A., v. 376, Issue 19, p.1593-1595.

178. Patel, K. M., and Sharma, P., 2011, *"Forward-backward asymmetry in top quark production from light colored scalars in SO(10) model"*, Journ. of High Energy Physics, v. 1104, p. 085 (1-22).

179. Prabhakar, S., Kumar, A., Banerji, J., and Singh, R.P, 2011, *"Revealing the order of a vortex through its intensity record"*, Optics Letters, v. 36, p. 4398-4400.

180. Resmi, V., Ambika, G., and Amritkar, R.E., 2011, *"General mechanism for amplitude death in coupled systems"*, Phy. Rev. E., v. 84, p. 046212 (12).

181. Rindani, S.D., and Sharma, P., 2011, *"Probing anomalous tbW couplings in single-top production using toppolarization at the Large Hadron Collider"*, JHEP, v. 11, 082 (1-28).

182. Sahoo, B.K., and Das, B.P., 2011, *"Parity nonconservation in ytterbiumion"*, Phys. Rev. A., v. 84, p. 010502 (R) (1-4).

183. Sahoo, B.K., and Das, B.P., 2011, *"Transition Properties of Low Lying States in Atomic Indium"*, Phys. Rev., A., v. 84, p. 012501 (1-5).

184. Sahoo, B.K., Pandey, R., and Das, B.P., 2011, *"The Search For A Permanent Electric Dipole Moment Using Atomic Indium"*, Phys. Rev. A., v. 84, p. 030502 (R) (1-4).

185. Sahu, R. and Kota, V.K.B., 2011, *"Deformed shell model results for two neutrino positron double beta decay of ^{84}Sr"*, Int. J. Mod. Phys. E., v. 20, p.1723-1733.

186. Sahu, R., Srivatava, P.C. and Kota, V.K.B., 2011, *"Deformed shell model results for two neutrino double beta decay of ^{82}Se"*, Can. J. Phys., v. 89, p. 1101-1105.

187. Samanta, G.K., and Ebrahim Zadeh, M., 2011, *"Dual-wavelength, two-crystal, continuous-wave optical parametric oscillator"*, Opt. Lett., v. 36, p. 3033-3035.

188. Samanta, G.K., Kumar, S.C., Devi, K., and Ebrahim Zadeh, M., 2012, *"High power, continuous-wave Ti: sapphire laser pumped by Fiber-laser green source at 532 nm"*, Opt. and Laser in Engineering, v. 50, p. 215-219.

189. Singh, A., Puri, S., and Mishra, H., 2011, *"Domain Growth in Chiral Phase Transitions"*, Nucl. Phys. A., v. 864, p. 176-202.

190. Srivastava, P.C. and Kota, V.K.B., 2011, *"Shell-model results in fp and $fpg_{9/2}$ spaces for $^{61,63,65}Co$ isotopes"*, Physics of Atomic Nuclei, v. 74, p. 971-978.

191. Srivastava, P.C., 2012, *"Structure of $^{71-78}Ga$ isotopes in the $f_{5/2}pg_{9/2}$ and $fpg_{9/2}$ spaces"*, J. Phys. G: Nucl. Part. Phys., v. 39, p. 015102 (1-10).

192. Vaity, P., and Singh, R.P., 2011, *"Self-healing property of optical ring lattice"*, Opt. Lett., v. 36, p. 2994-2996.

193. Varma, R.K, Banerjee, S.B., and Ambastha, A., 2012, *"Macro-scale observation of curl-free vector potential: A manifestation quantum modulation of the de Broglie wave"*, Eur. Phys. J. D., v. 66, p. 38.

194. Varma, R.K., 2012, *"Macro-scale matter wave generation in charged particle dynamics in a magnetic field, a consequence of quantum entanglement",* Eur. Phys. J. D, v. 66, p. 39.

195. Vyas, M., Kota, V.K.B., and Srivastava, P.C., 2011, *"One plus two-body random matrix ensembles with parity: Density of states and parity ratios"*, Phys. Rev. C., 83, p. 064301 (1-18).

Publications in Proceedings of Conference / Symposia / Workshops

Astronomy and Astrophysics

1. Anandarao, B.G., and Chakraborty, A., 2010, "PRL Mt Abu Observatory: New Initiatives", in *"Interstellar Matter and Star Formation: A multi-wavelength perspective"*, Astron. Soc., India Conf. Ser., v. 1, p. 211-216 (eds. Ojha, D.K.,).

2. Garcia Alvarez, D., 2011, et.al (B.G. Anandarao and Venkata Raman V., co-authors), *"16th Cambridge Workshop on Cool Stars, Stellar Systems and the Sun"*, Astron. Soc. Pacific Conf. Ser., v. 448, p. 609-616. (eds. Johns Krull, C.M., Browning, M.K., and West, A.A.,).

3. Kumar, A.A., and Jain, R., 2011, *"Multi-wavelength diagnostics of precursor phase in Solar flares"*, First Asia-Pacific Solar Physics Meeting ASI Conference Series, v. 2, p. 297-305, (eds. Choudhuri, A.R., and Banerjee, D.,)

4. Paul, B., Raichur, H., Jain, C., James, M., Devasia, J., and Naik, S., 2012, *"Orbital evolution of X-ray binaries and quasi-periodic oscillations in X-ray pulsars"*, ASInC, v. 3, p. 29-33.

5. Singal, A.K., 2011, *"Coherence inherent in an incoherent synchrotron radio source"*, Proceedings of International Conference on Diffuse Relativistic Plasmas RRI, Bangalore, J. Astrophys. Astr., v. 32, p. 447-450.

6. Singal, A.K., 2012, *"Our large peculiar motion in the universe determined from the sky brightness anisotropy",* Proceedings of the national conference on Applied Mathematics and Computational Physics, in Advances in Applied Mathematics and Computational Physics, World Education Publishers, Delhi, p. 113-122.

7. Vats, H.O., 2012, *"Interplanetary magnetic field and solar rotation"*, Planetary and Space Science, v. 63–64, p. 158-163.

Solar Physics

8. Gosain, S., 2011, *"Distribution of Magnetic Shear Angle in an Emerging Flux Region"*, Proc. I.A.U. Symp., v. 273, p. 347-350.

9. Gosain, S., and Venkatakrishnan, P., 2011, *"Evolution of Twist-Shear and Dip-Shear in Flaring Active Region NOAA 10930"*, Proc. I.A.U. Symp., v. 273, p. 212-215.

10. Maurya, R.A., and Ambastha, A., 2011, *"Variations in p-mode Parameters and Sub-surface Flows of Active Regions with Flare Activity"*, A.S.I. Conf. Series, v. 2, p. 189-195.

Planetary Sciences & PLANEX Program

11. Durga, P.K., and Murty, S.V.S., 2011, *"Wireless sensor networks (WSN) – An in situ remote sensing tool for planetary exploration"*, Signatures, Newsletter of the ISRC-AC, v. 23, p. 49-52.

12. Murty, S.V.S., and Ranjit, K.P.M., 2012, *"Noble gas isotopes: tracers of impactor signatures in lonar impact glasses"*, 43rd Lunar and Planetary Science Conference, Houston, Texas, USA, Abstract no.1423 (1-2).

13. Marhas, K.K., and Randhawa, J., 2012, *"Production of short lived radionuclides: Late-stage irradiation in the early solar system"*, 43rd Lunar and Planetary Science Conference, Houston, Texas, USA, Abstract no. 2410 (1-2).

14. Shanmugam, M., Vadawale, S., Acharya, Y.B., Goyal, S.K., Patel, A., Shah, B., and Murty, S.V.S., 2012, *"Solar X-ray monitor (XSM) on-board Chandrayaan-2 orbiter"*, 43rd Lunar and Planetary Science Conference, Houston, Texas, USA, Abstract no.1858 (1-2).

Space and Atmospheric Sciences

15. Acharya, Y.B., 2011, *"Planetary remote sensing and gamma ray Astronomy"*, Signatures, Newsletter of the ISRS–AC, v. 23, No.4, p. 29-35.

16. Gupta, S.P., 2012, *"Solar terrestrial relationship and space weather",* Proceedings of DST-SERC school on Seismo Electromagnetics, v. II, p. 189-205.

17. Pallamraju, D., 2011, *"Optical investigations of the Mesosphere and Lower Thermosphere"*, Proceedings of Workshop on Growth of Geomagnetism: Challenges and Opportunities in the Next Two Decades, Indian Institute of Geomagnetism, Navi Mumbai, India, p. 31-33.

Geosciences

18. Bluszcz, A., Li, S.H., and Singhvi, A.K., 2010, *"Proceedings of the Second Asia Pacific Luminescence and Electron Spin Resonance Dating"*, PART -1, Geochronometria, v. 37, p. 1-77.

19. Bluszcz, A., Li, S.H., and Singhvi, A.K., 2011, *"Proceedings of the Second Asia Pacific Luminescence and Electron Spin Resonance Dating"*, PART- 2, Geochronometria, v. 38, p. 189-303.

20. Deshpande, R.D., Dave, M., Singh, R.L., Gupta, S.K., 2011, *"IWIN Programme: New Hydrological Insights"*, Proceedings of the 14th ISMAS Symposium cum Workshop on Mass Spectrometry, Munnar, India, p. 95-108.

21. Gandhi, N., Singh, A., Prakash, S., and Ramesh, R., 2011, *"Variations in the nitrogen isotopic composition of Plankton in the Arabian Sea"*, Proc. ISMAS Symposium cum Workshop on Mass Spectrometry, Munnar, Kerala, v. XIV, p. 144-146.

22. Kumar, S., Watson, B., Putz, G. and Prepas, E., 2011, *"Modelling nitrogen in streamflow from Boreal forest watersheds in Alberta"*, Canada, using SWAT, Proceedings of International SWAT conference, Madrid, Spain, p. 417-429.

23. Laskar, A.H., Yadava, M.G., and Ramesh, R., 2011, *"Stable and radioactive carbon in Indian soils: implications to soil carbon dynamics"*, Proc. ISMAS Symposium cum Workshop on Mass Spectrometry, Munnar, Kerala, v. XIV, p. 255-258.

24. Managave, S.R., Sheshshayee, M.S., Borgaonkar, H.P., Bhattacharya, A., and Ramesh, R., 2011, *"Intra-annual carbon isotope variations in Indian Teak trees"*, Proc. ISMAS Symposium cum Workshop on Mass Spectrometry, Munnar, Kerala, v. XIV, p. 189-191.

25. Ramesh, R., Srivastava, R., Jani, R.A., and Singh, A.K., 2011, *"Monsoon onset signal in the stable oxygen and hydrogen isotopes in Rainfall"*, Proc. ISMAS Symposium cum Workshop on Mass Spectrometry, Munnar, Kerala, v. XIV, p. 48-53.

26. Rao, D.K., Jani, R.A., and Ramesh, R., 2012, *"Identification of source for excess methane in marine atmosphere over Arabian coast"*, Abstracts of 17th National Space Science Symposium held at Tirupati, 14-17 February, 2012, p. 12-13.

Theoretical Physics

27. Banerji, J., 2012, *"Ultra-sensitive Dual-mode Waveguide Interferometers"*, Proceedings of the 99th Session of the Indian Science Congress, *3-7 January, 2012, Bhubaneswar, India, p.40-41.*

28. Chatterjee, B., Mishra, H., and Mishra, A., 2011, *"Chiral symmetry breaking in 3-flavor Nambu-Jona Lasinio model in magnetic background"*, Nucl. Phys. A., v. 862-863, p. 475-478.

29. Joshipura, A.S., 2011, *"Neutrino mass models and CP violation"*, AIP Conf. Proc. v. 1382, p. 54-58.

30. Joshipura, A.S., and Patel, K.M., 2011, *"Unified description of fermion masses with quasi-degenerate neutrinos in SO(10)"* , AIP Conf. Proc., v. 1382, p. 115-117.

31. Kota, V.K.B., and Sahu, R., 2011, *"Algebraic IBM-ST and Mean-field DSM-T Models for N=Z Nuclei"*, Proceedings of the workshop on Frontiers in Gamma ray Spectroscopy (FIG09), TIFR, Mumbai, p. 83-93. (eds. Palit, R., and Pillay, R.)

32. Kedia, S., Kumar, A., and Singh, R.P., 2012, *"Experimental analysis of optical diffraction in self assembled photonic crystals"*, National Laser Symposium-20, 9-12 January, 2012, Anna University Chennai, India, p. 61 (1-4).

33. Kumar, A., Prabhakar, S., Vaity, P., and Singh, R.P., 2011, *"Spatial coherence properties of the one-dimensional projection of optical vortices"*, Frontiers in Optics, 16-20 October, San Jose, USA, OSA Technical Digest, paper FThG6 (1-2).

34. Singh, A., Puri, S., and Mishra, H., 2012, *"Domain growth and Ordering kinetics in Dense Quark Matter"*, proceedings of workshop on Critical Point and Onset of Deconfinement, CPOD 10, JINR, Dubna, Physics of Atomic Nuclei, v. 75, p. 689-692.

35. Singh, A., Puri, S., and Mishra, H., 2011, *"Kinetics of Chiral Phase Transitions in Quark Matter"*, Gribov-80 Memorial volume, Quantum Chromodynamics and Beyond, p. 527-540. (eds. Dokshitzer, Y., Levai, P., and Nyari, J.)

Books Edited/Review Articles

Books Edited

1. Chandra, H., 2012, Guest editor, Asian J of Physics Special volume: *"Studies in the mesosphere – lower thermosphere at low-latitudes",* v. 19 (4).

2. Managave, S.R., and Ramesh, R., 2011, *"Isotope dendroclimatology: a review with a special emphasis on the tropics",* in: Handbook of Environmental Isotope Geochemistry (Advances in Isotope Geochemistry), (ed: Baskaran, M.) Springer Verlag, Berlin, v. 1, p. 811-833.

3. Pallamraju, D., 2012, Special issue on *"Atmospheric Coupling Processes in the Sun-Earth System"*, J. Atmos. Sol.-Terr. Phys., (eds: Pallamraju, D., Gang Lu and Charles Lin), v. 75-76, 2012.

4. Srivastava, N., 2011, Special issue on *"Three dimensional aspects of CMEs, their source regions and interplanetary manifestations",* J. Atmos. Sol.Terres. Phys, Guest editors: Marilena Mierla, Nandita Srivastava and Luciano Rodriguez, v. 73, Issue 10.

5. Tripathy, G.R., Singh, S.K., and Krishnaswami, S., 2011, *"Sr and Nd Isotopes as Tracers of Chemical and Physical Erosion",* in Handbook of Environmental Isotope Geochemistry (Advances in Isotope Geochemistry), (ed: Baskaran, M.), Springer-Verlag Berlin Heidelberg, v. 1, p. 521-552.

Review Articles

1. Dewangan, D.P., 2012, *"Asymptotic methods for Rydberg transitions''*, Phys. Rep., v. 511, p.1-142.

2. Haider, S.A., Mahajan, K.K., and Kallio, E., 2011, *"Mars ionosphere: A review of experimental results and modeling studies"*, Rev. Geophys., v. 49, p. RG4001 2011RG000357. (1-37).

3. Joshi, B., Veronig, A., Manoharan, P.K., and Somov, B.V., 2012, *"Signatures of Magnetic Reconnection in Solar Eruptive Flares: A Multi-Wavelength Perspective",* Astrophys. Space Sci. Proc., (eds: Manfred Leubner and Zoltan Voros), Springer – Verlag Berlin Heidelberg, v. 33, p. 29-41.

4. Paul, B., and Naik, S., 2011, *"Transient High Mass X-ray Binaries"*, Bulletin of the Astronomical Society of India, v. 39, p. 429-449.

5. Srivastava, N., 2012, *"An overview of Multi Wavelength Observations of Coronal Mass Ejections and Related Phenomena",* Adv. Solar & Solar Terres. Phys., Georgeta Maris and Crisan Demetrescu, ISBN 978 81 308 0478 1.

Other Publications

1. Banerjee, D.P.K., and Ashok, N.M., 2011, *"Infrared Observations of V5588 Sgr", Astronomers Telegram,* 3345.

2. Banerjee, D.P.K., and Ashok, N.M., 2011, *"Near-Infrared Observations of Recurrent Nova T Pyx In Outburst",* Astronomers Telegram, 3297.

3. Chandrasekhar, T., 2011, *"A search at the edge of the Solar System – Discovery of Kuiper belt objects",* PLANEX NEWS LETTER, v.1, Issue 4, p. 4-6.

4. Munari, U., Ashok, N.M., Banerjee, D.P.K., Righetti, G.L., Dallaporta, S., Cetrulo, G. and Englaro, A., 2011, *"V5588 Sgr : Optical and near-IR spectroscopy",* Central Bureau of Astronomical Telegrams, 2723.

5. *Rajesh, T.A., Ramachandran, S., and Ubale, G.P., "An automated roof window system",* PRL Technical Report, PRL-TN-2012-101, Physical Research Laboratory, Ahmedabad, February, 2012.

Facilities and Services

Activities on the promotion of Official Language

As a part of implementation and progressive use of Hindi in PRL, the Hindi Pakhwada was celebrated at PRL from September 14 - 28, 2011. The highlights of the celebrations included word quiz, essay, elocution, Hamara Karya, self written poetry competition. A Technical Seminar in Hindi on "Contribution of PRL in Scientific/Technical Progress of India" was held at PRL on 20 March, 2012. Sixteen members presented their papers in this Seminar.

Vishwa Hindi Divas was organized in PRL on 10.1.2012 and an essay competition was held on Prospects of Use of Hindi in Scientific Work. Shri R.S. Gupta, Hindi Officer-II & OSD delivered lectures in Hindi at workshops held by various Departments like Space Applications Centre, Airport Authority, Food Corporation of India, Income Tax, Doordarshan, ONGC on different topics including Various applications of computers in Hindi.

Computer Centre

To cater to the High Performance Computing needs of our scientists, Computer Centre is equipped with High Performance Compute Cluster having 20 compute nodes, 1 master node with 64GB RAM on each node, 20TB storage capacity and 3.2 TF peak computing performance and 2.2 TF sustained computing performance. The HPC cluster has a Backup node, I/O node, Management node, Storage node, and a Visualization node. The HPC facility is homed in a special chamber that is maintained at controlled temperature and humidity and has a dual UPS system for round the clock operation. The primary network of HPC is with Infiniband and secondary network is Gigabit. Computer Center has Dell server having 16 AMD processors, 64GB RAM with 4TB disk capacity. Centre also has four HP servers, each having four AMD processors, 4 GB RAM, 1.5 TB disk space providing computing power with large disk storage. Computer centre has also IBM Power5 4 CPU based server providing additional computing power. The Internet connectivity is 10Mbps through BSNL Optical Fiber Cable. All these computing machines are connected to our high-speed (1Gbps) local area network (LAN) to provide easy, fast and reliable access to more than 300 PC's and a few workstations distributed throughout all the campuses of our laboratory. PRL dispensary in the colony campus opposite IIM is now connected to the Main Campus over an 1Gbps Optical Fiber link. Through this link, the PRL Medical Officers access the Dispensary database housed in the CoWAA cell in computer center. Through the same Optical Fiber link, the students and PDFs have a round the clock access to PRL LAN/Internet from their rooms via a few Wi-Fi devices installed in the buildings. Students from Thaltej Hostel also can access Internet throught a Wi-Fi device installed in the common room in the hostel. The connectivity between Udaipur Solar Observatory (USO), and PRL Main Campus is 2 Mbps through BSNL – MLLN

(Managed Leased Line Network). Mt.Abu is also connected to PRL main campus over 2 Mbps MLLN link provided by BSNL. Our Thaltej Campus is connected over a Optical Fiber 34 Mbps through BSNL-MLLN link. Thus, round the clock connectivity has been provided to users all the time from Thaltej, USO, and Mt. Abu. Our main campus is also connected to Thaltej via BSNL's 2 Mbps MLLN for voice communication providing intercom telephone facility between the campuses. The Centre provides centralized virus free E-mails by automatically scanning all incoming E-mails. Anti-Spam filter has been centrally installed to fight the Spam mails. The center also provides web enabled email service. Internet authorizations, monitoring and reporting functions have been added to have optimal usage of Internet bandwidth.

To cater to the High end computing needs, PRL has become resource partner of C-DAC's Grid Garuda Project. The Grid Garuda network is integrated to PRL LAN providing seamless access of Garuda resources to PRL scientists.

PRL SPACENET connectivity for Data, Intranet, and video conferencing has been established at Main Campus, USO and IR Observatory over IP to interact with ISRO centers.

Mathematical, numerical and visualization application software like IMSL, IDL, Mathematica, SigmaPlot, MATLAB, Lahey FORTARN 95, and Statistica etc. have also been installed to cater the needs of the scientific community.

Library & Information Services

Library always strives to act as a facilitator in the research carried out in the laboratory by making available latest resources in different subject areas. As a part of fulfilling this objective, PRL Library subscribes to full-text databases like ScienceDirect, IOP Archive, PROLA, GSA Archive, SPIE Digital Library, Science Archive (access from 1880) and Nature archive (access from 1987). As no library can be completely self-sufficient, it also provides document delivery service through ILL. The Library also assists the students in procuring the book-grant books.

In all, 371 books (scientific and general), 48 hindi books and 94 CDs/DVDs were added in the Main, Thaltej and USO libraries during 2011-12. Hundred and forty three (143) book grant requests were processed this year. During this period, number of visitors, visiting the library was 3525 and number of documents issued was 3905. The number of ILL requests for articles from other institutes fulfilled by PRL Library was 296 and that of requests of PRL staff fulfilled by other libraries was 310. Number of photocopies made, in house were 46154 and by outside agency were 44339.

The library homepage acts like a window through which it is possible to access the digital content subscribed by PRL as well as open access content. It gives link to 150 online journals out of the 158 journals subscribed by the library. It also provides access to the institutional repository consisting of journal articles published by the PRL authors from 1995 to present using the Greenstone Digital Library Software (GSDL software). More than 3000 articles by PRL authors are now part of the repository. PRL Theses from 1960 onwards (289) are now available full text for PRL users. About 30 E-books have been purchased this year for PRL users to keep pace with the changing technology. Ebooks page has been redesigned so as give access to the collection by subject as well as by title of the e-book. These collections can be accessed from library homepage (http://www.prl.res.in/~library).

Workshop

The Mechanical Workshop is used by scientists/engineers to fabricate or build suitable instruments for their research work. The workshop has a wide range of machines. These include Vertical machining centre, CNC lathe, conventional lathe & Milling machines, metal cutting machines, welding machines. The workshop is equipped with one CNC Lathe machine to carry out precise turning jobs. A state-of-the-art three axis Vertical Machining Center (VMC-850) computerized numerical controlled machine is installed recently and working successfully at PRL workshop. Software is available for design & development work which automatically transfers to the machine to manufacture the desired parts. This provides an opportunity for scientists to undertake important projects at the forefront of research/ technology. The workshop also carries out sheet and structural metal fabrication jobs. The high vacuum welding joints are also carried out by using TIG welding machine. Various high precision jobs including payload packages for satellite/rocket/balloon, ground based instrumentation, optical component adapters and mounts are being fabricated at the workshop.

Some of the major works carried out during the year are listed below:

(1) Cylindrical Mirror Analyser (CMA)

An energy analyser for charged particles (electrons or ions) has been fabricated. It consists of two co-axial SS304 cylinders of equal length. There are two annular slits close to the ends of the inner cylinder. Charged particles enter the annular gap through one slit. Mechanically, coaxial assembly of the cylinders is critical. The machining and positioning of the slit with accurate dimensions within the

Cylindrical Mirror Analyser (CMA) with experimental set-up

tolerance of 20 μ is required. In the present assembly, the inner cylinder is having outside diameter 42 mm and inside diameter of 40 mm at both ends. The inner cylinder has a variable wall thickness of 1 mm close to the ends and 2mm elsewhere. The outer cylinder has 95 mm outer diameter and 89 mm inner diameter. Slits made in the form of 3 annular sectors of included angle 108° are 3 mm width and are inclined at 45° to the wall. The inner cylinder has additional features within it to accommodate a detector and wire meshes to define the electric field.

(2) Temperature controlled Air manifold system

A temperature controlled ambient air manifold has been designed and developed for Aerosol Monitoring Laboratory. The system is made of cylindrical aluminum tube of length 457 mm and diameter 102 mm. The ambient air is sucked from its one side and aerosol instrument samples the air through its other end. The system can feed air to 5 aerosol instruments. The tube encloses a temperature and a humidity sensor, and is wrapped with an insulated nichrome heating cable. The assembly is encapsulated in a PVC tube to achieve thermal isolation. All components are silver anodized to protect them from oxidization.

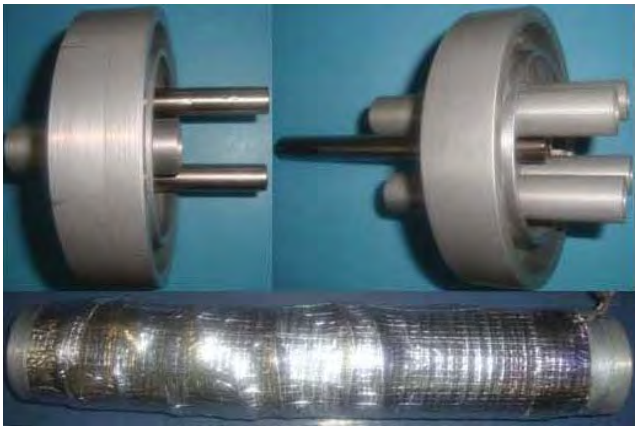

Temperature controlled Air manifold system

(3) Multi Heat Sink for Large Area Silicon Drift Detector

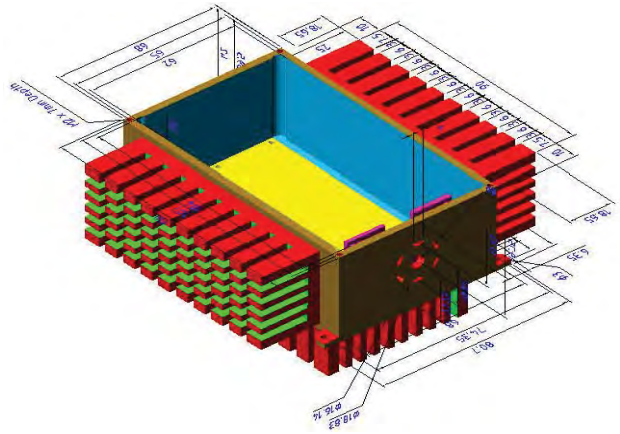

Multi Heat Sink For Large Area Silicon Drift

A large area (92 mm^2 Sensitive area) Silicon Drift Detector (SDD) is being used to realize very large area (736 $mm^{2)}$ low energy X-Ray Spectrometer. To achieve resolution of 200 eV @ 5.9 keV, detector has to be cooled by inbuilt Thermoelectric cooler (TEC). TEC dissipates about 4 watts of power to achieve "T ~ 65 °C. A Multi flange heat sink has been designed to effective radiate this 4 W heat at very fast Rate.

(4) Precision mirror mounts for Lidar

Two mechanical mounts are fabricated, for mounting mirrors, for pumping Laser beam into the atmosphere. These

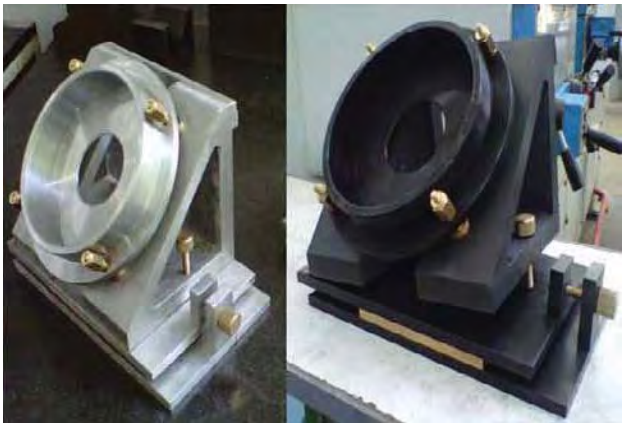

Precision Mounts

mounts are fabricated in workshop and having capability of steering and aligning Laser beam in XYZ plane. These are being used in the Lidar laboratory at Mount Abu.

(5) Time of Flight Mass Spectrometer (TOFMS)

Assembled Parts of TOFMS

In this mass spectrometer, atoms/molecules are ionized by electron impact, ion impact or photons. The mass spectrometer discriminate the detected ions on the basis of their mass to charge ratio due to an applied electric field. The required parts of a TOFMS are made in workshop. Three mesh holders, one barrel to mount channeltron detector and a drift tube with their mounting parts, like, rods, Teflon washers etc. are made in workshop. The assembled TOFMS is shown in fig. All parts/components needed critical machining operations and assembly.

(6) Laser ablation based cluster source

A cluster source based on laser ablation of a target accompanied by supersonic expansion of gas with the aim of production of a cluster beam is designed and fabricated. Provision is made for admitting high pressure gas and mounting quartz window for admitting high power laser beam. Three different types of cluster sources were fabricated of using materials like Aluminum, Brass and SS-304.

Laser Ablation based Cluster Sources

(7) Crystal holder

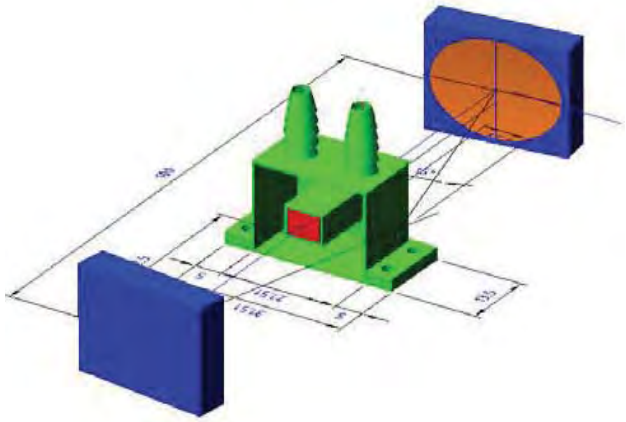

A compact crystal holder through which cold water can flow without making contact with the crystal has been designed and fabricated. The crystal is placed at the center of the oven as shown by red color. Cold water (temperature less than 18°C) entering into the holder (internal volume 50 cc) though one of the ports cools the holder and hence the crystal. The crystal holder is made of copper to take the advantage of high thermal conductivity. To avoid any leakage it is made in one piece with a cover.

(8) Other important jobs carried out in the workshop.

- A small rock sample cutting machine
- Solar Telescope work at Thaltej
- Digital Ionosonde Antenna work
- Airglow Photometer
- Calibration test setup for Source and Silicon Drift Detector Assembly
- Design of Electronics Work Bench
- Design of Solar X ray monitor sensor package for Chandrayaan-2 mission

Honorary Fellows

Professor J. E. Blamont

Professor P. Crutzen

Professor A. Hewish

Professor K. Kasturirangan

Professor D. Lal, FRS

Professor M. G. K. Menon, FRS

Professor U. R. Rao

Honorary Faculty

R. K. Varma
FNA, FASc, FNASc, NASI Senior Scientist

S. Krishnaswami
FNA, FASc, FNASc, FTWAS, INSA Senior Scientist

R. G. Rastogi
FNA, FASc, FNASc

S. K. Gupta
FNASc

A. C. Das

N. Bhandari
FNA, FASc, FNASc, INSA Honorary Scientist

D. P. Dewangan
FNASc

B.G. Ananad Rao

S. P. Gupta

Harish Chandra

H. S. S. Sinha

U. C. Joshi

R. Sridharan
FASc, FNASc, CSIR Emiritus Scientist

Honorary Technical Faculty

R. N. Misra

H.O. Vats

Academic Faculty

Name	Designation	Specialisation	Academic Qualification
Goswami J. N. *FNA, FASc, FNASc, FTWAS*	Director	Solar System Studies (Pre - Solar Processes)	Ph D, PRL, Guj. Univ. (1978)
Ambastha A. K.	Professor	Solar Plasma Physics, Coronal Structure and Polarization	Ph D, PRL, Gujarat Univ. (1981)
Amritkar R. E. *FASc, FNASc*	Senior Professor	Nonlinear Dynamics &Chaos	Ph D, IISc, Bangalore (1978)
Ashok N. M.	Senior Professor	Close Binary Stars, NovaeIR spectroscopy	Ph D, PRL, Gujarat Univ. (1983)
Baliyan K. S.	Associate Professor	AGNs, Comets, Atomic Physics, Milky Way	Ph D, Roorkee Univ. (1986)
Banerjee D.	Associate Professor	Thermoluminscence & Planetary Physics	Ph D, PRL, Gujarat Univ. (1996)
Banerjee D. P. K.	Professor	Novae, Be Stars,Planetary Nebulae, IR and Optical Studies	Ph D, PRL, Gujarat Univ. (1991)
Banerji J.	Professor	Classical Optics, Quantum Physics	Ph D, City Univ. (New York) (1982)
Bapat B.	Associate Professor	Atomic & Molecular Processes	Ph D, TIFR, Mumbai Univ. (1997)

Name	Designation	Specialisation	Academic Qualification
Bhatt J. R.	Associate Professor	Astrophysics	Ph D, IPR, MS Univ. (1992)
Bhattacharyya R.	Reader	Plasma Physics	Ph D Jadavpur Univ, Kolkata, (2006)
Bhushan Ravi	Scientist-SF	Oceanography and Paleoclimatology	Ph D, MS Univ.(2009)
Chakrabarty A.	Associate Professor	Extra- solar planets, Star Formation & Instrumentation	Ph D, PRL, Gujarat Univ. 1999)
Chakrabarty D.	Reader	Upper Atmoshere and Geomagnetic Storm	Ph.D, PRL, MLS Univ. (2008)
Chandrasekhar T.	Professor	High Angular Resolution Studies, Late type stars Solar Coronal, Studies Comets	Ph D, PRL, Gujarat Univ. (1982)
Deshpande R. D.	Scientist-SF	Application of Environmental Tracers in Hydrology	Ph D, PRL, MS Univ. (2007)
Gosain S.	Scientist-SD	Solar Physics and Instrumentation	Ph D, MLS Univ. (2007)
Goswami S.	Associate Professor	High Energy Physics	Ph D, Calcutta Univ. (1998)
Haider S. A. *FASc*	Professor	Planetary and Cometary Atmospheres	Ph D, Banaras Univ. (1984)
Kumar S.	Reader	Aquatic and Terrestrial Biogeochemistry	Ph.D, PRL, M. S. Univ., Vadodara (2004)
Jain R.	Professor	Solar Physics	Ph D, PRL, Gujarat Univ. (1983)
Janardhan P.	Professor	Solar Radio Astronomy & Space Weather	Ph D, PRL, Gujarat Univ. (1992)
Joshi B.	Reader	Solar Physics, Astronomy	Ph D, ARIES, Kumaun Univ. (2007)
Joshipura A. S. *FNA, FASc, FNASc*	Outstanding Scientist	Particle Physics	Ph D, Bombay Univ. (1979)
Juyal N.	Scientist-SF	Quaternary Geology & Paleoclimate	Ph D, M.S.Univ.(2004)
Kota V. K. B.	Senior Professor - H	Nuclear Physics	Ph D, Andhra Univ. (1977)
Kumar B.	Scientist-SD	Solar Physics	Ph D, PRL, MLS Univ. (2007)
Konar, Partha	Reader	Particle Physics	Ph D, Allahabad Univ.(2005)

Name	Designation	Specialisation	Academic Qualification
Lal S. *FNA, FASc, FNASc*	Senior Professor	Atmospheric Chemistry and Trace Gases	Ph D, PRL, Gujarat Univ. (1982)
Mahajan N.	Reader	Particle Physics	Ph D, Delhi Univ. (2003)
Marhas K. K.	Reader	Solar System studies	Ph D, PRL, DAVV Indore (2001)
Mathew S. K.	Associate Professor	Solar Magnetic & Velocity Fields	Ph D PRL, Gujarat Univ. (1999)
Mishra H.	Associate Professor	Strong Interaction Physics & Nuclear Astrophysics	Ph D, IOP, Utkal Univ. (1994)
Mohanty S.	Professor	Astroparticle Physics	Ph D, Wisconsin Univ. (1989)
Murty S. V. S. *FASc*	Senior Professor	Isotope Cosmochemistry	Ph D, IIT, Kanpur (1981)
Naik S.	Reader	High Energy Astro- physics, X-ray Binaries	Ph D,TIFR,Mumbai Univ. (2003)
Navinder Singh	Reader	Theoretical condensed matter and Statistical physics	PhD. RRI,Bangalore (2006)
Pallam Raju D.	Associate Professor	Space and Atmospheric Sciences	Ph D, PRL, DAVV Indore(1996)
Rai V.	Reader	Stable Isotope Cosmochemistry	Ph D, PRL, MS Univ. (2001)
Ramachandran S.	Associate Professor	Atmospheric AerosolsRadiative & Climate Impacts	Ph D, PRL, MS Univ. (1996)
Ramesh R. *FNA, FASc, FNASc, FTWAS*	Senior Professor	Paleoclimatology, Oceanography & Modelling	Ph D, PRL, Gujarat Univ. (1984)
Rangarajan R.	Associate Professor	Particle Physics & Cosmology	Ph D, Univ. of California, Santa, Barbara (1994)
Ray J. S.	Associate Professor	Isotope Geochemistry	Ph D, PRL, MS Univ. (1998)
Rengarajan R.	Scientist-SE	Atmospheric aerosols & aqueous geochemistry	Ph D, PRL, MLS Univ.(2004)
Rindani S. D. *FASc, FNA, FNASc*	Senior Professor-H	Particle Physics	Ph D, IIT, Bombay (1976)
Rastogi N.	Reader	Atmospheric & Aerosol Chemistry	Ph.D., PRL, MLSU, Udaipur (2005)
Sahoo B.K.	Reader	Atomic Physics	Ph D, Bangalore Univ.(2006)
Sahu L.K.	Reader	Atmospheric Science, Trace gases	Ph D, PRL, MLSU, (2005)

Name	Designation	Specialisation	Academic Qualification
Samanta G.K.	Scientist-SD	Laser and nonlinear optics	Ph D, Universitat Politecnica de Catalunya University, Barcelona, (2009)
Sarin M. M. *FASc, FNA, FNASc*	Senior Professor	Geochemistry and Oceanography	Ph D, PRL, Gujarat Univ. (1985)
Sarkar U. *FNA, FASc, FNASc*	Senior Professor	Particle Physics	Ph D, Calcutta Univ. (1984)
Sekar R.	Professor	Upper Atmospheric & Ionospheric Physics	Ph D, PRL, Gujarat Univ. (1991)
Sharma Som K.	Reader	Middle Atmosphere & Long Term Atmospheric Changes	Ph D, PRL, Gujarat Univ. (2010)
Ganesh S.	Scientist-SE	Milky Way, Comets, AGN, Astronomical polarimetry	Ph.D, Guj. Univ. (2011)
Sheel V.	Associate Professor	Modelling of Lower Atmosphere	Ph D, PRL, Gujarat Univ. (1996)
Singal A. K.	Associate Professor	Radio Astronomy & Astrophysics	Ph D, TIFR, Bombay Univ. (1986)
Singh A. D.	Associate Professor	Atomic Physics	Ph D, Bangalore Univ. (1998)
Singh R. P.	Scientist – SF	Laser Physics	Ph D, JNU, New Delhi (1994)
Singh S. K.	Associate Professor	Isotope Geochemistry	Ph D, PRL, MS Univ. (1999)
Singhvi A. K. *FNA, FASc, FNASc, FTWAS*	Outstanding Scientist	Palaeoclimatology and Geochronology	Ph D, IIT, Kanpur (1975)
Srivastava N.	Associate Professor	Solar Physics	Ph D, PRL, Ravi Shankar Shukla Univ. (1994)
Subramanian K. P.	Associate Professor	Experimental Atomic and Molecular Physics	Ph D, PRL, Gujarat Univ. (1987)
Thampi S.	Reader	Atmospheric Physics Thiruvananthapuram, Kerala,	Ph.D, VSSC, Univ. (2007)
Vadawale S. V.	Reader	High Energy Astrophysics and X - ray Spectroscopy	Ph D, TIFR, Mumbai Univ. (2003)
Venkatakrishnan P.	Senior Professor-H	Solar Physics	Ph D, Bangalore Univ. (1984)
Yadava M. G	Scientist-SF	Palaeoclimate, Radiocarbon dating and Stable isotopes	Ph D, PRL, DAVV Indore (2003)

Technical Faculty

Name	Designation
Acharya Y. B.	Engineer-G
Adhyaru P. R.	Engineer-SE
Narayanan R.	Scientist-SF
Rao D. K.	Scientist-SE
Shah A. B.	Engineer-SF
Shah K. J.	Computer-Scientist-SE
Shah R. R.	Engineer-SF
Shukla A. D.	Scientist-SE
Singh Mahendra	Sci./Eng.-SF
Ubale G. P.	Engineer-SF
Venkataramani S.	Scientist-SF



पी.आर.एल. में गतिविधियां
Events at PRL



























पी.आर.एल. में गतिविधियां
Events at PRL

पी.आर.एल. में गतिविधियां
Events at PRL



























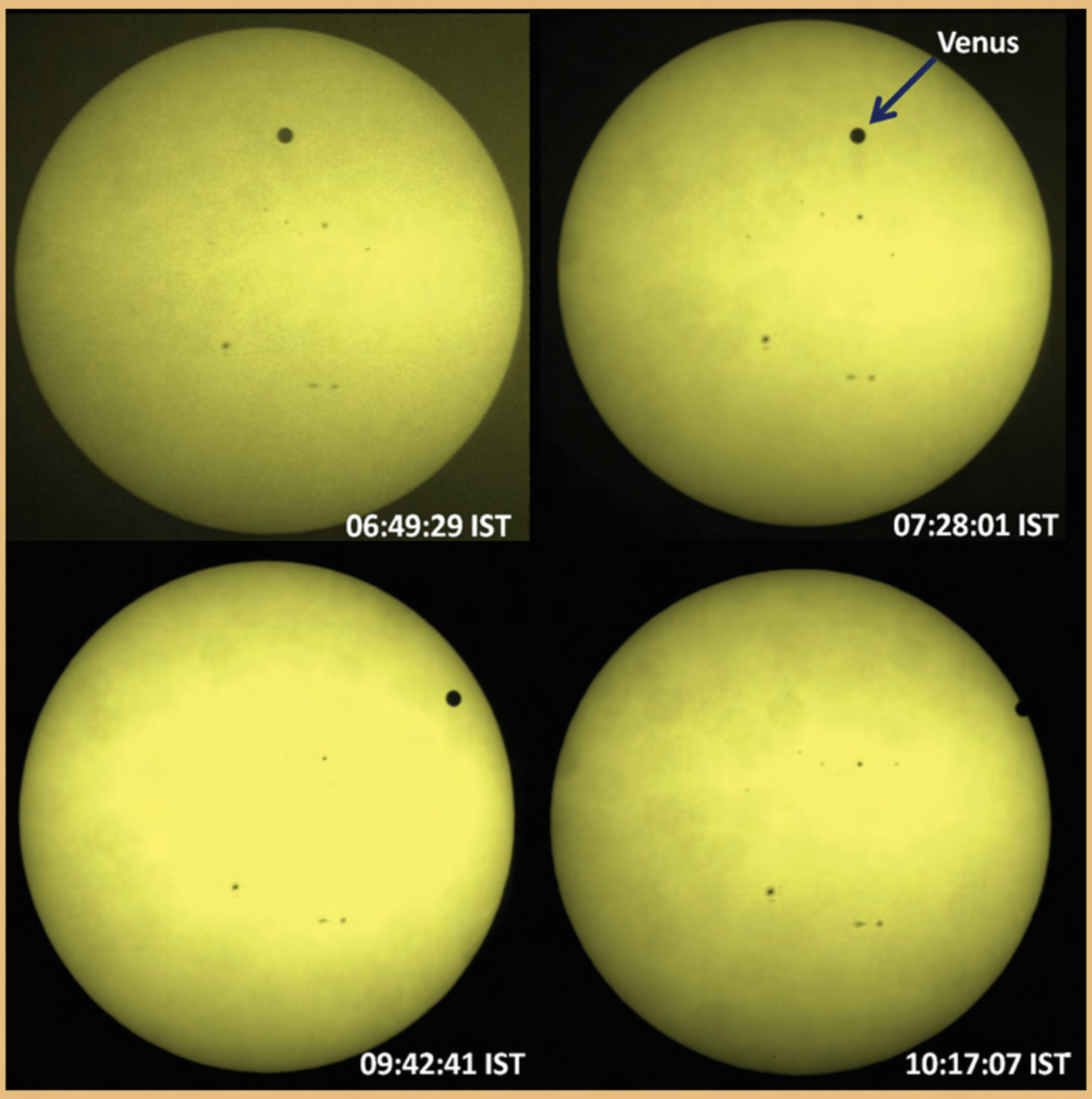
Venus
06:49:29 IST
07:28:01 IST
09:42:41 IST
10:17:07 IST